A PRIMER IN STRATEGIES TOWARDS THE ERA OF PRECISION MEDICINE

By

Warit Ruanglertboon

B.Pharm., M.Sc. (Pharmacology)

Thesis
Submitted to Flinders University
for the degree of

Doctor of Philosophy

College of Medicine and Public Health
11 November 2021

CONTENTS

LIST OF FIGURES

LIST OF TABLES

APPENDIX FIGURES

APPENDIX TABLES

DECLARATION

I certify that this thesis does not incorporate without acknowledgement any material previously submitted for a degree or diploma in any university; and that to the best of my knowledge and belief, it does not contain any material previously published or written by another person except where due reference is made in the text.

Warit Ruanglertboon

August 2021

ACKNOWLEDGEMENT

I would like to acknowledge that this project would not have been possible without the significant contribution of others, to whom words cannot express my gratitude.

Firstly, I would like to express my deepest sense of gratitude to my principal supervisor Associate Professor Andrew Rowland for his mentorship and guidance throughout my PhD studies. I am really grateful for your friendship, your expertise and the time we shared in the lab over the past 4 years in Adelaide. I thank equally to my co-supervisor Professor Michael Sorich and Dr. Ashley Hopkins for their guidance and support, especially during the later state of my candidature. Many thanks also to Associate Professor Robyn Meech for her co-supervision and advices of this thesis. A special thanks to Professor John Miners, who established a long-lasting collaboration with Thai pharmacology researchers throughout his successful career path. Without our fateful meeting, I could not be able to turn my life around this far.

I would like to thank my colleagues and friends, both past and present, for their friendship and helpful discussions. In particular, colleagues in precision medicine group, Dr. Zivile Useckaite, Lauren Newman and Alia Fahmy, and the others from discipline of Clinical Pharmacology, Dr. Julie-Ann Hulin, Dr. Nuy Chau, Dr. Sara Tommasi and Dr. Lu Lu. It has been a pleasure to work with you all over the years and be part of my life overseas. I thank Dr. Ahmad Abuhelwa, Natansh Modi and Sarah Badaoui who I mostly share my time during the very end of my candidature.

I would like to sincerely acknowledge the Royal Thai Government Scholarship for providing financial support and others invaluable advises. I will contribute what I have learned overseas back to our country in the best way I could do.

Finally, I dedicated this work to my family, friends and myself. This is the testament of my determination to make my dreams come true. I chose to endeavour in this path and keep embracing my dream no matter what happens in my life.

PUBLICATIONS ARISING DIRECTLY FROM THIS THESIS

- Ruanglertboon, W., Sorich, M.J., Rowland, A. et al. Effect of early adverse events resulting in sorafenib dose adjustments on survival outcomes of advanced hepatocellular carcinoma patients. Int J Clin Oncol (2020). https://doi.org/10.1007/s10147-020-01698-7
- Ruanglertboon, W., Sorich, M.J., Logan, J.M. et al. The effect of proton pump inhibitors on survival outcomes in advanced hepatocellular carcinoma treated with sorafenib. J Cancer Res Clin Oncol 146, 2693–2697 (2020). https://doi.org/10.1007/s00432-020-03261-3
- Ruanglertboon, W.; Sorich, J M.; Hopkins M A.; Rowland A., Mechanistic modelling identifies and addresses the risks of empiric concentration guided sorafenib dosing. Pharmaceuticals 2021, 14(5), 389; https://doi.org/10.3390/ph14050389.

ADDITIONAL PUBLICATIONS RELATED TO THIS THESIS

- Rowland, A, Ruanglertboon, W, Dyk, M, Wijayakumara, D, Wood, LS, Meech, R, Mackenzie, PI, Rodrigues, AD, Marshall, J-C & Sorich, MJ 'Plasma extracellular nanovesicle (exosome) derived biomarkers for drug metabolism pathways: A novel approach to characterise variability in drug exposure', British Journal of Clinical Pharmacology, vol. 85, issue 1, Jan 2019, pages 216-226

CONFERENCE PROCEEDINGS

- Ruanglertboon W. Characteristics of extracellular vesicles secreted by HepaRG following removal of media component. The Australasian Society of Clinical and Experimental Pharmacologists and Toxicologists (ASCEPT) annual scientific meeting, November 2019.
- Ruanglertboon W. Characteristics of extracellular vesicles secreted by HepaRG following removal of media component. The Australasian Society of Clinical and Experimental Pharmacologists and Toxicologists (ASCEPT) annual scientific meeting, November 2019.
- Ruanglertboon W., Rowland A., Sorich MJ. Detection of hepatic cytochromes P450 protein in plasma derived extracellular nanovesicles (exosomes). The Australasian Society of Clinical and Experimental Pharmacologists and Toxicologists (ASCEPT) annual scientific meeting, November 2018.

AWARDS IN SUPPORT OF THIS THESIS

- The Royal Thai Government Scholarship for the development of the Southern border of Thailand scheme., 2017 – 2022
- The British Journal of Clinical Pharmacology (BJCP) prize for trainee. Awarded by The British Pharmacological Society. The award was given for the best article by an early career researcher, for the article "Plasma extracellular nanovesicle (exosome) derived biomarkers for drug metabolism pathways: A novel approach to characterise variability in drug exposure" published in 2019 in issue 1 of the BJCP.
- Australasian Society of Clinical and Experimental Pharmacologists and Toxicologists (ASCEPT) travel grant, 2019

THESIS ABSTRACT

Precision medicine has emerged as a more refined iteration of clinical pharmacology and personalised medicine. The capacity for precision medicine to provide more nuanced and individualised estimates of drug exposure and effect has emerged due to advances in access to information and technologies. Several promising approaches have been invented to address the precision dosing, although some could not be practically usable in the real clinical setting. This thesis investigated into two distinct paradigms, including computational- and laboratory-based approach evaluating their essence in addressing the precision dosing of cancer medicines. In this thesis, sorafenib, an oral tyrosine kinase inhibitor, was selected as an exemplar drug to be extensively studied under the array of methods to address precision dosing.

Clinical epidemiology and data analysis using a big data from the pharmaceutical companies were conducted in the first two Chapters of the thesis. Notably, the current dataset was considered a "high-quality" data as it was originally derived from real patients enrolled in clinical trials. This section focussed on a current dosing guideline of sorafenib regarding dose adjustment during the therapeutic course. The prior assumption was made that dose adjustment of sorafenib due to AEs could lead to worse survival outcomes in the long term. However, the landmark analysis set at the end of the first cycle of treatment (28 days) to examine the effect of dose adjustment on the survival outcomes of sorafenib in advanced HCC patients observed no poorer outcomes. Moreover, patients experienced dose reduction due to the early AEs observed the association with an improved OS. It could be suggested that the long-term clinical benefits of sorafenib may be derived from high initial dose/plasma concentrations.

Previous studies showed a negative impact of PPI use on the clinical benefits derived from several TKIs, which sorafenib is a member of this class, such as erlotinib. Hence, concerning the effectiveness of sorafenib in patients that PPI was mandatory, a brief investigation of the effects of concomitantly used of PPI with sorafenib on the clinical outcomes was conducted. It was concluded that concomitant use of PPI with sorafenib was not associated with inferior clinical benefits. Noticeably, the finding of no association between concomitant PPI use and sorafenib outcomes was demonstrated for both OS and PFS in both univariable and adjusted analysis. This finding promotes confidence in prescribing PPI together with sorafenib in advanced HCC patients requiring PPI, leading to improving patients' quality of life.

Subsequent studies expanded on the outcomes of the clinical epidemiology analyses and involved the application of simulation and modelling-based analysis performed on Simcyp® platform to interrogate the capacity of concentration-guided sorafenib dose adjustment. The simulation was performed with and without model-informed initial dose selection (MIDS) to enhance the proportion of patients that achieve a sorafenib plasma concentration within a pre-defined optimal therapeutic. The results obtained

from the simulations revealed that covariates affecting sorafenib exposure were including hepatic CYP3A4 abundance, albumin concentration, BMI, BSA, sex and weight. By accounting for these covariates, it was possible to identified subjects at risk of failing to achieve a sorafenib $C_{max} \geq 4.78$ μg/mL with 95.0 % specificity and 95.2 % sensitivity. Concentration-guided sorafenib dosing with MIDS facilitated a sorafenib C_{max} within the range of 4.78 to 5.78 μg/mL for 38 of 52 patients who failed to achieve a $C_{max} \geq 4.78$ μg/mL with the standard dosing regimen. On the other hand, concentration-guided sorafenib dose adjustment without MIDS resulted in 33 of 52 patients who required dose adjustment achieving a $C_{max} \geq 5.78$ μg/mL.

The final section of this thesis was dedicated to laboratory-based biomarker discovery. The study aimed to verify the utility of extracellular vesicles (EVs) derived biomarkers, as part of the liquid biopsy, for the prediction of drug Absorption, Distribution, Metabolism and Excretion (ADMExosomes). Initially, a preliminary study to validate the availability of DME in EVs derived from human plasms was first conducted. Human plasma EVs was characterised before proceeding to other downstream experiments. The characterisation reported the particle size of 50-150 nm and a presentation of the small EV marker, Tsg101. EVs isolated from human plasma contained peptides and mRNAs originating from *CYP* (*1A2, 2B6, 2C8, 2C9, 2C19, 2D6, 2E1, 2J2, 3A4* and 3A5), *UGT* (*1A1, 1A3, 1A4, 1A6, 1A9, 2B4, 2B7, 2B10* and *2B15*), and NADPH-cytochrome P450 reductase. The number of unique peptides detected for each protein ranged between 2 and 19, with a mean of 9.65. In addition, 5 unique peptides originating from NADPH-cytochrome P450 reductase (the redox partner required for CYP activity) were also detected. While cytochrome b5 (34.5 kDa) was not detected in the current analysis as it was not contained within the window of protein bands analysed, the presence of this protein in human derived EVs has already been established.

Additional analysis following the confirmation of the availability of DME in EVs was conducted, proposing to verify the functionality aspect. *In vitro* hepatocyte cells line was used as the sources to produce a large amount, controllable and robust EVs. Meanwhile, the parallel experiments were conducted on human serum EVs obtained from healthy volunteers. The abundance of CYP3A4 and its catalytic activity derived from EVs samples were broadly evaluated. Targeted proteomics revealed the availability of CYP3A4 peptides derived from EVs isolated from HepaRG and human serum. Subsequently, determination of CYP3A4 catalytic activity was conducted using metabolite formation assay. LC-MS analysis detected 1OH midazolam and sorafenib N-oxide formation after incubation of human serum EVs with midazolam or sorafenib, respectively. However, no metabolite formation was observed from incubation of probe substrates with HepaRG EVs. The factors contributing to the positive metabolite formation derived from human serum EVs may be related to the integrity and conformation of CYP3A4 enzymes. However, complete attestation has not yet been identified in this thesis.

Taken together, the data presented in this thesis demonstrated a multidimensional approach to address precision dosing of sorafenib. The strengths and limitations of each technique were thoroughly investigated to explore the most appropriate method for the real clinical setting. Noticeably, the finding of DME panels and functionality provided an excellent opportunity to develop this knowledge to the real clinical diagnosis and treatment. Ultimately, this novel biomarker could serve as a bridging mediator not only to support an immediate dose monitoring and adjustment but also as a source to support model-informed precision dosing.

ABBREVIATIONS

Abbreviations	Definition
ACAT	Advanced Compartmental Absorption and Transit
AD	Alzheimer's disease
ADAM	Advanced dissolution, absorption, and metabolism
AE	Adverse event
AUC	Area under the curve
BCA	Bicinchoninic Acid
BCLC	Barcelona Clinic Liver Cancer
BSA	Bovine serum albumin
CAR	Constitutive androstane receptor
CAT	Compartmental Absorption and Transit
CKD	Chronic kidney disease
CTFR	Cystic fibrosis transmembrane conductance regulator
CYP	Cytochrome P450
DDI	Drug-drug interaction
ddPCR	Droplet Digital PCR
DME	Drug-metabolising enzyme
DMSO	Dimethyl sulfoxide
ECOG PS	Eastern Cooperative Oncology Group performance
EGF	Epidermal growth factor
ELV	Exosome- like particle
ER	Endoplasmic reticulum
ESCRT	The endosomal sorting complexes required for transport
Evs	Extracellular vesicles
FBS	Foetal bovine serum
FMOs	flavin-containing mono-oxygenases
GAPDH	Glyceraldehyde-3-phosphate dehydrogenase
GI	Gastrointestinal
GRs	Glucocorticoid receptors
HBV	Hepatitis B virus
HBx	Hepatitis B X protein
HCC	Hepatocellular carcinoma
HCV	Hepatitis C virus
HER2	Human epidermal growth factor receptor type 2
HLM	Human liver microsome
HSP	Heat shock protein
IIV	Inter-individual variability
IL	Interleukin
ILVs	Intraluminal vesicles
IVIVE	*in vitro/in vivo* extrapolation
LDL	Low-density lipoproteins
MAO	Monoamine oxidase
MV	Microvesicles
MVBs	Multivesicular bodies

NAFLD	Non-alcoholic fatty liver disease
NASH	Non-alcoholic steatohepatitis
NGS	Next generation sequencing
NRs	Nuclear receptors
NSAIDs	Nonsteroidal anti-inflammatory drugs
nSMase	Neutral sphingomyelinase
NTA	Nanoparticle tracking analysis
OATP	Organic-anion-transporting polypeptides
OS	Overall survival
PAHs	Polycyclic aromatic hydrocarbons
PBPK	Physiologically based pharmacokinetic
PCR	Polymerase chain reaction
PDGFR	Platelet-derived growth factor
PFS	Progression-free survival
PM	Poor metabolizer
PopPK	Populational pharmacokinetic
PPIs	Proton pump inhibitors
PXR	Pregnane X receptor
RCC	Renal cell carcinoma
RT-PCR	real-time quantitative PCR
RXR	Retinoid X receptors
SEC	Size-exclusion chromatography
SMase	Sphingomyelinase
TEM	Transition electron microscopy
TKIs	Tyrosine kinase inhibitors
Tsg101	Tumour susceptibility gene protein 101
UC	Ultracentrifugation
UGT	Uridine 5'-diphospho-glucuronosyltransferase
UM	Ultra-rapid metabolizer
US FDA	The United States Food and Drug Administration
VEGF	Vascular endothelial growth factor

CHAPTER 1: GENERAL INTRODUCTION

1.1 – A brief overview of the history of precision medicine

The concept of individualising a patient dose is not new. Over 500 years ago Swiss alchemist and physician Paracelsus (1493-1541) recognised that dose could resolve a remedy from a poison. While this concept has been refined significantly over time, the modern interpretation of dose individualisation by techniques such as therapeutic drug monitoring still dates back nearly 50 years to the early 1970s. Here, early reports describe the measurement of anticonvulsant [1] and phenobarbital [2] concentrations in blood being used to individualise doses, particularly in children. Similarly, in terms of the actions of a drug, over 100 years ago German Jewish physician and scientist Paul Ehrlich reasoned that even for complex infections characteristics of the pathogen could be targeted to kill the infection while leaving the host unharmed. This theory, termed Ehrlich's Magic Bullet, led to achievements including a cure for syphilis in 1909 and the precursor technique to bacterial Gram staining [3]. Ehrlich's methods for tissue staining also allowed for the distinction of different types of blood cells, which facilitated the diagnose and treatment of numerous blood diseases including haematological malignancies targeted by today's modern therapies.

The term "Personalised medicine" was firstly introduced in 1999 in an article "New Era of Personalised Medicine: Targeting Drugs for Each Unique Genetic Profile". The primary concept of personalised medicine was to provide a thorough treatment to each individual with an understanding of differences in genetic, epigenetic and clinical presentations. Personalised medicine utilises an individual data relating to medical history, family history, environmental factors and genetic factors to address the plausible disease prognosis. However, the term personalised medicine may somewhat imply that the treatment is individually designed for a person, which probably not entirely correct. Hence, the term "Precision medicine" was later introduced and can be defined as "an emerging approach for disease treatment and prevention that takes into account individual variability in genes, environment, and lifestyle for each person" according to the description provided by the US Precision Medicine Initiative program. Since the program was launched in 2015, the term "Precision Medicine" have become the preferred term in health community. Nevertheless, both personalised medicine and precision medicine, and their various historical predecessors share a mutual goal, which to maximise the treatment outcomes to best suit the patients based on the relevant pivot information such as genomic information, clinical presentation, omics data and patients' lifestyle.

A classic example of personalised medicine practice was the use of trastuzumab in patients who have the gene expression of the human epidermal growth factor receptor type 2 (HER2) positive. This example demonstrated the process of medical decision-making using apparent patient information as a critical consideration. Transtuzumab is a specially designed medicine to treat breast cancer patients who

have an overexpression of the HER2 gene. Patients with HER2 positive tended to receive more clinical benefit than patients who tested negative when treating with trastuzumab [4, 5]. Although there are still debates among researchers as to whether transtuzumab provides a clinical benefit in the treatment of tumours with both HER2 positive and negative expression [6], it cannot deny the fact that HER2 gene was used as a biomarker to guide/inform medical decision-making. For precision medicine, a classic example was depicted in a case of cystic fibrosis. The disease itself is described as a genetic disorder of cystic fibrosis transmembrane conductance regulator (CFTR) causing multiple organs damage. CTFR gene usually transcribes the protein for chloride ion channel; thus, the genetic aberrations of CTFR gene results in disruptive regulation of water and chloride ions [7]. Cystic fibrosis patients who have F508del (~ 88 % world-wide [8]) would gain the most benefit from combination therapy of ivacaftor and lumacaftor, showing an important of utilising the genomic data to guide the medical decision-making [9]. Thus, these are the results of the advancement in personalised/precision medicine which well-portrayed the significance of these disciplines. At present, the concept of precision medicine has been vigorously implemented in the field of oncology. Oncology is at the forefront of precision medicine, advancing beyond the typical treatment strategy based on a large, unstratified patients cohort. Precision medicine encourages a revolution of oncology practices to recognise more in utilising the individual's molecular profile to optimise the treatment strategy.

The prior examples illustrated the use of genomic information as a part to guide the optimal treatment plan. Both HER2 positive and F508del are categorised as biomarkers, one of the quintessential elements in modern precision medicine practice, especially cancers and other rare diseases. The traditional approach to identify the potential biomarkers may involve evaluating the pre-treatment characteristics, biochemical analysis and genetic testing. However, the methods to retrieve the data may take a more extended time to derive the necessary information to guide the precision dosing, which is practically not feasible to apply in a clinical setting. Analysing clinical trial data– a big data is a useful approach and very convincing as it deals with the data from the real patients. Nevertheless, the timeframe toward accessing the data can be unpredictable as some database require extensive and multiple regulatory approvals to access the database, which is impossible for an ongoing treatment scenario.

Precision dosing, a subcategory of precision medicine, exemplifies the trend of evidence-based pharmacotherapy [10, 11]. It considers any relevant aspect both in drug characteristics and patient characteristics (both disease state and physiological factors) to provide the most appropriate dosing strategy for the individual– individual dosing [12]. It is quintessential to acknowledge that drugs are, in numerous cases, the focal medium in overcoming the disease, either primary (directly treat the condition) or secondary (adjunctive treatment after medical interventions) contribution. The well-defined strategy in drug dosing would, eventually, increase patients' quality of life and reduce the long-term health-related cost to a nation. As thoroughly reviewed by Hopkins AH et al., precision dosing has its imminent role in optimising the dosing regimen, guiding/selecting the initial dose, and dose adaption

[13]. However, it could be a simple method to achieve the goal using only a laboratory-based approach or an intricate method using both laboratory- and computational-based approach in parallel to thrive for the precision dosing. Admittedly, identifying novel biomarkers could be a long-standing option as it could derive meaningful information supplies into any areas as mentioned earlier [14, 15].

Thus, there is a necessity to pursue the novel biomarkers, which has to be a non-invasive, high versatility that can be integrated into various research setting and contain meaningful information in order to promote a precision dosing. Recently, the blood-derived biomarker— extracellular vesicles (EV) have gained more attention as it contains genomic information and other proteins in its cargo. EV can be isolated from almost any biofluids such as plasma, serum, breast milk and urine. Thus, EV is a potential candidate for the precision dosing due to its versatility that can be incorporated into a part of liquid biopsy, which considered as a less invasive and relatively safe method. The array of methods and their importance in precision medicine such as using a computational simulation, data analysis and a scientific experiment is described in this chapter. The in-depth detail of factors affecting variability in drug exposure and pharmacokinetic profile is also provided. Finally, the literature review of EVs was introduced with a description of the previous reports of its promising role as a novel biomarker in precision medicine.

1.2 – Pharmacokinetics

Pharmacokinetics describes the passage of a drug through the body. For an orally administered drug this incorporates the processes of Absorption, Distribution, Metabolism and Excretion, and is often referred to as ADME. Human tend to come across various therapeutic compounds, chemicals and xenobiotics throughout the entire lifespan either or not as an intention. Sometimes, the xenobiotics can be a poisonous substance that causes detrimental to the body; thus, throughout the evolution, the human body has developed an effective mechanism for the disposition of drugs and xenobiotics in the body.

1.3 – Drug metabolism

Drug metabolism is an integral element of pharmacokinetics. The simplified way to describe the whole process of drug metabolism is the sequential order of transforming the compounds to the altered form that more apparent to be eliminated from the body. The enzymes that involved in the process of biotransformation are classified as drug-metabolising enzymes (DME). The metabolic capability of DME spans over xenobiotics substance as well. For a correction of literary, a recent textbook suggested the name "xenobiotic-metabolising enzymes" as the more appropriate definition [16].

In order to be absorbed into the body, most drugs and other xenobiotics have a characteristic of high lipophilicity. They require a process of functionalisation where the reactive groups are attached to the compound, deriving more hydrophilic derivatives that efficiently enough to be eliminated. However, some drugs are reported to eliminate without any structure modification, an unchanged form.

Nevertheless, the majority of drugs are, relatively, needed to slightly undergo structure modification to facilitate the disposition.

The liver is major site of metabolism in the body, both for endogenous and exogenous substances. In addition to the liver, the small intestine and kidney's also serve as important sites of metabolism. In particular metabolism in the small intestine serves as a barrier to oral drug exposure, while conjugation in the kidneys dramatically enhances the water solubility of lipophilic compounds and enhances transporter utilisation. In addition to these organs, DME are also found at the other sites of the body. Several pieces of evidence reported the present of DME in diverse organs/tissues such as lung [17], brain [18] and, to a lesser extent, skin [19]. Hence, these organs/tissues are, to a limited degree, contribute to the biotransformation of drugs and other xenobiotics, which should be categorised as part of the drug metabolism process.

Drug metabolism has traditionally been divided into two main reactions, phase I and phase II reactions, which were considered to occur in consecutive order [20]. However, the term phase I and phase II reactions may be outmoded. David et al. described the term to be misleading and inaccurate due to inconsistent in grouping and categorisation [21]. For example, the general idea regarding phase II metabolism is increasing the hydrophilicity of the compound for excretion purpose. In fact, some phase II mechanism leads to a reduction in hydrophilicity such as N-acetylation of aromatic amines. Thus, the alternative approach to group the drugs and xenobiotics metabolism into groups might be functionalisation (oxidation and reduction), conjugation and nucleophilic trapping reactions.

The predominant enzymes responsible for functionalisation reactions are the Cytochrome P450 (CYP) superfamily. However, there are also groups of non-CYP oxidative enzymes involved in xenobiotics oxidations such as flavin-containing mono-oxygenases (FMOs), monoamine oxidase (MAO).

1.4 – Cytochrome P450

The CYP enzymes are the heme-containing proteins superfamily found in variety of living organisms such as in bacteria and human. This enzyme superfamily is mainly responsible for metabolising endogenous and exogenous substances. The CYP enzymes are membrane-bound enzyme which found inside the lipid bilayer of endoplasmic reticulum (ER) in hepatocyte (**Figure 1**). Apart from CYPs, the UDP-glucuronosyltransferase (UGT) enzyme superfamily and the other DMEs are also found in this lipid bilayer of ER within hepatocyte.

As reviewed by Furge et al, the characterisation of CYP was performed using carbon monoxide binding spectra and found a strong absorption at 450 nm, which resulted in the 'P450' nomenclature to this type of enzymes [22, 23]. Also, because of the presence of cysteine residue which attach to the heme group, this difference makes the identity of CYP distinct to the other heme-containing protein such as haemoglobin which has histidine residue attaches to the heme instead. The CYP enzymes require a

supplement of electrons and other cofactors in order to fully activate the catalytic reactions. One of the important cofactors for CYP metabolism is nicotinamide adenine dinucleotide phosphate (NADPH), which is the source of O_2 and H^+ that will supply to CYP reaction cycle. Moreover, the reaction requires CYP-NADPH oxidoreductase enzyme which bound adjacent to the CYP enzyme. The mechanism of CYP metabolism begins when the substrate enters the hepatocyte and consequently embedded into the lipid bilayer of ER where it come into contact with CYP enzyme. The overview of metabolic consequence of drugs and other xenobiotics as shown in **Figure 2**.

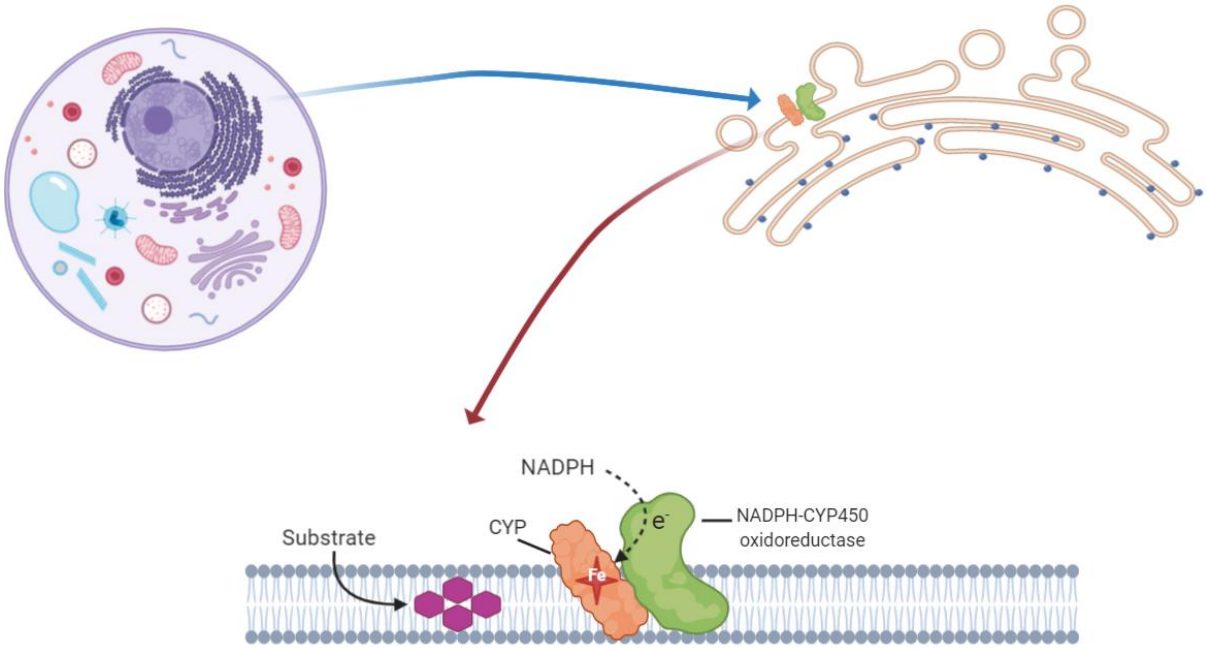

Figure 1 – Localisation of CYP450 in cells. The figure showed microscopic level of CYP450 embedded in the lipid bilayer of ER. NADPH-CYP oxidoreductase is in adjunct to CYP and play a role to supplement electron to the CYP-related metabolic reaction. Figure created with BioRender.com.

CYP enzymes are responsible for most of the functionalisation reactions of clinically used drugs [16]. Due to their extensive capability in terms of biotransformation, CYP enzymes are not limited to only one enzyme per one substrate. In fact, a single CYP isoform is able to metabolise the vast majority of substrates those share similarity in features such as the functional groups in the compound structure. Moreover, a single compound can also be metabolised by several CYP isoforms in different molecular catabolism. Thus, the overlapping of substrate specificity among CYP isoforms add a certain degree of complex into metabolism aspect. As aforementioned, the CYP enzymes have expansive role of exogenous metabolism but, on the other hand, also involves in controlling endogenous compound such as cholesterol synthesis and steroid hormone metabolism [24]. For example, the CYP19 family which is also known as aromatase is responsible for testosterone metabolism only. Thus, some of the CYPs

that majorly involve in endogenous compound tend to have a limited activity and substrate of catabolism compare to the CYPs that involve in exogenous metabolism.

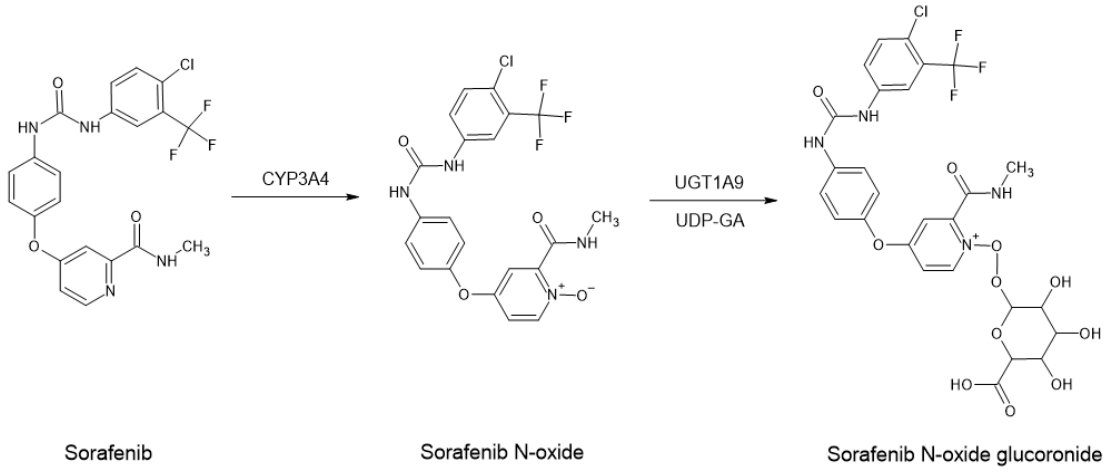

Figure 2 – Metabolism of sorafenib. CYP3A4 responsible for the oxidation of sorafenib to obtain sorafenib N-oxide. UGT1A9 together with UDP-GA as a cofactor conjugate sorafenib N-oxide with glucuronic acid to increase the hydrophilicity.

More than 50 CYP enzymes have been identified in humans, with twelve CYP identified to be involved in drug metabolism including CYP1A1, 1A2, 1B1, 2A6, 2B6, 2C8, 2C9, 2C19, 2D6, 2E1, 3A4, and 3A5. These enzymes are highly abundant in the liver. In this review, only a few CYPs family and isoforms are selected according to its significant in metabolising clinically use drugs. The selected CYP in this review are including CYP1A subfamily (CYP1A1, CYP1A2), CYP2 family (CYP2C9, CYP2C19, CYP2D6) and CYP3 family (CYP3A4). The overview of CYP and its level of expression in human liver as shown in **Figure 3** [25].

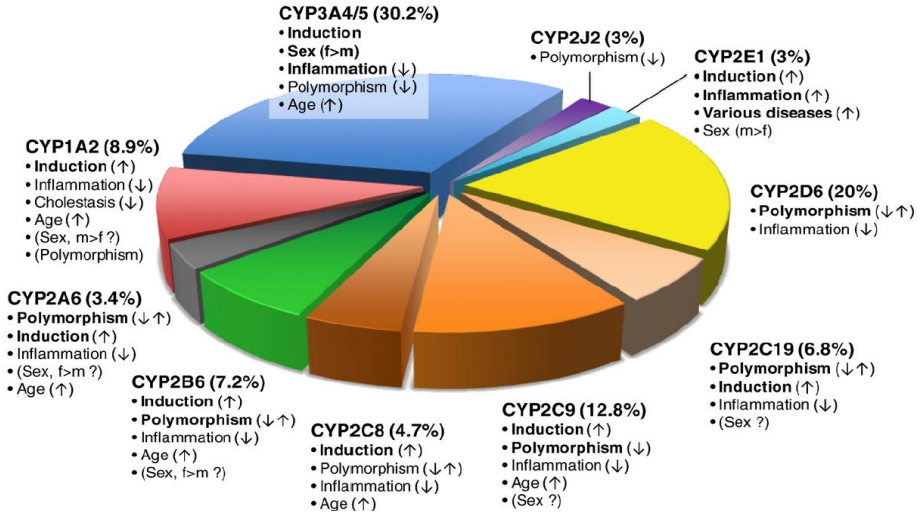

Figure 3 – The illustration shows the proportion of CYP expression in human liver. [Taken from Zanger et al. (2013)].

Table 1. Example of major CYP isozymes and its substrates, inducers and inhibitors.

CYP	Substrate	Inducers	Inhibitors
1A2	Clozapine Caffeine Propranolol Theophylline Aminophylline Mirtazapine	Carbamazepine Phenobarbital Tobacco	Amiodarone Cimetidine Ciprofloxacin
2C9	Irbesartan Losartan Ibuprofen Celecoxib Phenytoin Diclofenac Naproxen Meloxicam Glipizide Glibenclamide Tolbutamide Warfarin	Carbamazepine Griseofulvin Phenytoin Rifabutin Rifampin St. John's wort	Amiodarone Clopidogrel Efavirenz Fluconazole Valproic acid Sulfamethoxazole Fluorouracil Disulfiram Isoniazid
2C19	Clopidogrel Clozapine Diazepam Omeprazole Esomeprazole Lansoprazole Pantoprazole Rabeprazole Phenytoin Phenobarbital Fluoxetine Thalidomide Propranolol	Artemisinin Barbiturates Carbamazepine Phenytoin Rifampin St. John's wort	Cimetidine Efavirenz Fluconazole Isoniazid Modafinil Omeprazole Oxcarbazepine Voriconazole
2D6	Amitriptyline Carvedilol Chlorpheniramine Chlorpromazine Codeine Dextromethorphan	Pregnancy-related hormone	Amiodarone Bupropion Diphenhydramine Haloperidol Thioridazine Quinidine

	Diphenhydramine Haloperidol Imipramine Metoclopramide Metoprolol Risperidone Thioridazine Tramadol Venlafaxine		Fluoxetine Imatinib
3A4	Atorvastatin Simvastatin Pioglitazone Clarithromycin Clonazepam Erythromycin Itraconazole Ketoconazole Alprazolam Triazolam Midazolam Bromocriptine Bupropion Ziprasidone Donepezil Amlodipine Felodipine Nifedipine Verapamil	Rifampicin Carbamazepine Phenobarbital Oxcarbazepine Phenytoin Griseofulvin St. John's wort Modafinil	Midazolam Grapefruit juice Ketoconazole Itraconazole Fluconazole Indinavir Ritonavir Isoniazid Atazanavir Amiodarone

1.5 – CYP family

1.5.1 – CYP1A subfamily

CYP1A1 and CYP1A2 are the important enzymes in this subfamily. CYP1A1 expresses at a deficient level in liver but the high level in lung, intestine, lymphocytes and placenta instead (thus, categorised as the extrahepatic site). In contrast, CYP1A2, which shares 80 % similarity of amino acid identity to CYP1A1, expresses mainly in the liver. CYP1A1 also be called as aryl hydrocarbon hydroxylase which responsible for inactivation of procarcinogen. Both CYP1A1 and CYP1A2 are highly induced by polycyclic aromatic hydrocarbons (PAHs) generated from most cigarette smoke. CYP1A1 is

responsible for metabolising various of the commonly clinical used drugs including propranolol, amiodarone, flunarizine and R-warfarin.

On the other hand, CYP1A2 is reported to metabolise numerous important clinically use drugs such as psychotropic agents (tacrine, clozapine, olanzapine), local anaesthetics (lidocaine and ropivacaine), acetaminophen and propranolol. The summary of drugs that are metabolised by CYP1A2, as shown in **Table 1**. The common inducers of CYP1A2 include cigarette smoking and omeprazole [26, 27]. Cigarette smoking also the most problematic cause that alters the basal activity of CYP1A2 due to the induction property toward the CYP1A2 enzyme. One study in a group of patient who had been prescribed clozapine and used around more than three months without withdrawing cigarette smoking reported a necessity of dosage titration of clozapine [28]. In addition, the clearance rate of non-smokers was found to be significantly lower compared to the active smokers. As a result, the average maintenance dose in smokers was 382 mg/day, which is significantly higher than non-smoker (197 mg/day) at $P < 0.01$.

Caffeine is the other substrate that perturbative the activity of CYP1A2. As such, smokers who also drink caffeine tend to develop caffeine tolerance faster than non-smoker [29]. The study showed that higher coffee-drinking behaviour was associated with the number of a smoking habit. In contrast, the consumption of tea and heavy smoking showed no change in the manner of consuming. The fact that tea contains less caffeine compared to coffee, thus less likely to be influenced by the cigarette-induced CYP1A2 activity.

1.5.2 – CYP2 family

CYP2C9 is predominantly expresses in the liver and accounts for 20 % of total hepatic CYP450 proteins based on the protein content in human liver microsomes [30]. In addition, CYP2C9 is responsible for approximately 15 % of metabolising clinically used drugs which is the third most contributing drug-metabolising enzyme behind CYP3A4 and CYP2D6 [31]. Clinical drugs which are metabolised by CYP2C9 are including antidiabetic drugs (e.g. glipizide, glibenclamide), anticonvulsant drugs (e.g. phenytoin, phenobarbital), anticoagulants (warfarin), antihypertensive agents (e.g. irbesartan, losartan), diuretics and nonsteroidal anti-inflammatory drugs (NSAIDs) (e.g. celecoxib, naproxen, meloxicam)

CYP2C19 is another important isoform in CYP2C subfamily. *CYP2C19* was found to be highly genetic polymorphism such as *CYP2C19*1*, *CYP2C19*2*, *CYP2C19*3*, *CYP2C19*4*, *CYP2C19*5* and *CYP2C19*17*. The genetic polymorphism of *CYP2C19* showed a diversity effect on the rate of drug metabolism in the different individual. The *CYP2C19*2*, found 2-5 % in Caucasians and 18-23 % in Japanese, was known for a characteristic of poor metaboliser (PM) to its substrate. The patient who has *CYP2C19*2* tend to experience less effective of clopidogrel treatment due to the undermining in the prodrug activation process resulting in a state of clopidogrel resistant [32]. *CYP2C19*2* allelic variant

was reported to cause aberrant splicing, which results in the loss of enzyme activity. This led to a reduction in the efficacy of clopidogrel compared to the patients who have the wild type of *CYP2C19* (*CYP2C19*1*). In contrast, patients who have the variant *CYP2C19*17* was found to associate with a massive increase in enzyme activity compared to the wild type [33]. The CYP2C19 enzyme was found responsible for metabolising proton pump inhibitors (omeprazole, lansoprazole, pantoprazole, rabeprazole), anticonvulsant (phenobarbital, phenytoin, mephenytoin), antidepressants (citalopram, escitalopram, desipramine, clomipramine) and antiplatelet agent (clopidogrel, *R*-warfarin).

CYP2D6 is the other isoforms that have been extensively studied since 1977 [34]. The enzyme CYP2D6 is responsible for metabolising around 25 % of prescribing medicine generally antipsychotics (e.g. risperidone, haloperidol, chlorpromazine) and antidepressants drugs (e.g. nortriptyline, amitriptyline). The genetic polymorphism of *CYP2D6* was found among different ethnicities as approximately 6-10% of the Caucasian population found to express a PM, whereas only 1% was found among the Chinese, Koreans and Japanese. On the other hand, the ultra-rapid metaboliser (UM) was predominantly found in the Ethiopians, whereas this characteristic found only 1-2 % in the Caucasians.

The clinical relevance regarding the variability of *CYP2D6* variant is related to the metabolism of drugs used in the central nervous system, especially antipsychotic agents. The discrepancy in the rate of metabolism due to genetic polymorphism can lead to a serious neurological adverse event (AE) such as parkinsonism. Moreover, antipsychotic agents tend to be used for an extended period of therapeutic course partly due to the complexity of the disease itself. As such, it provokes numerous concerns regarding the potential serious AE, which consequently lead to alleviation in clinical outcomes of antipsychotics treatment, which are the primary challenge in the treatment of the psychiatric disorder.

1.5.3 – CYP3A subfamily

The CYP3A subfamily is the only member in the CYP3 family found in human. Generally, the primary CYP3A isoenzyme is CYP3A4 and CYP3A5 where CYP3A7 is one of the isoforms that only expressed during foetal development and can be found minimally in the liver and intestine in an adult human. [35]. CYP3A4 and CYP3A5 are the most well-characterised isoforms in this subfamily in which the CYP3A4 has a more prominent role in drug-metabolism. CYP3A4 exhibits the most extensive metabolising property and profoundly expressed in the liver. The CYP3A4 enzyme metabolises over 30 % of clinically used drugs, which cover a wide range of drug class such as lipid-lowering agents (e.g. simvastatin, atorvastatin), macrolide antibiotics (e.g. erythromycin, clarithromycin), antituberculosis (e.g. rifampicin, rifabutin, isoniazid), psychotropic drugs (carbamazepine, alprazolam, midazolam). CYP3A4 enzyme is also known as highly inducible and modulation by numerous compounds which can consequently lead to a high probability of drug-drug interaction issues. CYP3A4 enzyme is also known as highly inducible and modulation by numerous compounds which can consequently lead to a high probability of drug-drug interaction issues. The induction of CYP3A4

enzyme was reported to initiate at the molecular level involving the activation of nuclear receptors (NRs). The Pregnane X receptor (PXR), the constitutive androstane receptor (CAR) and glucocorticoid receptor (GR) were the NRs found to involve in the process CYP3A4 enzyme induction.

1.6 – Induction of drug metabolising enzyme: case of CYP3A4

The mechanism of enzyme induction initiates at the level of gene transcription. The primary induction mechanism arises from the ligand-receptor complex in which most of the receptors, in this case, are NRs. NR is a large group of receptors, which can be categorised into four main types (type I, II, III, IV) [36] and has a distinct mechanism of ligand-receptor interaction compare to the others. For example, type I nuclear receptors reside in the cytoplasm, which forms a partial attachment to the chaperone proteins such as heat shock protein (HSP). The ligands of type I nuclear receptors, such as estrogen, bind to the receptor once entering the cytoplasm and consequently dislodge the receptor from the chaperone. The ligand-receptor complex then undergoes homodimerisation then enter the nucleus (**Figure 4**) [37]. The ligand-receptor complex interacts with other coactivators then subsequently allow the target gene activation process. Induction of CYP3A4 initiates via one of the NR superfamilies, the PXR. Generally, PXR is responsible for drug metabolism, cholesterol metabolism, bile acid transport and inflammation. PXR expresses as an orphan NR type which requires partially binding of a ligand to the receptor before translocating the complex into the nucleus.

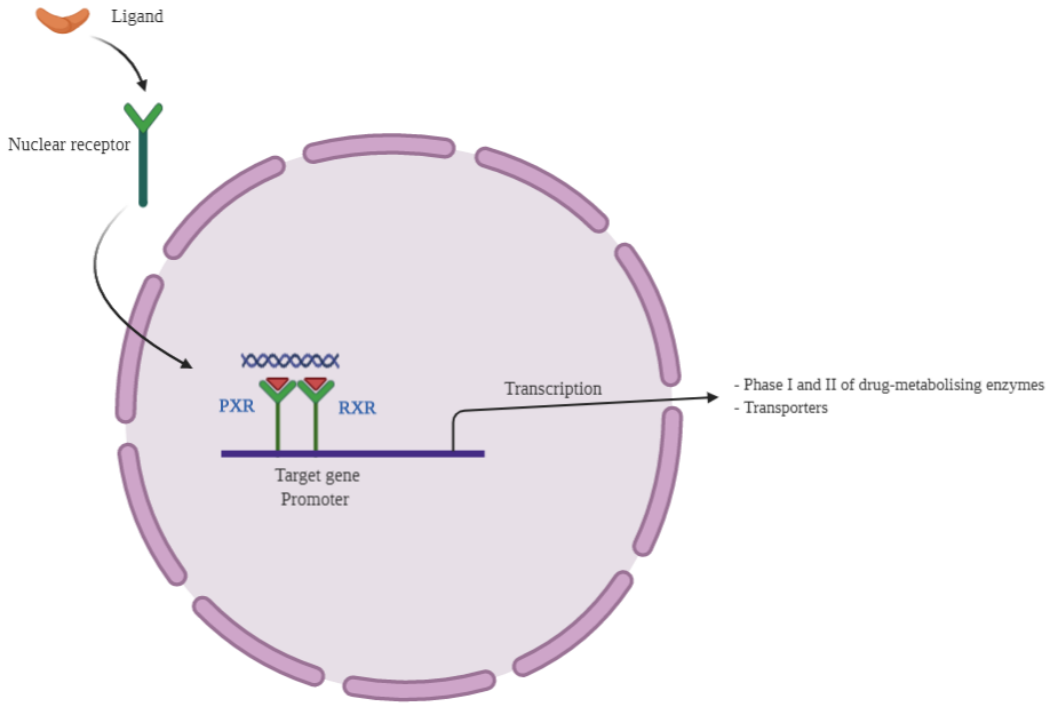

Figure 4 – A schematic of drug-metabolising enzyme induction via nuclear receptors. Figure created with BioRender.com.

Successful binding of the ligand-receptor complex then translocated to the nucleus of the cells where a subsequent binding to retinoid X receptors (RXR) at the promoter of the target genes occur. Activation of PXR increases the transcriptional rate of CYP3A4 enzyme as it is one of the target genes of PXR responsive elements [38]. Therefore, the activation of PXR results in an elevation of CYP3A4 expression, which in turn lead to an increase in CYP3A4 enzyme activity—the induction state.

1.7 – Drug-drug interaction

Drug-drug interactions (DDI) may occur when two or more drugs are administered concurrently, the result of which is in an alteration in drug effects. Drug interaction may broadly divide into two main categories according to the mechanistic of interactions, either pharmacokinetic or pharmacodynamic interactions (**Figure 5)**. Pharmacokinetic interactions are subdivided into four subcategories aligned to the process of pharmacokinetics. Pharmacokinetic interactions mostly occur during the process of drug metabolisms, in the form of enzyme induction/inhibition, such as in the case of phenobarbital and warfarin. Phenobarbital is a CYP2C9 inducer in which if it is administered at the overlapping with the other CYP2C9 substrate such as warfarin, the duration of warfarin action may decrease leading to treatment failure [39].

PPIs are the other group of drugs that have been a significant concern in producing pharmacokinetically interactions. One of the primary concerns is in the area of the effects of cancer medicines. Recent reports found several significant effects of using PPI with cancer medicines, particularly tyrosine kinase inhibitors (TKIs) due to intragastric pH changes. This has been observed in the case of using PPI with erlotinib, one of the TKI drugs. Generally, the orally administered drugs, especially solid dosage form, are governed by many factors, such as surface area of absorption and dissolution profile [16]. Erlotinib is an orally administered TKI indicated for patients who suffer from non-small cell lung cancer (NSCLC). Previous literature found that NSCLC patients who received erlotinib concomitantly with PPI showed a lower plasma erlotinib concentration significantly than those without PPI administration. The investigator speculated that the reduction of erlotinib plasma concentration was due to the physicochemical property of erlotinib. As erlotinib has a characteristic of a weak acid, the solubility is predominantly affected by the increase of intragastric pH (less acidic) as a result of the co-administered PPI [40].

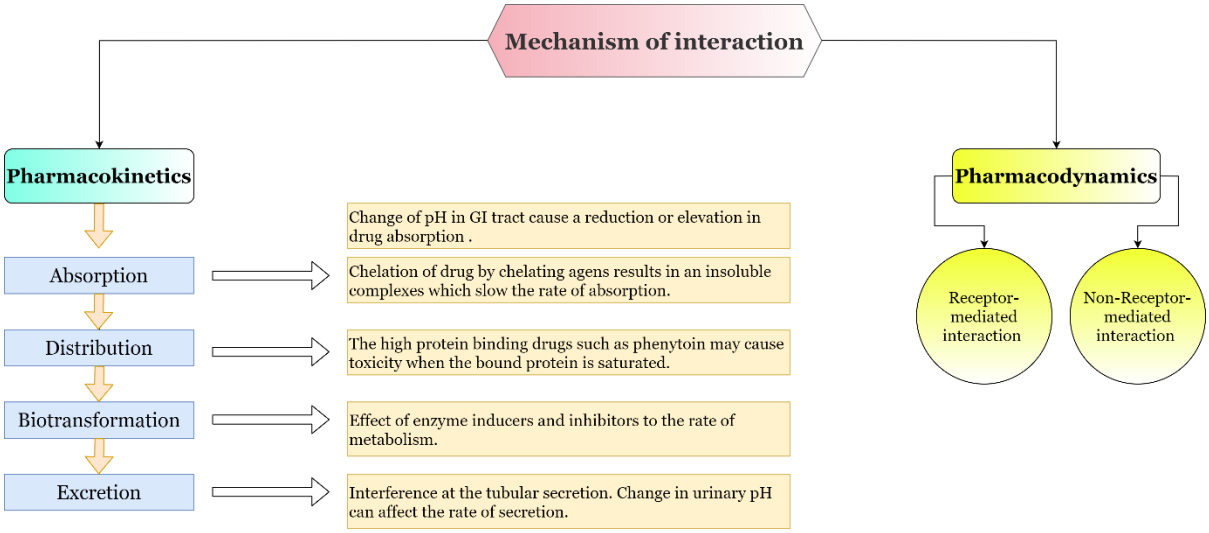

Figure 5 – Diagram shows the mechanism of drug interactions and examples.

Pharmacodynamic interactions are situations when co-administered drugs influence each other's effect directly. For example, diazepam, an allosteric modulator of $GABA_A$ receptor, enhance the psychodepressant effects of alcohol when both of them are concurrently consumed. Mechanistically, diazepam binds to the benzodiazepine receptor on the $GABA_A$ receptor, which facilitates the binding of GABA to its receptor resulting in an increase of Cl^- ion influx causing the membrane to be more hyperpolarisation. Alcohol also binds to the $GABA_A$ receptor but in a different site from diazepam but able to cause an increase in Cl^- ion influx and hyperpolarisation (**Figure 6**) [41]. Thus, these two agents are able to cause an exorbitant influx of Cl^- ion when administered at a similar period as a result of the synergistic effect.

This image has been removed due to copyright restriction. Available online from [https://pharmrev.aspetjournals.org/content/62/1/97.long/ Uusi-Oukari M, Korpi ER. Regulation of GABA(A) receptor subunit expression by pharmacological agents. Pharmacol Rev. 2010 Mar;62(1):97-135. doi: 10.1124/pr.109.002063. Epub 2010 Feb 1. PMID: 20123953.]

Figure 6 – A schematic shows different biding site of $GABA_A$ receptors between benzodiazepines and ethanol. [Taken from Uusi-Oukari, M. and E.R. Korpi (2010)].

The consequences follow drug interactions possibly appear in a variety of effect. The additive effect is the combined response of drug, which equal to the summation from each agent acting alone (1 + 1 = 2). Synergistic is similar to additive, but the total response is greater than the summation from each agent ($1+1 \geq 2$). Also, the synergistic effect tends to originate from two different mechanisms of action, which are stimulated at the same time. The concurrent effects of each drug enhance the overall outcomes in

which exceeding the additive summation [16]. On the other hand, antagonism interaction constitutes the interference of drug action where one of the concurrently administered drugs compromise the effect of another drug.

Drug interaction does not necessarily result in an undesired outcome. Instead, utilising the proper interaction may result in the better treatment outcomes. For example, ritonavir indirectly enhances the effect of protease inhibitor by prolonging the duration of action due to its capability as a CYP3A4 inhibitor. Hence, the biotransformation of indinavir is delayed deriving an extended duration of action. Therefore, ritonavir/indinavir combination increased plasma indinavir concentrations significantly as observed in AUC (185 – 450 %) and C_{max} (21 – 110 %) compared to indinavir alone [42]. Similar situation was observed in the case of clopidogrel and a medicinal plant St. John's Wort. Clopidogrel, a platelet aggregation inhibitor, is a prodrug that required a two-step bioactivation by CYP enzymes to obtain an active metabolite which binds specifically to P2RY12 purinergic receptor (**Figure 7**) [43]. By co-administering clopidogrel with St. John's Wort, the result is an enhancing of platelet inhibition effect of clopidogrel. St John's Wort contains hyperforin which constitute a potent ligand for the PXR receptor, thus upregulating the genotypic expression of *CYP2C19* and *CYP3A4*. The results of patients those received a 14-day treatment of St John's Wort before administering clopidogrel showed an increase in the inhibitory activity of platelet aggregation (IPA) when measured at 2, 4 and 6 hours after exposing to clopidogrel [44].

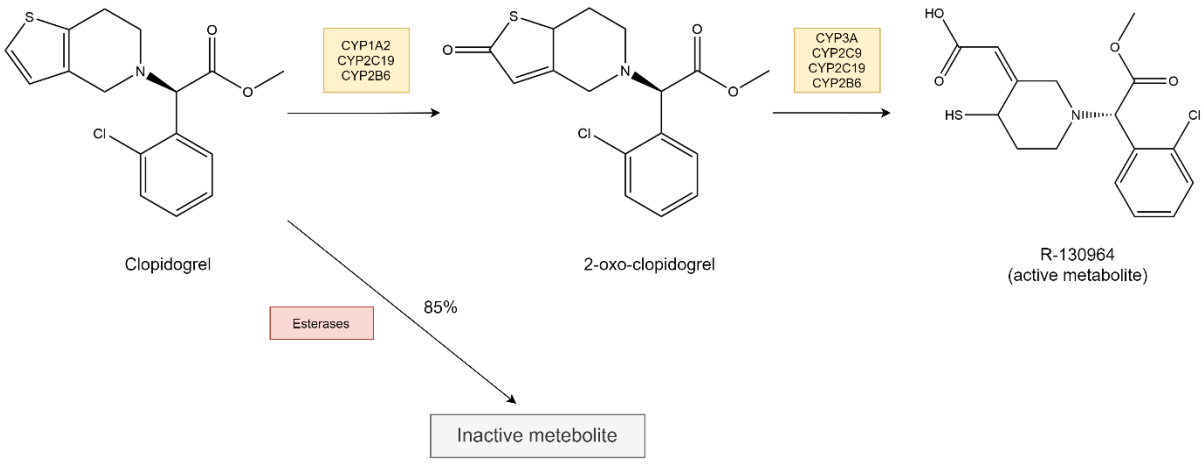

Figure 7 – Biotransformation of clopidogrel.

In summary, drug interactions have a variety of possible outcomes. Some drugs may need an exact plasma level to exhibit the full therapeutic effects such as anticancer drugs and antibiotics. These groups of drugs are prone to affect by concomitant medicines, which may, in the worst-case scenario, lead to treatment failure. Thus, understanding/identifying the effect of DDIs, especially with the common concomitant drugs such as analgesic agents, acid lowering agent or other metabolic syndrome drugs

would be beneficial in clinical practices. Patients who strongly rely on the treatment efficacy such as cancer patients would also gain a profit from this knowledge.

1.8 – Pharmacokinetic variability

The variability in the pharmacokinetics of drug exposure is the phenomenon that is observed when the pharmacokinetic profiles varies between individuals receiving the same dose of the same drug. The source of variability may be the phenotype and/or genotype of each individual or may result from environmental sources. Difference in patient demographic such as age, sex, race and comorbidity (diabetes, hepatic/renal impairment) may contribute to the variation in drug exposure. Genetic polymorphism results in PM/UM characteristics is the typical epitome of genotype-related exposure variability. Warfarin, an antiplatelet agent, is an example of drug that has already identified to be affected by both phenotype and genotype factors. Warfarin is mainly metabolised by CYP2C9 whereas evidences found that patients who have the variants *CYP2C9*2* and *CYP2C9*3* required only 45 % of standard dose to achieve the treatment efficacy as these variants were identified as PM [45]. PM characteristic of warfarin leads to the risk of bleeding when using in the standard dose as the rate of metabolism is lower, thus requiring a dose reduction to prevent the AE. The other model example is in the case of *CYP2C19* variants and PPI. Previous literature reported that *CYP2C19* polymorphism, both UM and PM, was associated with the pharmacokinetic variability of PPI. While the *CYP2C19*2* and **3* were reported to produce no function and decreased enzyme function (predicted phenotype as PM), the *CYP2C19*17* was reported to produce an increase in enzyme function (predicted phenotype as UM) [46]. First-generation PPIs, including omeprazole, lansoprazole and pantoprazole, were affected by this genetic polymorphism due to 80% of them being metabolised by CYPC19. Therefore, an individual with a characteristic of CYP2C19 UM, which exhibit an extensive rate of metabolism, would require a dose-escalation of drugs to treat a particular condition such as *H.pylori* infection.

Drug-interactions also play an important role in the heterogeneity of drug response. Patients with chronic diseases such as hypertension, diabetes mellitus and cancers are by default use more than one agent to control the disease at an extended of time. In the case of cancer patients, evidence reported that patients tend to have a notable record of concomitantly using proton-pump inhibitors (PPIs) and metabolic syndrome-related drugs with cancer medicines [47, 48]. PPIs are among the most concerning drug groups that could cause pharmacokinetically interactions on account of their intrinsic capability. PPI acts by inhibiting H^+-K^+ ATPase– proton pump in an irreversible manner, leading to an alteration in GI acidity (pH). As such, the altered acidity environment in the GI tract could, potentially, affect the absorption of pH-sensitive co-administered drugs [49]. For instance, the previous studies observed an increase in mortality rate in cancer patients who use PPIs concomitantly with a recently developed tyrosine kinase inhibitors (TKIs) such as erlotinib, imatinib and sunitinib indicating a negative effect of PPI on some TKIs efficacy [50]. Hence, this emphasizes the importance of identifying the source of

pharmacokinetic variability, which would ultimately lead to a better treatment strategy toward the precision dosing practice.

The strategy to address the pharmacokinetic variability can be performed in many fashions. The computational pharmacologists may attempt to thrive this issue by using model-informed precision dosing either top-down (opulation pharmacokinetics; PopPK) or bottom-up (Physiologically based pharmacokinetic; PBPK) approach. On the other hand, the experimental pharmacologists may embark on the *in vitro* model using different cellular models to thoroughly characterise the pharmacokinetic profile of the investigated drug.

1.9 – In vitro determination of pharmacokinetics

The study of the pharmacokinetic profile of drugs can be easily initiated using *in vitro* platform. The i*n vitro* platforms provide high flexibility in profiling multiple aspects of primary pharmacokinetics, such as determining the fate of the test compound, defining the proportion of plasma protein binding and identifying the permeability capacity [51]. Of all the aspects, determine the fate of the compound is one of the most crucial components in the *in vitro* pharmacokinetics study [52]. Generally, the rich source of protein that contains an appropriate level of DME is used to determine the enzyme responsible for metabolising the test compound. Human liver microsome (HLM) is among the most common protein source in the *in vitro* drug disposition study [51, 53]. However, the inconsistency of DME expression between batch and availability has been the primary concern in using HLM as the protein source [54, 55]. Freshly isolated primary human hepatocyte (PHH) are the other preferred proteins source for studying preclinical drug metabolism. The primary role of PHH in the preclinical drug metabolism study is verifying the characteristic of enzyme induction/inhibition of the test compound. Nonetheless, PHH tends to lose the liver-specific gene expression over time compared to the initial stages of cultivation. Moreover, verifying the reliable source of obtaining PHH is the other significantly challenging issue to be considered. The recent development hepatocyte cell line, HepaRG, has become an adequate substitution for HLM and PHH due to its comparable expression profile and high consistency of expression between the batch. Thus, HepaRG has been considered to be a suitable test system to serve multi-purposes *in vitro* drug metabolism study. Such example as seen in the European Commission guideline for the *in vitro* method of assessing the CYP enzyme induction of the studied compounds using HepaRG [56].

1.10 – HepaRG: a novel cell lines for studying drug-metabolising enzyme.

HepaRG is a human hepatoma cell lines derived from patient who suffered from hepatocarcinoma and hepatitis C virus [57, 58]. HepaRG has a unique characteristic as a bipotent progenitor which able to differentiate into two types of the cell population, including hepatocyte-like and biliary-like morphology. Unlike the other *in vitro* hepatic cell lines such as HepG2, HepaRG express a high level

in a wide range of xenobiotic-metabolising enzymes, especially DMEs. Moreover, HepaRG also expresses various transporter genes and transcription factors (PXR, CAR, AhR, PPARα). Generally, primary human hepatocyte (PHH) is the long-time mainstay in the *in vitro* hepatocyte model because of its wide range of expression in DMEs. However, a lack of consistency of gene expression level between batch is one of the major drawbacks of PHH. In contrast, HepaRG showed a stable expression of DME genes between batch, which provide higher reliability across multiple experiments.

1.10.1 – Culturing and basic features of HepaRG

The initial morphology of undifferentiated HepaRG after seeding is epithelial-like morphology. When fully differentiated, HepaRG expresses two distinct morphology including hepatocyte-like and biliary-like morphology. HepaRG can be obtained in two forms either fully differentiated or undifferentiated state. Generally, the fully differentiated usually can be purchased from the various certified biomedical vendors, although they are mostly available in one-time used. On the other hand, the undifferentiated HepaRG can be obtained mainly from a special agreement to the Rennes institute. Although the process to obtain the undifferentiated HepaRG may slightly complicated, it comes with multiple advantages. Undifferentiated HepaRG has an unlimited production size as long as the passage number is not exceeded passage 20. Cell bank can be made during culture production, which increases the availability of several experiments.

The undifferentiated HepaRG maintains epithelial phenotype during the first few days of culturing **(Figure 8A)**. The base media of HepaRG is mainly William's E media with additional of essential supplements [57, 59]. HepaRG undergoes proliferation state around day 3 to day 7 after start seeding then reach confluency around day 10. After day 10, cells morphology starts to differentiate into hepatocyte- and biliary-like cells **(Figure 8B)**. At day 14, the base media with additional 2 % dimethyl sulfoxide (DMSO) is introduced to facilitate the differentiation program. Cells reach maximum differentiation after 14 days of exposure to DMSO-containing media. The fully differentiated HepaRG expressed a feature of mature hepatocytes with high expression in drug-metabolising enzymes genes, liver-specific markers and other transcription factors [57, 59, 60].

1.10.2 – Seeding, confluency and trans-differentiation behaviour

The hepatocyte-like cells of HepaRG are the primary source producing DME activity. The immunochemical analysis showed positive staining of CYP3A4 only in hepatocyte-like cells but not in biliary-like cells [61]. Cells damage caused by a high dose of acetaminophen (20 mM) observed the significant loss of hepatocyte-like cells, diminishing CYP2E1 and CYP3A4 activity [62]. The confluency of HepaRG during the culturing is the main factor promoting the expression of liver-specific functions of the cells. Generally, the level of confluency in HepaRG align in parallel with the progress

of culturing. Troadec et al. described the progress of HepaRG culturing into 4 stages including 1. Proliferation 2. Confluence 3. Superconfluence, and 4. Differentiation [63].

HepaRG at proliferation state showed an exponential growth rate. The cells form a monolayer and spread to the entire area of culture support, hence gradually entering the confluence state. Notably, it was reported that cells at the proliferation state observed no liver-specific or related functions. Up to the superconfluence state, genes that regulate body fluids in response to stimuli and immunity become highly-regulated. Meanwhile, genes that regulate cell motility and signal transduction become repressed at the superconfluence state [61]. At differentiated state, genes that regulate the metabolism of lipids and organic acids become more active than in progenitor state, which results in the display of liver-specific functions. HepaRG cells retain liver-specific functions for the additional 2 weeks when maintain in media supplemented with DMSO.

1.10.3 – Stable expression of liver-specific function of HepaRG

HepaRG is available to be utilised in the experiments as soon as the end of the differentiation process (30-32 days after seeding). It has been shown that the functional and expression of HepaRG are stable up to six weeks of culturing [60, 64]. Cells morphology showed a minimally change during 4 additional weeks of maintaining in DMSO-supplemented media. Moreover, the functional stability test was conducted using both RT-qPCR and enzyme activity assay. RT-PCR data showed that DME genes and transporter expression remained highly stable in any time period after differentiation [64]. Moreover, HepaRG exhibit stable enzyme activity and induction capability as well in the long-term culturing. Cells showed at least 2-fold induction of CYP3A4 and CYP1A2 enzyme activity following incubation with rifampicin or 3-Methylcholanthrene, respectively [65, 66].

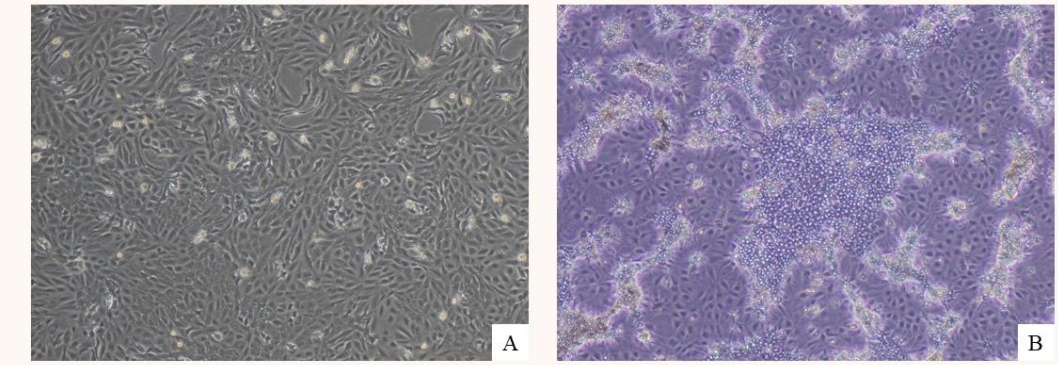

Figure 8 – Photomicrograph of HepaRG (A) undifferentiated HepaRG (B) differentiated HepaRG.

1.11 – In vitro - In vivo correlation

The extrapolation of *in vitro* data to predict *in vivo* hepatic clearance has been extensively investigated [67-70]. This area of research has observed promising outcomes when applying to predict the CYP and UGT-catalysed functionalisation. As mentioned elsewhere in this thesis, each individual CYP and UGT isoform responsible for metabolising particular compounds; however, there is a certain degree of overlapping in compound selectivity. This could lead to the consequence in which DDI occurs due to differences in the level of enzyme expression and genetic polymorphisms among each individual. Understanding the enzyme responsible for the biotransformation of a drug and relevant information regarding the factors affecting enzyme activity would allow a concrete prediction of drug elimination in real patients [67-70].

The most common approach to estimate *in vivo* CL_H is to apply an *in vitro* - *in vivo* extrapolation (IVIVE). Utilising alternative enzyme sources such as human liver microsomes (HLM), human hepatocytes cell lines, or recombinant proteins as the source of enzymes is an alternative approach to characterise the *in vitro* CL_{int} [71]. The important kinetics parameters (K_m and V_{max}) can be calculated based on product formation rate over a substrate concentration range (between 1/5 K_m to 3 K_m). The CL_{int} is then calculated using V_{max}/K_m under an assumption of initial rate condition [67, 72-74]. From here, whole liver CL_{int} can be transformed into the expression for a mathematical model of hepatic clearance, using the well-stirred model as the most commonly used approach, to estimate *in vivo* CL_H and E_H. This approach is illustrated in **Figure 9**.

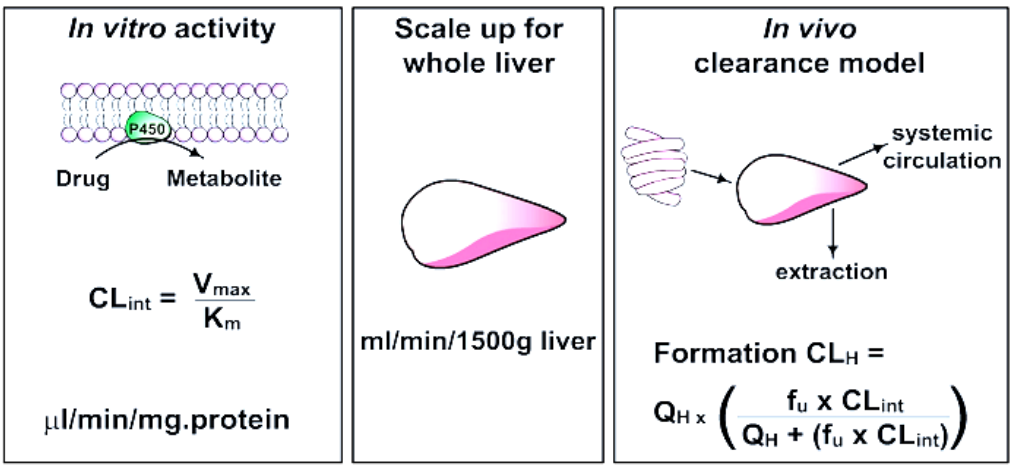

Figure 9 – Approach for calculating in vivo CL_H from kinetic constants determined for metabolite formation in vitro using the well-stirred model of hepatic clearance. [Taken from Miners (2002)].

Although a concept of IVIVE has been widely implemented, there are several concerns regarding the approach. It has been observed that using HLM as the enzyme source to conduct IVIVE during the initial drug development tend to result in under-predicted of in vivo CL_{int} and CL_H, especially in drugs eliminated by CYPs or UGTs [67, 75-77]. In addition, the variability of enzyme expression profile between a batch of HLM is another short-coming for this method. The alternative approach, such as using different enzyme source or computational modelling, have been proposed [78, 79]. Of all the available *in vitro* platforms, HepaRG tends to be the most reliable candidate due to its expression profile and robustness between batch. Further discussion regarding HepaRG as in the succeeding section.

1.11.1 – Enzyme kinetics

The key feature of enzyme kinetics is the saturability of the rate-limiting step of enzyme-catalysed reactions. Generally, most of the enzyme-catalysed reactions follow the characteristic of first-order kinetics (**Figure 10**). First-order kinetics is described as at low substrate concentration the rate of product formation is directly proportionate with the substrate concentration. Nevertheless, the rate of product formation gradually reaches the limit, and eventually zero, following the further increase in substrate concentration [80].

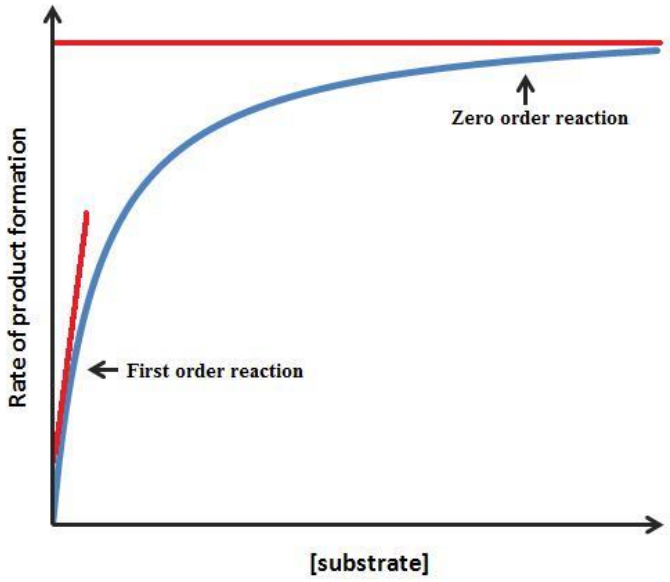

Figure 10 – Dependence of rate of product formation on substrate concentration for a typical enzyme catalysed reaction, showing substrate concentration ranges associated with first- and zero-order kinetics.

The explanation proposed by Michaelis and Menten described that there are two steps in respect to enzyme-mediated reactions [81, 82]. The first reaction revolves around the binding between substrates and enzymes. The enzyme-substrate complex is the intermediate complex obtained from the first reaction under the contingency of reversible binding between the two molecules. Subsequently, dissociation of the intermediate complex yields the end product of the reaction and the regenerated enzyme. Consequently, Briggs and Haldane proposed that although the binding between enzyme and substrate was in a reversible manner, it is not necessary to be in equilibrium [83]. Thus, the expanded enzyme-mediated reactions can be illustrated by the schematic shown in **Figure 11**:

Figure 11 – Schematic representation of an enzyme mediated reaction where k_1 is the rate of ES complex formation, - k_{-1} is the rate of ES dissociation reverse to enzyme and substrate, and k_2 is the rate of ES dissociation resulting in product (P) formation. The overall rate of reaction is restricted by the amount of available free enzyme and by the degradation of the ES complex.

Following the assumption of the first-order kinetics, enzyme concentration will be limited by the given amount of the substrate concentration. Thus, enzyme concentration reaches the saturation threshold as a result of a further increase in substrate concentration. At the saturation threshold, the enzyme concentration represents the total concentration of enzyme present, $[E_0]$. As such, the total rate of the reaction will be correlated to the substrate concentration which is equal to $k_2[E_0]$. Therefore, the presented condition determines the maximal initial velocity (V_{max}) that can occur for a given enzyme concentration (**Equation 1**):

$$\textbf{Equation 1.} \qquad V_{max} = k_2 \times [E_0]$$

1.11.2 – Michaelis-Menten kinetics

The original Michaelis and Menten with a subsequent application of the steady-state assumption, an enzyme kinetic model was developed. This expanded model is capable of quantifying the rate of an enzymatic-mediated reaction [80]. The model can be mathematically described in the **Equation 2**, which is commonly referred to as the Michaelis-Menten equation:

$$\textbf{Equation 2.} \qquad Rate\ (v) = \frac{V_{max} \times [S]}{K_m + [S]}$$

1.12 – Physiologically-based pharmacokinetic modelling (PBPK)

PBPK modelling and simulation is an extension of traditional IVIVE and part of the system pharmacology discipline. Generally, the system pharmacology aims to create a prediction platform to investigate the interaction of the interested compound to the whole-body system. PBPK considers the molecular interaction of compound to the physiological repositories, including absorption, organ distribution, metabolism pathway and excretion (**Figure 12**). Recently, PBPK has become an emerging tool in drug discovery and development. The US Food and Drug Administration (FDA) and European Medicines Agency (EMA) incorporated the PBPK into the guideline for drug approval and regulatory submission. Hence, this emphasises the significant role of PBPK in the contemporary research era.

PBPK focuses on the population variables in equal importance as the compound variables to build the predictive algorithm. As such PBPK is capable for the prediction of the pharmacokinetic profile, drug-drug interaction and drug exposure during the disease state. Moreover, PBPK can be utilised to support designing clinical trials, as it is capable of guiding the most optimum dosing regimen for the study.

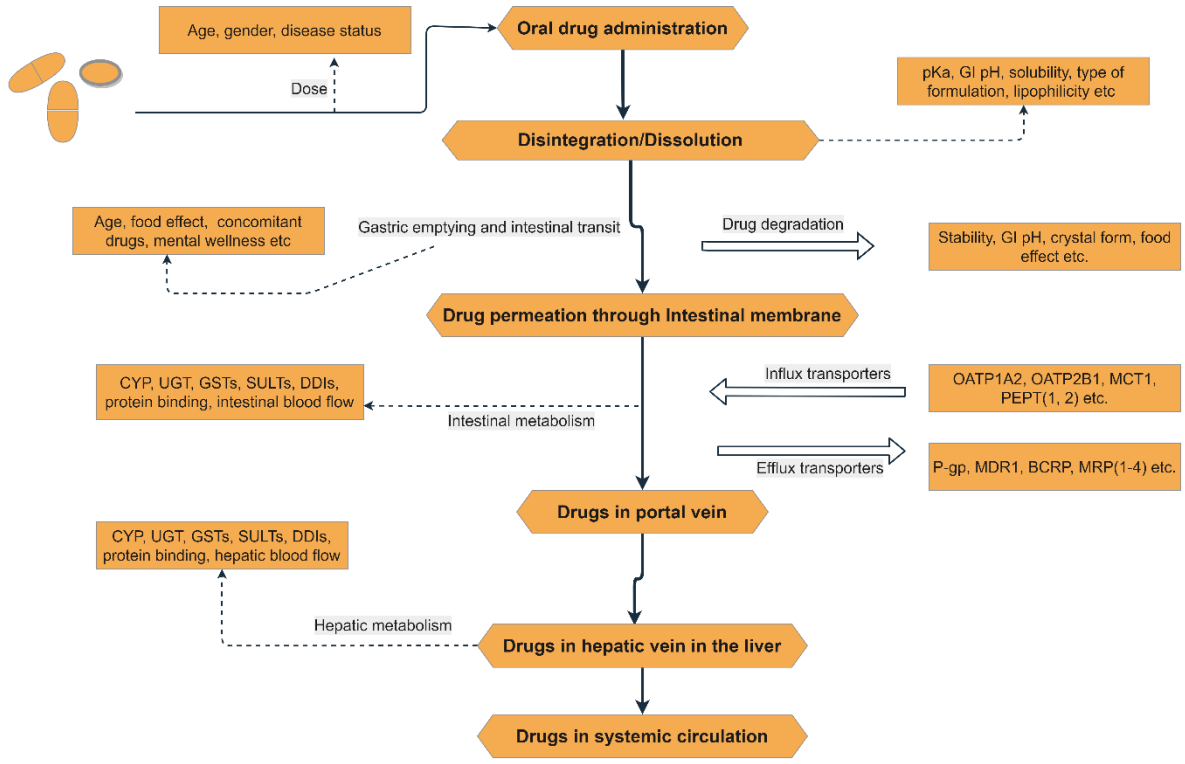

Figure 12 – A schematic diagram of the steps and factors affecting oral drug absorption.

Typically, PBPK models are constructed based on the physiological property of the target species. In human, the virtual physiological systems are built based on the established knowledge in organ functions. The primary focus of the physiological part revolves around the organs responsible for drug disposition and metabolism, such as GI tract (absorption) and the liver (metabolism). These organs are

assembled into compartments and assigned a specific parameter to represent the functional characteristics whereby interaction to the other compartment also considered, thus creating "system data". On the other hand, virtual pharmacological compounds are constructed by considering physicochemical property (solubility, pKa, molecular weight) and physiological interaction (protein binding, metabolic pathway, permeability). Data from the previous literature that relevant to the interested compound have a significant contribution to the model development. Importantly, the more data can be gathered; the better-refined compound model can be constructed. Some parameters may be absent from the prior literature or unable to define; further calculation/estimation is the only option to obtain the data. Nevertheless, the estimated data is needed to validate before applying to the actual modelling and simulation.

1.12.1 – The modelling approach of PBPK to predict oral drug absorption.

1.12.1.1 – Dispersion model

Dispersion model rationalises the concept of the intestine as a single uniform tube with constant dispersion profile, stable axial dispersion and continuous rate of absorption. It is considered the first model to simulate the time-dependent of GI absorption. The original dispersion model disregards the effect of first-pass metabolism, which derive a major drawback to the model. Therefore, the original dispersion model tended to overestimate the absorption of drugs that undergo pre-systemic metabolism. Furthermore, the original model neglects the mechanism of drug absorption as it assumes the absorption occurs only in passive diffusion manner [84]. Thus, the lack of the actual compound interaction with the other processes such as efflux transporters results in the overprediction of absorption.

Subsequently, the dispersion model was integrated as part of PK-Sim®, which is a whole-body PBPK software [85]. PK-Sim® addresses the major drawback of the original dispersion model by taking into account the pre-systemic metabolism and the interaction of drugs to the transporters. As such, PK-Sim® has gradually become a standard tool to predict absorption of the oral dosage form during drugs development. Its flexibility to adjust the drug release profiles is the most useful function over the other platforms.

1.12.1.2 – Compartmental Absorption and Transit (CAT) model.

The CAT model is the further developed version of oral single-compartment absorption model. The CAT model integrates the features of a compartment and dispersion model to overcome the limitation in the complex of absorption kinetics [86]. The main focus of the model is the intestinal flow properties. Yu et al simplify the multiple segments of the small intestinal tract into multiple compartments which the finalised model is the seven-compartment transit model [86]. The model assigns the first compartment as the duodenum whereas the second and third compartments are assigned as the jejunum.

The remaining four compartments all represent the ileum (**Figure 13**). All compartments have different volumes and flow rates, yet, they all share the same transit rate constant.

The CAT model was firstly employed to predict the absorption of drugs with an assumption of non-degradable and highly water-soluble. Thus, poorly water-soluble drugs or rapidly degradation are not well-compatible to use this absorption model. Nonetheless, the limitations were later addressed lead to the successful application to predict several poorly water-soluble drugs such as digoxin and griseofulvin [87].

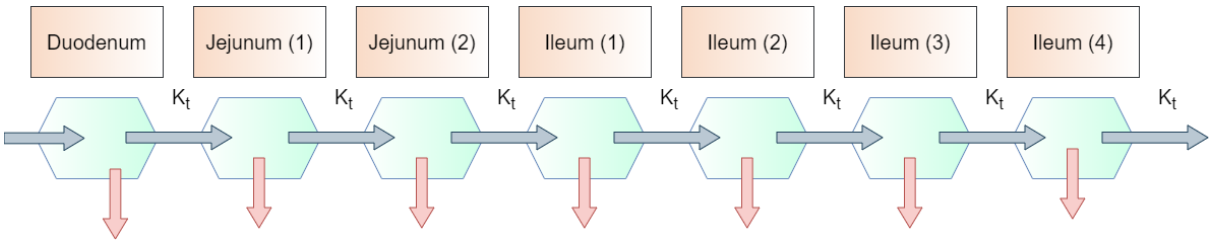

Figure 13 – A schematic diagram of the Compartmental Absorption and Transit (CAT) model.

1.12.1.3 – Advanced Compartmental Absorption and Transit (ACAT) model.

ACAT model is the modified version of the CAT model with the additional front end and back end to the base model. The additional front end is pre-systemic metabolism whereas the back end is the process of colon absorption. Thus, the model consists of nine compartments; stomach (front end), seven main compartments and colon (back end) (**Figure 14**). ACAT model takes into account the property of drug including the physicochemical characteristics (solubility, permeability), chemical stability (degraded, undegraded), gut wall metabolism and the effect of drug formulation on the rate of pharmacokinetics. The GastroPlus™ software (Simulation plus Inc., USA) is an example of the implementation of ACAT PBPK model. Parameters customisation in the GastroPlus™ such as GI transit time, pH, permeability and drug formulations can be explicitly assigned to the designate compartment allowing versatility to adjust the model.

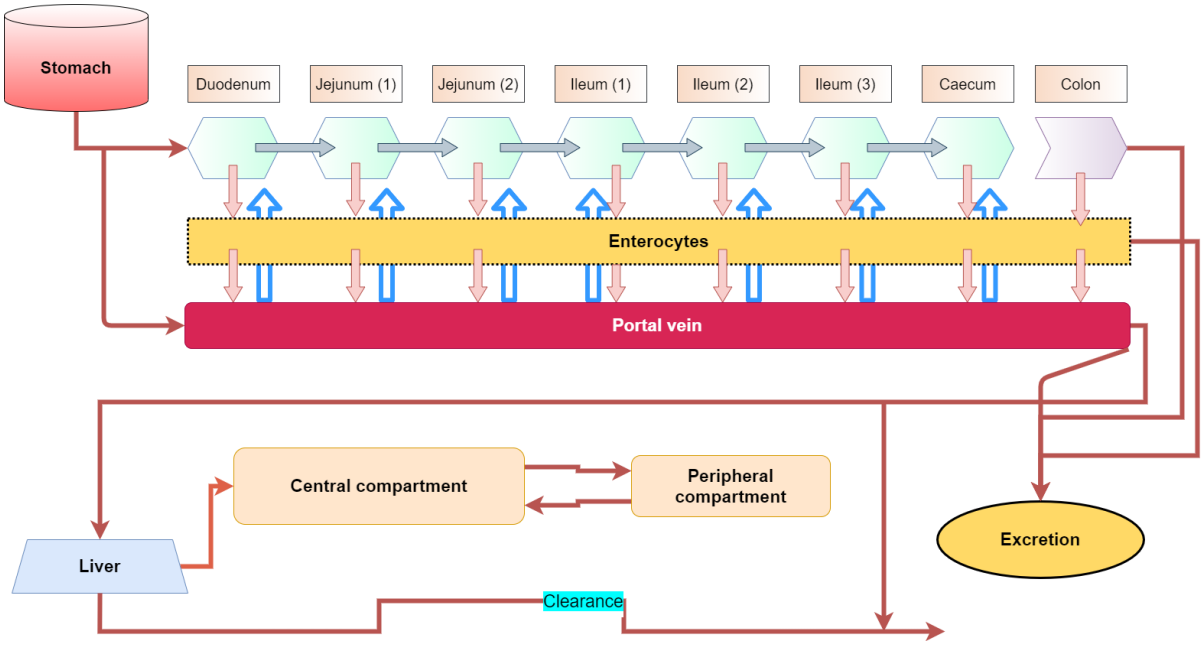

Figure 14 – A schematic diagram of the Advanced Compartmental Absorption and Transit (ACAT) model.

1.12.1.4 – Advanced Dissolution, Absorption, and Metabolism (ADAM) model.

The ADAM model was developed based on the CAT model with the additional consideration of fundamental GI tract physiology (**Figure 15**). Thus, gastric/small intestine emptying time and the capacity of the small intestine are also considered in the model. Furthermore, ADAM model also takes into account for the heterogeneity of GI tract, gut-wall permeability, enterocytic blood flow, gut-wall degradation and metabolism. Drug metabolism parameters are taken into consideration in the model as well. The parameters are including the hepatic CYP abundance, UGT abundance and the transporter profile. The ADAM model is implemented in Simcyp® software (Certara, UK). The unique function of Simcyp® is it incorporates a priori which consider the factor of inter-individual variability (IIV) based on physiological characteristics.

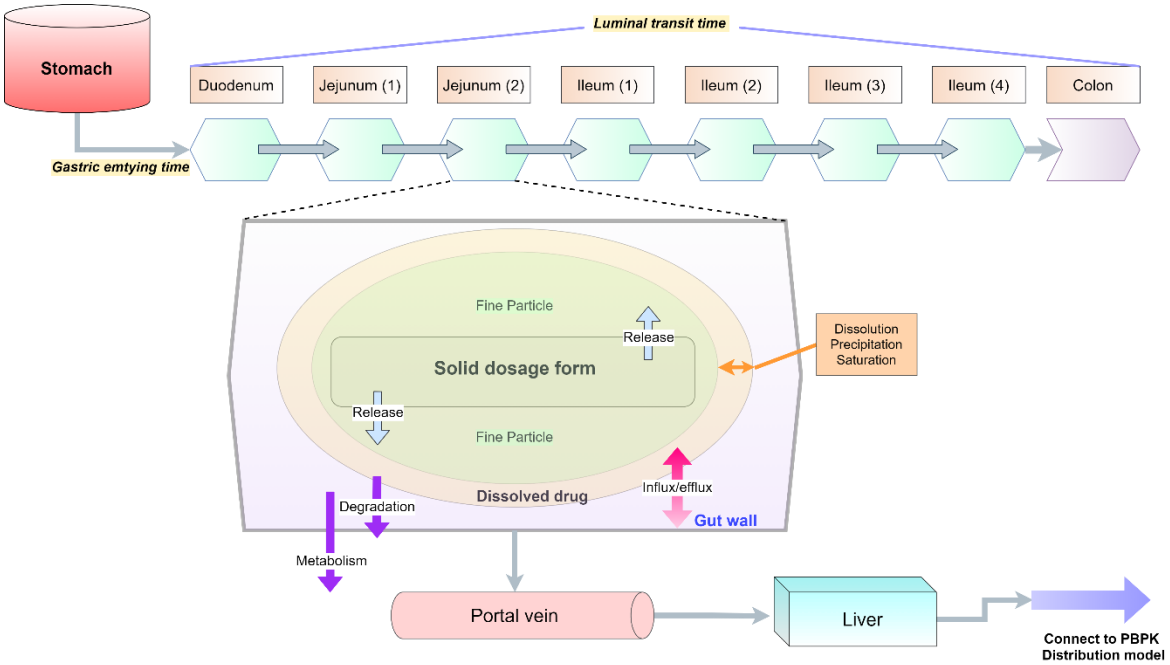

Figure 15 – A schematic diagram of the ADAM model.

1.13 – Simcyp® PBPK

Simcyp® PBPK simulator is one of the proprietary simulators capable of modelling and simulation the process of pharmacokinetics including oral absorption or IV injection, distribution and elimination (metabolism and renal excretion). In general, the platform generates the pharmacokinetic profiles based on the virtual population, which can be manually specified the demographic data such as age, gender and race, thus creating groups of distinct characteristics cohort (**Table 2**). Unlike other platforms, Simcyp® provides the built-in function for the concomitant administration with the other compounds, mainly the classical enzyme inducers/inhibitors. This function allows the opportunity to investigate the potential metabolically-related drug interactions of the compound of interested. Additionally, the results of modelling and simulation from Simcyp® are calculated across populations, not only the "average" individual, thus enabling further interrogation to individuals who have a particular characteristic.

Simcyp® is considered as a "bottom-up" approach in pharmacokinetic modelling. The model is built by combining the data of drug characteristics with the knowledge of anatomical characteristics of the body (including organs and tissues) (**Figure 16**) (**Table 3**). In contrast, the "top-down" method was well-represented by PopPK in which the pharmacokinetic model was empirically constructed based on the observed data from the available clinical trial data. PopPK theoretically seemed more realistic as clinical trial data was categorised as a high-quality. However, this approach was unable to predict drug effects, either therapeutic or toxicity on some inaccessible tissues such as the brain.

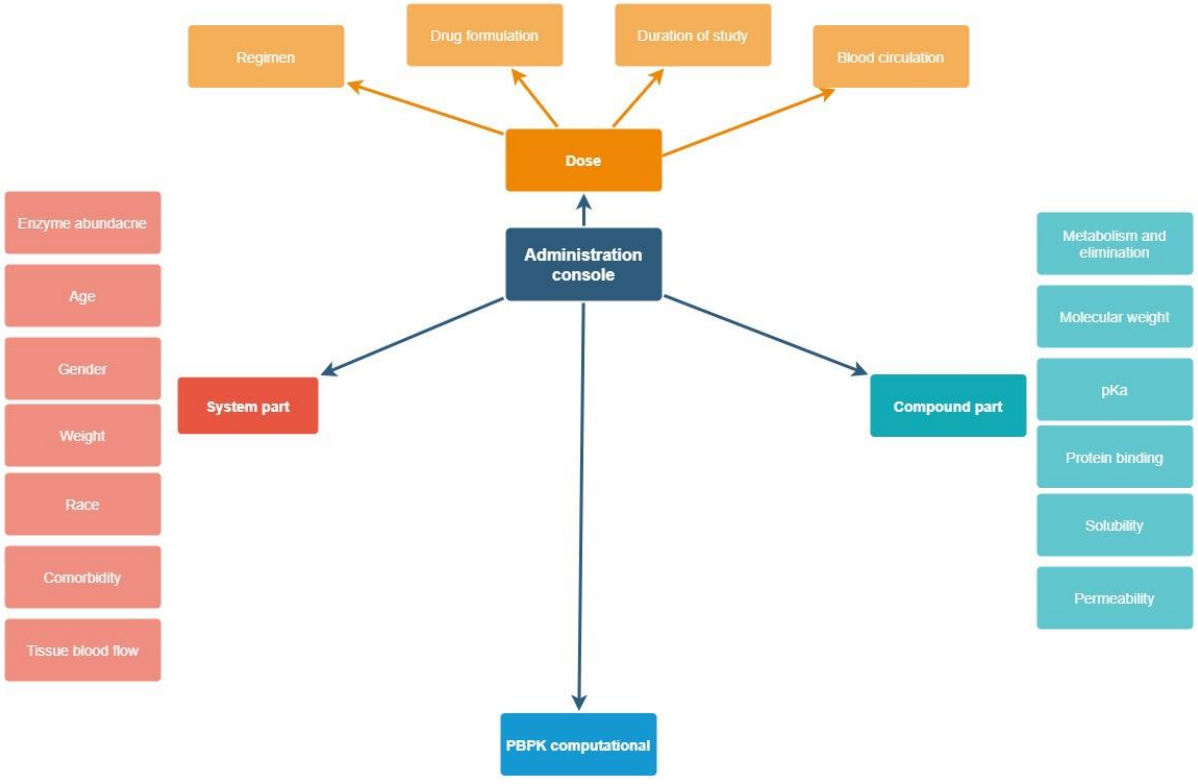

Figure 16 – Overview of the structure Simcyp® PBPK simulator.

Table 2. Example of data requirement for constructing a PBPK model in Simcyp® simulator.

Parameter	Unit	Note
Drug data		
Physicochemical property		
Molecular weight	g/mol	-
$LogP_{O:W}$	-	-
Species	Base, Acid, Neutral	-
pKa	-	-
Protein binding	-	-
Blood/Plasma partitioning	f_{up}	-
Permeability	B:P	-
Dosage form	10^{-6} cm/s	Immediate release, control release, etc.
V_{max} and K_m	pmol/min/mg, µmol/L	-
Enzyme contribution to the metabolism	-	Data from In vitro reaction phenotyping
Hepatic transport (Passive transport, P-gp)	-	-
System data		
Gender proportion	-	-
Weight	kilograms	-
Ethnicity	-	-
Age	years	-
Body surface area (BSA)	m^2	-
Trial design		
Food consumption	-	Fast/Fed, high-fat content
Sampling time	-	-
Dosage regimen	-	once daily, twice daily, etc.
Duration of study	days, weeks, months	-
P-gp: P-glycoprotein, CYP: cytochrome P450, V_{max}: maximum velocity, K_m: Michaelis-Menten constant		

Table 3. List of input data that can be used in Simcyp® simulator.

Category	Input data
Drug formulations	Immediate release, control or extended release, intravenous injection
Absorption	First order kinetics, compartmental model, CAT model, ADAM model. ADAM sub-model allows an adjustment in gastric emptying time, intestinal transit time, drug-specific solubility profile, dissolution and permeability
Metabolism	The metabolism profiles were able to generate based on Human liver microsomes Recombinant CYP and UGT enzymes Human hepatocytes Human kidney microsomes Human intestinal microsomes
Population	The available ethnicities are including Caucasian, Chinese, Japanese. Type of virtual population groups are including Healthy, patients with comorbidities such as obese, renal impairments, hepatic impairments
Drug-drug interactions	Built in a set of common enzyme inducers (rifampicin) and inhibitors (ketoconazole)
Trial designs	Able to specify the route of administration, single and multiple dosing regimen, number or participant per virtual trial
Type of simulations	Full-PBPK, partial-PBPK

1.13.1 – Applications of Simcyp® PBPK

In recent years, PBPK modelling and simulation have become an essential supporting data especially during the stage of drug discovery and development. Generally, the newly developed compound data tend to be limited and mostly derived from *in vitro* study and animal study. Simcyp® provides an opportunity to expand the available data to predict the following outcome due to particular clinical settings such as co-administered the investigated drug with enzyme inducers.

Over the past few years, Simcyp® has gained its recognition as a tool to provide a piece of supporting information in order to serve the requirement for regulatory review agencies. The major leading agencies that acknowledge the significant role of Simcyp® are including the US FDA and the EMA. The other application of Simcyp® PBPK such as:

1.13.1.1 – Extrapolation and prediction of drug exposure in special populations.

Simcyp® is regularly employed to extrapolate the pharmacokinetic profile from the virtual healthy volunteers to a particular case of patients. This includes patients who highly likely have minimal available data such as paediatric, renal/hepatic impairments patients. The success story was observed in the model-informed dosing regimen of imatinib in paediatrics using the extrapolation from virtual adult populations [88].

1.13.1.2 – Study of drug-drug interaction.

Simcyp® plays a significant role in predicting the potential of drug-drug interactions (DDI). In recent years, it has seen an ongoing improvement of the model-prediction performance for several compounds. The model refinement has continuously performed in order to increase the simulation reliability to the greatest extent. An excellent example to demonstrate the utility of PBPK in this aspect was shown in the study of PBPK modelling of atorvastatin. The study investigated the interaction between atorvastatin and the enzyme inhibitor to determine the possibility of serious adverse events (AEs) [89]. In addition, this study had further incorporated the knowledge of liver uptake via organic anion-transporting polypeptide (OATP) 1B1 and 1B3 into the model as an extension to the similar previous study [90]. The result was the refined model of atorvastatin capable of investigating the DDI lead to rhabdomyolysis when co-administered with enzyme inhibitor of CYP3A4 (rifampicin, clarithromycin and itraconazole) and OATP (rifampicin and cyclosporine).

1.13.1.3 – Guiding for adjusting dosage and regimen in renal impairment patients.

Renal impairment such as chronic kidney disease (CKD) or other conditions that observed a compromised renal function was recognised as a state of awareness for drug administration. Renal impairment patients have a reduction in glomerular filtration and tubular secretion depends on the level of severity. This leads to a significant decrease in clearance for drugs that mainly eliminated via renal. Thus, having a tool to predict drug clearance in the different magnitude of renal functions would support the decision-making for dose adjustment in renal impairment patients. Such epitomes were observed in the case study of ceftazidime and digoxin where PBPK was chosen to test the prediction capability in a particular population. Ceftazidime is one of the third-generation cephalosporin serves as a broad spectrum β-lactamase-resistant agent. It was reported to be eliminated mainly via glomerular filtration without any interaction with transporters. Thus, the mentioned characteristics make ceftazidime a suitable compound to assess the competency of PBPK model to predict the pharmacokinetics in renal

impairment patients. The results from Li et al. observed a comparable pharmacokinetic profile between the data generated from Simcyp® simulator and the prior clinical study data [91]. Although the Simcyp® model could not precisely apply in the high severity of renal impairments, the prediction performance was still under 1.5-fold margin of error. Another example of the application of Simcyp® PBPK in renal impairments was the extensive development of the kidney PBPK model for digoxin. Digoxin, a cardiac glycoside, has long been recognised for its narrow therapeutic range in treating congestive heart failure. The effective therapeutic window between 0.5 – 0.8 ng/ml were associated with the desired treatment outcome. However, the greater the plasma digoxin over 1.2 ng/ml, the higher possibility to observe adverse events and mortality [92]. Simcyp® PBPK of the kidney model for the regional difference in tubular surface area was earlier established [93] and optimised later on for digoxin by incorporating OATP4C1 and P-gp [94]. Hence, the optimised digoxin Simcyp® PBPK model was successfully developed and able to predict the PK profile of digoxin in special populations such as elderly whereas a slight overestimation trend was observed in virtual renal impairment patients [94].

1.13.1.4 – In vitro/in vivo extrapolation.

One of the base function yet very important of Simcyp® PBPK simulator is its capability to predict *in vivo* drug clearance using in vitro metabolic data or so-called *in vitro/in vivo* extrapolation (IVIVE). Simcyp® simulator has the interface to input data from in vitro studies such as kinetics data from human liver microsome or even recombinant enzymes both CYP and UGT by default. Thus, this premise allows researchers to conduct a preliminary study using PBPK simulation to help to identify the variability in the virtual population before conducting of clinical trials. This aspect has been proved and developed so far, as shown in prior studies [95-97]. In practical, the extrapolation is performed by accounting the protein content in HLM or related microsomal proteins combined with the well-stirred liver model to calculate hepatic blood clearance. Fully applicable of IVIVE was observed as in the case of rosiglitazone. Rosiglitazone, an insulin sensitiser for treating diabetes mellitus, is primarily metabolised in the liver by CYP2C8 enzyme whereas CYP2C9 and 1A2 are the secondary. Previous literature reported variability in rosiglitazone exposure due to genetic polymorphism of CYP2C8, especially *CYP2C8*3*. Importantly, the metabolic activity of *CYP2C8*3* to rosiglitazone was reported to be higher than the wild type. Thus, the following study conducted by Rowland K et al. employed Simcyp® modelling to further investigate the impact of CYP2C8 genotype on the degree of DDI. The study utilised the capability of trimethoprim as CYP2C8 inhibitor to demonstrate the magnitude of DDI with rosiglitazone between different genotypes. The results found an equivalent concentration-time profile of rosiglitazone and trimethoprim generated from Simcyp® with the *in vivo* data [98]. Thus, it emphasises the other significant role of Simcyp® to promote the precision dosing among patient with different genotypes.

1.14 – Sorafenib

Sorafenib is an oral TKI which inhibit cancer-cell proliferation, angiogenesis and accelerate the apoptosis rate *in vitro* [99, 100]. Sorafenib has been widely used in the treatment of several types of cancers as US FDA approved sorafenib for advanced renal cell carcinoma (RCC) and advanced Hepatocellular carcinoma (HCC). Similarly, the European Medicines Agency also approved sorafenib for the diagnosis, as mentioned above.

1.14.1 – Physicochemical properties

Sorafenib is categorised as a very poor soluble drug. The solubility of sorafenib is $3.59x10^{-2}$ mg/L at 25°C (US EPA; Estimation Program Interface (EPI) Suite. Ver. 4.11. Nov, 2012. Available from, as of Mar 6, 2014: http://www.epa.gov/oppt/exposure/pubs/episuitedl.htm. The low solubility of sorafenib directly affects the absorption in the gastrointestinal tract resulting in the low value of bioavailability (38-49 %).

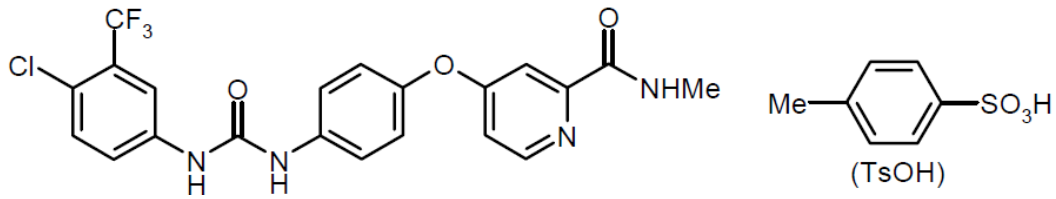

Figure 17 – Chemical structure of sorafenib tosylate.

Sorafenib tosylate (**Figure 17**) showed a better solubility at very high acidic pH (0.034 mg/100 mL at pH 1) whereas increased pH results in lower solubility (0.013 mg/100 ml at pH 4.5). As pH is one of the factors of sorafenib solubility, an acid-suppressing agent such as PPIs and histamine-2 receptor antagonist could theoretically interfere the solubility lead to reduced bioavailability of sorafenib.

1.14.2 – Pharmacology

1.14.2.1 – Mechanism of action

Sorafenib acts as a potent inhibitor of VEGFR subtype 1,2 and 3, PDGFR-beta (PDGFRβ) and fibroblast growth factor receptor 1 (FGFR1). Furthermore, *in vitro* studies of sorafenib observed the inhibitory activity to several Raf-kinase isoforms involved in the process of angiogenesis and tumour growth (**Figure 18**) [101, 102].

This image has been removed due to copyright restriction. Available online from [https://mct.aacrjournals.org/content/7/10/3129.long/ Scott M. Wilhelm, Lila Adnane, Philippa Newell, Augusto Villanueva, Josep M. Llovet and Mark Lynch. Mol Cancer Ther, October 1 2008 (7) (10) 3129-3140; DOI: 10.1158/1535-7163.MCT-08-0013.

Figure 18 – Mechanism of action of sorafenib. [Taken from Willhelm et al. (2008)].

1.14.2.2 – Absorption

Sorafenib reaches peak plasma concentration approximately within 3 hours after oral administration. The second absorption was observed at 8-12 hours and 24 hours after the first administration suggesting an enterohepatic recirculation characteristic. High-fat diet (50 % fat; 900 calories) affect the absorption of sorafenib by reducing 29 % of the bioavailability compared to fasted and moderate-fat diet (30% fat; 700 calories) [103]. Thus, sorafenib is recommended to administer without food.

Dose escalation of sorafenib observed a fluctuation at the dose of 400 mg twice daily. The twice-daily regimen of 600 and 800 mg observed a slightly greater AUC than the 400 mg dose but not at the significant level. Sorafenib reaches the steady-state at day 7 after the first dosing. Preclinical study of sorafenib tosylate absorption was conducted in multiple animal species such as, female beagle dogs and male Wistar rats. The absorption of sorafenib following either oral or intravenous observed a higher absorption ratio in rodents (78.6 % in female CD-1 mice and 79.2 % in male Wistar rats) compared to in female beagle dogs (67.6 %).

1.14.2.3 – Distribution

Sorafenib exhibits a high protein binding to human plasma proteins (99.5 %). Albumin is the major binding proteins whereas alpha-globulins and low-density lipoprotein (LDL) are the subsequence. The ratio of sorafenib distribution between red blood cell and plasma is reported as 1.33.

Sorafenib is a high lipophilicity (LogP [partition octanol-water] = 3.8). Besides, sorafenib also has a high permeability based on *in vitro* model using Caco-2 cells. Transporting ratio of sorafenib from basolateral to apical side and from apical to the basolateral side of sorafenib in Caco-2 cells were 4.7 (0.1 µM sorafenib) and 2.5 (1 µM sorafenib) respectively. pH directly affects protein binding of sorafenib as the reported fraction unbound at pH 6.78 was 1.8 % then decreased to 0.165 % at pH 7.99.

1.14.2.4 – Metabolism

Biotransformation of sorafenib mainly occurs in the liver using CYP3A4 enzyme follow by glucuronidation mediated by UGT1A9 enzyme (**Table 4**). Sorafenib parent compound was found mostly in plasma which accounts for 73 % of the identified metabolites in human at steady state. The

primary metabolite of sorafenib, sorafenib N-oxide (metabolite M2) obtains from N-oxidation at pyridine ring of parent compound. Hydroxylation of the N-methyl group of parent compound results in metabolite M3. Combining of metabolites M2 and M3 results in the formation of metabolite M1[104].

Table 4. Metabolites of sorafenib

Substance	Reaction to obtain the metabolite	Plasma	Faeces	Urine
Sorafenib	Parent compound	73 %	50.7 %	Not detected
Metabolite M1	Metabolite M2 + M3	Not detected	Not detected	Not detected
Metabolite M2	N-oxidation	16.7 %	Not detected	Not detected
Metabolite M3	N-methyl hydroxylation	Trace amount	0.4 %	Not detected
Metabolite M4	Demethylation	1 %	1.2 %	Not detected
Metabolite M5	Oxidative metabolite	Not detected	Not detected	Not detected
Metabolite M6	Carboxylic acid	Trace amount	19.1 %	Not detected
Metabolite M7	Glucoronide of sorafenib	0.5 %	Not detected	Not detected
Metabolite M8	Glucoronide of metabolite M2	Not detected	Not detected	Not detected

Enterohepatic recirculation of sorafenib was observed and described by two main mechanisms; 1) The metabolite M7 is glucuronidated follow by biliary excretion of the by-product to gut. In the gut, the glucuronic acid is cleaved to yield sorafenib then undergo reabsorption. 2) Oxidation of sorafenib results in metabolite M2 which undergo biliary excretion into the gut. Colonic bacteria reduce metabolite M2 to sorafenib then undergo reabsorption. The other metabolites and the biotransformation cascade as shown in **Figure 19**.

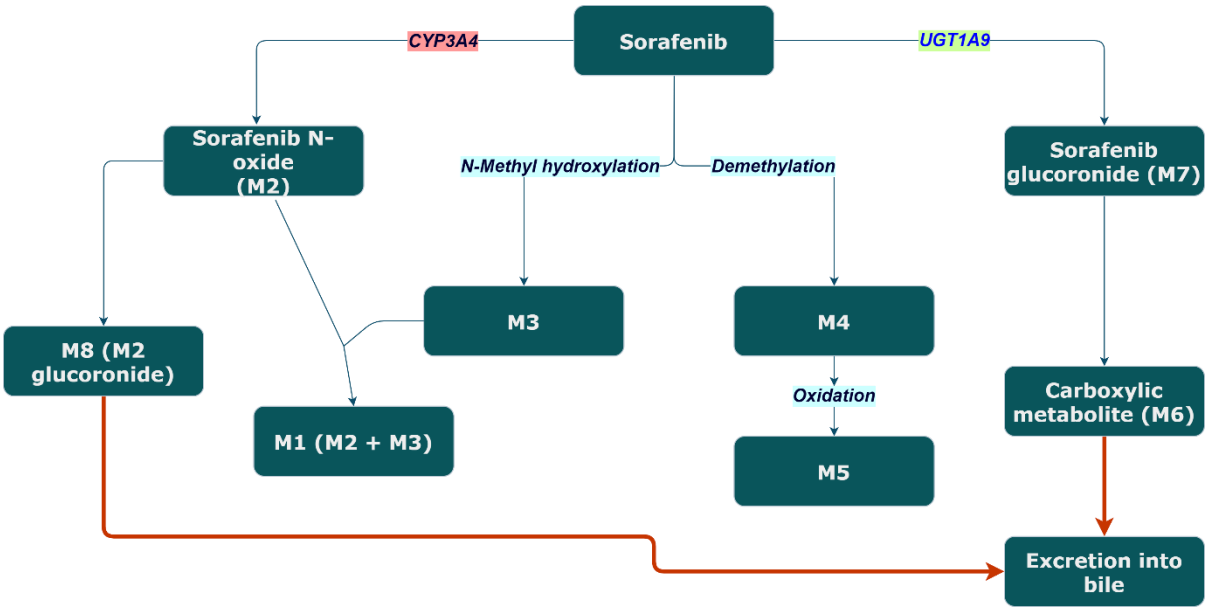

Figure 19 – A schematic of sorafenib metabolism.

1.14.2.5 – Indication

The US FDA approves sorafenib as the first-line treatment option for advanced/unresectable HCC with characteristics of Barcelona Clinic Liver Cancer (BCLC) stage B and a well-preserved liver function (Eastern Cooperative Oncology Group performance (ECOG PS) grade 0 – 2. Sorafenib is also approved to be used in renal cell carcinoma. The recommended dose of sorafenib is 800 mg (400 mg of a tablet twice daily). The AEs associated with sorafenib exposure tend to occur within the first cycle of treatment [105, 106]. Dose adjustment is allowed as recommended by the product manual. Dose adjustments are including either reducing dose of the daily intake or temporary withdraw sorafenib for a period of time [107].

1.14.2.6 – Factor affecting sorafenib exposure

Due to sorafenib available in oral dosage form, several cautions need to be exercised when using in patients. Sorafenib is reported to be negatively affected by a high-fat diet. As mentioned earlier, sorafenib is highly advised to be administered separately with a particular diet to avoid compromised drug absorption. Moreover, the absorption of sorafenib was reported to be influenced by the acidity environment as higher pH reduces the solubility of sorafenib; thus, lowering the absorption. Moreover, the solubility of sorafenib was to be affected by the intragastric pH. As a high acidic environment favour the solubility, whereas more basic environment lowers the solubility. Theoretically, drugs that could alter intragastric pH to be less acidic (pH > 5), such as PPIs, are highly likely to compromise sorafenib exposure.

1.15 – Extracellular vesicles (EVs) as novel biomarkers in precision medicine.

The research field of EVs, particularly small EVs – exosomes, has become one of a centre of attention which seen a dramatic increase in research output within the last decade. The earlier study of exosomes focused on the molecular consequence, such as its physiological activity role. [108]. Exosomes was thought to act as the carrier of cellular by-product for disposition purpose without any other significant functions. However, evidence has proved that exosomes are more than a garbage bag to dispose of cellular waste material. Instead, it contains intact molecular constituents encapsulated within well-structured lipid bilayer similar to the cell membrane [109, 110]. The first report of the availability of genomic materials encapsulated inside EVs by Valadi et al. was in 2007, since then the field of study has expanded to a greater extent.

As the field has progressed, the definition of each EV has been more refined to precisely describe the particular EV investigated in the study. Generally, EVs are small (50 to 1,000 nm) membranous vesicles that are secreted by all cells in the body and are found in various biological fluids (e.g. blood, urine, saliva, lymph, cerebrospinal fluid, breast milk). There are many different types of EVs, including exosomes, ectosomes, apoptotic bodies, microvesicles (MV) as shown in **Figure 20** [111-113]. Each

EV has distinct characteristics regarding the biogenesis, secretion, morphology, abundance and composition of cargos. Exosomes is one of the smallest subpopulations of EV. They are 50-150 nm in diameter, contain proteins, small molecules and various forms of nucleic acid (miRNA, mRNA, tRNA and DNA) as shown in **Figure 21**. Current literature indicates that unlike many types of EVs, exosomes are explicitly packaged and enriched for particular cargo associated with their biological function [114, 115]. With that being said, proteomic and genomic analysis of exosomes demonstrated a non-specific element to the packaging of exosome cargo, which appears to more broadly represent the cell/tissue of origin [116, 117]. Hence, the finding attracted researches from a distinct field of study to investigate in small EVs as it showed the feasibility in using EVs as a novel tool for their field of expertise such as drug delivery system, disease biomarker). In this thesis, the term small EVs is used interchangeably with exosomes as the current isolation methods are unable to purely captured a particular EV types. However, this thesis focused only the small EV population, thus; the subsequent experimental chapter (**Chapter 5**) were designed and optimised to only investigated the small EVs.

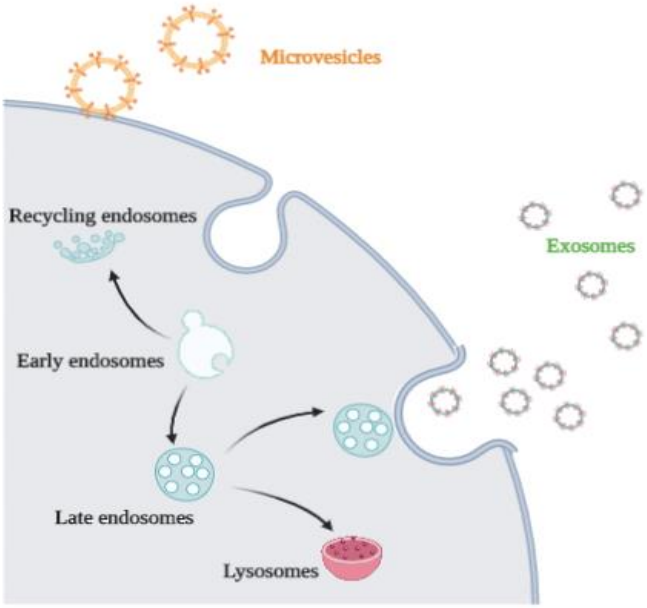

Figure 20 – small EVs serve as a mediator of cell to cell communication. The figure shows the fate of small EVs from secretion by hosts cell and uptake by recipient cells via two mechanisms either (a) internalisation by plasma membrane or (b) taken directly by recipient cells. Figure created with BioRender.com.

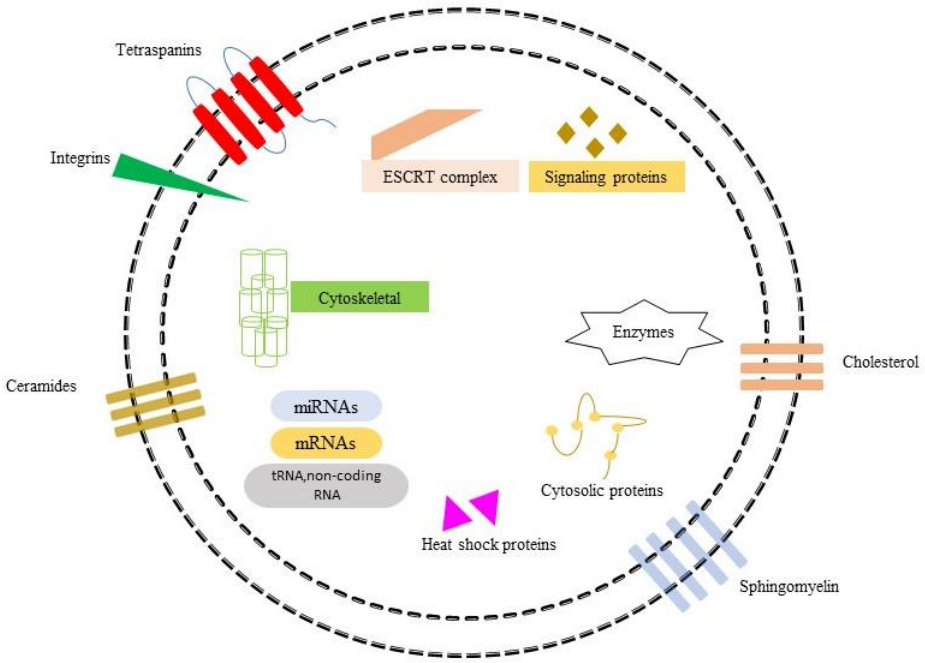

Figure 21 – A schematic of the overall composition of small EVs, exosomes. The figure shows three main components including proteins (surface and internal), nucleic acids and lipid components. Figure created with BioRender.com.

1.15.1 – Biogenesis of EVs

As roughly narrated about the cellular cascade of small EVs secretion, this section will focus more on each step of the biogenesis pathway toward the secretion of MV and exosomes type. Exosomes biogenesis may roughly divide into two main pathways, including the endosomal sorting complexes required for transport (ESCRT) -dependent and ESCRT-independent.

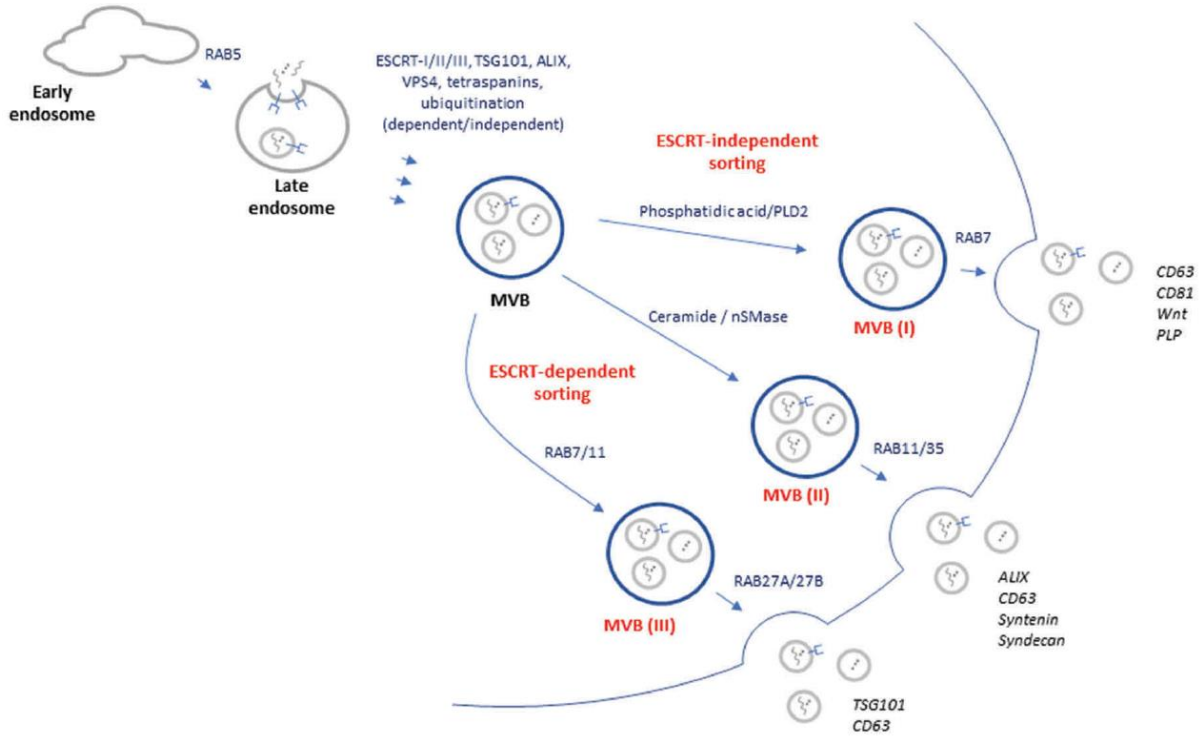

Figure 22 – Schematic of biogenesis pathway of small EVs. The figure showed two main biogenesis mechanisms including ESCRT-dependent and ESCRT-independent. [Taken form Greening and Simpson (2018)]

The ESCRT-dependent pathway begins during the early development of endosome before shifting to the late endosome. In this state, the intraluminal vesicles (ILV) start to accumulate and pack inside the multivesicular bodies (MVBs), ready for the ESCRT to facilitate the sorting process. Generally, ESCRT has four different main subtypes, including ESCRT-0, I, II, and III, which are all involved in protein sorting process (**Figure 22**). Several pieces of evidence showed that ESCRT complexes have a crucial role in exosomes secretion either promotion or demotion, as shown in **Figure 23**. Evidence also supported that interfering ESCRT-0 proteins, tumour susceptibility gene protein 101 (Tsg101), STAM and HRS reduce the secretion of exosomes in Hela cells. In contrast, silencing four of the ESCRT-III including CHMP4C, VPS4B, VTA1 and ALIX led to the increase in exosomes secretion instead [118]. ALIX was thought to facilitate the process of exosomes secretion; however, the above-mentioned results contradict the prior finding [119]. According to the EV database, ALIX and syntenin shared the most frequently identified markers in exosomes (ExoCarta). ALIX, syntenin and syndecan were found co-accumulated in EV isolated from the human breast cancer cell lines, MCF-7. Further investigation also found that the increased level of syntenin was associated with a proportionated increase in ALIX, syndecan and the other exosomal markers [119]. Thus, it is still unclear for the relationship between ALIX and exosomes secretion as evidence showed controversial findings. Notwithstanding, it could

make a logical assumption that different cell types require different cargo sorting complex leads to slightly diverse in cellular composition [118, 119].

This image has been removed due to copyright restriction. Available online from [https://www.nature.com/articles/nrm.2017.125/ van Niel, G., D'Angelo, G. & Raposo, G. Shedding light on the cell biology of extracellular vesicles. Nat Rev Mol Cell Biol 19, 213–228 (2018). https://doi.org/10.1038/nrm.2017.125.

Figure 23 – In-depth details of biogenesis cascade of small EVs. The figure depicted each sorting complex that involve to each other in order to form and secrete small EVs [Taken from van Niel et al. (2018)].

The other biogenesis mechanism of small EVs is ESCRT-independent pathway. Ceramide is the main component for this biogenesis pathway as reported by Trajkovic et al. [120]. The study reported that small EVs contain high amounts of sphingomyelin and cholesterol while containing less phosphatidylcholine compared to the total cellular membrane. Sphingomyelin could be derived from ceramide by hydrolysis of phosphocholine moiety using the enzyme sphingomyelinase (SMase). Although the biogenesis of small EVs is roughly divided into two main pathways, there is still unclear whether any molecular hybridisation between the pathways associate to the conglomeration of small EVs or not. [121]. As mentioned above, small EVs transcribed from different cells of origin possibly undergo a particular sorting mechanism suitable for each cell types. Thus, it is highly likely that there is a reciprocal mechanism promoting small EVs secretion in different scenarios. Further investigation to evaluate this hypothesis still needs to be conducted for more understanding of these phenomena [110, 122, 123].

1.15.2 – Proteins in small EVs

Proteins derived from small EVs (particularly exosomal proteins) have been studied extensively. The level of focus provided to exosomal proteins is comparable to the level of focus provided to exosomal RNA. The advance in proteomics analysis reveals the two common proteins category found in most small EVs. The first category is the group of essential vesicular component, including protein found in the plasma membrane, endosomal proteins and proteins needed for cell adhesions. The example of proteins commonly found in small EVs are listed in **Table 5**.

Table 5. Common identified protein in small EVs.

Protein category	Example
Cell adhesion	Lactadherin, Integrins, Thromospondin-1, Claudin-1
Cell structure and motility (including cytoskeleton)	Actin, Myosin, Tubulins, Vimentin, Cofilin-1, Radixin, Erzin
Tetraspanins	CD9, CD63, CD81, CD82, CD53
Heat shock proteins (HSP)	HSP90, HSP70, HSP27, HSP60
Membrane transport	PG regulatory-like protein, CD13
Trafficking and membrane fusion	Annexins, Clathrin heavy chian-1, Dynamin, Syntaxin-3, Synaptosomal-associated protein
Multivesicular body biogenesis	Alix, TSG101, Rab proteins, Vacuolar sorting protein
Metabolic enzymes	Glyceraldehyde-3-phosphate dehydrogenase (GAPDH), Pyruvate kinase isozymes M1/M2, Fatty acid synthase, ATP citrate lyase, ATPase, Aspartate aminotransferase, Aldehyde reductase
Antigen presentation	Human leukocyte antigen (HLA) class I and II/peptide complexes
Transcription and protein synthesis	Histones, Ribosomal proteins, Ubiquitin
Iron transport	Transferrin receptor
Signaling proteins	Syntenin-1, Guanine nucleotide-binding protein (G-proteins), GTPase HRas (HRAS), Ras-related protein Rap-1b/2b

As mentioned earlier, the accessory proteins class that required for forming internal membrane budding during the sorting of MVBs is a group of ESCRT proteins. This group of proteins facilitates the ILV formation and later exosomes. Thus, ESCRT proteins such as ALIX or Tsg101 can be used as a marker to verify the classification of EV (**Table 6**).

Apart from the general essential proteins found in small EVs, the other set of proteins are directly related to the cell of origin. Each cell has its own unique protein expression phenotype which able to transport to the EVs. For example, small EVs derived from cerebrospinal fluid were found abundant in amyloid-beta protein, a by-product of amyloid protein precursor catabolism. The amyloid-beta protein was found to be one of the markers of Alzheimer's disease (AD) as reported by many pieces of evidence [124-126]. Evidence reported that accumulation of amyloid-beta in neuronal cells was the primary factor associated with synaptic dysfunction. Furthermore, the high accumulation density of amyloid-beta proteins leads to the formation of plaques– amyloid plaques, one of the pathological hallmarks of AD [127]. The earlier study from Takahashi et al. observed the high level of amyloid-beta proteins localised in MVBs in the brain of AD patients compared to non-AD patients [128]. Importantly, it was later confirmed that the amyloid-beta oligomers were the main adverse factor inducing neurotoxicity and

disease propagation. Sinha et al. found that small EVs isolated from AD brains contain a large number of amyloid-beta oligomers compared to non-AD. Evidence showed that small EVs derived from AD brains could transfer the pathological elements to the naive cell suggesting its potential role as a mediator in cell-to-cell communication [129]. The other disease propagation phenomenon via small EVs was observed in HBV transmission to the naive hepatocytes and energy transportation between cardiomyocytes during glucose deprivation state [130, 131].

Since small EVs contain a specific cargo depends on the cellular of origin; thus hypothetically, it can be used to reciprocate the status of its radical as well. Currently, there is still an inadequate understanding of EVs, including exosomes, and DME. As DMEs are proteins, it can be assumed that small EVs-derived from the liver where the DME is highly expressed should also carry the DME proteins in the cargo. The advance in proteomics analysis revealed DME and cofactors peptides in exosomes isolated from rat hepatocytes suggesting a strong support to the hypothesis [117]. Hence, considering that hepatic-derived small EVs represent a miniature illustration of the actual enzymatic status in the liver, proving this concordance would lead to an establishment of using small EVs as a novel non-invasive biomarker to determine the actual DME status in hepatocytes.

Table 6. List of identified protein using LC-MS/MS from rat hepatocyte-derived small EVs. Adapt from Conde-Vancells et al. 2008.

Protein category	Name
Xenobiotics and endogenous compounds metabolism	Cytochrome P450: 2A1, 2B3, 2C11, 2D1 2D3, 2D10, 2D18, 2D26 UDP-glucuronosyltransferases: 2B2, 2B3 and 2B5 NADPH-cytochrome P450 reductase Alcohol dehydrogenase 1 and Epoxide hydrolase 1 Cytochrome b5
Transmembrane	CD63, CD81 and CD82 Membrane-associated progesterone receptor Asialoglycoprotein receptor
Cells adhesion	Lactadherin Clathrin heavy chain Alix Annexins: A2, A4, A5, A6
Signalling proteins	Guanine nucleotide-binding protein sub beta 2-like 1 Guanine nucleotide-binding G(s) α, and G(i) -α2
Protein synthesis and post-transductional	40S ribosomal protein SA, S3, S4(X), S6 60S ribosomal protein L6 and L7

Lipid Metabolism	Acyl-coenzyme A oxidase 2, peroxisomal Fatty aldehyde dehydrogenase Fatty acid synthase and ATP-citrate synthase
Carbohydrate and Amino-acid Metabolism	Alpha-enolase L-lactate dehydrogenase A chain Pyruvate carboxylase Fructose-1,6-bisphosphatase 1, aldolase A
Miscellaneous	Cytochrome b5 Ferritin heavy chain Ferritin light chain 1 ATP synthase subunits α and β

1.15.3 – RNA in small EVs.

Small EVs became a centre of attention as a potential biomarker for disease and diagnostic due to the ease of detecting mRNAs and miRNAs in exosomes by Valadi et al [132]. It leads to the subsequent interesting assumption that small EVs may play a crucial part in cell-to-cell communication as it can remotely transfer genomic information to the other cells. Exosomes have the feature of lipid bilayer membrane which capable of protecting the enclosed material from any digestive enzymes. This assertion was testified by the use of a couple of detergents including Triton-X100 and RNase A enzyme. RNase A enzyme is capable of RNA digestion, whereas Triton-X100 is capable of disrupting the lipid bilayer integrity. The isolated small EVs incubated with only RNase A enzymes showed an amplifiable of the polymerase chain reactions within the margin of error compared to non-treated small EVs. However, when firstly incubated small EVs with Triton-X100 follow by RNase A enzyme, the polymerase chain reaction (PCR) results were outside the margin of error [133].

Similar to the study of exosomal proteins, exosomal RNA is the other approaches that has significantly been studied during the last decade. Several cutting-edge technologies such as Droplet Digital PCR (ddPCR), real-time quantitative PCR (RT-PCR) and Next generation sequencing (NGS) facilitate the identifying of the genetic material shuttled by small EVs [134]. Moreover, the study about exosomal RNA was reported to span almost the entire biofluids including urine [135], cerebrospinal fluids [136], breast milk [137], semen [138] and cell culture supernatant [132].

To sum up, both mRNA, miRNA and other related trace element which potentially play a role in cell-to-cell signalling/modulation can be found in small EVs [132, 139-141] which in turn support the significant role of small EVs as a novel method of cell signalling mechanism. By applying this knowledge to any other type of liquid biopsy tracking method, detecting of rare disease and/or alteration of homeostasis is unquestionably possible.

1.15.4 – Perspective in small EVs, exosomes, as a novel biomarker in precision medicine: current challenge.

One of the main challenges in EV research field is the purification of EV. During the last decade, many researchers in EV field have come to realise that there is no such a way to solely isolated a particular population of EV from the source of origin. The currently available approaches tend to utilise the physicochemical properties of EV as a mechanism of isolation. Such an example is the isolation of EV using ultracentrifugation. Ultracentrifugation (UC) is the method of choice for many research group as it has less complexity both in the fundamental and the required equipment. The advantage of UC is the capability of scaling which suitable for working with a large volume of samples such as cell culture conditioned media. However, transition electron microscopy revealed that many EVs isolated from UC showed a substantial loss of integrity. The membranous collapse or fusing was often observed in EV isolated by UC [142]. The method itself requires multiple incremental steps of centrifugation both intermediate and the extended amount of time; thus, it is nearly impossible to apply this isolation method to a standard clinical diagnostic setting. Using kit isolations is the other option that considered to be more pragmatic. This option comes with many pros such as fewer isolation steps, highly reproducible, require less instrument needed to perform the isolation, and most of them are portable. One of the drawbacks in using kit isolation is the higher cost per sample. Although UC may give a low recovery rate and post some risks to the vesicles integrity, the cost per sample isolation is at least 10-times lower than any kit isolations. Therefore, choosing the optimum performance of isolation with the most cost-effectiveness is an essential element in EVs researches, especially if aiming to integrate into clinical translation.

On the other hand, if one intends to maximise the isolation purity to the greatest extent, the most convincing technology would befall into employing the immunocaptured-based isolation. The method would provide more insight into organ-specific EVs as immunocapture could apply the organ-specific marker to isolate a particular EVs population from biofluids specifically. On the other hand, the cost per isolation for this approach tend to exceed other proprietary kit isolation due to its versatility in modification, anyhow further development and optimisation still required. Thus, using conditioned media from mammalian cells should be the current method of choice to investigate the nature of the organ-specific EVs. The knowledge developed from the cell-based EVs would indeed become a ground understanding for the later *in vivo* study of organ-specific EVs.

Apart from the downside regarding the challenging in EV isolation, its inherent properties have demonstrated their potential utility in various research fields. The majority of researchers aim to use EVs for a pre-emptive action to determine any abnormality occurring in the body. Gene expression assay and proteomics profiling have been extensively used to analyse its molecular cargo as they are the main approaches to elucidate the roles of EVs from a different source of origin. As EVs are generally

available in a very tiny amount, sacrificing any proportion of EVs sample has to be wisely spent. Thus, the better the sensitivity of the detection method, the better possibility to analyse the same sample in many paradigms. The advanced in proteomics also provide the workability of combining EVs in clinical translation as EVs could serve as a non-invasive source of biomarkers as an extension from a standard liquid biopsy [143, 144]. Hence, this has placed the position of EVs in high regard as a worthy biomarker to investigate its possible role in a modern precision dosing.

1.16 – Research aims

The current challenge of precision medicine and precision dosing is translational from bench to bedside. There are limitations in each precision dosing approach, such as the analysis of clinical trial data and PBPK modelling need a decent amount of data as a base requirement of the entire process. This thesis aimed to demonstrate a broad view of the array of the current methods in precision medicine, including PBPK modelling, clinical epidemiology and biomarkers discovery which are the three major elements in precision medicine. Herein, sorafenib was used as the model drug in this thesis to implement the aforementioned precision dosing approaches. Sorafenib is the essential element to treat advanced HCC patients, although a degree of heterogeneity in drug exposure was frequently reported. Investigating into the potential source of variability and revalidating the factor affecting drug exposure would lead to patients' greatest benefit. Moreover, this thesis sought to develop a novel approach in precision dosing using circulatory biomarkers – EVs to track the variability in DMEs. Ultimately, this approach will enable the biopsy-like information to be captured, allowing the changes in enzymatic status to be timely monitored. Thus, this would lead to better tailoring the treatment strategy to each patient; thereby, the benefits of drugs therapy are optimised.

The hypothesis underpinning this thesis is that precision dosing strategies may provide complementary or unique insights to optimise the dosing of sorafenib. In order to address this hypothesis, the following specific aims were evaluated:

- **Aim 1.**

Evaluate the effect of early AEs resulting in sorafenib dose adjustments on survival outcomes of advanced HCC patients using individual patient level data from randomised clinical trials.

- **Aim 2**.

Evaluate the effect of PPIs on the survival outcomes in advanced HCC patients treated with sorafenib using individual patient level data from randomised clinical trials.

- **Aim 3**

Part A. Develop and validate a whole body PBPK model for sorafenib and apply this model to identify the physiological and molecular factors affecting variability in sorafenib exposure.

Part B. Utilise the model developed in ***Aim 3A*** to evaluate the performance of (i) fixed sorafenib dosing, (ii) concentration guided sorafenib dosing based on therapeutic drug monitoring alone and (iii) concentration guided sorafenib dosing based on therapeutic drug monitoring with model-informed initial dose selection (MIDS), with respect to achieving a therapeutic sorafenib plasma concentration.

- **Aim 4**

Part A. Establish the functionality of plasma EV derived biomarker to predict the exposure of CYP3A4 substrates such as sorafenib.

Part B. Develop am *in vitro* model based on the HepaRG cell line to study DMEs in hepatocyte-derived EVs.

CHAPTER 2: EFFECT OF EARLY ADVERSE EVENTS RESULTING IN SORAFENIB DOSE ADJUSTMENTS ON SURVIVAL OUTCOMES OF ADVANCED HEPATOCELLULAR CARCINOMA PATIENTS.

2.1 – Function of Chapter

This first results chapter establishes the potential importance of precision medicine in terms of maximising the efficacy and minimising toxicity within the context of anti-cancer medicines. In this chapter, the impact of the reduction in dose intensity, through dose reduction, interruption or discontinuation, on survival outcomes was evaluated. Historically, for systemic cytotoxic anti-cancer drugs any reduction in dose intensity has been associated poorer treatment outcomes and inferior survival. As such, reduction in dose intensity for newer anti-cancer medicines is also viewed negatively despite the marked differences in the pharmacodynamic principles underpinning the use of these drug classes. In this first chapter of the thesis, the relationship between reduction in dose intensity and survival is evaluated. This thesis chapter has been reviewed and published in full as:

Ruanglertboon, W., Sorich, M.J., Rowland, A. et al. Effect of early adverse events resulting in sorafenib dose adjustments on survival outcomes of advanced hepatocellular carcinoma patients. Int J Clin Oncol ***25,*** *1672–1677 (2020).*

The chapter has been reproduced for this thesis with kind permission from International journal of clinical oncology (License ID 1141056-1) in **Appendix 6**. Formatting and minor changes in wording have been made to conform to the remainder of this thesis.

2.2 – Introduction

Hepatocellular carcinoma (HCC) is the third most common cause of cancer-related death [145]. Sorafenib, a tyrosine kinase inhibitor (TKI), is the recommended first line treatment option for advanced/metastatic HCC with demonstrated improvements in overall survival (OS) and progression-free survival (PFS) compared to previous options [146, 147]. Nevertheless, there is still heterogeneity in survival outcomes and adverse outcomes between patients who receive sorafenib therapy [146, 148].

Sorafenib is initiated at a dose of 400 mg twice daily for the treatment of advanced HCC [149]. Within clinical trials approximately 40 % of patients treated with sorafenib require a dose interruption and 30 % require a dose reduction due to adverse events (AEs). Studies indicate that AEs most commonly occur within the first month of sorafenib therapy, with frequent AEs including hand-foot syndrome and diarrhoea [107, 146, 150, 151]. Studies have demonstrated that diarrhoea and hand-foot syndrome early after sorafenib initiation were associated with improved survival outcomes [152, 153]. However, studies have not investigated the associations between dose adjustments due to sorafenib induced AEs and survival outcomes. The primary aim of the study was to evaluate the impact of early AEs requiring sorafenib dose interruptions or dose reductions on survival outcomes in patients with advanced HCC. An exploratory analysis of the association between pre-treatment patient characteristic and early sorafenib dose adjustments induced by AEs was conducted.

2.3 – Methods

2.3.1 – Study Design and Patients

The study was a secondary analysis of the sorafenib arm of phase III clinical trial NCT00699374 which included participants with locally advanced or metastatic HCC [154]. Participants were initiated on sorafenib at 400 mg twice daily on 4-week cycles. Dose reductions and treatment interruptions were permitted in response to AEs according to the registered product insert [154]. When necessary, doses were reduced to 400 mg once daily, and then 400 mg dose every other day.

Individual participant data (IPD) was accesses in this study from www.projectdatasphere.org. Secondary analysis of anonymized IPD was deemed negligible risk research by the Southern Adelaide Local Health Network, Office for Research and Ethics and was exempt from review.

2.3.2 – Predictors and outcome data

The primary outcome was OS, with PFS assessed as a secondary. PFS was evaluated using according to the Response Evaluation Criteria in Solid Tumours (RECIST) version 1.0 [155].

AEs were defined by grade according to the Common Terminology Criteria for Adverse Events version 3.0 (CTCAE) [149]. AEs requiring sorafenib dose adjustments were categorised as 'dose reduction', 'dose interruption' and 'discontinuation'. AE within the first 28 days of sorafenib therapy leading to dose adjustment were the primary focus of this analysis.

Supplementary analyses were undertaken for hand-foot syndrome AEs occurring in the first 28 days of sorafenib therapy and relative dose intensity (actual divided by planned cumulative dose [156, 157]) of sorafenib over the first 28 days of therapy. Sorafenib relative dose intensity was calculated and classified into two groups (<50 % vs ≥50 %) as previously described [156].

Available pre-treatment characteristic data included sex, age, race, weight, Eastern Cooperative Oncology Group performance status (ECOG PS), estimated glomerular filtration rate, Barcelona Clinic Liver Cancer (BCLC) staging, history of hepatitis B or C infection, number of metastatic site, the presence of liver metastases, oesophageal varices, liver cirrhosis, non-alcoholic steatohepatitis and portal vein thrombosis.

2.3.3 – Statistical analysis

A landmark Cox proportional hazard analysis was used to evaluate the association between early AEs requiring sorafenib dose adjustments and OS/PFS. Associations were reported as hazard ratios (HR; event outcomes) with 95 % confidence intervals (95% CI) and P values. The landmark was set at 28 days (end of 1st cycle) after sorafenib initiation, with individuals who progressed or died within the first 28 days of therapy excluded from analysis. The landmark was derived according to a balance of being as early as possible (as early markers of response are more useful, and there is a loss of individuals/power as the landmark time increases due to the event occurring before the landmark) and ensuring enough AEs had occur before the landmark time (as only AEs before the landmark count in the analysis technique). Kaplan-Meier analysis was used to estimate and plot survival outcomes according to sorafenib dose adjustment categories.

As an exploratory analysis, univariable Cox proportional hazard analysis was used to evaluate the association between pre-treatment characteristics and early AEs requiring sorafenib dose adjustments within the first 28 days of therapy.

2.4 – Results

2.4.1 – Patient Characteristics

Data from 542 patients with advanced HCC who received sorafenib therapy were available. **Table 7** provides a summary of the patient characteristics. Prior to day 28th, 16 participants were excluded from

the analysis due to disease progression, including 10 participants who died. Median follow-up in the population was 22 [95% CI: 21-24] months.

Table 7. Summary of patient characteristics.

Parameters	Total No. 542
Sex	
Female	85 (16%)
Male	457 (84%)
Age (years)	
[18, 50]	128 (24%)
[50, 60]	148 (27%)
[60, 70]	149 (27%)
[70, 84]	115 (21%)
Missing	2 (0%)
Race	
Asian	417 (77%)
Non-Asian	125 (23%)
Weight at baseline	64 (57 - 74)
Baseline ECOG score	
0	289 (53%)
1	250 (46%)
Missing	3 (1%)
BCLC stage	
B	89 (16%)
C	452 (83%)
Missing	1 (0%)
Involved disease site - liver	495 (91%)
Number of involved disease sites (including liver)	
1	223 (41%)
2	214 (39%)
3	89 (16%)
4	16 (3%)
Oesophageal varices	
Yes	156 (29%)
No	376 (69%)
Missing	10 (2%)
Hepatitis B	
Yes	287 (53%)
No	245 (45%)
Missing	10 (2%)
Hepatitis C	
Yes	118 (22%)
No	414 (76%)
Missing	10 (2%)
Liver cirrhosis	
Yes	247 (46%)
No	285 (53%)
Missing	10 (2%)
Estimated glomerular filtration rate (ml/min/1.73 m^2)	
[90, 257]	301 (56%)
[60, 90]	190 (35%)
[45, 60]	30 (6%)
[6, 45]	19 (4%)
Missing	2 (0%)

Data are median (IQR) or number of patients (%)

2.4.2 – Dose adjustment and predictors

Figure 24 presents the incidence of AEs requiring dose adjustments of sorafenib within each of the first 10-cycles of therapy. Within the first 28 days, 128 (51.6 %) had a dose interruption, 97 (39.1 %) had a dose reduction and 23 (9.3 %) discontinued the treatment.

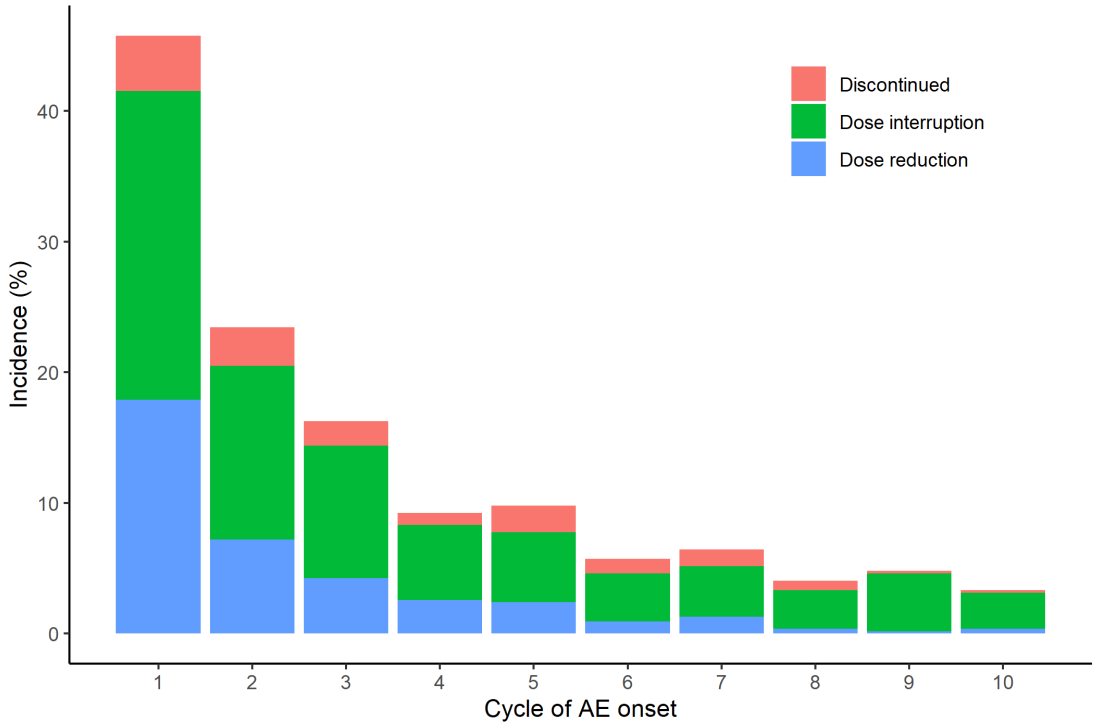

Figure 24 – Proportion of the study cohort with an adverse event leading to adjustment of sorafenib dosing over the first 10 cycles of sorafenib treatment.

Univariable Cox proportional analysis data identified older age, Asian race, lower weight, history of hepatitis C infection, and absence of liver metastases as associated with an increased risk of experiencing an AEs within the first 28 days of sorafenib therapy which requires a dose adjustment ($P < 0.05$; **Table 8**).

Table 8. Univariate analysis in predictors of AE related to dose adjustment within first 28 days.

	No. patients	Events/Patients (%)	HR	95% CI	P
Sex	542				0.056
Female		47/85 (55%)	1.00		
Male		201/457 (44%)	0.63	0.40 to 1.01	
Age (years)	540				0.021
[18, 50]		52/128 (41%)	1.00		
[50, 60]		58/148 (39%)	0.94	0.58 to 1.53	
[60, 70]		72/149 (48%)	1.37	0.85 to 2.20	

[70, 84]		65/115 (57%)	1.90	1.14 to 3.16	
Race	542				0.001
Asian		207/417 (50%)	1.00		
Non-Asian		41/125 (33%)	0.50	0.33 to 0.75	
Weight at baseline	542		0.98	0.96 to 0.99	<0.001
Baseline ECOG score	539				0.922
0		133/289 (46%)	1.00		
1		114/250 (46%)	0.98	0.70 to 1.38	
BCLC stage	541				0.780
B		42/89 (47%)	1.00		
C		206/452 (46%)	0.94	0.59 to 1.48	
Involved disease site - liver	542				
No		28/47 (60%)			
Yes		220/495 (44%)	0.54	0.30 to 1.00	0.049
Number of involved disease sites (including liver)	542		0.90	0.73 to 1.11	0.322
Oesophageal varices	532				
No		172/376 (46%)			
Yes		70/156 (45%)	0.97	0.66 to 1.40	0.854
Hepatitis B	532				
No		115/245 (47%)			
Yes		127/287 (44%)	0.90	0.64 to 1.26	0.535
Hepatitis C	532				
No		173/414 (42%)			
Yes		69/118 (58%)	1.96	1.30 to 2.97	0.001
Liver cirrhosis	532				
No		140/285 (49%)			
Yes		102/247 (41%)	0.73	0.52 to 1.03	0.071
Estimated glomerular filtration rate (ml/min/1.73 m^2)	540				0.974
[90, 257]		136/301 (45%)	1.00		
[60, 90]		89/190 (47%)	1.07	0.74 to 1.54	
[45, 60]		13/30 (43%)	0.93	0.44 to 1.98	
[6, 45]		9/19 (47%)	1.09	0.43 to 2.76	

CI=confidence interval, OR=odds ratio

2.4.3 – Effect of early AEs related dose adjustment on survival outcomes

At day 28, there was a significant relationship between early AEs requiring sorafenib dose adjustment within the first 28 days with OS (HR [95%CI]; dose interruption = 0.9 [0.7 - 1.2]; dose reduction = 0.6 [0.5 - 0.9]; discontinuation = 1.7 [0.9 - 3.4]; P = 0.005) (**Table 9**). There was no significant relationship between early AEs requiring sorafenib dose adjustment with PFS (HR [95%CI]; dose interruption = 1.2 [1 - 1.5]; dose reduction = 0.9 [0.7 - 1.1]; discontinuation = 1.1 [0.2 - 7.7]; P = 0.148) (**Table 9**). **Figure 25** presents Kaplan-Meier estimates of OS and PFS by AE induced dose adjustment category within the first 28 days of sorafenib therapy. **Figure 26** presents a forest plot of OS by patient subgroups for AEs requiring dose reductions versus no action in the first 28 days of sorafenib treatment – indicative that the association between dose reduction due to AEs within the first 28 days of sorafenib and favourable OS was consistent across patient subgroups. **Figure 27** presents a forest plot of PFS by patient subgroups for AEs requiring dose reductions versus no action in the first 28 days of sorafenib treatment. No association between dose reduction due to AEs within the first 28 days of sorafenib were observed across patient subgroups.

Table 9. Summary of the association between dose adjustment following AEs within first 28 days of sorafenib treatment with OS and PFS.

		OS			PFS		
Action	**N**	**Median [95% CI] time to event (months)**	**HR [95% CI]**	**P**	**Median [95% CI] time to event (months)**	**HR [95% CI]**	**P**
No action	292	10 [8 – 11]	1	0.005	4 [3 – 4]	1	0.148
Dose interruption	125	9 [8– 15]	0.91[0.7 – 1.2]		3 [3 – 4]	1.2 [1 – 1.5]	
Dose reduction	95	15 [12 – 22]	0.6 [0.5 – 0.9]		4 [3 – 6]	0.9 [0.7 – 1.1]	
Discontinuation	14	3 [2 – NA]	1.7 [0.9 – 3.4]		NA	1.1 [0.2 – 7.7]	

N - sample size, CI - confidence interval, HR - hazard ratio, OS - overall survival, PFS - progression-free survival, NA - No data

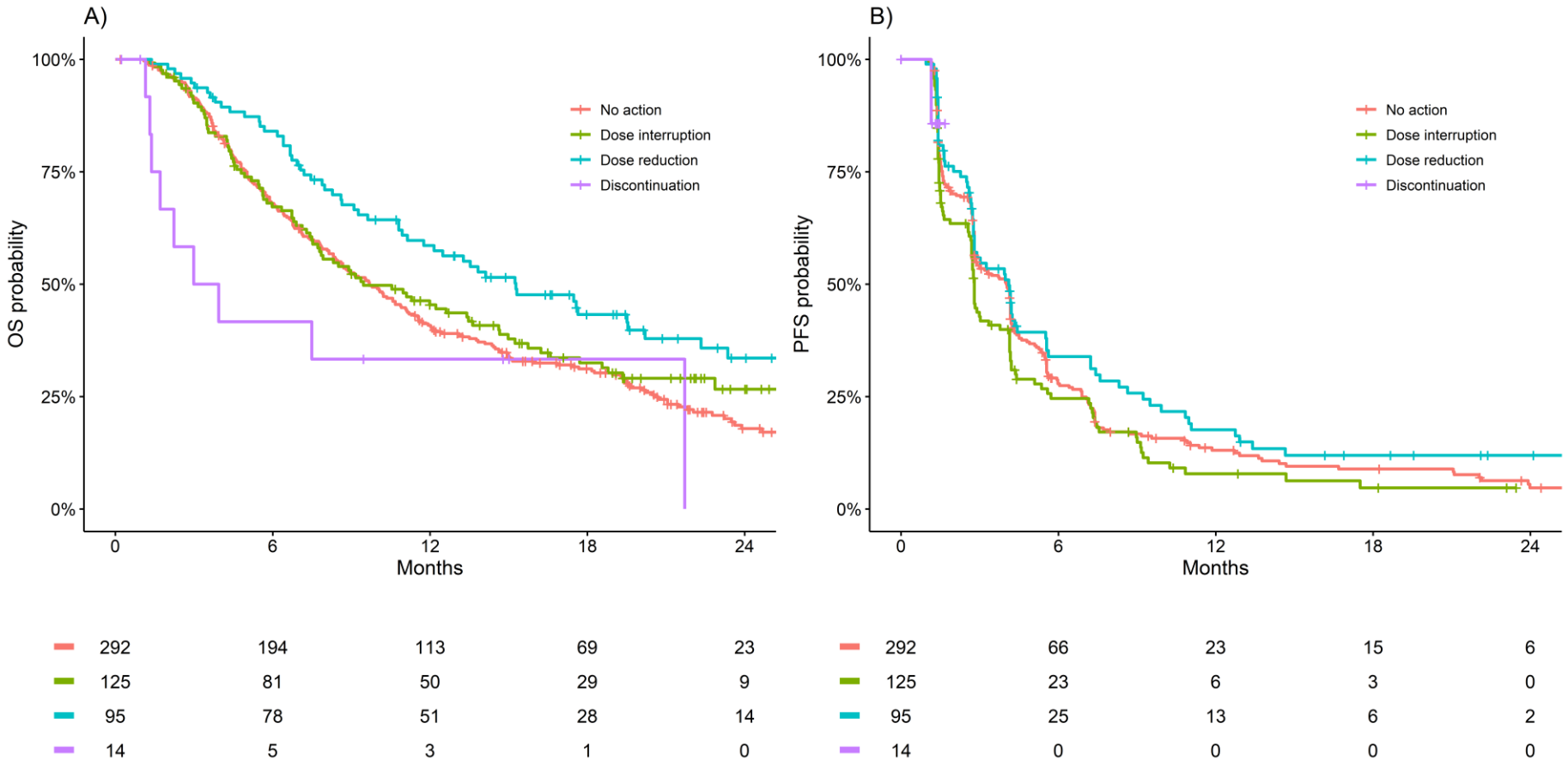

Figure 25 – Kaplan-Meier estimates of OS (A) and PFS (B) by AE induced dose adjustment category within the first 28 days of sorafenib therapy.

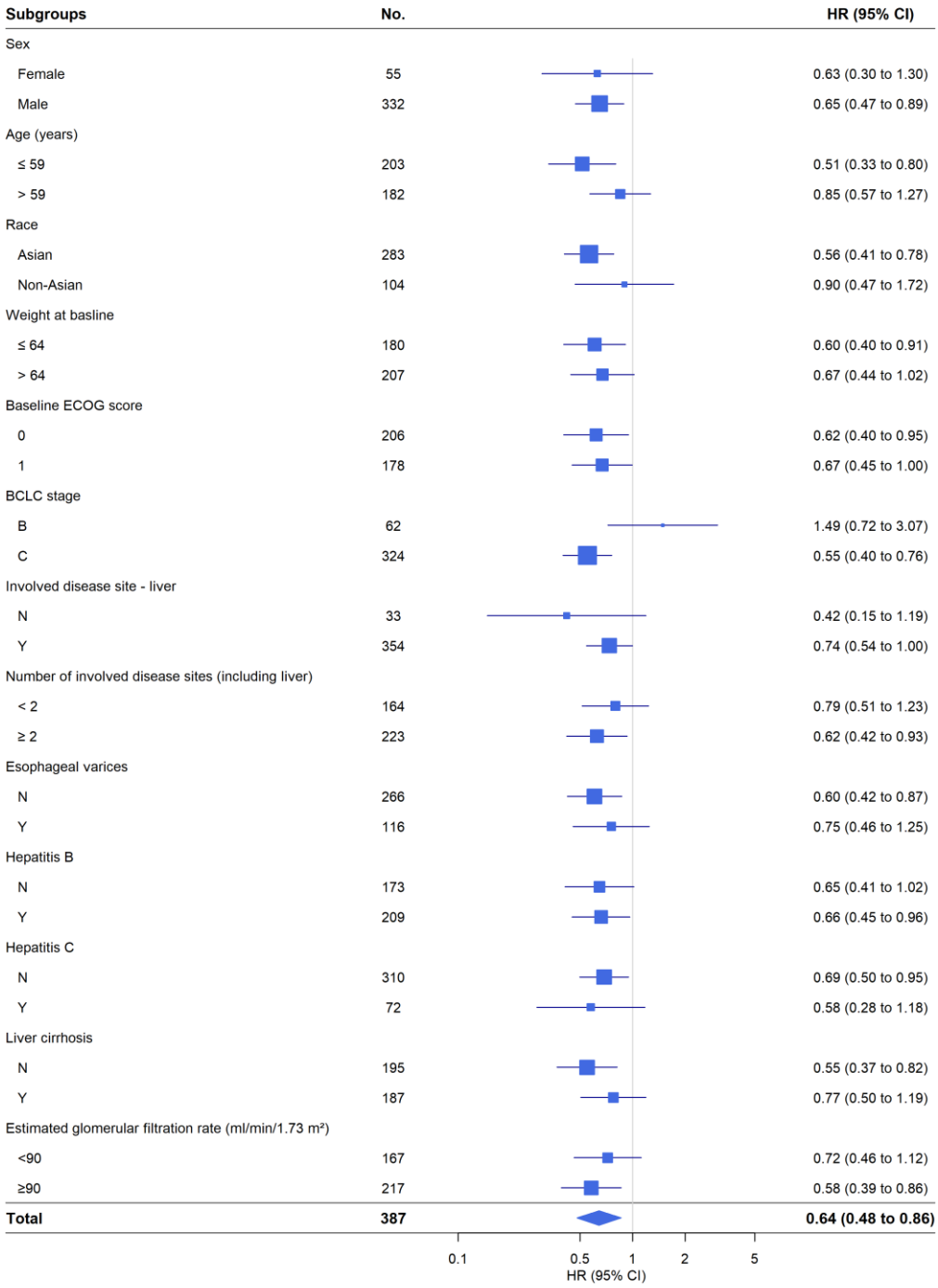

Figure 26 – Forest plot summary (HR 95%CI) of OS by patient subgroups for dose reductions versus no action in the first 28 days of sorafenib treatment.

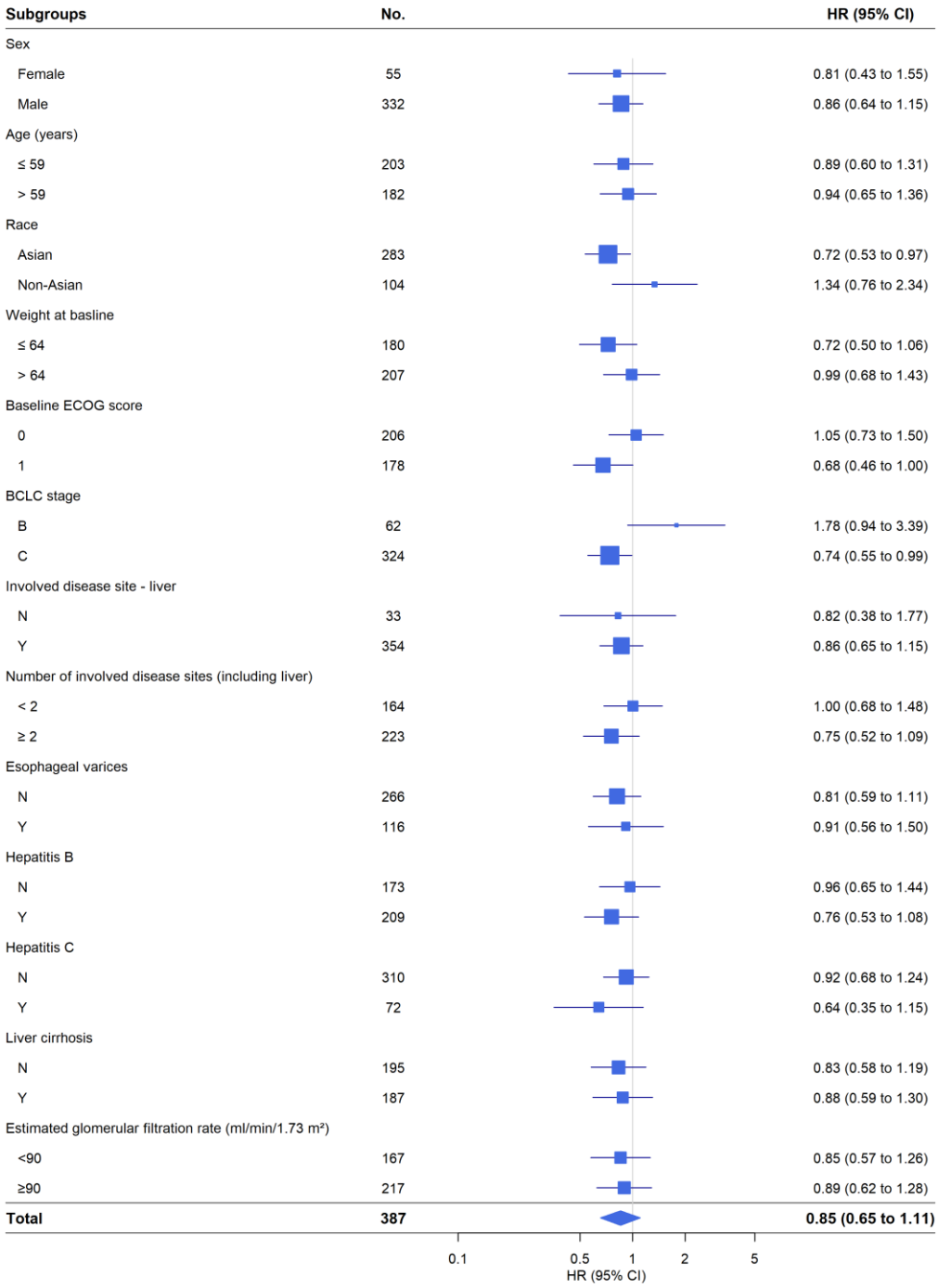

Figure 27 – Forest plot summary (HR 95%CI) of PFS by patient subgroups for dose reductions versus no action in the first 28 days of sorafenib treatment.

2.4.4 – Supplementary analyses

Higher sorafenib dose intensity (≥50 % vs <50 %) over the first 28 days was associated with less favourable OS (HR [95% CI]; 1.4 [1.0 - 1.9], P = 0.035), however, there was no significant association with PFS (HR [95% CI]; 1.0 [0.8 - 1.4], P = 0.775) (**Table 10**). Hand-foot syndrome in the first 28 days of sorafenib therapy was associated with favourable OS (HR [95% CI]; 0.9 [0.8 - 0.9], P = 0.005) but not PFS (HR [95% CI]; 1.0 [0.9 - 1.1], P = 0.785).

Table 10. Association between RDI in first 28 days of sorafenib treatment with OS and PFS.

			OS			PFS	
RDI within first 28 days	N	Median time to event (days)	HR [95% CI]	P	Median time to event (days)	HR [95% CI]	P
< 50 %	79	465	1	0.035	88	1	0.775
≥ 50 %	447	298	1.4 [1.0 – 1.9]		105	1.0 [0.8 – 1.4]	

N - sample size, CI - confidence interval, HR - hazard ratio, OS - overall survival, PFS - progression-free survival

2.5 – Discussion

To the best of the authors knowledge, this is the first study to report on the effects of dose adjustment of sorafenib due to AEs on survival outcomes of advanced HCC patients. Our analysis showed that dose adjustments were not associated with worse survival outcomes. In addition, patients who experienced dose reduction due to AEs within the first 28 days of therapy had more favourable OS compared to patients who required no dose adjustments.

The precision dosing of cancer medicines requires evidence to inform the effect of dose changes on cancer patient outcomes. This information is currently lacking for sorafenib use in advanced HCC. Several studies have explored alternate dosing strategies for sorafenib [158, 159]. A retrospective study assessed initiating sorafenib at < 800 mg daily, identifying non-inferior outcomes compared to 800 mg daily [158]. Meanwhile, dose escalation above 800 mg daily has been observed to improve survival in a subset of patients [159]. The current recommended dosing strategy of sorafenib in HCC is 800 mg daily, with dose reduction in response to AEs. In this study, HCC patients initiated sorafenib at 800 mg daily and dose interruptions and reductions in response to toxicity were not observed to worsen survival outcomes, in fact, patients who required a dose reduction had favourable OS. Such evidence provides strong support for the current dosing guidelines of sorafenib in HCC. Thus, our study highlights a need for caution when investigating lower than recommended initial doses –there is the potential that high initial doses/plasma concentrations ultimately drive long term benefits. In addition, this study supports

future investigations of dose escalation strategies in patients who have not experienced AEs, as a mechanism to improve survival in patient who have not required a dose adjustment.

A finding that sorafenib dose adjustments due to AEs are not associated with worse survival outcomes is not surprising. Similar results have been shown for other targeted cancer medicines including vemurafenib, afatinib and ado-trastuzumab emtansine [160-162]. In part, this is due to AEs potentially reflecting a subgroup of patients with high plasma concentrations or patients more pharmacodynamically sensitive to the medicine – particularly where AE reflects an 'on-target' toxicity. Supporting the findings of this study, prior research has demonstrated a concentration-effect relationship for sorafenib and that the early occurrence of hand-foot syndrome and diarrhoea with sorafenib may be associated with improved survival outcomes [105, 163, 164]. A similar association between the occurrence of hand-foot syndrome in the first 28 days of sorafenib therapy with favourable OS was observed in this study on supplementary analysis.

In this study it was identified that older age, Asian race, lower weight, history of hepatitis C infection, and absence of liver metastases were associated with increased dose adjustments of sorafenib due to AEs. Such evidence provides support for subgroups of patients who require increased monitoring to minimise the negative quality of life impacts of AEs which ultimately require dose adjustments.

This study used large high-quality data, consistent with contemporary practice. A landmark approach was utilised to avoid potential time biases. Furthermore, the landmark time of 28 days is an early time to provide functional information for clinical decisions, while capturing a significant of portion of required dose adjustments. Another significant strength of the study was that the association between dose reductions and favourable OS was consistent with supplementary analysis of sorafenib dose intensity and findings across patient subgroups (**Figure 26**). Variability in associations of sorafenib dose adjustment with OS/PFS were identified, this may be due to PFS being an imperfect surrogate affected by variability in timing of assessments, investigators and measurement biases [165, 166]. Further OS associations may be confounded by subsequent therapies or crossover [165, 166]. Nonetheless dose adjustment of sorafenib due to AEs did not worsen PFS or OS. Thus, both endpoints are in concordance with supporting current dosing guidelines.

In conclusion, dose adjustment of sorafenib due to AEs did not compromise the survival outcomes of advanced HCC patients, with dose reduction associated with improved OS. Further, older age, Asian race, lower weight, history of hepatitis C infection, and absence of liver metastases were associated with an increased risk of experiencing an AEs requiring a sorafenib dose adjustment. Such evidence provides support for the current dosing guidelines of sorafenib in advanced HCC, and an indication of subgroups who require increased monitoring to minimise the potential quality of life impacts of AEs.

CHAPTER 3: THE EFFECT OF PROTON PUMP INHIBITORS ON SURVIVAL OUTCOMES IN ADVANCED HEPATOCELLULAR CARCINOMA TREATED WITH SORAFENIB.

3.1 – Function of Chapter

Chapter 2 demonstrated the significance of 'on-target' toxicity led to the adjustment of dose intensity of sorafenib in advanced HCC patients, which resulted in no poorer survival outcomes. Thus, it was an exceptional example of the crucial function of precision dosing in cancer medicine.

The current chapter of this thesis centred around the aspect of the effect of concomitant medicines on the clinical outcomes derived from sorafenib. The concomitant medicine that was primarily investigated in the study was the class of proton pump inhibitors (PPIs). The previous literature suggested that concomitantly use PPIs with tyrosine kinase inhibitors (TKIs), a class of drug that sorafenib belong to, resulting in reduced clinical outcomes derived from TKIs. Herein, the effect of PPIs on the survival outcomes of sorafenib was explicitly analysed. This thesis chapter has been reviewed and published in full as:

Ruanglertboon, W., Sorich, M.J., Logan, J.M. et al. The effect of proton pump inhibitors on survival outcomes in advanced hepatocellular carcinoma treated with sorafenib. J Cancer Res Clin Oncol ***146,*** *2693–2697 (2020).*

The chapter has been reproduced for this thesis with kind permission from Journal of Cancer Research and Clinical Oncology (License ID 5131100971819) in **Appendix 6**. Formatting and minor changes in wording have been made to conform to the remainder of this thesis.

3.2 – Introduction

Sorafenib is an oral tyrosine kinase inhibitor (TKIs) and the current mainstay first-line treatment for advanced hepatocellular carcinoma (HCC) [167]. Sorafenib acts as a potent inhibitor of vascular endothelial growth factor (VEGFR) subtype 1, 2 and 3, platelet-derived growth factor-beta (PDGFRβ) and fibroblast growth factor receptor 1 (FGFR1) [101, 102].

Recently, clinical studies reported a high degree of inter-individual variability in the pharmacokinetic profile of sorafenib [168]. It is suggested that sorafenib has a limited absorption capacity in the gastrointestinal (GI) tract due to its low solubility profile. In addition, sorafenib's oral bioavailability may be limited by factors that increase intragastric pH, which resultantly decrease the solubility and potentially lower the fraction of sorafenib absorbed from the gastrointestinal tract (f_a) [50].

In clinical practice, cancer patients often take both cancer and non-cancer medicines. Medicines for chronic diseases such as metabolic syndromes and acid-lowering agents being among the most reportedly used non-cancer medicines in cancer patients [47, 48]. A current hypothesis is that concurrent proton pump inhibitor (PPI) administration may reduce the bioavailability of oral TKIs, particularly those with dissolution profiles sensitive to pH changes [168-170]. Recent research indicates that PPIs may impact the survival of cancer patients treated with gefitinib [171] and erlotinib [40]. Further, Sharma et al. [50] indicated that PPIs may impact TKIs as a class, albeit the data was dominated by lung cancer patients treated with erlotinib. However, the efficacy and dissolution profile of all TKIs are not the same and to date there has been no large high-quality analysis to investigate the impact of PPI use on the survival outcomes of advanced HCC patients treated with sorafenib.

Thus, using individual-participant data from the phase III clinical trial NCT00699374, this study aimed to evaluate the impact of PPI use on the survival outcomes of advanced HCC patients initiating sorafenib treatment.

3.3 – Methods

3.3.1 – Patient population

The study was a secondary analysis of the phase III clinical trial NCT00699374 (sorafenib arm only) [154]. Participants were assigned to receive sorafenib at 400 mg twice daily on 4-week cycles for the treatment of locally advanced or metastatic HCC.

Individual-participant data (IPD) were accessed in this study via www.projectdatasphere.org. Secondary analysis of anonymized IPD was deemed negligible risk research by the Southern Adelaide Local Health Network, Office for Research and Ethics and was exempt from review.

3.3.2 – Predictors and outcomes

The primary assessed outcome was overall survival (OS), with progression-free survival (PFS) assessed as the secondary outcome. PFS was evaluated according to Response Evaluation Criteria in Solid Tumours (RECIST) version 1.0 [155]. PPI use at the time of sorafenib commencement (baseline) was assessed as the primary covariate. Baseline PPI use was the focus, as PPIs are commonly used for extended time periods.

Available pre-treatment characteristic data included age, sex, weight, race, Eastern Cooperative Oncology Group performance status (ECOG PS), number of metastatic sites, alpha-fetoprotein (AFP), neutrophil to lymphocyte ratio, Barcelona clinic liver cancer stage (BCLC), sum of longest diameter of target lesions, history of hepatitis B or C infection, history of alcohol abuse, liver cirrhosis, oesophageal varices, portal vein thrombosis, non-alcoholic steatohepatitis, serum haemoglobin and gamma glutamyl transferase concentrations.

3.4 – Statistical analysis

Cox proportional hazard analysis was used to evaluate the association between baseline PPI use and OS/PFS. Associations were reported as hazard ratios (HR) with 95% confidence intervals (95% CI) and probability (P) values. Univariable and analyses adjusted for known prognostic factors were conducted. Complete case analyses were conducted. Kaplan-Meier analysis was used to estimate and plot survival outcomes. Statistical analyses were performed using R version 3.5.

3.5 – Results

3.5.1 – Patient characteristics

There were 542 patients with advanced HCC who received sorafenib in the clinical trial, 122 patients were concomitantly using a PPI at baseline. A summary of patient characteristics is presented in **Table 11**. Median follow-up in the population was 22 [95% CI: 21-24] months.

Of the 122 using a PPI at baseline, 34 were using esomeprazole, 19 lansoprazole, 22 omeprazole, 28 pantoprazole and 19 rabeprazole. The indications for PPI use were ulcers (n = 37), gastritis (n = 36), gastroesophageal reflux disease (n = 20) and others (n = 29). Of the 122 using a PPI at baseline, 81 used PPI therapy for the entire period of receiving sorafenib treatment. Of the 41 patients who had PPI free periods while on sorafenib, the median [inter-quartile range] number of days on PPI therapy within the first month was 30 [19-30] - an indication that even in these patients PPI use was frequent.

Table 11. Summary of patient characteristics.

	Total (n = 542)	PPI non-users (n = 420)	PPI users (n = 122)
Age (years)			
< 55	192 (35%)	162 (39%)	30 (25%)
55 to 67	182 (34%)	138 (33%)	44 (36%)
≥ 67	166 (31%)	118 (28%)	48 (39%)
Missing	2 (<1%)	2 (<1%)	0 (0%)
Sex			
Female	85 (16%)	65 (15%)	20 (16%)
Male	457 (84%)	355 (85%)	102 (84%)
Weight at baseline	64 (57 - 74)	63 (57 - 73)	67 (58 - 77)
Race			
Asian	417 (77%)	338 (80%)	79 (65%)
Non-Asian	125 (23%)	82 (20%)	43 (35%)
Baseline ECOG score			
0	289 (53%)	217 (52%)	72 (59%)
1	250 (46%)	202 (48%)	48 (39%)
Missing	3 (1%)	1 (<1%)	2 (2%)
Number of involved disease sites (including liver)			
1	223 (41%)	168 (40%)	55 (45%)
2	214 (39%)	172 (41%)	42 (34%)
3	89 (16%)	70 (17%)	19 (16%)
4	16 (3%)	10 (2%)	6 (5%)
Alpha Fetoprotein (mcg/L)			
Median (IQR)	277 (13 - 4000)	328 (15 - 4458)	86 (8 - 2770)
Missing	22 (4%)	16 (4%)	6 (5%)
Neutrophil to lymphocyte ratio at baseline (10^9/L)			
Median (IQR)	2.6 (1.9 - 3.9)	2.5 (1.8 - 3.9)	3.0 (2.0 - 3.9)
Missing	14 (2.6%)	9 (2.1%)	5 (4.1%)
BCLC stage			
B	89 (16%)	64 (15%)	25 (20%)
C	452 (83%)	356 (85%)	96 (79%)
Missing	1 (<1%)	0 (0%)	1 (1%)
Sum of longest diameter of target lesion at baseline			
Median (IQR)	108 (56 - 170)	100 (51 - 160)	127 (76 - 192)
Missing	6 (1%)	3 (1%)	3 (2%)
Hepatitis B			
Yes	287 (53%)	241 (57%)	46 (38%)
No	245 (45%)	170 (40%)	75 (61%)
Missing	10 (2%)	9 (2%)	1 (1%)
Hepatitis C			
Yes	118 (22%)	81 (19%)	37 (30%)
No	414 (76%)	330 (79%)	84 (69%)
Missing	10 (2%)	9 (2%)	1 (1%)
Alcohol abuse			
Yes	81 (15%)	56 (13%)	25 (20%)
No	451 (83%)	355 (85%)	96 (79%)
Missing	10 (2%)	9 (2%)	1 (1%)
Liver cirrhosis			
Yes	247 (46%)	188 (45%)	59 (48%)
No	285 (53%)	223 (53%)	62 (51%)
Missing	10 (2%)	9 (2%)	1 (1%)
Portal vein thrombosis			
Yes	161 (30%)	122 (29%)	39 (32%)
No	371 (68%)	289 (69%)	82 (67%)
Missing	10 (2%)	9 (2%)	1 (1%)
Oesophageal varices			
Yes	156 (29%)	114 (27%)	42 (34%)

No	376 (69%)	297 (71%)	79 (65%)
Missing	10 (2%)	9 (2%)	1 (1%)
Non-alcoholic steatohepatitis			
Yes	16 (3%)	11 (3%)	5 (4%)
No	516 (95%)	400 (95%)	116 (95%)
Missing	10 (2%)	9 (2%)	1 (1%)
Haemoglobin (g/L)	133 (122 - 146)	134 (123 - 147)	131 (118 - 141)
Gamma Glutamyl Transferase (U/L)			
Median (IQR)	130 (62 - 250)	124 (60 - 250)	148 (72 - 252)
Missing	7 (1%)	7 (2%)	0 (0%)

3.5.2 – The effect of concomitant use of sorafenib and PPI on survival outcomes

On univariable analysis, there were no associations between baseline PPI use and OS (HR [95%CI]; 1.01 [0.80 - 1.28], P = 0.93) nor PFS (0.96 [0.76 - 1.21], P = 0.73) in advanced HCC initiated on sorafenib (**Table 12, Figure 28**). Further on adjusted analysis, no significant association with OS (1.10 [0.82-1.41], P = 0.62) nor PFS (1.11 [0.86 – 1.44], P = 0.41) was identified (**Table 12**).

Table 12. Summary of association between baseline PPI use status and survival outcomes.

			Univariable			**Adjusted***	
	PPI	**n**	**HR (95% CI)**	**P**	**n**	**HR (95% CI)**	**P**
OS	No	420	1.00	0.93	377	1.00	0.62
	Yes	122	1.01 (0.80 - 1.28)		105	1.10 (0.82 - 1.41)	
PFS	No	420	1.00	0.73	377	1.00	0.41
	Yes	122	0.96 (0.76 - 1.21)		105	1.11 (0.86 – 1.44)	

CI = confidence interval, HR = hazard ratio, n = number of subjects

*Analysis adjusted for age, sex, weight, race, baseline ECOG, number of metastatic site, baseline AFP, neutrophil to lymphocyte ratio, baseline BCLC, sum of longest diameter of target lesion at baseline, history of hepatitis B or C infection, history of alcohol abuse, liver cirrhosis, oesophageal varices, portal vein thrombosis, non-alcoholic steatohepatitis, baseline haemoglobin, baseline gamma glutamyl transferase

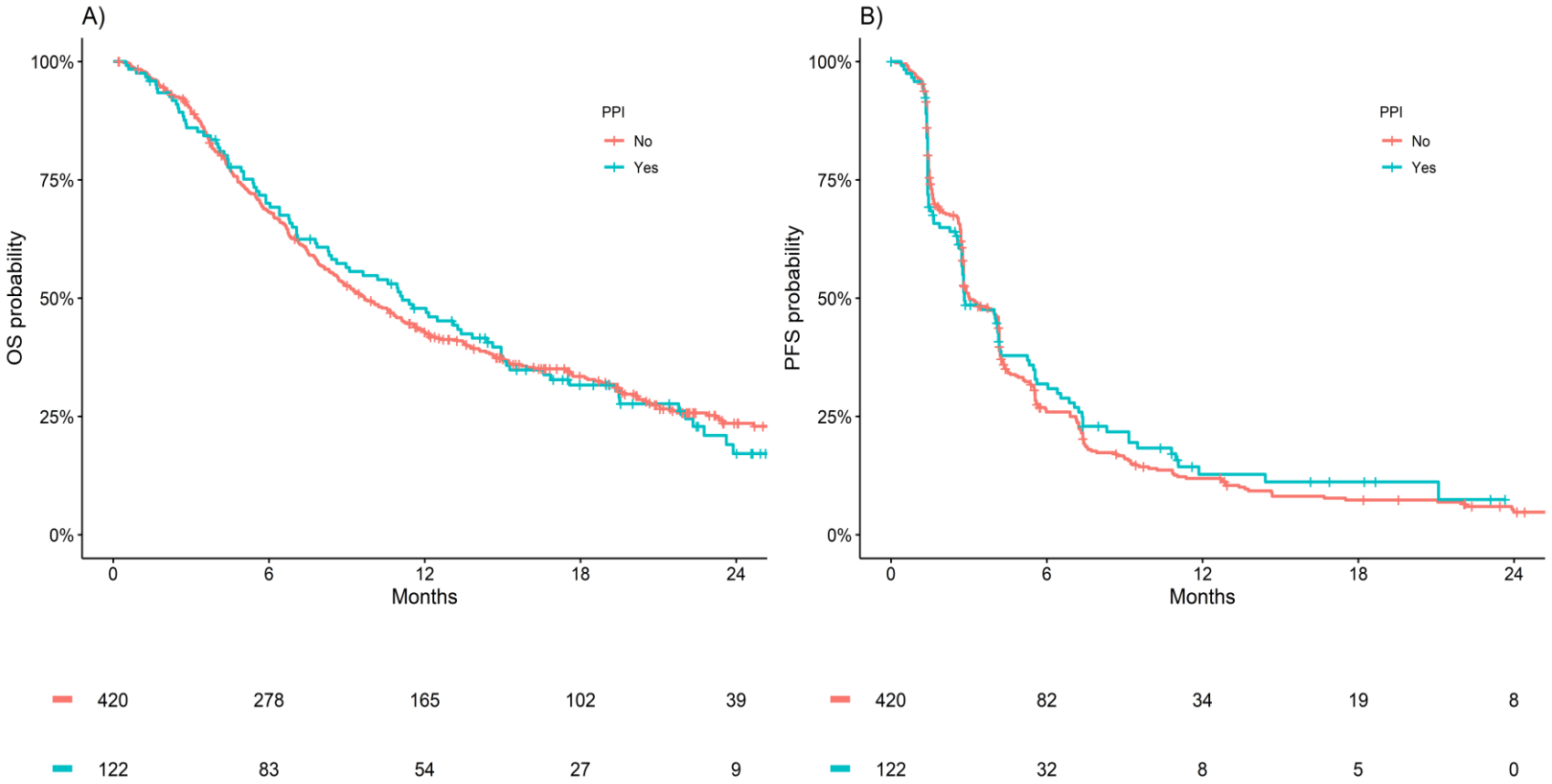

Figure 28 – Kaplan-Meier estimates of OS (A) and PFS (B) by PPI status.

3.6 – Discussion

Orally administered cancer medicines can be affected pharmacokinetically or pharmacodynamically by other co-administered drugs. For example, rifampicin which is a potent CYP3A4 inducer, reduces the area under the curve (AUC) and C_{max} of sunitinib exposure by 23 and 46 %, respectively [40, 172]. Similarly, it is mechanistically rationalised that PPIs irreversibly bind to the H^+/K^+-ATPase pumps altering intragastric pH from being highly acidic (pH = 1 - 4) to less acidic (pH > 6), thus potentially reducing gastrointestinal dissolution and absorption of oral TKIs [40]. It is further hypothesised that this effect may be unfavourable to the survival outcomes achieved with TKIs, which require an acidic environment for intestinal absorption. However, the potential impact of PPIs on outcomes of advanced HCC patients treated with sorafenib has been minimally explored. Here, we highlighted that concomitant PPI use with sorafenib in advanced HCC patients was not associated with altered survival outcomes.

To date, there has been preliminary research on the effect of PPIs on the therapeutic outcomes associated with TKIs. For example, Sharma et al. [50] conducted a pooled analysis of Surveillance, Epidemiology, and End Results (SEER)-Medicare database indicating that concomitant PPI use with a TKI was associated with an increased risk of death. However, the dissolution and pharmacodynamic profiles of all TKIs are not the same. Thus, while Sharma et al. [50] indicated PPI use was associated with negative outcomes for TKIs and specifically erlotinib (the majority of the population) – no effects on imatinib or sunitinib were identified and the associations for sorafenib were not presented. Thus, to the best of our knowledge the present study is the largest analysis of the association between concomitant PPI use and survival outcomes of advanced HCC patients treated with sorafenib – of which no association with altered survival outcomes were identified. These results are similar to the Lalani et al. [173] study which found no association between PPI use and survival outcomes in a pooled cohort of renal cell carcinoma (RCC) patients, treated with sorafenib, sunitinib or axitinib.

While a post-hoc analysis, the data used in this study was large high-quality data collected within clinical trial and the dosing strategy assessed is consistent with contemporary practice. Another strength of this study is the result of no association between concomitant PPI use and sorafenib outcomes was demonstrated for both OS and PFS (on univariable and adjusted analysis). It is acknowledged that Child-Pugh class A, ECOG PS of 0 or 1 and adequate organ function were inclusion criteria, and the presence of clinically relevant ascites was an exclusion criteria of NCT00699374 [154]. A notable limitation was an inability to assess the type, dose or compliance to the documented PPI use. Nonetheless, at least 80 % of those using a PPI at baseline did so for a condition requiring long term treatment. Future research will aim to confirm if the results are consistent between specific PPIs and if the non-association extends to other acid lowering agents such as H2 receptor antagonists. A limitation

of this study is the restricted range of settings evaluated. Future research should include the evaluation of sorafenib used for advanced RCC and its use in other lines of therapy.

3.7 – Conclusions

The concomitant use of a PPI with sorafenib in advanced HCC patients was not associated with altered survival outcomes. Our analysis further shows the importance of assessing the impact of PPIs on TKIs on a per medicine basis as the dissolution and pharmacokinetic profile of all TKIs are not the same.

CHAPTER 4: MECHANISTIC MODELLING IDENFIFIES AND ADDRESSES THE RISKS OF EMPIRIC CONCENTRATION GUIDED SORAFENIB DOSING

4.1 – Function of Chapter

Chapter 2 and **3** utilised the secondary analysis of "Big data" to demonstrate the importance of precision medicine. Big data analysis is one of the contemporary research in the modern era, which could potentially support decision-making in real-world practices. On the other hand, computational modelling and simulation have seen increases in applications, including pharmacological research.

In terms of precision medicine, computational simulation has already been implied to support decision making in clinical practice, especially for the drugs or conditions that require meticulous consideration such as sorafenib [174-177]. Currently, the knowledge of the optimal therapeutic index of sorafenib plasma concentration is minimal. The evidence regarding the minimum effective concentration and minimum toxicity concentration were taken from only small cohorts. As such, this chapter aimed to apply computer simulation to evaluate the capability of concentration-guided sorafenib dose adjustment, with and without model-informed drug dosing, to increase the proportion of patients that achieve the designated plasma concentration. This thesis chapter has been reviewed and published in full as:

Ruanglertboon, W.; Sorich, J M.; Hopkins M A.; Rowland A., Mechanistic modelling identifies and addresses the risks of empiric concentration guided sorafenib dosing. Pharmaceuticals 2021, 14(5), 389; https://doi.org/10.3390/ph14050389.

Formatting and minor changes in wording have been made to conform to the remainder of this thesis.

4.2 – Introduction

Sorafenib is an orally administered small molecule kinase inhibitor (KI) used in the treatment of advanced hepatocellular (HCC) and renal cell (RCC) carcinomas. Sorafenib is a potent inhibitor of multiple kinase receptors including the vascular endothelial growth factor receptor (VEGFR), endothelial growth factor (subtype 1, 2 and 3), platelet-derived growth factor-beta (PDGFRβ) and fibroblast growth factor receptor 1 (FGFR1). Variability in sorafenib exposure between individuals and within an individual over time has been identified as a potential source of heterogeneity in treatment efficacy and tolerability [178, 179]. The area under the plasma concentration curve (AUC) and maximal concentration (C_{max}) for sorafenib following has been reported to vary more than 50 % with standard 400 mg dosing [180-182]. Variability in gastrointestinal absorption due to limited and pH dependent solubility has been proposed as a major source of variability in exposure [183], however concomitant proton pump inhibitor (PPI) use, which is reported to reduce KI absorption [50], has been demonstrated to have no impact on survival outcomes in HCC [184] and RCC [173, 185] patients treated with sorafenib.

A sorafenib $C_{max} \geq 4.78$ μg/mL has been associated with superior overall survival in RCC and HCC patients, albeit with a higher incidence of hypertension, while a sorafenib $C_{max} \geq 5.78$ μg/mL has been associated with an increased incidence of grade II toxicity, the most common of which is hand foot skin reactions [186, 187]. While the evidence for these thresholds is derived from a single observational study in 52 individuals, these values have been cited as target concentrations in multiple reviews addressing individualised sorafenib dosing [188, 189]. The dose escalation protocol that has been proposed for sorafenib to increase from 400 mg to 600 mg twice daily [190]. This approach is based on a sub-analysis of a phase II trial demonstrating a clinical benefit in patients who increased from 400 mg to 600 mg sorafenib twice daily following disease progression at the 400 mg dose [191]. Notably the association of this dose escalation with sorafenib plasma concentration has not been evaluated.

The potential benefits of individualised KI dosing has gained interest in recent years [11, 192, 193] and a number of strategies available to both inform initial dose selection and facilitate dose adaption [13]. Therapeutic drug monitoring (TDM) is an established method to facilitate concentration-guided dose adaption but requires significant clinical and analytical resources to quantify the drug of interest and establish a robust evidence base. To date, few cancer medicines have met the level of evidence required to implement TDM in a clinical setting [194-196].

Model-informed initial dose selection (MIDS), often underpinned by a population pharmacokinetic (Pop-PK) or physiologically-based pharmacokinetic (PBPK) model, has emerged as a strategy to assist initial dose selection either to complement or replace TDM [197-200]. PBPK modelling and simulation is an established tool in drug discovery and development, where it is used to predict factors affecting PK and support the design of clinical trials [201, 202]. PBPK is a “bottom-up” approach whereby the

concentration-time profile of a drug is simulated based on physiochemical and *in vitro* data [203, 204]. Novel clinical applications for PBPK have been proposed involving the prediction of clinical drug-drug interactions, identification of physiological covariates impacting drug exposure and informing initial dose selection [198, 204-206].

The primary objective of this study was evaluated the capacity of concentration-guided sorafenib dose adjustment, with and without MIDS, to increase the proportion of patients that achieve a sorafenib C_{max} within a concentration range of 4.78 to 5.78 μg/mL. A full body PBPK model for sorafenib was first developed and validated, then used to identify physiological and molecular covariates associated with between subject variability in sorafenib exposure.

4.2 – Methods

4.2.1 – Development and Verification of the sorafenib PBPK model structural model

Sorafenib absorption was simulated using the advanced dissolution, absorption, and metabolism (ADAM) sub-model which incorporates membrane permeability, intestinal metabolism and transporter-mediated uptake and efflux. The ADAM sub-model was used in conjunction with a full-body PBPK model, containing compartments and drug distribution characteristics for all organs. All simulations were performed using Simcyp® (version 19.1, Certara, UK). The differential equations underpinning the model have been described previously [207].

4.2.2 – Development of the sorafenib compound model

The physicochemical, blood binding, absorption, distribution, elimination parameters utilised to construct the sorafenib compound model were summarised in **Table 13**. Physicochemical properties were based on published literature and documents [103, 208]. Metabolism and elimination parameters were incorporated based on reported intersystem extrapolation factor (ISEF) adjusted *in vitro* CYP and UDP-glucuronosyltransferase (UGT) data (**Figure 29**).

Table 13. Model inputs used to build the sorafenib compound model.

Parameter	Value	Source
Physicochemical properties		
Molecular weight	464.82 g/mol	[103]
Log $P_{o:w}$	4.54	
Hydrogen bond donor	3	[103]
Species	Base	
Protein binding		
B/P	0.55	[103]
f_{up}	0.0048	[103]

Absorption (ADAM model) f_a k_a (L/hr)	 0.99 1.75	 Predicted Predicted
Permeability P_{eff}, man (10^{-4} cm/s) Caco-2 (10^{-6} cm/s)	 4.01 24.1	 Predicted
Formulation Solid formulation	Immediate release	[103]
In vivo pharmacokinetic properties (full PBPK model) Prediction model K_p scalar	 1 0.7	 Predicted
CYP metabolism: ISEF adjusted recombinant enzyme kinetics (CL_{int}; µL/min/pmol CYP3A4	2.6	[209]
UGT metabolism: ISEF adjusted recombinant enzyme kinetics (CL_{int}; µL/min/mg) UGT1A9	20.1	[209]

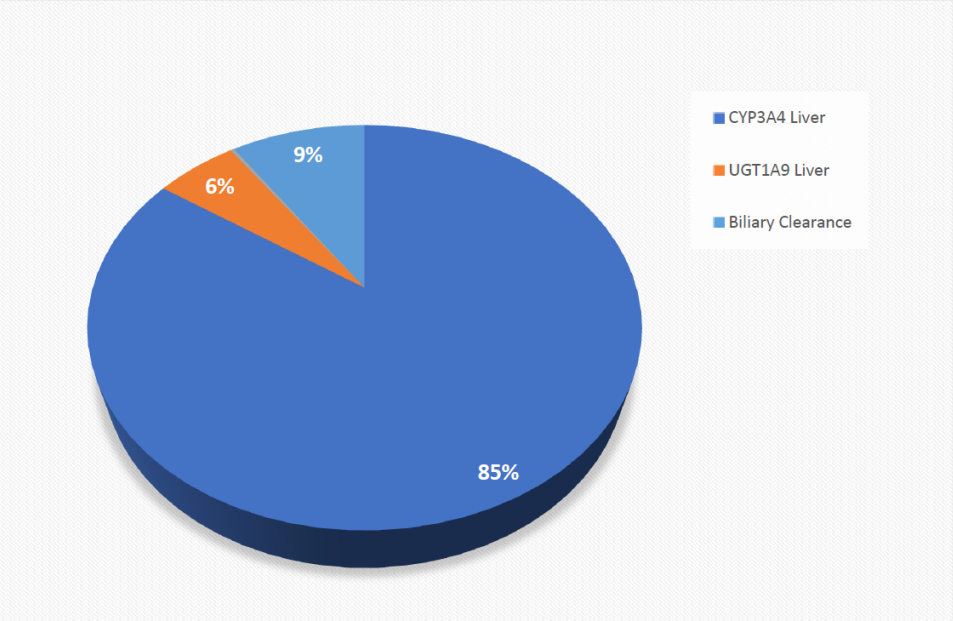

Figure 29 – The pie chart demonstrated the relative contribution of CYP3A4 and UGT1A9 to simulated sorafenib elimination based on the predicted model.

4.2.3 – Population model

As no clinical trials evaluating sorafenib exposure have been performed in healthy volunteers, verification of the sorafenib compound model was performed using Sim-Cancer population cohort. Simulations performed to assess the physiological and molecular characteristics driving between-subject variability in sorafenib exposure at steady state also utilised the Sim-Cancer population cohort. The physiological and pathological characteristics of the Sim-cancer population have been determined based on a meta-analysis of cancer patients enrolled in clinical trials [210].

4.2.4 – Simulated trial designs

During the model development stage, simulations included 10 trials with 10 subjects per trial (100 subjects total). During the verification stage, simulations were performed in 10 trials matched for sample size, dose, age range and sex distribution in the protocol described for the observed trial. Unless specified otherwise, parameters defining sorafenib exposure were assessed over 24 hours following a single dose at 9:00 AM on day 1.

4.2.5 – Validation of the sorafenib compound model

The sorafenib compound model was validated by comparing simulated AUC and C_{max} values to reported observed values from matched clinical trials undertaken in cancer patients. A mean simulated parameter estimated within 2-fold of the mean observed parameter and contained within the 90 % confidence interval for the observed parameter was applied as the criteria to accept the model accuracy. The model goodness-of-fit was further verified by visual inspection of the overlay of mean simulated and observed sorafenib concentration-time profiles from individual clinical trials. Simulated C_{max} values were normalised to account for the mean fold error (MFE) between simulated and observed values determined from multiple dose validation studies when evaluating simulations against the observed target concentration range (4.78 to 5.78 µg/mL).

4.2.6 – Physiological and molecular characteristics driving variability in sorafenib exposure

The validated sorafenib compound model was used to evaluate associations between physiological and molecular covariates and steady-state sorafenib AUC and C_{max} [197]. A trial comprising 1,000 subjects from the Sim-Cancer population was simulated over 15 days with 400 mg of sorafenib administered orally in a fasted-state every 12 hour for 14 days starting at 9:00 am on Day 1. The steady state sorafenib AUC was determined over 12 hours following the final dose of sorafenib at 9:00 pm on Day 14. The

steady state sorafenib C_{max} was determined as the maximum concentration following the final dose at 9:00 PM on Day 14.

Associations between physiological and molecular characteristics and sorafenib log transformed AUC and C_{max} were evaluated by univariate and multivariate linear regression. Continuous variables were checked for normality and non-linearity of association, sex was coded as a binary variable. A multivariable linear regression model to predict the log transformed sorafenib C_{max} was developed by stepwise forward inclusion of individually significant characteristics identified in the univariable regression analysis based on a probability of F to enter ≤ 0.05. The multivariable model (MIDS) predicted C_{max} was determined by back transformation of the model predicted log transformed C_{max}. The capacity of MIDS to identify subjects with a sub-therapeutic simulated sorafenib C_{max} determined by scaling the reported threshold for simulation accuracy was evaluated using classification matrix analysis and is summarised as model sensitivity and specificity. The predictive performance of MIDS was assessed by receiver operating characteristic curve (ROC) analysis. Statistical analysis was conducted using R version 4.0.2 and IBM SPSS Statistics for Windows version 23 (Release 2015, IBM, Armonk, NY).

4.2.7 – Impact of dose individualisation

A simulation was conducted to evaluate the capacity of concentration-guided sorafenib dose adjustment to achieve a steady state sorafenib C_{max} within the range 4.78 to 5.78 µg/mL. Sorafenib exposure was simulated in a cohort of 500 subjects from the Sim-Cancer population (20 to 50 years old, 50 % female) over 14 days with 400 mg sorafenib administered orally in a fasted-state every 12 hour starting at 9:00 am on Day 1. Sorafenib C_{max} was determined following the final dose at 9:00 pm on Day 14. Sorafenib exposure in subjects who failed to achieve a Day 14 normalised simulated $C_{max} \geq 4.78$ µg/mL was simulated over an additional 14 days with sorafenib administered at a dose of 600 mg every 12 hour starting at 9:00 am on Day 15. The post dose adjustment sorafenib C_{max} was determined following the final dose at 9:00 pm on Day 28.

A simulation was conducted in the same cohort to evaluate the benefit of MIDS at baseline in conjunction with concentration-guided sorafenib dose adjustment. Demographic characteristics for the Sim-Cancer cohort were used to predict the normalised simulated Day 14 sorafenib C_{max} based on the multivariable model described previously. Based on MIDS subjects with a predicted sorafenib $C_{max} \geq 4.78$ µg/mL received 400 mg sorafenib twice daily, while subjects with predicted sorafenib $C_{max} < 4.78$ µg/mL received 500 mg sorafenib twice daily. Sorafenib exposure was simulated over 28 days as described for concentration-guided sorafenib dose adjustment without MIDS, with C_{max} evaluated at Day 14 and Day 28 and a dose increase to 600 mg between Day 15 and Day 28 for individuals who failed to achieve a Day 14 $C_{max} \geq 4.78$ µg/mL.

4.3 – Results

4.3.1 – Verification of the sorafenib PBPK compound model

The accuracy of the sorafenib compound model was assessed in nineteen age and sex matched cohorts from single or multiple ascending dose (100 to 800 mg) trials. Mean simulated and observed AUC and C_{max} values and the corresponding simulated/observed ratios are presented in **Table 14** along with a summary of the verification trial characteristics (i.e. age range, sex, sample size and dose). The mean (± standard deviation; SD) simulated/observed AUC and C_{max} ratios for the single-dose cohorts (n = 37) were 1.92 (± 1.11) and 1.50 (± 1.7), respectively. The mean (± SD) simulated/observed AUC and C_{max} ratios for the multiple-dose (typically 14 days) cohorts (n = 14) were 1.50 (± 0.72) and 1.17 (± 0.63), respectively. Variability in model performance, indicated by large SD for parameter ratios, was driven by heterogeneity in observed parameters between trials. A representative sorafenib concentration-time profile depicting overlayed with the mean concentration-time profile and 90 % confidence interval (CI) for the observed data was shown in **Figure 30**. The accuracy of the sorafenib compound model was considered acceptable on the basis that mean simulated parameters were within 2-fold of the respective mean observed parameter and contained within the 90 % CI for the observed parameter. Simulated Day 14 and Day 28 sorafenib C_{max} values were divided by 1.17 to account for simulation to observed MFE in multiple dose studies when evaluating simulated parameters against the observed target C_{max} range. Results of sensitivity analyses performed to evaluate the impact of input parameters with measurement uncertainty (CL_{int} for CYP3A4 and UGT1A9 pathways, fraction unbound, B/P ratio and LogP) on sorafenib kinetic parameters are shown in **Figure 31**.

Table 14. Verification of the impact of drug interactions on sorafenib exposure.

Trials	Age (median [range])	Female (%)	Dosing regimen	Trial	C_{max} (mg/L)	AUC (mg/L.hr)
Strumberg D, Clark JW, Awada A et al. [180]	60 [18 - 75]	36 %	Single dose 100 mg (n = 3)	Observe	2.69	83.80
				Simulated	0.55	6.93
				Ratio	4.89	12.09
			Single dose 400 mg (n = 3)	Observe	3.42	107.00
				Simulated	2.21	27.72
				Ratio	1.55	3.86
			Multiple dose 100 mg (n = 3)	Observe	2.31	23.80
				Simulated	1.42	14.60
				Ratio	1.63	1.63
			Multiple dose 200 mg (n = 3)	Observe	2.84	16.10
				Simulated	2.84	29.20
				Ratio	1.00	0.55
			Multiple dose 400 mg (n = 5)	Observe	9.35	71.70
				Simulated	5.68	58.39
				Ratio	1.65	1.23
			Multiple dose 600 mg (n = 8)	Observe	9.81	79.00
				Simulated	8.53	87.59
				Ratio	1.15	0.90
Minami H, Kawada K, Ebi H et al. [211]	63 [32 - 73]	32 %	Single dose 100 mg (n = 3)	Observe	0.43	9.40
				Simulated	0.53	6.40
				Ratio	0.81	1.47

			Single dose 200 mg (n = 15)	Observe	0.74	24.30
				Simulated	1.12	13.42
				Ratio	0.66	1.81
			Single dose 400 mg (n = 6)	Observe	1.21	35.4
				Simulated	2.11	25.51
				Ratio	0.57	1.39
			Single dose 600 mg (n = 7)	Observe	1.41	40.50
				Simulated	3.13	37.21
				Ratio	0.45	1.09
Awada A, Hendlisz A, Gil T et al. [181]	58 [42 - 79]	43 %	200 mg BID mg (n = 3) Day 1	Observe	3.63	24.90
				Simulated	1.57	8.80
				Ratio	2.31	2.83
			400 mg BID mg (n = 9) Day 1	Observe	3.04	24
				Simulated	3.18	28.17
				Ratio	0.96	0.85
			600 mg BID mg (n = 12) Day 1	Observe	4.56	30.40
				Simulated	4.81	42.65
				Ratio	0.95	0.71
			200 mg BID mg (n = 3) Day 7	Observe	9.01	83.40
				Simulated	3.48	36.20
				Ratio	2.59	2.30
			400 mg BID mg (n = 9) Day 7	Observe	9.90	82.70
				Simulated	6.61	68.79
				Ratio	1.50	1.20

			600 mg BID mg (n = 12) Day 7	Observe	11.50	94.80
				Simulated	10.10	109.72
				Ratio	1.14	0.86
			200 mg BID mg (n = 3) Day 21	Observe	6.33	50.50
				Simulated	4.05	45.57
				Ratio	1.56	1.11
			400 mg BID (n = 5) Day 21	Observe	10	76.50
				Simulated	7.8	87.33
				Ratio	1.28	0.88
			600 mg BID (n = 12) Day 21	Observe	9.24	77
				Simulated	11.36	125.74
				Ratio	0.81	0.61

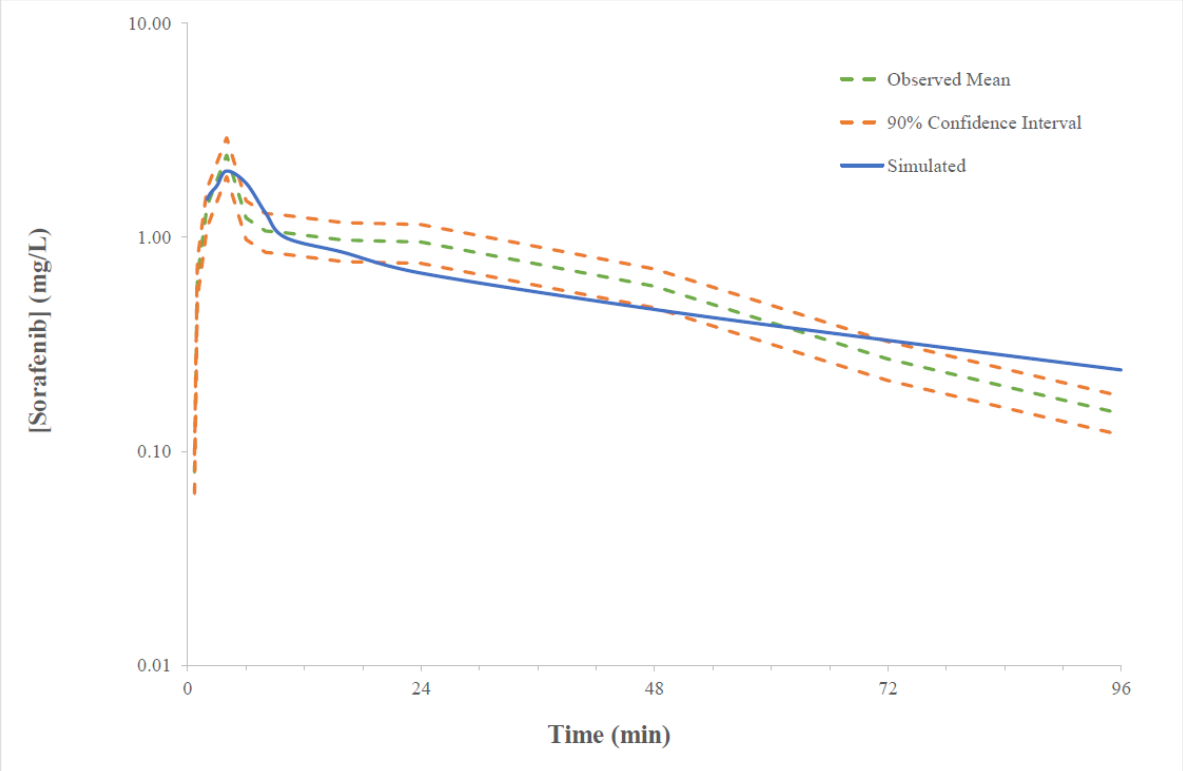

Figure 30 – Representative overlay of simulated and observed (range) plasma concentration time curve of sorafenib (0 - 96 hours) following 400 mg twice a day dosing. Solid blue line represented the mean model predicted exposure, dashed green line represented the mean observed exposure and dashed orange represented minimal and maximal 90% confidence intervals for the observed data.

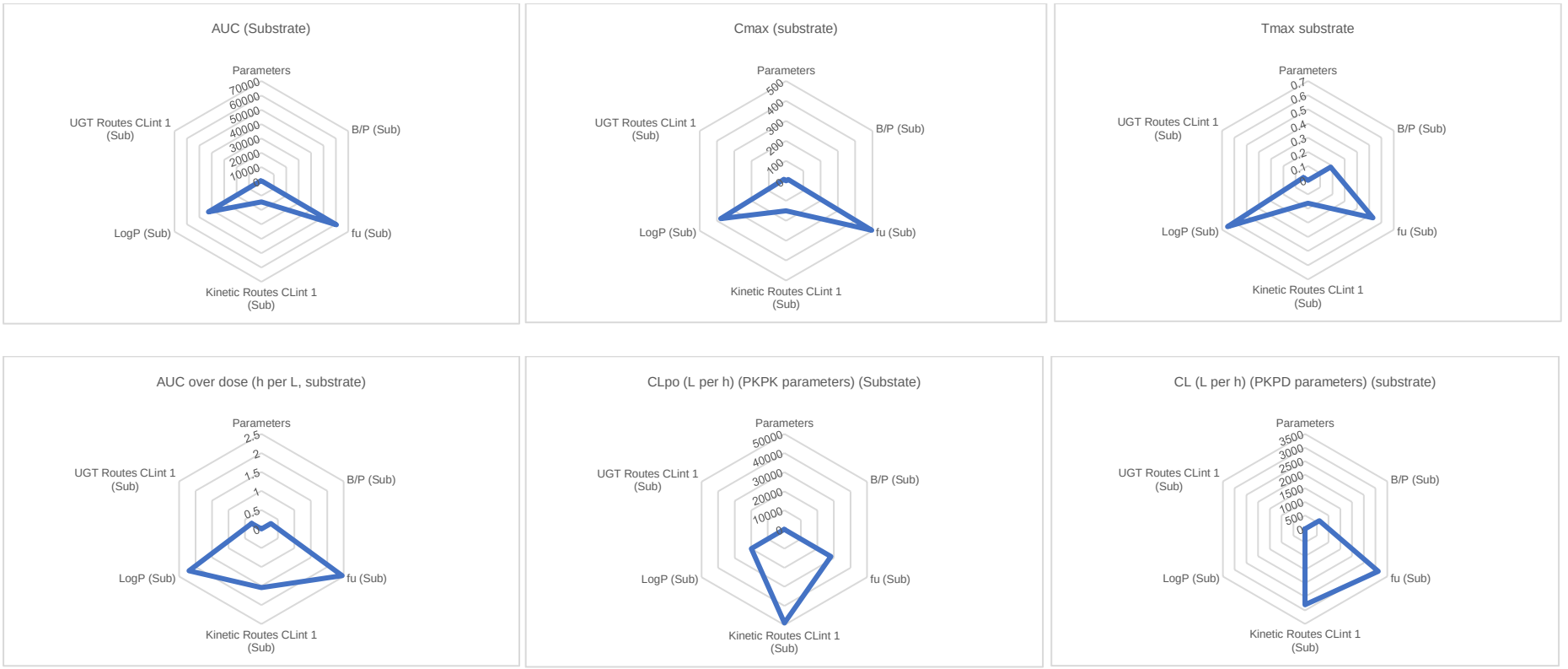

Figure 31 – Sensitivity analysis to evaluate the impact of the compound model input parameter on the simulation outcome (both pharmacokinetic and pharmacodynamic parameters). The relationship between examined parameters and input parameters was provided as a series of subanalyses

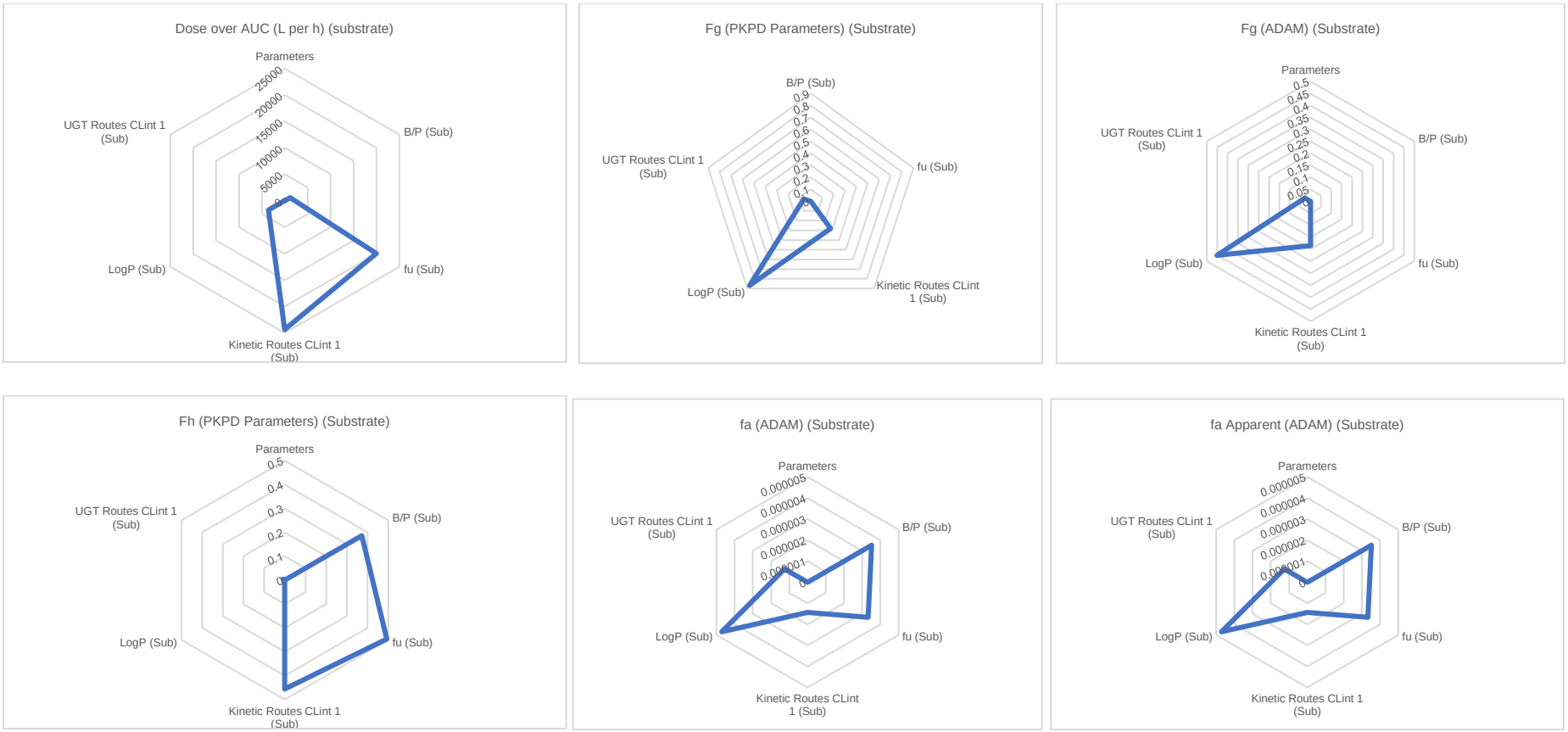

Figure 31 (cont.) – Sensitivity analysis to evaluate the impact of the compound model input parameter on the simulation outcome (both pharmacokinetic and pharmacodynamic parameters). The relationship between examined parameters and input parameters was provided as a series of subanalyses

4.3.2 – Sorafenib exposure in cancer patient

The summary of the mean, SD and range of steady-state sorafenib AUC and C_{max} parameters defining exposure in 1,000 virtual cancer patients is presented in **Table 15**. Consistent with reported clinical trial data [181, 182, 211], the simulation revealed variability of greater than an order of magnitude in sorafenib exposure; the steady state AUC ranged from 22.7 to 270 mg/L.hr (mean 99.2 mg/L.hr), while C_{max} ranged from 2.3 to 23.2 µg/mL (mean 8.9 µg/mL).

Table 15. Summary of physiological and molecular characteristic considered in regression analyses.

Parameter	Mean	Standard Deviation	Range	
			5th centile	95th centile
Sorafenib Exposure				
Steady state C_{max} (mg/L)	8.92	3.35	4.58	15.3
Steady state AUC (mg/L.hr)	99.2	39.6	48.7	176
Physiological Characteristics				
Female (%)	50			
Age (years)	40.4	9.05	22.6	49.6
Weight (kg)	74.6	14.8	53.0	102
Height (cm)	170	9.38	155	184
BMI (kg/m^2)	25.9	4.28	19.8	33.4
Cardiac output (L/hr)	312	38.0	254	381
Haematocrit (%)	38.0	4.86	30.7	46.5
Albumin (g/L)	39.5	7.26	28.9	53.0
GFR ($mL/min/1.73m^2$)	109	24.2	53.3	217
Liver CYP abundance (pmol P450)				
CYP3A4	8523459	4988135	1378085	44856000
Liver UGT abundance (pmol protein)				
UGT1A9	1773543	873240	4051	5530162
Intestinal CYP abundance (pmol P450)				
CYP3A4	64549	38872	9653	322094
Intestinal UGT abundance (pmol protein)				
UGT1A9	16689	11925	1621	63907

Abbreviations: BMI = body mass index, GFR = glomerular filtration rate, CYP = cytochrome P450, UGT = Uridine 5'-diphospho-glucuronosyltransferase.

4.3.3 – Physiological and molecular characteristics driving variability in sorafenib exposure

Univariate logistic regression analysis evaluated correlations between physiological and molecular characteristics and sorafenib steady state C_{max} threshold at > 4.78 mg/L (**Table 16**) in a cohort of 1,000 Sim-Cancer subjects. Statistical analysis of multivariable linear regression with stepwise inclusion of parameters revealed the primary covariates driving variability in sorafenib AUC were hepatic CYP3A4 abundance, albumin concentration, body mass index (BMI), body surface area (BSA), sex and weight (**Figure 32**).

Table 16. Logistic regression analysis of therapeutic C_{max} threshold of > 5.5926 mg/L.

Parameter	OR	95% CI	Regression *p* value	C-statistic
Physiological Characteristics				
Sex (Male/Female)	1.06	0.71 to 1.58	0.792	0.51
Age[#] (years)	1.23	1.00 to 1.52	0.050	0.56
Weight[#] (kg)	0.53	0.46 to 0.61	<0.001	0.76
Height[#] (cm)	0.65	0.53 to 0.81	<0.001	0.61
Body Surface Area (m^2)	0.02	0.01 to 0.04	<0.001	0.74
BMI (kg/m^2)	0.82	0.79 to 0.86	<0.001	0.73
Albumin (g/L)	1.07	1.04 to 1.10	<0.001	0.62
Creatinine (µmol/L)	1.00	0.99 to 1.02	0.636	0.53
GFR[#] ($mL/min/1.73m^2$)	0.13	0.06 to 0.29	<0.001	0.66
CYP3A4 abundance (µmol P450)				
Intestinal	0.16	0.00 to 22.4	0.469	0.5
Hepatic	0.57	0.52 to 0.63	<0.001	0.96
UGT1A9 abundance (µmol P450)				
Intestinal[#]	0.16	0.84 to 1.17	0.903	0.49
Hepatic	0.49	0.40 to 0.61	<0.001	0.69

[#] Age per ten years incremental, weight per 10 kg incremental, height per 10 cm incremental, GFR per 100 ml incremental, intestinal UGT1A9 per 10,000 pmol incremental
OR = odd ratio, CI = confidence interval, BMI = Body Mass Index, GFR = Glomerular filtration rate.

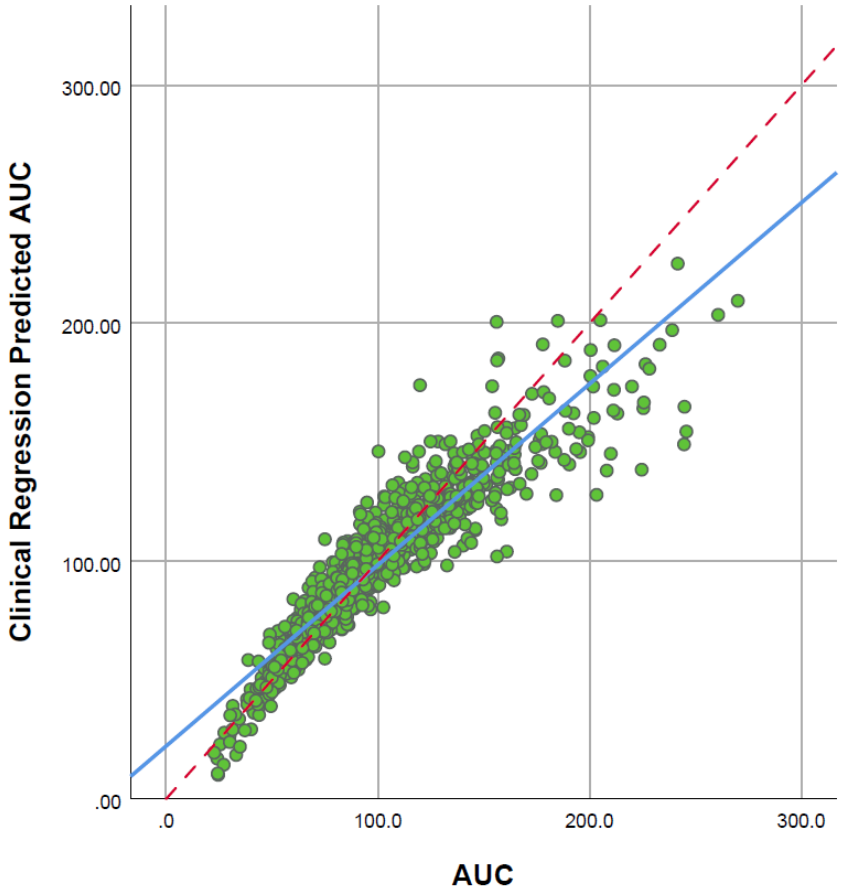

Figure 32 – Correlation of model predicted steady-state sorafenib concentration predicted sorafenib AUC. Blue solid line represents the regression line (model-fitted line) for the model-predicted steady state sorafenib concentration and predicted AUC. Red dash line represents a reference line.

Table 17. Multivariable linear regression model performance characteristics.

Model	R^2	Std. Error of the Estimate	R^2 Change	AUC ROC	AUC ROC change
a	0.631	0.24141	0.631	0.953	0.953
b	0.781	0.18614	0.150	0.981	0.028
c	0.868	0.14458	0.087	0.990	0.009
d	0.873	0.14156	0.006	0.991	0.001
e	0.883	0.13619	0.010	0.991	-
f	0.883	0.13595	0.001	0.991	-

Model predictors (a) hepatic CYP3A4 abundance; (b) hepatic CYP3A4 abundance, albumin concentration; (c) hepatic CYP3A4 abundance, albumin concentration, BMI; (d) hepatic CYP3A4 abundance, albumin concentration, BMI, body surface area; (e) hepatic CYP3A4

abundance, albumin concentration, BMI, body surface area, sex; (f) hepatic CYP3A4 abundance, albumin concentration, BMI, body surface area, sex, weight; (g) hepatic CYP3A4 abundance, albumin concentration, BMI, body surface area, sex and weight.

A summary of the performance characteristics for the multivariable linear regression model is shown in **Table 17**. The covariate most strongly associated with variability in sorafenib AUC was hepatic CYP3A4 abundance, inclusion of albumin concentration and BMI resulted in substantial improvement in multivariable model fit. Stepwise inclusion of additional the covariates BSA, sex and weight resulted in minor improvements in model performance (R^2 change ≤ 0.010). No other covariate met the stepwise inclusion criteria (probability of F to enter ≤ 0.05). These parameters formed the basis of the MIDS. The AUC of the ROC for the MIDS predicted steady state AUC was 0.991 (**Figure 34**). Sixty- three subjects (6.3 %) from the Sim-Cancer cohort failed to achieve a Day 14 C_{max} > 4.78 µg/mL. MIDS predicted individuals that failed to achieve a therapeutic sorafenib C_{max} with. 95.2 % sensitivity (60 / 63 sub-therapeutic individuals) and 95.0 % specificity (809 / 937 therapeutic individuals) (**Table 18**, **Figure 34**). Shown in **Figure 33**, differences in albumin concentration between participants were associated with changes in f_u.

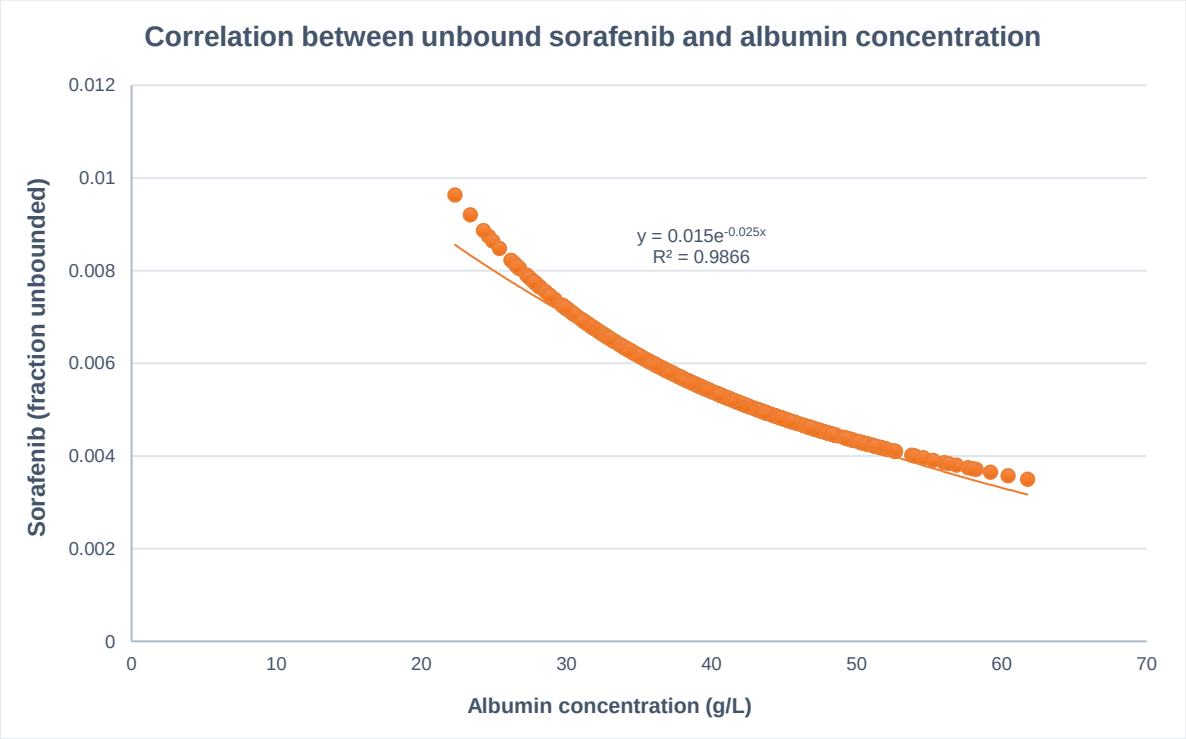

Figure 33 – Correlation between unbound sorafenib and albumin concentration.

Table 18. Classification matrixes describing the capability of linear regression models to identify individuals with a sub-therapeutic sorafenib steady state C_{max}.

		Predicted Therapeutic C_{max}		Percentage correct
		Sub-therapeutic	Therapeutic	
Observed Therapeutic C_{max}	Sub-therapeutic	60 (true negative)	3 (false negative)	95.2
	Therapeutic	47 (false positive)	890 (true positive)	95.0

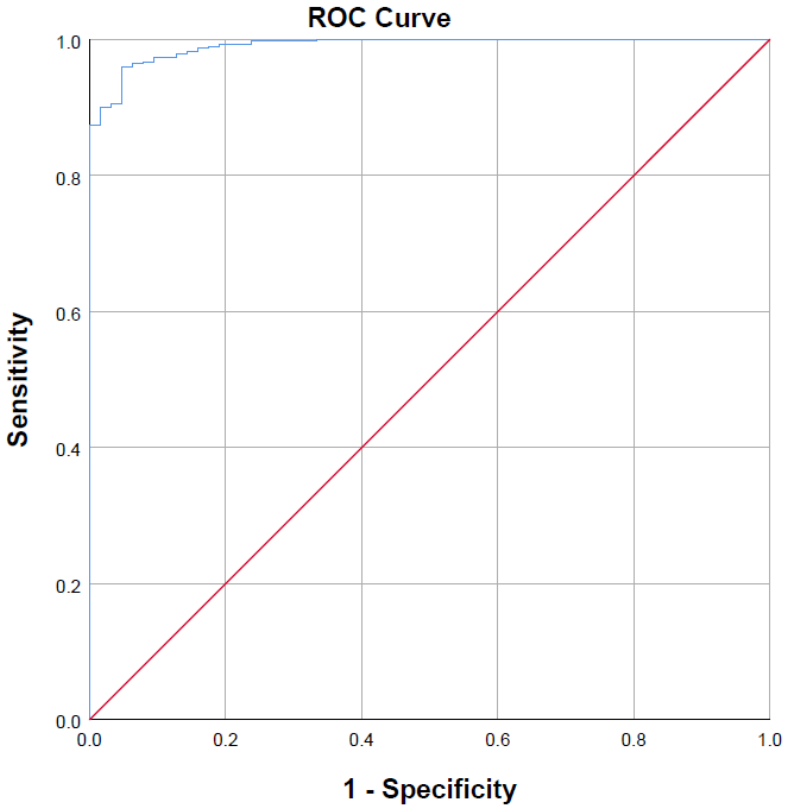

Figure 34 – Receiver operating characteristic (ROC) curve demonstrating the prediction performance of a predicted steady state sorafenib AUC.

4.3.4 – Impact of dose individualisation

The proportion of participants with a simulated sorafenib C_{max} below, within and above the target 4.78 to 5.78 µg/mL range at Day 14 and Day 28 based following flat 400 mg dosing, concentration-guided

dosing and concentration guided dosing with MIDS is reported in **Table 19**. Concentration guided sorafenib dosing without MIDS identified that 12.4 % of subject (62/500) failed to achieve a Day 14 $C_{max} \geq 4.78$ µg/mL with 400 mg twice daily dosing. Increasing the sorafenib dose to 600 mg twice daily in individuals who failed to achieve a Day 14 sorafenib $C_{max} > 4.78$ µg/mL, while retaining the 400 mg twice daily dose for those who did achieve a Day 14 sorafenib $C_{max} \geq 4.78$ µg/mL resulted in 99 % of subjects (495/500) achieving a Day 28 $C_{max} \geq 4.78$ µg/mL. Concentration guided sorafenib dosing without MIDS resulted in an additional 43 subjects achieving a Day 28 $C_{max} > 5.78$ µg/mL compared to flat 400 mg dosing.

Table 19. Number of participant below, within and above target concentration range with different sorafenib dosing protocols.

Dosing Protocol	Day 14			Day 28		
	< 4.78 µg/mL	**4.78 to 5.78 µg/mL**	**> 5.78 µg/mL**	**< 4.78 µg/mL**	**4.78 to 5.78 µg/mL**	**> 5.78 µg/mL**
Flat dosing	62	116	322	62	116	322
Concentration guided dosing	62	116	322	5	130	365
Concentration guided dosing with MIDS	34	135	331	5	164	331

On the basis of MIDS, 52 subjects were allocated to receive an initial sorafenib dose of 500 mg and 448 subjects were allocated to receive an initial sorafenib dose of 400 mg. Concentration guided sorafenib dosing with MIDS resulted in 6.8 % (34/500) subjects failing to achieve a Day 14 $C_{max} \geq 4.78$ µg/mL. Increasing the sorafenib dose to 600 mg twice daily in individuals who failed to achieve a Day 14 sorafenib $C_{max} \geq 4.78$ µg/mL, while retaining the MIDS informed twice daily dose for those who did achieve a Day 14 sorafenib $C_{max} \geq 4.78$ µg/mL resulted in 99 % (495/500) of subjects achieving a Day 28 $C_{max} \geq 4.78$ µg/mL. Concentration guided dosing with MIDS resulted in an additional 9 subjects achieving a Day 28 $C_{max} > 5.78$ µg/mL compared to flat 400 mg dosing. Post-hoc analysis demonstrated that 3 of these subjects would have a $C_{max} < 4.78$ µg/mL with 400 mg dosing, while the remaining 6 subjects could have retained a Day 28 $C_{max} \geq 4.78$ µg/mL while avoiding a Day 28 $C_{max} > 5.78$ µg/mL with a dose reduction from 500 mg to 400 mg following assessment of C_{max} on Day 14, however dose reduction was not incorporated into the simulation protocol.

4.4 – Discussion

The present study demonstrated that concentration guided dosing with MIDS facilitates therapeutic sorafenib exposure in 99 % of subjects within 28 days while minimising the number of additional subjects at risk of supra-therapeutic dosing compared to concentration guided dosing alone. Multivariable linear regression modelling demonstrated that variability in simulated sorafenib AUC and C_{max} is associated with hepatic CYP3A4 abundance, albumin concentration, BMI, sex, age and weight.

Logistic regression modelling of these covariates predicted individuals likely to fail to achieve sorafenib $C_{max} \geq 4.78$ mg/L with high sensitivity and specificity (95.2 % and 95 %, respectively). Incorporation of these parameters into an MIDS algorithm that allocated subjects to a 400 mg or 500 mg initial sorafenib dose resulted in a 50 % reduction in the number of subjects that failed to achieve a Day 14 $C_{max} \geq 4.78$ mg/L. When used in conjunction with concentration guided dosing at Day 14, this protocol resulted in 99 % of subjects attaining a Day 28 $C_{max} \geq 4.78$ mg/L.

The current study also highlights the potential danger of empiric concentration guided dosing in terms of placing patients at an increased risk of toxicity. In the absence of MIDS, 69 % of subjects (43/62) that underwent a dose escalation from 400 to 600 mg on Day 14 experienced a C_{max} on Day 28 that is associated with increased risk of grade II toxicity. Compared to concentration guided dosing alone, the concentration guided dosing with MIDS protocol reduced the number of additional subjects at increased risk of grade II toxicity on Day 28 ($C_{max} \geq 5.78$ mg/L) from 43 to 9.

PBPK modelling and simulation is an established tool to support drug discovery and development, and is a core element of the regulatory approval process in many jurisdictions [212]. Recent studies have further demonstrated the potential role of PBPK in predicting covariates affecting variability in drug exposure resulting from either patient characteristics or the drugs' physicochemical properties [197, 198], giving rise to the intriguing potential for this platform to support model informed precision dosing [199, 205]. Since the introduction of imatinib in 2001 there has been a growing evidence base supporting a role for concentration guided KI dosing, despite this implementation of KI dose individualisation has remained challenging. Many early studies focussed on a potential role for TDM guided KI dosing, however, sufficient evidence has yet to be generated to support widespread implementation for any KI. This has led to the exploration of novel approaches to facilitate precision KI dosing, which have included model informed precision dosing based on integrated simulation/prediction platforms such as PK-Sim®, GastroPlus™, Phoenix™, and Simcyp® [199, 213-215].

The target concentration range and dose escalation protocol used in the current study were based on the best current evidence [186, 191]. The main limitation to this study remains the lack of independent verification of the 4.78 to 5.78 µg/mL target C_{max} range. Further, when considering the clinical implementation, it is also important to note that the rate at which sorafenib is absorption from the GIT varies > 5-fold [183]. Variability in the rate of intestinal absorption results in marked variability in the time taken to reach C_{max} for sorafenib (1 to 6 hours). As such, in the absence of full PK (AUC) sampling, which is not practical in a clinical setting, concentration guided sorafenib dosing based on a C_{max} target is unlikely to be robust.

Liver CYP3A4 abundance was identified as the dominant characteristic driving variability in sorafenib AUC and C_{max}. By accounting for this characteristic alone, it was possible to identifying subjects with

a sub-therapeutic sorafenib C_{max} with a specificity of 74.6 % and a sensitivity of 96.3 %. When hepatic CYP3A4 abundance was considered along with readily attained data regarding albumin concentration, BMI, BSA, sex and weight in combination with albumin concentration, these two parameters accounted for > 88 % of multivariable model performance in terms of R^2, specificity and sensitivity (**Table 17**). These data suggest that consideration of liver CYP3A4 abundance may provide sufficient power to prospectively identify patients who are likely to require a higher sorafenib dose in order to achieve a therapeutic plasma concentration. Importantly, recent work in this [216] and other [217, 218] laboratories has demonstrated that quantification of extracellular vesicle (EV) derived CYP3A protein, mRNA and *ex vivo* activity robustly describes variability in CYP3A activity in humans.

This study identified the major physiological and molecular characteristics associated with between subject variability in sorafenib exposure to be hepatic CYP3A4 abundance, albumin concentration, BMI, BSA, sex and weight. Initial dose selection informed by a model accounting for these covariates resulted a quicker and more effective concentration guided sorafenib dosing.

CHAPTER 5: EVALUATION OF THE VALUE OF EXTRACELLULER VESICLES AS NOVEL BIOMARKER IN DRUG METABOLISING ENZYMES: THE EXPLORATORY ANALYSES

5.1 – Function of this Chapter

Chapters 2 and **3** of this thesis demonstrated the substantial variability in sorafenib plasma concentration and the potential importance of this variability in terms of defining efficacy and tolerability for this drug. Additionally, **Chapter 4** of this thesis defined the physiological and molecular characteristics that were most strongly associated with variability in sorafenib exposure. While several characteristics such as gender, body surface area, BMI and even albumin concentration can be readily evaluated using existing strategies, there is currently no endogenous marker to robustly characterise an individual CYP3A4 abundance and functions. For sorafenib, differences in CYP3A4 abundance between individuals was identified as the most important characteristic associated with variability in sorafenib exposure, accounting for around 60 % of the variability in the univariate linear regression analysis and as the top variable in the multiple linear regression analysis [219].

4-beta-hydroxycholesterol (4-β-HC) is an endogenous small molecule that has been proposed as a marker of CYP3A4 function [66, 220]. Changes in 4-β-HC concentration within an individual pre- and post- an intervention have been demonstrated to correlate well with induction of CYP3A4 expression [66]. However, marked variability between individuals in the activity of alternate biological pathways involved in cholesterol synthesis and metabolism limit the utility of 4-β-HC as a marker of between subject variability in CYP3A4 activity [221]. As such, the final chapter of this thesis primarily sought to explore extracellular vesicles as a novel source of biomarkers to define CYP3A4 abundance. Exploratory analyses were also performed to determine the breadth of drug metabolising enzymes (DME) that could be studied using EVs.

5.2 – Introduction

One of the approaches in precision medicine is to identify novel biomarkers to serve as a tool to assist the decision-making in drug administration and dosing. Previous chapters have demonstrated two possible approaches to address precision medicine; nevertheless, they were unlikely feasible to be applied in a clinical setting. Thus, there is an urge to identify a novel biomarker which holds a versatility yet well-suited in any scale of clinical setting. Recently, liquid biopsy has drawn much attention as its notion as a minimally invasive diagnostic approach compared to more invasive approaches such as tissue biopsy [222-224]. More importantly, the traditional tissue biopsy may not be feasible in some patients, such as patients who have late-stage cancer, multiorgan metastasis or in a deplorable health condition. Whereas, liquid biopsy not only offers less invasive approach, but also allows the process to be readily repeated and more applicable, regardless of the location of the tumour [225-227].

Liquid biopsy utilises biofluid-derived materials as a source of the subsequent downstream experiments. Currently, there are three main areas of liquid biopsy which have been extensively studied, including circulating tumour cells (CTCs), cell-free DNA (cfDNA) and extracellular vesicles (EVs) [228-230]. The efficiency of cfDNA has long been observed as a robust preventive biomarker, especially in cancers [231-233]. A good example of the successful use of cfDNA can be observed such as in the case of COLVERA® test kit for surveillance of relapsed colorectal cancer after primary treatment [234]. Nonetheless, most of the application tends to focus on the detection of the mutated gene released from tumour cells. Using of cfDNA may be useful as a preventive minimal invasive diagnostic approach; however, it is unlikely to further develop into any meaningful quantitative interpretation. On the other hand, EVs, mainly the small-diameter subpopulation – small EVs, demonstrated the capability to preserve its cargo with lipid-bilayer property, thus prolonging its content from the degradation [235-238]. This feature also facilitates cell-to-cell communication as the secreted small EVs were found to function as an intercellular messenger [239-243]. Thus, there is more opportunity of using small EVs for the further downstream experiment, unlike cfDNA that mostly restricted to qualitative-based evaluation [244, 245].

Drug metabolism is the principal part of drug disposition. The enzymes that involve in the process of drug metabolism are generally categorised as DMEs. Within DMEs, there are two prominent enzyme families; cytochrome P450 (CYP) and UDP-glucuronosyltransferase (UGT) account for the metabolic clearance of more than 70 % of drugs that are subject to metabolism [25, 246, 247]. DMEs are found to be highly expressed in the liver with a lesser degree in the small intestine [248-251]. Thus, supposedly, the cargo of liver-derived small EVs should contain liver-specific proteins, RNAs, and other genetic material related to its originate. Previously, proteomics analysis of small EVs isolated from rat hepatocyte could identify a large number of proteins related to DMEs along with general small EVs proteins [117]. Prior commencing this thesis, there was no evidence regarding the identification of

DMEs focusing on CYPs and UGTs in human plasma/serum small EVs. The research question underpinning this chapter was; could EV-derived CYP3A4, the predominant liver CYP isoform, proteins and mRNA are used as markers to predict the variability in exposure to medicine cleared by this enzyme? To achieve the research question, series of experimental plan were conducted including:

- Evaluation of the isolation capability of EVs from human plasma/serum and cell culture supernatant.
- Determination of the presence of CYP and UGT enzymes in EVs at protein and mRNAs level.
- Demonstration of the functional activity of the EVs-derived proteins from human plasma/serum and cell culture supernatant using the validated high turn-over rate probe substrate (midazolam).
- Demonstration of the capacity to metabolise sorafenib using the same *ex vivo* assay conditions.

  Experimental design for this Chapter is summarised in **Figure 35**.

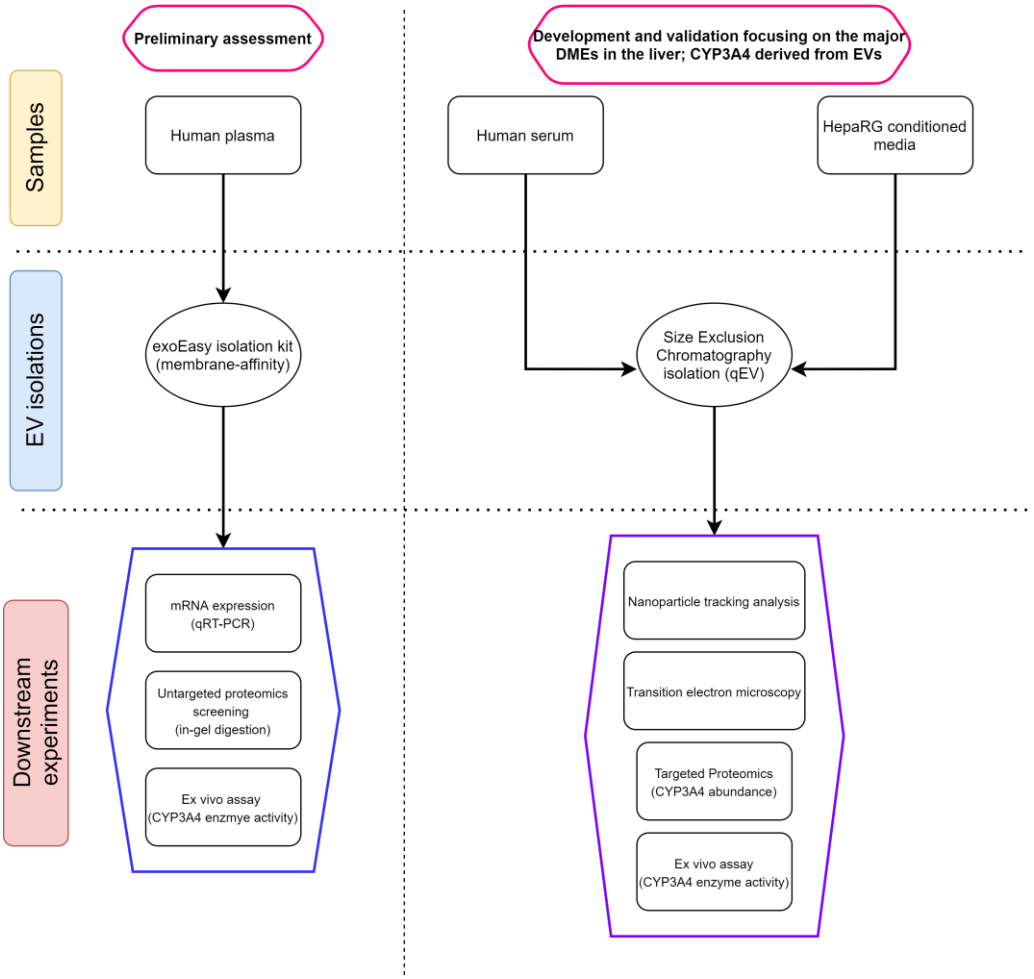

Figure 35 – Experimental design.

5.3 – Materials and Methods

5.3.1 – In vitro *cell culture*

5.3.1.1 – Cell Culture

Undifferentiated HepaRG cells were donated by Biopredic international (Rennes, France) under MTA agreement. Cells were grown in William's E media supplemented with 2 mM Glutamax, 10 % foetal bovine serum (FBS), 100 IU/mL penicillin, 100 µg/mL streptomycin, 5 µg/mL bovine insulin, and 50 µM hydrocortisone hemisuccinate. Cells were maintained in growth media for 14 days to allow proliferation. At day 15, cells cell growth media was replaced with growth media containing 1 % DMSO for 3 days, before culturing in differentiation media containing 2 % DMSO for 18 days. Media was replaced every 2-3 days throughout the culturing process. HepaRG cell differentiation is shown in **Appendix 3**.

To passage the cells, media were removed and cells were washed with sufficient amount of sterile PBS and detached from the flask by the addition of 2 mL (for T75) 0.05 % trypsin/0.53 mM EDTA in PBS solution and incubated at 37°C for less than 3 minutes.

For induction study (**Appendix 3**), HepaRG cells were cultured in induction media (William's E media supplemented with 2 mM Glutamax, 100 IU/ml penicillin, 100 µg/mL streptomycin, 4 µg/ml bovine insulin, and 50 µM hydrocortisone hemisuccinate). Rifampicin was dissolved in DMSO at 1,000-fold to the desired final concentration in order to minimise DMSO concentration to less than 0.1 % in the incubation. Cells were cultured in induction media with presence or absence of 10 µM rifampicin for 48 hours with media and drug renewal every 24 hours. At 48 hours, cells were harvested by removing the media followed by wash briefly with sufficient sterile Dulbecco's phosphate-buffered saline (D-PBS). Cells were scraped from the attachment using cells scrapper before transferring to the collection tubes.

5.3.1.2 – Cell conditioned medium (CM) preparation

The conditioned media were harvested by direct transfer to collection tubes using a pipette. A total of 250 mL of media were collected (25 mL per flask, 10 flasks per experiment). Media were centrifuged at 2,500 g for 15 minutes at 4°C for two cycles before EVs isolation was subsequently performed. The number of cells was counted using Neubauer Haemocytometer Cell Counting Chamber (Adelab Scientific, Australia). The cells were suspended in PBS (1x) and further diluted to an appropriately working range between 250,000 cells and 2.5 million cells per mL. The volume of 20 µL of diluted samples was introduced into the Neubauer chamber by slowly placing the pipette tip at the edge of the chamber covered by coverglass. Release the suspension slowly to fill an entire chamber.

5.3.1.3 – Tangential flow filtration (TFF)

Tangential flow filter (TFF, HansaBioMed) was used to concentrate CM, exactly as per manufacturer's recommendation. Each 150 mL of CM was concentrated to 3 mL (i.e. concentrated by a factor of 50), prior to isolation using size exclusion chromatography (SEC) column.

5.3.2 – EV isolation from cell CM

5.3.2.1 – Size exclusion chromatography (SEC)

Concentrated HepaRG CM EVs were isolated using qEV2 column (Izon Science). SEC columns were left to stand in an upright position at room temperature (RT) for 30 minutes, in order to achieve operational temperature range (18-24°C). EVs isolations was performed as per manufacturer's recommendation. Briefly, filter reservoir was rinsed with 5 mL of 0.2 µm filtered PBS and attached to the column (avoiding trapped air bubbles between the reservoir and the column). Bottom cap of the column was removed allowing the buffer (filtered PBS) to run through the column. Column was washed with 60 mL of 0.2 µm filtered PBS before sample loading.

Following column wash, 2 mL of CM was loaded into the filter reservoir. Void flow-through of 14 mL was discarded and subsequent 10 mL of flow-through containing EVs was collected in 10 mL collection tube (Corning). EVs containing flow-through was further concentrated using Amicon ultra-15 filter unit (Merck Milipore). Briefly, Amicon filters were washed by applying 4 mL of 0.2 µm filtered PBS and centrifuging at 4,000 g at 10°C in a swing-arm bucket centrifuge for 15 minutes. Flow-through was discarded and 10 mL of dilute qEV sample was added to the reservoir of washed Amicon filter unit. Sample was centrifuged for 30 minutes at 4,000 g at 10°C. Concentrated qEV sample (200 µL approximately) was transferred from Amicon filter unit reservoir into a Protein LoBind tube. Sufficient volume of 0.2 µm filtered PBS was added to concentrated qEV samples to obtain total sample volume of 200 µL (for normalisation purposes). The overview of the work flow is illustrated in **Figure 36**.

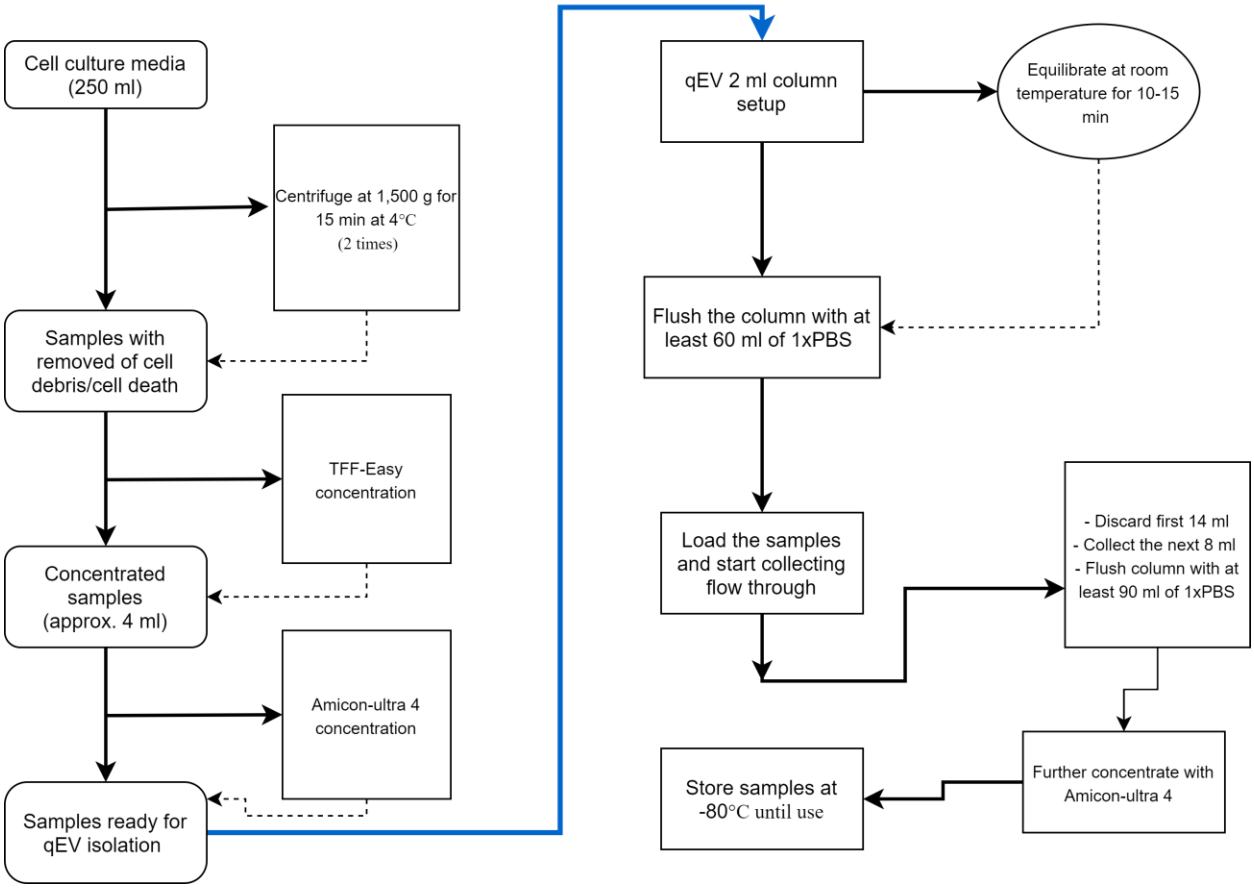

Figure 36 – Overview of small EVs isolation from HepaRG conditioned media.

5.3.3 – EV isolation from human serum

5.3.3.1 – Collection of blood/serum/plasma

Eight millilitres of whole blood was collected into Z Serum Sep Clot Activator (serum collection) or EDTA tubes (plasma collection, Greiner Bio-One, Frickenhausen, Germany) or using a 21-gauge Vacuette Safety Blood Collection sealed vacuum device (Greiner Bio-One, Frickenhausen, Germany) from healthy participants that provided informed consent. To ensure sample quality the device was primed by collecting a 5 mL 'discard' tube immediately prior to sample collection. Serum was isolated from whole blood within 60 minutes of sample collection by two cycles of centrifugation at 2,500 g for 15 minutes at 4°C. Plasma was isolated immediately after collection by two cycles of centrifugation at 2,500 g for 15 minutes at 4 °C.

5.3.3.2 – Size exclusion chromatography (SEC)

Human serum EVs were isolated using the same method as described in *5.3.2.1*, except 2 mL of human serum was loaded into filter reservoir instead of 2 mL of cell CM.

5.3.3.3 – Human plasma EV isolation by exoEasy kit: membrane affinity-based isolation

ExoEasy Maxi kit is a membrane affinity-based isolation kit from Qiagen (Qiagen, Germany). The kit applies the membrane affinity with spin column mechanism to facilitate the purification of EVs. Human plasma samples were filtered using 0.2 µm syringe filters. Approximately 2 – 4 mL of the resulting filtrate was mixed with 1.25 volumes of binding buffer (Qiagen XBP) and the resulting mixture was added to the reservoir compartment of the spin columns. All centrifugation steps were performed at RT. Firstly, samples were centrifuged for 5 minutes at 500 g, flow-through discarded. Wash buffer (10 µL; Qiagen XWP) was added to the reservoir compartment and the columns were centrifuged for 5 minutes at 4,000 g, flow-through discarded. Subsequently, elution buffer (400 µL; Qiagen XE) was added to the reservoir compartment and the spin columns were transferred to fresh collection tubes. Sample columns were incubated at RT for 90 seconds followed by centrifugation for minutes at 500 g. The resulting flow-through was reapplied to the reservoir compartment and incubated at RT for further 90 seconds (**Figure 37**). Sample containing columns were centrifuged for 5 minutes at 4,000 g. Resulting the flow-through containing EVs was stored at –80°C until needed for downstream analyses.

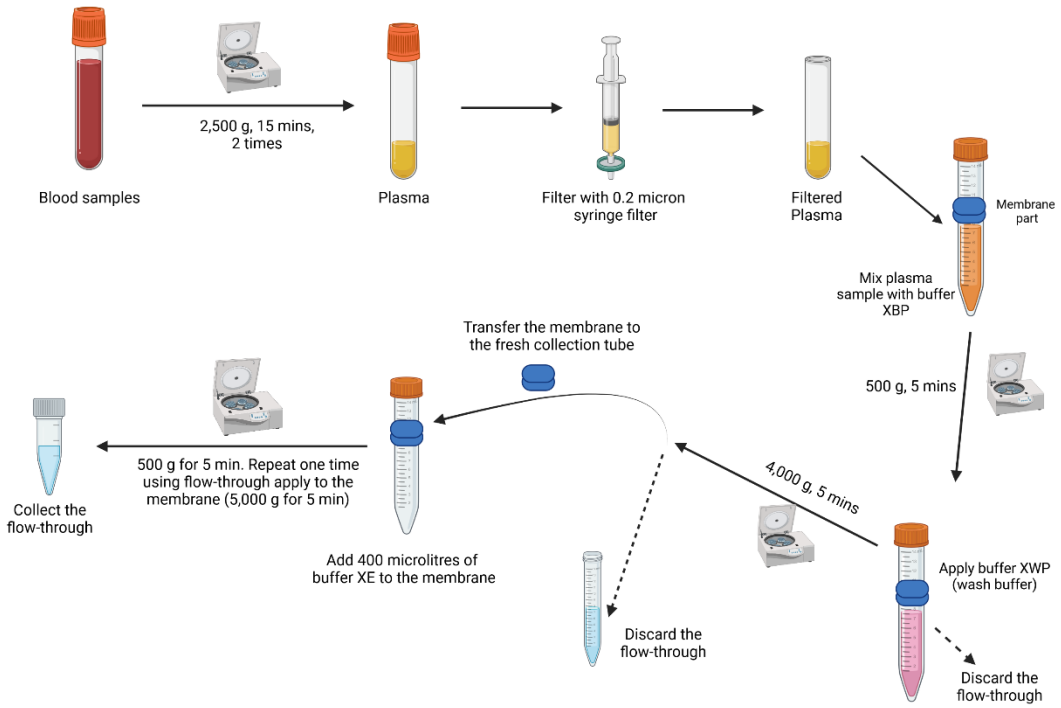

Figure 37 – A schematic representation of exoEasy kit isolation workflow (Adapt from: Qiagen exoEasy Maxi kit Handbook) Figure created with BioRender.com.

5.3.4 – Western blotting to determine TSG101

Approximately 25-40 µg total protein of samples were diluted 1:4 in sample loading buffer (4x Sodium dodecyl sulphate (SDS)-PAGE buffer) and heated at 95°C for 5 minutes. Proteins were separated by

SDS-PAGE (4 % stacking gel, 10 % separation gel) at RT; at 80 V for 20 minutes and 150 V for 60-80 minutes through stacking gel and separating gel, respectively using Biorad® Mini-Protean II Cell equipment. Proteins were transferred on to nitrocellulose membrane (BioRad®) in an ice-cooled Mini Trans-Blot Cell apparatus (BioRad®) at 20 V overnight at 4°C. Membrane was washed briefly once with Tris-buffered saline (TBST) with 0.2 % Tween-20 and blocked in 5 % (w/v) blocking buffer (TBST + 5 % non-fat dry milk) on shaker for 100 at RT. Rinse the membrane briefly with sufficient TBST then incubated the membrane with primary antibody (1:1000) and 1 % blocking buffer for overnight on the shaker at 4°C. Subsequently, relocated the membrane to RT followed by washing 3 times using TBST (10 minutes per wash). The membrane was incubated with the anti-species-specific Horseradish peroxidase labelled IgG (1:2000), 1:10000 BioRad® Precision Plus Strep-Tactin HRP conjugates and 1 % blocking buffer for 1.5 hours. The membrane was washed in TBST for 3 more times (10 minutes per wash). Membrane-bound peptides conjugated with horseradish peroxidase were detected by chemiluminescence (Roche Diagnostics, Mannheim, Germany) and subsequently exposed to Omat autoradiographic film (Eastman Kodak, Rochester, NY, USA). Autoradiographs were processed manually with AGFA developer, fixer and replenisher reagents.

5.3.5 – Transmission electron microscopy (TEM)

Samples were prepared adapting a previously published protocol with a slight modification [252]. Briefly, specialised carbon-coated grids (Ted-Pella B 300M; Ted-Pella, Redding, CA, USA) were cleaned and hydrophilized using plasma glow discharge for 15 seconds (Gatan SOLARUS Advanced Plasma Cleaning System, Gatan, Inc., Pleasanton, CA, USA) before using in the samples preparation process. Five-µL of sample in 0.2 µm filtered PBS was placed on carbon-coated grids for 5 minutes. Wash the carbon-coated grids briefly for 15 seconds at RT with 0.2 µm filtered PBS. Subsequently, the carbon-coated grids were contrasted with 2 % uranyl acetate for 3 minutes at RT washed once then examined by FEI TECNAI Spirit G2 TEM (Thermo Fisher Scientific, Waltham, MA, USA) operated at 100 kV. TEM images were acquired at 30,000x and 68,000x.

5.3.6 – Nanoparticle tracking analysis (NTA)

Nanoparticle tracking analysis (NTA) was performed to determine the abundance and size distribution of the isolated EVs isolated from human serum and HepaRG conditioned media. NTA was performed using the NanoSight NS300 (Malvern Panalytical, Malvern, United Kingdom, Software Version 3.4). Human serum EV samples and HepaRG EV samples were diluted between 1:1000 and 1:5000 using freshly 0.2 µm filtered PBS; five 60 seconds videos were captured and analysed under constant flow conditions (flow rate 50) using NTA 3.4 software.

5.3.7 – Extraction of total RNA from EVs using exoRNeasy kit

EV isolations for downstream extraction of RNA is described in Section *5.3.3.3*. Following washing XWP buffer, the column was transferred to the new collection tube and 700 µL of QIAzol lysis agent (Qiagen) was added directly to the membrane. Columns were centrifuged at 5,000 g for 5 minutes to collect the lysate. Chloroform (90 µL) was added to the lysate, and the mixture was incubated at RT for 2-3 minutes and centrifuged at 12,000 g for 15 minutes at 4°C. Centrifugation separated the samples into 3 phases: the partition of RNA in the upper colourless aqueous phase, DNA partition in the interphase, and the organic phase. Aqueous phase (approximately 200 µL) was transferred to a new 1.5 mL tube and two volumes of 100 % ethanol were added (approximately 400 µL). The total volume of mixture around 600 µL was transferred to RNeasy MinuteElute spin column (Qiagen. Column was topped up with the sample and centrifuged at ≥ 8,000 g for 15 seconds at RT until the remaining sample was loaded. Seven hundred µL washing buffer RWT was added to the column and columns was centrifuged at 8,000 g for 15 seconds. 500 µL of buffer RPE was added to the column, followed by 8,000 g centrifugation for 15 seconds. The step was repeated using 500 µL RPE buffer and followed by centrifugation at 8,000 g for 2 minutes. Spin column was placed in a new 2 mL collection tube and centrifuged at 18,000 g for 5 minutes with the lid open, allowing the membrane to dry. Following centrifugation, column was transferred to a new 1.5 mL collection tube and 14 µL of RNase-free water was added directly to the centre of the membrane (The lid of the spin column was closed and the column was left to stand for 1 minute. The column was centrifuged at 18,000 g for 1 minute to elute the total RNA from the membrane.

5.3.8 – Generation of cDNA using Superscript VILO cDNA synthesis kit.

The RNA was reverse transcribed to cDNA using the SuperScript™ VILO™ cDNA Synthesis Kit according to the manufacturer's protocol (Invitrogen). Master mix was prepared mixing 4 µL of 5x VILO reaction mix, 2 µL of 10x SuperScript Enzyme Mix (per reaction) and added to RNA sample (140 ng per reaction) then use DEPC-treated water bring to 20 µL. Mix the reaction tubes gently and incubate at 25°C for 10 minutes, follow by 42°C for 60 minutes, then terminate the reaction at 85°C at 5 minutes. The cDNA can be kept at -80°C until use.

5.3.9 – Detection of CYP and UGT mRNA in EVs isolated from plasma.

Primer sets used are detailed in the **Table 20**. Assay setup used for PCR was: 20 µL reactions containing 1x GoTaq qPCR Master Mix, 0.5 µM each primer and template cDNA equivalent to 20-40 ng input RNA. PCR conditions used for quantitative analysis were: 95°C for 15 minutes (activation); 40 of 15 second cycles of 95°C; 15 seconds at 60°C (annealing) and 72°C for 20 seconds; and a ramped melting

curve analysis between 55 and 95°C with 4 seconds, 1°C steps. Data was acquired during the 72°C extension phase of each cycle.

Table 20. Primer sequences used in gene expression assays.

Genes		Forward Primer sequence	Backward Primer sequence
CYP	*1A1*	GGTCAAGGAGCACTACAAAACC	TGGACATTGGCGTTCTCAT
	1A2	CAGAAGCTTCAAGCACAGCGAGAACTAC	CAAGGATCCGGGTCTTGTCGATGGCCGA
	2C8	TGTAAAACGACGGCCAGT	CAGGAAACAGCTATGACC
	2C9	TACAATACAATGAAAATACATG	CTAACAACCAGACTCATAATG
	2C19	TGTAAAACGACGGCCAGT	CAGGAAACAGCTATGACC
	2D6	GCAAGAAGTCGCTGGAGCAGTG	CTCACGGCTTTGTCCAAGAGAC
	2E1	GCCATCAAGGATAGGCAAGA	TCCAGAGTTGGCACTACGACT
	3A4	AGTATGGAAAAGTGTGGGGCT	TGGAGACAGCAATGATCGTAA
	3A7	CTATGATACTGTGCTACAGT	TCAGGCTCCACTTACGGTCT
UGT	*1A1*	ATGCTGTGGAGTCCCAGGGC	CCATTGATCCCAAAGAGAAAACC
	1A6	CTTTTCACAGACCCAGCCTTAC	TATCCACATCTCTCTTGAGGACAG
	1A9	GAGGAACATTTATTATGCCACCG	CCATTGATCCCAAAGAGAAAACC
	2B4	TCTACTCTTAAATTTGAAGTTTATCCTGT	TCAGCCCAGCAGCTCACCACAGGG
	2B10	TGACATCGTTTTGCAGATGCTTA	CAGGTACATAGGAAGGAGGGAA
	2B17	GTGTTGGGAATATTCTGACTATAATATA	CAGGTACATAGGAAGGAGGGAA
	2B15	ATCCCAATGACGCATTCACTCTTAAACTC	CAGGTACATAGGAAGGAGGGAA

5.3.10 – Proteomics screening to determine the abundance of DMET in EVs

Proteomics in-gel digestion was performed to determine the abundance of DMET peptides in EVs isolated from plasma. Briefly, in-gel trypsin digestion was performed on 40 to 70 kDa bands excised from 1D-SDS PAGE gels. Gel fragments were destained and dehydrated at RT by adding 100 µL of acetonitrile. Protein bands were reduced using 10 µmol/L dithiothreitol (DTT) then alkylated using 50 µmol/L iodoacetamide (IAA) by incubating gel fragments at 60°C for 30 minutes. Gels were dehydrated using 100 µL acetonitrile and digested with trypsin at an enzyme-to-protein ratio of 1:20 for 16 hours at 37°C. Peptides were extracted by adding acetonitrile at a final concentration of 50 %. Peptides were

separated by LC performed on a Waters XBridge BEH C18 column (150 mm × 0.3 mm, 3.5 µm) with a 45 minutes acetonitrile gradient using an AB Sciex Ekspert 400 nanoHPLC. Column elutant was monitored using an AB Sciex 5600+ triple time of flight MS operating in positive ion mode, with rolling collision energy and dynamic accumulation enabled. Three technical replicates were performed for each sample. *De novo* sequencing was performed on raw MS data using Peaks Studio v7.0 software.

5.3.11 – Targeted proteomics for the quantification of DMET in EVs

Targeted proteomics was performed using an in-solution digestion approach to quantify the abundance of the targeted DMET. CYP3A4 proteins were quantified. Briefly, samples were thawed slowly on ice. Protein samples (50 µL) were diluted in sufficient amount of 1xPBS to make 100 µL starting volume. Samples underwent a freeze-thawing process for three-cycle using dry-ice and water bath (set at 37ºC). 50 mM ammonium bicarbonate (pH 8) was added, followed by 200 mM DTT to the sample. Samples were incubated at 60ºC for 90 minutes on a heat block. Samples were allowed to cool down to RT for 15 minutes. For the alkylation step, 400 mM iodoacetamide was added to the samples, followed by incubation for 60 minutes in the dark. Upon alkylation, 2.5 µg of trypsin (Trypsin Gold, Promega) was spiked into the reduced and alkylated protein sample and digestion was carried out for 12 hours in the shaking water bath set to 37ºC. Digestion was quenched with formic acid (10 % v/v) and pelleting the excess debris by centrifugation at 16,000 g at 4°C for 10 minutes. 100 µL of clear supernatant was carefully removed and transferred to the LC-MS vial, 7 µL was injected for LC-MS/MS analysis.

During the LC-MS/MS run, peptides were separated on an Agilent HPLC column (AdvanceBio peptide map, 2.1 x 100 mm, 2.7 µm). HPLC mobile phases consisted of 0.1 % formic acid in 100 % de-ionised water v/v (A) and 0.1 % formic acid in 100 % Acetonitrile v/v (B). After the 0 minutes, initial hold at 90 % A and 10 % B, mobile phase composition began with 90 % A and 10% B for 3 minutes. The gradient then changed to 40 % A and 60 % B for 10 seconds. The flow rate was set at 0.3 mL/minute. Agilent triple quadrupole mass spectrometer optimized for selected SRM and quantification was performed using the Water MS Quantitative software.

5.3.12 – Ex vivo CYP activity assay

5.3.12.1 – Enzyme activity assay to determine the protein functionality from cell lysates.

HepaRG cells were lysed by resuspending in Tris-EDTA buffer (pH 7.4) then performed four freeze-thawing cycles using dry-ice and water bath set to 37ºC. Milli-Q water, 1 M potassium phosphate buffer and cell lysates were added to 1.5 mL Eppendorf Tubes. Cell lysates were replaced with an equal volume of Milli-Q water for no protein control. Samples (in duplicate) were pre-incubated in the absence of NADPH for 10 minutes in a shaking water bath at 37ºC. Following pre-incubation, NADPH was added to initiate reactions. The final incubation volume was 200 µL. Midazolam and NADPH were

replaced with an equal volume of Milli-Q water for no substrate and no cofactor controls, respectively. Samples were incubated in a shaking water bath at 37ºC for 60 minutes. Reactions were terminated with the addition of 400 µL of ice-cold 0.1 % (v/v) formic acids in methanol. Samples were centrifuged at 16,000 *g* for 15 minutes at 4ºC. 300 µL of the clear supernatant was removed from each tube and transferred to 2 mL LC vials fitted with 400 µL pulled-point glass inserts. Vials were then capped and transferred to the LC-MS for analysis.

5.3.12.2 – Enzyme activity assay to determine the protein functionality from EVs

EVs were isolated from HepaRG conditioned media using the methods as described elsewhere. The activity assay was carried similar to cell lysates with a slight modification. Briefly, Milli-Q water, 1 M potassium phosphate buffer and cell lysates were added to 2 mL LoBind Eppendorf Tubes. EVs were replaced with an equal volume of 1xPBS for no protein control. Samples (in duplicate) were pre-incubated in the absence of midazolam and NADPH for 24 hours in a shaking water bath at 37ºC. After 24 hours, midazolam followed by NADPH was added to initiate the reactions. The final incubation volume was 100 µL. Midazolam and NADPH were replaced with an equal volume of Milli-Q water for no substrate and no cofactor controls, respectively. Samples were incubated in a shaking water bath at 37ºC for 24 hours. Reactions were terminated with the addition of 100 µL of ice-cold 0.1 % (v/v) formic acids in methanol. Samples were centrifuged at 16,000 *g* for 15 minutes 37ºC. 100 µL of the clear supernatant was removed from each tube and transferred to 2 mL LC vials fitted with 250 µL pulled-point glass inserts. Vials were then capped and transferred to the LC-MS for analysis.

5.4 – Results

5.4.1 – Western blotting

Small EV presence was confirmed by Tsg101 protein expression in EVs lysates isolated from human plasma and from CM from HepaRG cells. As expected, significantly lower expression of Tsg101 in HepaRG cell lysates, compared to EVs (**Figure 38**).

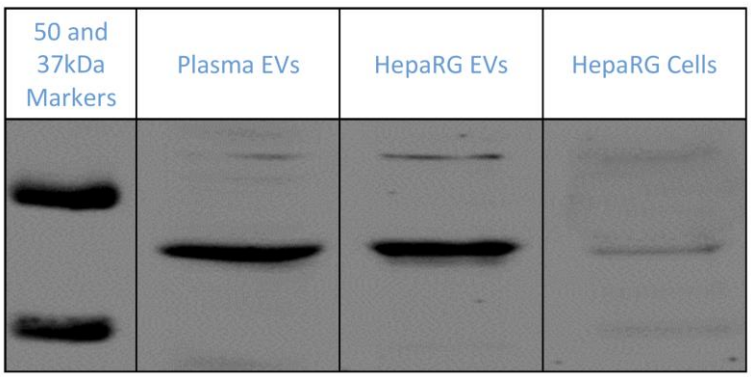

Figure 38 – Immunoblot demonstrating Tsg101 (44 kDa) expression in human plasma and HepaRG EV isolated by exoEasy kit.

5.4.2 – CYP and UGT mRNA expression in plasma EVs

The presence of *CYP 1A2, 2C8, 2C9, 2D6, 2E1* and *3A4*, and *UGT 1A1, 1A9, 2B4, 2B7* and *2B10* mRNAs in EVs isolated from human plasma was confirmed by real-time PCR. The relative expression of individual CYP and UGT mRNAs in EVs were reported in **Table 21**.

Table 21. Expression of CYP and UGT mRNA in plasma EVs. Data was partially generated by Wijayakumara D.

Family	Gene	Cycle time (Ct)
CYP	*1A2*	31.72
	2C8	32.63
	2C9	33.29
	2E1	29.60
	3A4	32.35
UGT	*1A1*	34.34
	1A9	34.78
	2B4	29.49
	2B7	33.27
	2B10	32.18
	2B15	30.22

5.4.3 – CYP and UGT proteins detected in EV isolated from plasma

Mass spectrometry based proteomic profiling of EVs isolated from human plasma detected 188 unique peptides originating from CYP 1A2, 2B6, 2C8, 2C9, 2C19, 2D6, 2E1, 2 J2, 3A4 and 3A5, and UGT 1A1, 1A3, 1A4, 1A6, 1A9, 2B4, 2B7, 2B10 and 2B15. The unique peptides attributed to each protein are summarized in **Table 22**. The number of unique peptides detected for each protein ranged between 2 and 19, with a mean of 9.65. In addition, 5 unique peptides originating from NADPH-cytochrome P450 reductase (the redox partner required for CYP activity) were also detected. The capacity to detect peptides originating from CYP and UGT proteins was confirmed in plasma from 3 individuals. It is worth further noting that while cytochrome b5 (34.5 kDa) was not detected in the current analysis as it

was not contained within the window of protein bands analysed (40 to 70 kDa), the presence of this protein in human-derived small EVs has already been established.

Table 22. Proteomics analysis of human plasma EVs at target gel band 40 to 70 kDa.

Family	Enzyme	Number of Unique Peptides	Peptide Sequences
CYP	1A2	16	ASGNLIPQEK DTTLNGFYIPK ELDTVIGR FLTADGTAINKPLSEK FLWFLQK GRPDLYTSTLITDGQSLTFSTDSGPVWAAR HSSFLPFTIPHSTTR IGSTPVLVLSR LSDRPQLPYLEAFILETFR MMLFGMGK NPHLALSR NTHEFVETASSGNPLDFFPILR TVQEHYQDFDKNSVR VDLTPIYGLTMK YGDVLQIR YLPNPALQR
	2B6	8	FHYQDQEFLK FSDLLPMGVPHIVTQHTSFR HRETLDPSAPK IAMVDPFFR KTEAFIPFSLGK YGDVFTVHLGPR YGFLLMLK YPHVAER
	2C8	14	DQNFLTLMK EALIDNGEEFSGR EHQASLDVNNPR GLGIISSNGK LPPGPTPLPIIGNMLQIDVK MLQIDVK NLNTTAVTK RFDYKDQNFLTLMK RFNENFR SDYFMPFSAGK

			SFTNFSK SHMPYTDAVVHEIQR VQEEIDHVIGR YGLLLLLK
	2C9	16	EALIDLGEEFSGR FDYKDQQFLNLMEK FGLKPIVVLHGYEAVK FSLMTLR GFGIVFSNGK GIFPLAER GKLPPGPTPLPVIGNILQIGIK ILEKVK ILQIGIK LPPGPTPLPVIGNILQIGIK NVAFMK RFSLMTLR SHMPYTDAVVHEVQR VQEEIER YALLLLLK YFMPFSAGK
	2C19	5	GHFPLAER GHMPYTDAVVHEVQR LNENIR MVVLHGYEVVK QNQQSEFTIENLVITAADLLGAGTETTSTTLR
	2D6	12	AFLTQLDELLTEHR DIEVQGFR EALVTHGEDTADRPPVPITQILGFGPR EVLNAVPVLLHIPALAGK FGDIVPLGVTHMTSR FHPEHFLDAQGHFVKPEAFLPFSAGR FSVSTLR LLDLAQEGLKEESGFLR RFSVSTLR RPEMGDQAHMPYTTAVIHEVQR RVQQEIDDVIGQVR SQGVFLAR
	2E1	12	EALLDYKDEFSGR FGPVFTLYVGSQR FITLVPSNLPHEATR

			FSLTTLR HFDYNDEK LHEEIDR MVVMHGYK PAFHAHR VVMHGYK YGLLILMK YPEIEEK YSDYFKPFSTGK
	2J2	3	FTFRPPNNEK LFVSHMIDK VIGQGQQPSTAAR
	3A4	18	APPTYDTVLQMEYLDMVVNETLR DNIDPYIYTPFGSGPR DVEINGMFIPK EIDAVLPNK EMVPIIAQYGDVLVR ETQIPLK EVTNFLR FALMNMK GVVVMIPSYALHR HRVDFLQLMIDSQNSK KDVEINGMFIPK LGIPGPTPLPFLGNILSYHK LQEEIDAVLPNK LSLGGLLQPEKPVVLK NKDNIDPYIYTPFGSGPR RPFGPVGFMK SLLSPTFTSGK YWTEPEK
	3A5	7	APPTYDAVVQMEYLDMVVNETLR DSIDPYIYTPFGTGPR DTINFLSK DVEINGVFIPK LDFLQLMIDSQNSK LDTQGLLQPEKPIVLK LGIPGPTPLPLLGNVLSYR
NADPH-cytochrome P450 reductase		5	DGALTQLNVAFSR FAVFGLGNK IQTLTSSVR

			KKEEVPEFTK TALTYYLDITNPPR
UGT	1A1	6	DGAFYTLK EDVKESFVSLGHNVFENDSFLQR ESFVSLGHNVFENDSFLQR EVTVQDLLSSASVWLFR GHEIVVLAPDASLYIR PLSSHSDHMTFLQR
	1A3	6	GDFVMDYPR GHQAVVLTPEVNMHIK LLTTNSDHMTFMQR SMAMLNNMSLVYHR VLVVPIDGSHWLSMR YLSIPTVFFLR
	1A4	2	GHQAVVLTPEVNMHIKEEK YLSIPAVFFWR
	1A6	19	AMAIADALGK DIVEVLSDR DRPVEPLDLAVFWVEFVMR DTLNFFK DVDIITLYQK FSDHMTFSQR GAGVTLNVLEMTSEDLENALK GHEIVVVVPEVNLLLK IPQTVLWR IYPVPYDQEELK KAMAIADALGK NDLLGHPMTR SFLTAPQTEYR SPDPVSYIPR VLEMTSEDLENALK WLPQNDLLGHPMTR YDFVLEYPR YEELASAVLK YQSFGNNHFAER
	1A9	4	AFAHAQWK ILLGFSDAMTFK TDFVLDYPK TYSTSYTLEDLDR
	2B4	9	FEVYPVSLTK

			HSGGLLFPPSYVPVVMSELSDQMTFIER IHHDQPVKPLDR IPFVYSLR PTTLSETMAK TEFEDIIK TILDELVQR VLVWPTEFSHWMNIK WAELPK
	2B7	16	ANVIASALAQIPQK DLLNALK FDGNKPDTLGLNTR IEIYPTSLTK IPQNDLLGHPK IQHDQPVKPLDR QHDQPVKPLDR SLSFSPGYTFEK TILDELIQR VDFNTMSSTDLLNALKR VGIPLFADQPDNIAHMK VINDPSYK VLVWAAEYSHWMNIK WDQFYSEVLGR WIPQNDLLGHPK WSDLPK
	2B10	7	FDGNKPDALGLNTR HSGGFIFPPSYVPVVMSK LEVYPTSLTK LSDQMTFMER PSYKENIMK TEFENIIMQLVK TVINDPSYKENIMK
	2B15	8	AEMWLIR FSVGYTFEK GAALSVDIR IHHDQPMKPLDR LPQNDLLGHPK NYLEDSLLK TILEELVQR WLPQNDLLGHPK

5.4.4 – TEM analysis

High-resolution TEM was used to evaluate the EVs sample background/purity, sample composition, and EVs structure. Representative images from EVs sample isolated by qEV70 2 mL SEC column displayed clear background with limited non-EVs contamination. Moreover, most EVs were 50 - 150 nm in size and surrounded by intact membrane (**Figure 39**). Similarly, EVs isolated by SEC from HepaRG CM, were round, undamaged and surrounded by intact membrane (**Figure 40**). Sample integrity and EVs morphology were similar between EVs from both sources.

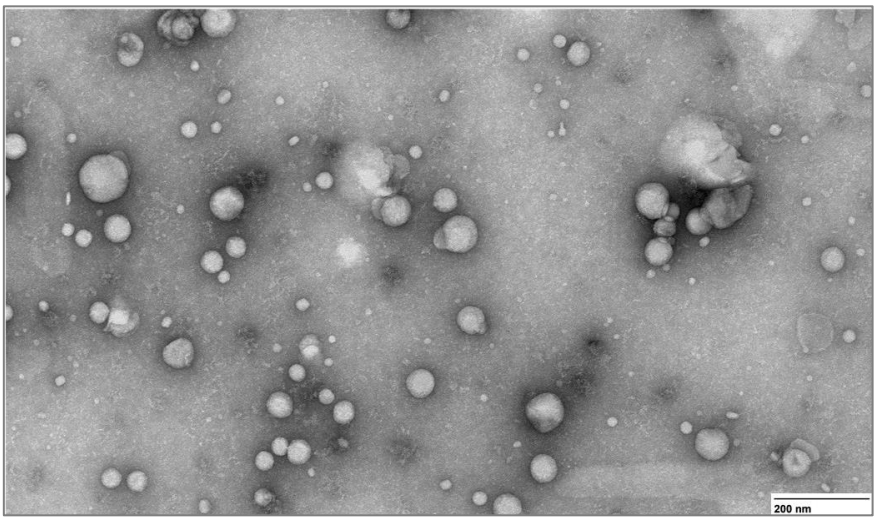

Figure 39 – Characterisation of human serum EVs using TEM. Direct mag: 30,000x, no sharpening, normal contrast. Scale bar = 200 nm.

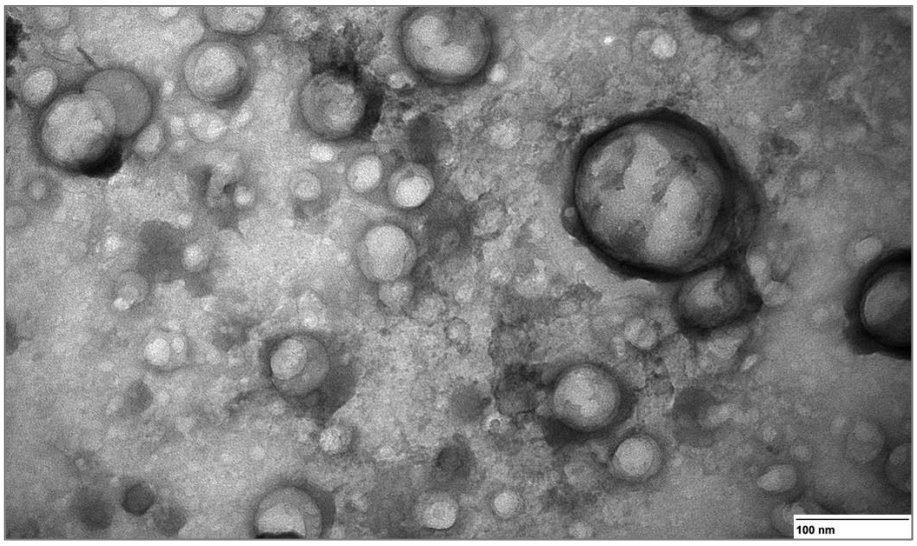

Figure 40 – Characterisation of HepaRG EV secreted EVs using TEM. Direct mag: 68,000x, no sharpening, normal contrast. Scale bar = 100 nm.

5.4.5 – Particles distribution

Nanoparticle tracking analysis (NTA) of the particle size distribution of EVs isolated from human serum demonstrated a median [interquartile range; IQR] diameter of isolated nanovesicles was 138.2 [105.9 – 171.9 nm; **Figure 41**]. The mean (± SD) yield of EVs isolated from human serum was 3.5 x 10^{11} ± 5.02 × 10^{11} particles/mL of serum (equivalent to around 7 x 10^{10} particles/2 mL starting serum volume).

HepaRG EVs demonstrated a median [IQR] diameter of isolated nanovesicles was 133.7 [124.5 – 139.7 nm; **Figure 41**]. The mean (± SD) yield of EVs isolated from conditioned media was 8.3 x 10^{11} ± 6.6 × 10^{11} particles/mL of conditioned media (derived from approximately 1,500 million cells; 150 million cells/flask, total of 10 flasks).

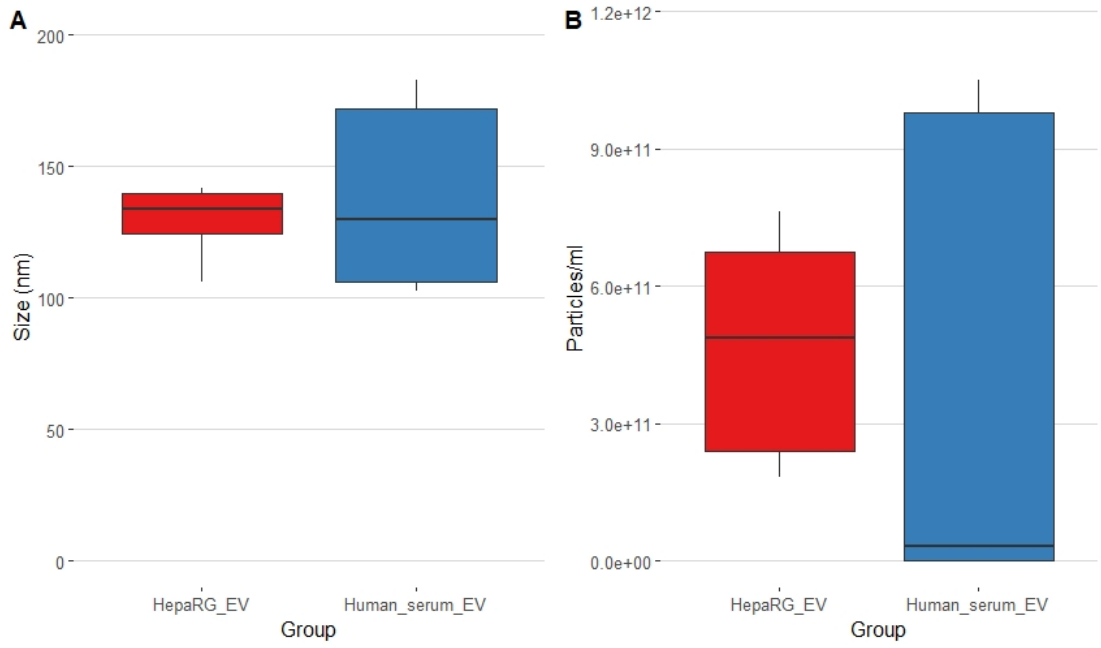

Figure 41 – NTA analysis of human serum EVs and HepaRG EVs samples, where A: median particle size (nm) and B: particle concentration; particles/mL).

5.4.6 – Abundance of CYP3A4 peptide: targeted proteomics analysis

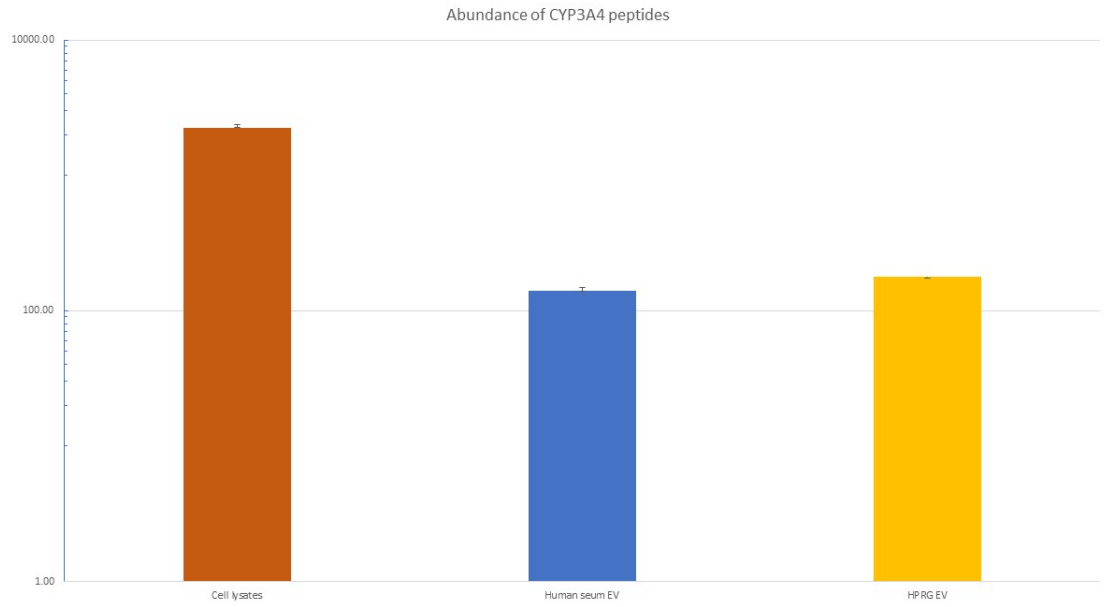

Figure 42 – Abundance of CYPA4 peptides derived from HepaRG cells lysate, human serum EVs and HepaRG EVs. Error bars represent the mean ± SD generated from three independent experiments.

CYP3A4 proteins were detected both in the human serum EVs and HepaRG EVs, whereas HepaRG lysates were used as a positive control to reassure the validity of the experiment. Interestingly, the presence of CYP3A4 peptides in human serum EVs and HepaRG EVs was similar in quantity, albeit the starting volume of each sample was different (2 mL of human serum vs 250 mL HepaRG conditioned media; **Figure 42**). For human serum EVs, samples were obtained from three different healthy volunteers. For HepaRG EVs, data were generated from three different biological replicates.

5.4.7 – Functional activity of CYP3A4 using midazolam as probe substrate

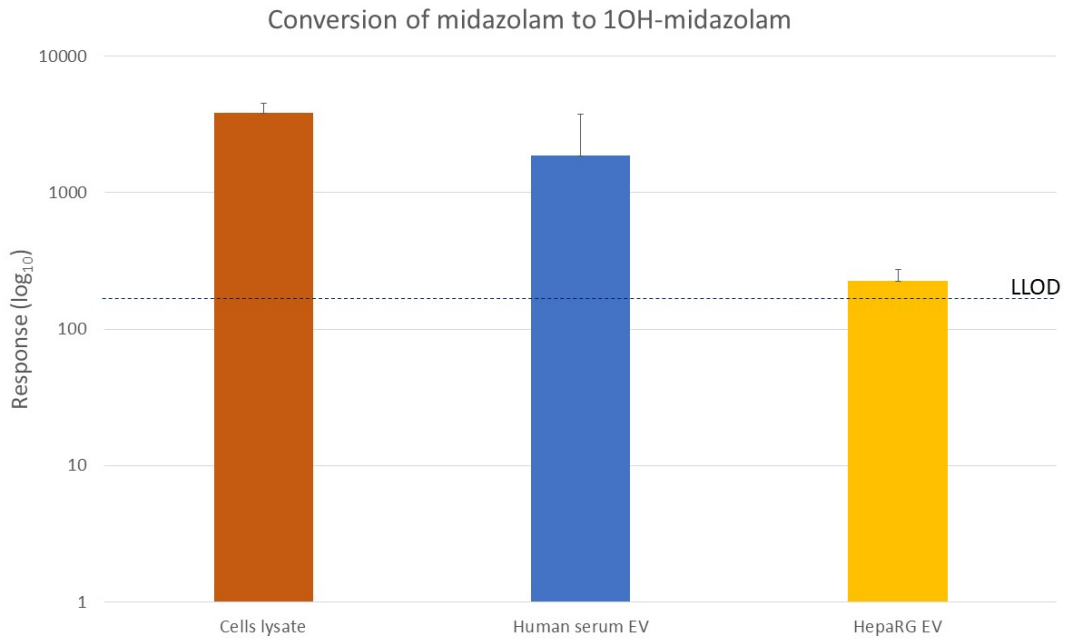

Figure 43 – Conversion of 1OH-midazolam following ex vivo activity assay. Error bars represent the mean ± SD generated from three independent experiments. LLOD = lower limit of detection.

The conversion of 1OH-midazolam was measured as a representative of CYP3A4 functionality. HepaRG lysates were used as positive control, whereas no protein input was served as a blank. Human serum EVs used in this analysis were the aliquoted samples from the proteomics analysis. The presence of 1OH-midazolam was observed following the incubation of midazolam with human serum EVs suggesting the functionally active of CYP3A4 enzyme (**Figure 43**). However, the inter-individual variability was observed as seen in the high magnitude of the standard deviation presented as error bar (response ± SD; 1862.41 ± 1886.83). On the other hand, the functionality of CYP3A4 was observed in HepaRG EV sample although the response was substantial lower compared to human serum EV (response ± SD; 224.73 ± 48.72). Noticeably, there was less variability in the functional activity of CYP3A4 enzyme derived from HepaRG EVs compared to human serum EV.

5.4.8 – Functional activity of CYP3A4 using sorafenib as probe substrate.

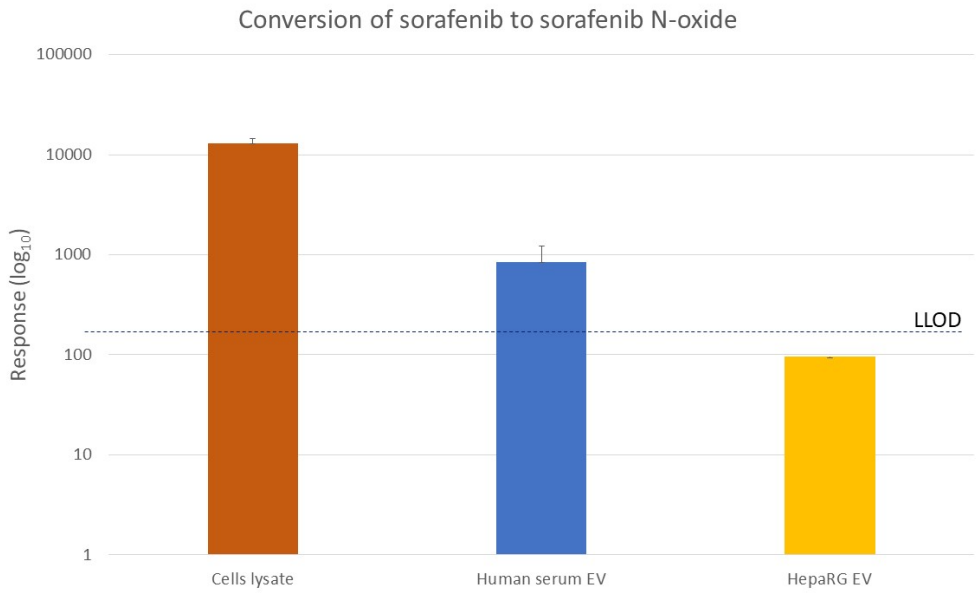

Figure 44 – Conversion of sorafenib N-oxide following ex vivo activity assay. Data derived from cells lysate and HepaRG EVs were generated from biological triplicates. Data derived from human serum EVs was generated based on three different healthy volunteers. LLOD = lower limit of detection.

The conversion of sorafenib N-oxide was barely observed in human serum EVs and HepaRG EVs (**Figure 44**). HepaRG lysates was used as a positive control for the experiments, which observed a formation of sorafenib N-oxide following *ex vivo* incubation assay. There was a detectable amount of sorafenib N-oxide conversion derived from the human serum EVs sample. On the other hand, there was no conversion of sorafenib N-oxide derived from HepaRG EVs.

5.5 – Discussion

The research field of EVs is a highly advancing area during the past decade. At the time this chapter commenced, there was still a lack of systematic approaches to properly researching this field of research. Moreover, as this research area is at the initial phase, several undiscovered elements are yet to be investigated. Unquestionably, the premise stemmed both limitations and opportunities in this research area. The finding of genomic material in small EVs by Valadi et al. [132] was the breakthrough factor in enlightening the countless possibilities of using small EVs in various research objectives. Thenceforth, several studies revealed the significant role of small EVs in cell-to-cell communication, cell signalling, and a certain degree of tumorigenesis; thus, strengthening a wide range of its novel utilities [253-258].

Several recent evidence has displayed a convincing role of small EVs as liquid biopsy. The features of lipid-bilayer membrane of small EVs serve as a physical barrier protecting the cargo from any catalytic activity. Herein, the images of small EVs isolated from human serum were captured by TEM presenting a round-shaped vesicle with around 100 nm in diameter, which are the classical features of small EVs, exosomes. Moreover, further characterisation of the size distribution of the human serum sample and HepaRG CM using NTA analysis observed the median [IQR] was 138.2 [105.9 – 171.9] diameter of isolated nanovesicles, which coincide with the reported size of small EVs population [235, 259, 260]. Identification of the small EVs marker using Western blot analysis to target anti-Tsg101 observed a clear protein band between the reference band of 37 to 50 kDa, which is the reported molecular weight of Tsg101 (44 kDa) [261, 262].

This chapter verified the suitability of small EVs to be used as a novel marker for ADME pathways. Herein, the data were presented in both at mRNA level, and protein level acquiring from RT-PCR and proteomics analysis, respectively. RT-PCR and mass spectrometry-based proteomics are considered to be powerful tools in biomarker discovery both in sensitivity and specificity [263-266]. RT-PCR hold a core concept of traditional PCR in which the gene of interested would be able to amplify only if the targeted cDNA template presence in the sample [267-269]. Likewise, proteomics analysis utilised *de novo* sequencing to identify the available peptide fragments related to the original full protein sequence [270-272]. Hence, the positive results obtained from these two techniques rely absolutely upon the abundance of targeted proteins, RNA in the sample. In this, proteomic screening and RT-PCR analyses demonstrated the presence of multiple CYP and UGT proteins and mRNAs in small EVs isolated from plasma (**Tables 21 and 22**). These data are supported by prior untargeted profiling of small EVs isolated from human urine showing detectable levels of protein from all subcellular compartments including the endoplasmic reticulum, which explicitly identified CYP2D6 [273]. A recent study proposed the specific packaging and circulation of *CYP2E1* in exosomes on the basis of mRNA expression [217]. Here, we similarly demonstrate that of the isoforms screened, *CYP2E1* accounted for 63.5 % relative CYP mRNA expression in small EVs. Notably, *CYP2E1* is also the predominant mRNA detected in human liver, accounting for 34.5 % of total hepatic CYP mRNA expression, and 67.9 % of relative expression for the isoforms screened. Kumar et al. [217] also demonstrated protein expression for multiple CYP in exosomes, although their conclusions in regard to protein quantification must be considered in the context that protein expression was quantified by immunoblot band intensity using isoform specific antibodies. As band intensity depends on the efficiency of antibody binding, the lack of external standardization precluded meaningful comparison of protein abundances.

Targeted proteomics analysis revealed the abundance of CYP3A4 peptides both in human serum EVs and HepaRG cell-released EVs. The CYP3A4 enzyme was the focus in this chapter as it is the predominant CYP isoform in the human liver, responsible for metabolising around 30% of clinically

used drugs, including sorafenib [16]. Although, the amount of the quantified CYP3A4 peptides was comparable between different sample types, it needed to be recognised that their originality was different. Human serum EVs were derived from a 2 mL starting volume of serum, whereas HepaRG EVs derived from 250 mL cultured media with supplementary serial concentration procedures prior to EVs isolation (derived from approximately 120 - 150 million cells per flasks, 10 flasks). Nevertheless, targeted proteomics quantification was inadequate to determine the functionality of the investigated protein as the apparent peptides abundance may be derived from the inactive enzyme. Thus, the apparent number of peptides quantification was insufficient to conclude the research hypothesis of using EVs as a marker for DMEs. As such, subsequent analysis was conducted focusing on the functional activity of CYP3A4 derived from EVs. The functional assay was performed using *ex vivo* CYP activity assay. The activity of CYP3A4 enzyme was measured by the conversion of 1OH-midazolam and/or sorafenib N-oxide as they are the main metabolite derived from CYP3A4 functionalisation. Herein, the functional activity of CYP3A4 was able to be detected from both human serum EVs and HepaRG EVs. Interestingly, whilst the amount of peptide abundance between samples was comparable as mentioned earlier, the functionality of the enzyme was different. Human serum EVs showed around 10-fold higher enzyme activity than HepaRG EVs, yet the observed enzyme activity derived from human serum EVs also noted a large degree of variability. The variability of CYP3A4 functionality observed from human serum EVs was not surprising. As human serum samples were taken from different healthy volunteers, the observed variabilities were representative of inter-individual variability [274]. On the other hand, the *in vitro* system of HepaRG is generally well-controlled and easily standardises the batch process. Such processes included the timeframe of media replenishing, collecting and harvesting. As a result, it has shown consistency in CYP3A4 functionality derived from HepaRG EVs.

The higher CYP3A4 functional activity derived from human serum EV could be described in several speculations. Firstly, enzymes are specialised-type of proteins in which the protein conformation is one of the critical role affecting its functionality. Generally, structure perturbation of proteins could lead to protein malfunction due to changing in its reactivity, selectivity and affinity. However, the current understanding regarding the apparent conformation of EVs-derived CYP3A4 is still limited. In addition, the current analytical setting during the candidature was unable to resolve this contingency. However, it is worth exploring the presumption mentioned above as it may unveil the biological relevance of EVs, which could lead to improvement in the later step of this biomarker discovery attempt. The other speculation that could affect EVs-derived enzyme activity differences is the sample collection procedure. Human serum samples were collected arbitrarily from healthy volunteers, whereas HepaRG media was harvested in a specific manner. Currently, there is limited information regarding the timeframe of the cargo-loading process, which reportedly a particular mechanism depends strongly on the cell of origin [275]. As such, it is possible that the lower the functional activity of EVs-derived CYP3A4 isolated from HepaRG conditioned media compared to human plasma EVs conceivably due

to the inadequate sorting mechanism of DME into the EVs. Such an example has been observed during the developmental process of EV characterisation and isolation in HepaRG CCM (**Appendix 3**). Furthermore, EV isolated from different timeframes and conditions expressed variability in the size distribution profile. This phenomenon strongly suggested a necessity to study further in the perspective of the molecular biology of EVs in both cell culture models and humans.

Nevertheless, identifying this speculation was beyond the scope of this thesis. Further investigation focussing on the proteins composition in a different timeframe of sample collection, both human plasma/serum and *in vitro* EVs, would elucidate this speculation. Thus, there are still several paradigms need to be addressed prior implementing small EVs into the real-life clinical practice.

5.6 Acknowledgement

The author would like to thank Dr. Zivile Useckaite for providing academic support regarding TEM and NTA analysis. Additionally, the author would like to thank Dhilushi Wijayakumara for providing academic support regarding Western blot analysis and mRNA quantification analysis. The author would like to thank Flinders proteomic facility and Adelaide microscopy for providing access to the required instruments to complete this thesis chapter.

CHAPTER 6: CONCLUSIONS

Thesis summary

The strategy to address precision dosing as part of the big picture of 'precision medicine' can be performed in several approaches. The works presented in this thesis only recapitulated a small part of the currently applicable precision dosing and precision medicine methods. Two chapters of this thesis were dedicated to a post-hoc analysis from clinical trial data – a big data analysis. One of those two chapters was focused on verifying the effect of the early dose adjustment and survival outcomes in advanced HCC patients treated with sorafenib. The following study was simultaneously conducted using the same dataset focusing on the possible drug-drug interaction (DDI) affecting sorafenib clinical benefits. Subsequently, the following chapter was dedicated to computational simulation and modelling using Simcyp® PBPK platform as a model-informed drug dosing strategy supporting clinical practice. address the factors affecting variability in sorafenib exposure. Finally, the last part of the works was invoked around laboratory-based biomarker discovery. As biomarker discovery was part of the key research to fulfil the ethos of precision medicine, thus the presenting works were the exploratory research that endeavoured a novel biomarker to track variability in DMEs. In the chapter, EVs were extensively studied both *ex vivo* and *in vitro* models to validate its potential role as a tool to track the variability in DMEs.

The study in **Chapter 2** and **3** demonstrated an expanded horizon of computational-based approach to address the precision dosing of sorafenib. Big data analytics using R programming (https://www.r-project.org) was the primary tool in investigating the designated dataset. A phase III clinical trial data obtained from data sharing source (https://www.projectdatasphere.org) was utilised to investigate two crucial research questions, which result in the reports in those two Chapters. **Chapter 2** focussed on the impact of dose adjustment during the early treatment initiation period on the long-term survival outcomes in advanced HCC patients treated with sorafenib. On the other hand, **Chapter 3** mainly interrogated the effect of DDI on the treatment benefit of sorafenib. The finding in **Chapter 2** was the very first time to demonstrate the effect of the early dose adjustment of sorafenib due to AEs on the survival outcomes in advanced HCC patients. It appeared that there were no worsening survival outcomes in patients who underwent early dose adjustment, either dose reduction or dose interruption. In contrast, patients who took no action or withdrew sorafenib showed poorer survival outcomes, both OS and PFS. Furthermore, additional cautions for particular patient characteristics were also provided in the analysis. These subgroups of patients possibly required additional monitoring as the analysis suggested a higher susceptibility to develop AEs, which lead to sorafenib dose adjustments. **Chapter 2** emphasised the significance of the initial dose of sorafenib as it seemed that the optimal starting dose associated with better long-term clinical benefits. The circumstance when experiencing specific toxicity following the administration of cancer medicine can be implied as an "on-target" toxicity. Several

studied showed that patients who experienced particular toxicities after commencing a cancer medicine tend to obtain a better clinical outcome [160, 276, 277].

Subsequently, **Chapter 3** utilised the same dataset as in **Chapter 2** but focussed on DDI paradigm during cancer treatments. Unquestionably, DDI as part of the polypharmacy issue is the underrated issue in long-term management in cancer therapy [278-281]. Using multiple medications were commonly observed among elderly patients in which the number of medications seems to be associated with age [282, 283]. Although some medications are mandatory for life-threatening chronic diseases, however, some are not admittedly necessary, such as herbal medicines. Among the frequently used non-cancer medicines in cancer patients, PPIs were one of the most concerning groups to cause DDI with orally cancer medicines [284-286]. PPIs have a prolonged duration of action with primary mechanism to alter intragastric pH to be less acidic, which compromised the absorption of pH sensitive drugs such as erlotinb and capecitabine [40, 285]. Hence, it is a reasonable assumption to speculate that similar interaction is highly likely to occur in sorafenib. This had led to the primary analysis in **Chapter 3** to evaluate the effect of concomitant use of PPIs and sorafenib on survival outcomes in advanced HCC patients. The results from **Chapter 3** made clarity to the safety concern regarding the impact of PPIs on sorafenib efficacy, where no worsening survival outcomes were observed. The finding has given better confidence to advanced HCC patients regarding safety concern when PPI is required during sorafenib's treatment course. However, the analyses were conducted focussing only on PPIs, whereas, in reality, there are several classes of gastric acid suppressants on the market. Future research can be conducted in two possible directions to expand the understanding of this circumference. Firstly, the larger study population from any other completed clinical trials are required to evaluate the impact of each PPI on sorafenib and/ or other cancer medicines. The analysis in **Chapter 3** only evaluates PPIs as a class, although each PPI has somewhat different characteristics. The population expansion would increase the analysis power, capable of extensive investigation on each different PPIs and other relevant research questions. The larger dataset also leads to the subsequent second direction in which the other available gastric acid suppressants could be further examined. As such, the analysis focuses on Histamine-2 receptor antagonist (H2RA), antacids, and alginate-based raft forming agents will be conducted as they were the secondarily frequently used acid suppressant to PPI [287, 288].

Chapter 2 and **Chapter 3** demonstrated the capability of clinical epidemiology where post-hoc analysis of the clinical trial data – a large high-quality data was utilised to the greatest extent. Moreover, they have also illustrated the contemporary researches in which the available data sources were maximally utilised in order to promote better precision dosing [289-291]. However, the strength of this type of approach aligns with its unavoidable shortcoming. The most prominent limitation of clinical epidemiology is variation of time to complete a single investigation [292]. By default, the timeframe to obtain the desired dataset until thoroughly analyses may require exorbitant of time [293]. The complexity of research questions also contributes to the length of time to finish the analysis, to a certain

extent. Unquestionably, this is unlikely to comply with the on-demand real-time precision dosing scenario. Hence, clinical epidemiology tends to be an excellent candidate for a sustainable approach to address precision dosing in a non-time constraints fashion [294, 295]. Nevertheless, to reciprocate the instantaneous precision dosing in a clinical setting, a congruous optional approach is required.

Using PBPK modelling and simulation to evaluate factors affecting the variability in sorafenib exposure signified a modern approach to guide precision dosing in cancer medicine (**Chapter 4**). PBPK is a versatile tool suitable for interrogating potential factors affecting the pharmacokinetics-pharmacodynamics of newly-developed/launched drugs. The important role of PBPK has been observed not only in drug discovery and development but also as a reassuring tool to support the regulatory submission [296, 297]. Herein, PBPK was employed to investigate factors affecting variability in sorafenib exposure and further implemented to evaluate whether the composed MIDS could improve the exposure profile or not. Following the results derived from the simulation data, liver CYP3A4 abundance was the predominant factor driving the variability in sorafenib exposure. The other patients' characteristics, including albumin, BMI, BSA, gender and weight were also, to a lesser degree, contributed to the variability in sorafenib exposure. A multivariable linear regression modelling accounted for the covariates mentioned above is possible to predict individual failing to achieve therapeutic threshold of sorafenib with high sensitivity (95.2%) and specificity (95%). The ADAM absorption sub-model in Simcyp® simulator was chosen to characterise a full-PBPK profile of sorafenib as it was the most appropriate module for the present modelling. This sub-model considered a multidimensional paradigm for modelling such as multiple compartmental interactions and intrinsic physicochemical property, hence allow the robustness of exposure profile to be simulated [208, 298]. As a result, the observed and simulated profile of sorafenib exposure demonstrated a concurring absorption phase, as shown in the C_{max} and T_{max} value. Subsequently, PBPK simulation in conjunction with MIDS accounted for crucial parameters contributing to the variability of sorafenib exposure results in 99% of subjects achieving therapeutic threshold.

Although the analysis was able to reveal the potential factors affecting the variability of sorafenib exposure, there are still several elements yet to improve. Evidence showed that sorafenib exhibit enterohepatic recirculation (EHC), as aforementioned elsewhere in this thesis, thus it poses a complexity during the construction of the compound model in Simcyp® platform. Simcyp® is the proprietary platform which somewhat limited the advanced configuration setting. As such, the developer restricts the ADAM sub-model in Simcyp® simulator not to enable EHC when the compound model is specified as oral dosage form. Hence, the simulation was conducted while recognising an impediment, to a certain extent, due to this factor. Similarly, several previous studies observed the challenges of building a compound model of sorafenib, such as in the case of Lokesh et al. Lokesh et al. described sorafenib absorption model as a one-compartment with additional four gastrointestinal transit compartments and semi-mechanistic EHC. Although the model was successfully developed to

portray the delayed absorption and the present of EHC, the residual error of plasma concentration was very high (50%) [183]. As such, this reflects the current challenges of model-informed precision dosing for the compounds manifesting an intricated physicochemical property. Essentially, further development for the more versatile or even cross-platform simulator would be necessary to enhance the prediction performance to a greater extent [299-301].

At present, the new concept of virtual twins is perhaps the most explicit perspective in model-informed precision dosing area. [199, 205]. This concept is still based on the current Simcyp® PBPK modelling, but it takes into account more individual patient-oriented data such as organ size, local/systemic inflammatory status, DMEs profile (both genotype and phenotype) and haematological parameters [199, 205]. A successful application of virtual twins was first shown in the case of prediction of olanzapine exposure. In the study, the virtual twins were created for each individual by individualising the Simcyp® virtual healthy population with corresponding data from real patients recruited in the counterpart. Patient characteristics were specifically assigned the CYP2C8 genotype and CYP1A2 phenotype based on additional laboratory finding performing in parallel during the study [205]. Although a thriving performance of virtual twins, it was also suggested that the superior prediction performance could be obtained only when the activities of DMEs in the major organs were sufficiently defined. Admittedly, it is almost impossible to verify DMEs activity in every patient as surgical tissue biopsies cause a painful and higher risk to patients. Thus, it has led to the significance in the finding of potential novel ADME biomarkers to estimate DMEs abundance, as shown in **Chapter 5**.

The conclusion derived from the two chapters in clinical epidemiology and the proposed perspective in **Chapter 4** led to the exploratory research focussing on biomarker discovery. Ultimately, the novel biomarkers should serve as a supporting interplay between computational and laboratory-based to succeed the precision dosing. A liquid biopsy was considered an appropriate source to explore in the novel biomarkers during this thesis was commencing. Liquid biopsy is a concept referring to any blood or other biofluid-derived material that can be used to provide a genetic landscape or track the cellular status of the organ of interested [302-305]. Unlike tissue biopsy, this approach offers a nearly pain-free sample collection, which allows more accessible to a wide range of patients. EVs were the centres of an extensive study in this thesis as the main objective of **Chapter 5** was to evaluate its role as a tool to track variability in DME. Herein, a preliminary study hypothesising the abundance of DME genes and proteins expression in human plasma EVs was firstly conducted. This was to serve as a proof of concept as the ultimate goal of the study is to apply the knowledge in a real clinical setting. Thus, if there is no relevant information regarding the hypothesis, it would be futile in continuing the study. Human plasma EVs were successfully isolated with reporting the size range of 50-150 nm and the presence of EVs marker, Tsg101. Subsequently, RT-PCR analysis of the RNA extracted from the samples revealed the abundance of several CYPs and UGTs, suggesting the expression of DMT gene in human plasma EVs. On the other hand, proteomics analysis using in-gel digestion method aiming to the protein band at 40-

70 kDa revealed the abundance of DME peptides derived from human plasma EVs. Noticeably, the peptides of accessory cofactors for drug metabolism were additionally found in the human plasma EVs. Thus, the finding provides a convincing indication for developing EV as a biomarker for drug metabolism pathway (ADMExosomes).

The confirmation of DME expression derived from human plasma EVs has led to a subsequent work focusing on the functionality perspective. Here, the *in vitro* model of hepatocytes, HepaRG was introduced as the primary source to study ADMExosomes. Notably, *in vitro* model is a flexible medium suitable for the initial phase of research and development. It holds several important advantages such as high consistency and reproducibility, relatively low cost, ease of pharmacological manipulations [306]. Unlike *ex vivo*, *in vitro* model has more accessible in which the sample can be collected, almost, anytime in large portion amount with no ethical consideration involved [307]. HepaRG is a well-established hepatocyte cell lines with highly expressed in a panel of DMEs. Upon obtaining from a different laboratory, HepaRG was briefly validated as it was the first time the cells were introduced into the new facility. Meanwhile, optimisation of EVs isolation from *in vitro* HepaRG model was conducted in parallel. During this optimisation period, it had seen a phenomenon of EVs secretion associated with different cells conditions. One of the validation processes was to verify the inducibility of HepaRG in response to typical enzyme-inducing agents. Such processes require removing FBS and DMSO from the maintenance media to recalibrate the basal enzyme activity. It was found that the EVs isolated from the cell during FBS and DMSO-deprived had a different profile compared to the normal condition. Such difference can be seen from the smaller size distribution and higher EVs concentration from the first 24 hours after DMSO and FBS deprivation (**Appendix 3**). It could be assumed that removing the essential media components afflicts cellular environments, leading to change in EVs profile. Evidently, introducing moderate stress to the cells such as hypoxic incubation and acidic pH [308, 309] resulting in the promotion of EVs secretion. Moreover, perturbating energy production in the cells by inhibiting glycolysis and oxidative phosphorylation results in an increased number of EVs secretion [310]. Although the instigating mechanisms were different, they shared the similar concept of interfering the normal condition of cells culture and maintenance. Hence, the finalised culturing condition of HepaRG in the actual study was William's E media with essential additives as mentioned elsewhere in **Appendix 3**.

The abundance and functionality of ADMExosomes derived from HepaRG and human serum were subsequently evaluated as the primary focus of **Chapter 5**. Human serum samples were used mainly in the subsequent study due to the availability of samples. Prior work conducted in this laboratory demonstrated that plasma and serum are equivalent in terms of EVs derived CYP3A4 protein abundance. Herein, CYP3A4 enzyme was the major CYP isoforms extensively studied as it has a broad catalytic capability and most abundant among other enzymes in the liver. Proteomics analysis observed the presence of CYP3A4 peptides from both HepaRG and human serum EVs suggesting the relevant

of enzymes in the EVs. However, only human serum EVs produced catalytic activity of CYP3A4 but not HepaRG EVs. Formation of 1OH-midazolam or sorafenib N-oxide was observed after incubation human serum EVs with midazolam or sorafenib, respectively in the *ex vivo* assay. Although the volume of media harvested from HepaRG was considerably large (250 mL), there was no meaningful catalytic activity of CYP3A4 observed. This might be suggested that the abundance of CYP3A4 peptides derived from HepaRG EVs as found in the proteomic analysis may not be entirely functioning. Importantly, it has to be acknowledged that the method to verify the catalytic activity and abundance were in a different principle. The label-free, MS2 product ion scan method as part of proteomics analysis was employed to quantify the abundance of CYP3A4 in EVs samples. This method delivers high precision, sensitivity and reproducibility to quantify/ qualify the protein of interest from the biological samples [311-313]. Nevertheless, proteomics analyses investigate only a fraction of the entire protein sequence to determine the actual abundance in the investigated samples [314, 315]. However, it could not explicitly define the integrity or conformation of the proteins of interest. In contrast, functionality assessments, such as *ex vivo* assay, rely strongly on the integrity of the proteins. Admittedly, the catalytic activity of enzymes depends profoundly on the protein conformation, which is highly likely related to proteins' integrity [316-318]. Evidence supported that even small protein modification remotely from the active site could alter protein dynamic and overall enzyme mechanisms [319, 320]. In the case of CYP3A4, three major conformations have been confirmed based on computational analysis of crystal structures [321]. Nevertheless, it is beyond the scope of this thesis to determine the conformation-related enzyme activity. However, an in-depth analysis of this aspect needs to be addressed as it could potentially impact the catalytic functions. On the other hand, it is also unknown regarding the abundance of any other relevant accessory cofactors for xenobiotics metabolism such as cytochrome b5. Cytochrome b5 serves as one of the electron donors in the catalytic cycle of CYP450. Although its abundance was confirmed in EVs secreted from several cells, there is no information regarding its absolute abundance and functionality perspective [322, 323].

This thesis highlighted multidimensional approaches to address precision dosing, especially for the group of drugs that requires close attention, such as cancer medicines. Here, sorafenib was selected as an exemplar of drugs with a particular pharmacokinetic profile and one of the first-line option for cancer patients in the advanced stage. Although this thesis demonstrated several achievements either obtaining from computational-oriented or laboratory-oriented works, typical limitations could still be observed across those two paradigms. The laboratory-oriented work involving the exploratory of EVs research showed great potential as a new supporting player in the modern precision dosing as part of the precision medicine. Nevertheless, it requires further elucidation and elaboration to apply this cutting-edge knowledge to clinical reality.

REFERENCE

1. Least, C.J., Jr., G.F. Johnson, and H.M. Solomon, (1975) Therapeutic monitoring of anticonvulsant drugs: gas-chromatographic simultaneous determination of primidone, phenylethylmalonamide, carbamazepine, and diphenylhydantoin. Clin Chem. 21(11): p. 1658-62.
2. Ce, P. and R. Ts, (1975) Phenobarbital plasma levels in neonates. Clinics in Perinatology. 2: p. 111.
3. Ros-Vivancos, C., M. González-Hernández, J.F. Navarro-Gracia, J. Sánchez-Payá, A. González-Torga, and J. Portilla-Sogorb, (2018) Evolution of treatment of syphilis through history. Rev Esp Quimioter. 31(6): p. 485-492.
4. Mass, R.D., M.F. Press, S. Anderson, M.A. Cobleigh, C.L. Vogel, N. Dybdal, G. Leiberman, and D.J. Slamon, (2005) Evaluation of clinical outcomes according to HER2 detection by fluorescence in situ hybridization in women with metastatic breast cancer treated with trastuzumab. Clin Breast Cancer. 6(3): p. 240-6.
5. Giordano, S.H., S. Temin, S. Chandarlapaty, J.R. Crews, F.J. Esteva, J.J. Kirshner, I.E. Krop, J. Levinson, N.U. Lin, S. Modi, et al., (2018) Systemic Therapy for Patients With Advanced Human Epidermal Growth Factor Receptor 2–Positive Breast Cancer: ASCO Clinical Practice Guideline Update. Journal of Clinical Oncology. 36(26): p. 2736-2740.
6. Ithimakin, S., K.C. Day, F. Malik, Q. Zen, S.J. Dawsey, T.F. Bersano-Begey, A.A. Quraishi, K.W. Ignatoski, S. Daignault, A. Davis, et al., (2013) HER2 Drives Luminal Breast Cancer Stem Cells in the Absence of HER2 Amplification: Implications for Efficacy of Adjuvant Trastuzumab. Cancer Research. 73(5): p. 1635-1646.
7. Clunes, M.T. and R.C. Boucher, (2007) Cystic Fibrosis: The Mechanisms of Pathogenesis of an Inherited Lung Disorder. Drug discovery today. Disease mechanisms. 4(2): p. 63-72.
8. *Cystic Fibrosis Foundation. Cystic Fibrosis Foundation Patient Registry 2019 Annual Data Report.* Cystic Fibrosis Foundation: Bethesda.
9. Wainwright, C.E., J.S. Elborn, B.W. Ramsey, G. Marigowda, X. Huang, M. Cipolli, C. Colombo, J.C. Davies, K. De Boeck, P.A. Flume, et al., (2015) Lumacaftor–Ivacaftor in Patients with Cystic Fibrosis Homozygous for Phe508del CFTR. New England Journal of Medicine. 373(3): p. 220-231.
10. Polasek, T.M., S. Shakib, and A. Rostami-Hodjegan, (2018) Precision dosing in clinical medicine: present and future. Expert Review of Clinical Pharmacology. 11(8): p. 743-746.
11. Darwich, A.S., K. Ogungbenro, O.J. Hatley, and A. Rostami-Hodjegan, (2017) Role of pharmacokinetic modeling and simulation in precision dosing of anticancer drugs. Translational Cancer Research: p. S1512-S1529.
12. Tyson, R.J., C.C. Park, J.R. Powell, J.H. Patterson, D. Weiner, P.B. Watkins, and D. Gonzalez, (2020) Precision Dosing Priority Criteria: Drug, Disease, and Patient Population Variables. Frontiers in pharmacology. 11: p. 420-420.
13. Hopkins, A.M., B.D. Menz, M.D. Wiese, G. Kichenadasse, H. Gurney, R.A. McKinnon, A. Rowland, and M.J. Sorich, (2020) Nuances to precision dosing strategies of targeted cancer medicines. Pharmacology Research & Perspectives. 8(4): p. e00625.
14. De Ruysscher, D., J. Jin, T. Lautenschlaeger, J.X. She, Z. Liao, and F.S. Kong, (2017) Blood-based biomarkers for precision medicine in lung cancer: precision radiation therapy. Transl Lung Cancer Res. 6(6): p. 661-669.
15. Centanni, M. and L.E. Friberg, (2020) Model-Based Biomarker Selection for Dose Individualization of Tyrosine-Kinase Inhibitors. Frontiers in Pharmacology. 11(316).
16. Laurence L. Brunton, R.H.-D., Björn C. Knollmann, *Goodman & Gilman's: The Pharmacological Basis of Therapeutics*. 2017, McGraw-Hill Education: United States of America.
17. Zhang, X., Q.-Y. Zhang, D. Liu, T. Su, Y. Weng, G. Ling, Y. Chen, J. Gu, B. Schilling, and X. Ding, (2005) Expression of cytochrome p450 and other biotransformation genes in fetal and adult human nasal mucosa. Drug Metabolism and Disposition. 33(10): p. 1423-1428.
18. Dutheil, F., S. Dauchy, M. Diry, V. Sazdovitch, O. Cloarec, L. Mellottée, I. Bièche, M. Ingelman-Sundberg, J.P. Flinois, I. de Waziers, et al., (2009) Xenobiotic-metabolizing enzymes

and transporters in the normal human brain: regional and cellular mapping as a basis for putative roles in cerebral function. Drug Metab Dispos. 37(7): p. 1528-38.
19. Baron, J.M., T. Wiederholt, R. Heise, H.F. Merk, and D.R. Bickers, (2008) Expression and function of cytochrome p450-dependent enzymes in human skin cells. Curr Med Chem. 15(22): p. 2258-64.
20. Barnes, J.M., (1960) Detoxication Mechanisms. The Metabolism and Detoxication of Drugs, Toxic Substances and Other Organic Compounds. British Journal of Industrial Medicine. 17(3): p. 244-244.
21. David Josephy, P., F. Peter Guengerich, and J.O. Miners, (2005) "Phase I and Phase II" Drug Metabolism: Terminology that we Should Phase Out? Drug Metabolism Reviews. 37(4): p. 575-580.
22. Garfinkel, D., (1958) Studies on pig liver microsomes. I. Enzymic and pigment composition of different microsomal fractions. Arch Biochem Biophys. 77(2): p. 493-509.
23. Furge, L.L. and F.P. Guengerich, (2006) Cytochrome P450 enzymes in drug metabolism and chemical toxicology: An introduction. Biochemistry and Molecular Biology Education. 34(2): p. 66-74.
24. Zhang, Y.-Y. and L. Yang, (2009) Interactions between human cytochrome P450 enzymes and steroids: physiological and pharmacological implications. Expert Opinion on Drug Metabolism & Toxicology. 5(6): p. 621-629.
25. Zanger, U.M. and M. Schwab, (2013) Cytochrome P450 enzymes in drug metabolism: Regulation of gene expression, enzyme activities, and impact of genetic variation. Pharmacology & Therapeutics. 138(1): p. 103-141.
26. van der Weide, J., L.S. Steijns, and M.J. van Weelden, (2003) The effect of smoking and cytochrome P450 CYP1A2 genetic polymorphism on clozapine clearance and dose requirement. Pharmacogenetics. 13(3): p. 169-72.
27. Andersson, T., C.G. Regårdh, M.L. Dahl-Puustinen, and L. Bertilsson, (1990) Slow omeprazole metabolizers are also poor S-mephenytoin hydroxylators. Ther Drug Monit. 12(4): p. 415-6.
28. van der Weide, J., L.S. Steijns, and M.J. van Weelden, (2003) The effect of smoking and cytochrome P450 CYP1A2 genetic polymorphism on clozapine clearance and dose requirement. Pharmacogenetics and Genomics. 13(3): p. 169-172.
29. Bjørngaard, J.H., A.T. Nordestgaard, A.E. Taylor, J.L. Treur, M.E. Gabrielsen, M.R. Munafò, B.G. Nordestgaard, B.O. Åsvold, P. Romundstad, and G. Davey Smith, (2017) Heavier smoking increases coffee consumption: findings from a Mendelian randomization analysis. International Journal of Epidemiology. 46(6): p. 1958-1967.
30. Zhang, H.F., H.H. Wang, N. Gao, J.Y. Wei, X. Tian, Y. Zhao, Y. Fang, J. Zhou, Q. Wen, J. Gao, et al., (2016) Physiological Content and Intrinsic Activities of 10 Cytochrome P450 Isoforms in Human Normal Liver Microsomes. J Pharmacol Exp Ther. 358(1): p. 83-93.
31. Isvoran, A., M. Louet, D.L. Vladoiu, D. Craciun, M.-A. Loriot, B.O. Villoutreix, and M.A. Miteva, (2017) Pharmacogenomics of the cytochrome P450 2C family: impacts of amino acid variations on drug metabolism. Drug Discovery Today. 22(2): p. 366-376.
32. Brandt, J.T., S.L. Close, S.J. Iturria, C.D. Payne, N.A. Farid, C.S. Ernest Ii, D.R. Lachno, D. Salazar, and K.J. Winters, (2007) Common polymorphisms of CYP2C19 and CYP2C9 affect the pharmacokinetic and pharmacodynamic response to clopidogrel but not prasugrel. Journal of Thrombosis and Haemostasis. 5(12): p. 2429-2436.
33. Deshpande, N., S. V, R.K. V V, M. H V V, S. M, R. Banerjee, M. Tandan, and N.R. D, (2016) Rapid and ultra-rapid metabolizers with CYP2C19*17 polymorphism do not respond to standard therapy with proton pump inhibitors. Meta gene. 9: p. 159-164.
34. Mahgoub, A., J.R. Idle, L.G. Dring, R. Lancaster, and R.L. Smith, (1977) Polymorphic hydroxylation of Debrisoquine in man. Lancet. 2(8038): p. 584-6.
35. Burk, O., H. Tegude, I. Koch, E. Hustert, R. Wolbold, H. Glaeser, K. Klein, M.F. Fromm, A.K. Nuessler, P. Neuhaus, et al., (2002) Molecular mechanisms of polymorphic CYP3A7 expression in adult human liver and intestine. J Biol Chem. 277(27): p. 24280-8.
36. Sever, R. and C.K. Glass, Signaling by nuclear receptors. Cold Spring Harbor perspectives in biology. 5(3): p. a016709-a016709.

37. Chai, X., S. Zeng, and W. Xie, (2013) Nuclear receptors PXR and CAR: implications for drug metabolism regulation, pharmacogenomics and beyond. Expert Opin Drug Metab Toxicol. 9(3): p. 253-66.
38. Istrate, M.A., A.K. Nussler, M. Eichelbaum, and O. Burk, (2010) Regulation of CYP3A4 by pregnane X receptor: The role of nuclear receptors competing for response element binding. Biochem Biophys Res Commun. 393(4): p. 688-93.
39. Cropp, J.S. and H.I. Bussey, (1997) A review of enzyme induction of warfarin metabolism with recommendations for patient management. Pharmacotherapy. 17(5): p. 917-28.
40. Ohgami, M., T. Kaburagi, A. Kurosawa, K. Doki, T. Shiozawa, N. Hizawa, and M. Homma, (2018) Effects of Proton Pump Inhibitor Coadministration on the Plasma Concentration of Erlotinib in Patients With Non-Small Cell Lung Cancer. Ther Drug Monit. 40(6): p. 699-704.
41. Uusi-Oukari, M. and E.R. Korpi, (2010) Regulation of $GABA_A$ Receptor Subunit Expression by Pharmacological Agents. Pharmacological Reviews. 62(1): p. 97-135.
42. Cressey, T.R., N. Plipat, F. Fregonese, and K. Chokephaibulkit, (2007) Indinavir/ritonavir remains an important component of HAART for the treatment of HIV/AIDS, particularly in resource-limited settings. Expert Opinion on Drug Metabolism & Toxicology. 3(3): p. 347-361.
43. Holmes, D.R., G.J. Dehmer, S. Kaul, D. Leifer, P.T. O'Gara, and C.M. Stein, (2010) ACCF/AHA Clopidogrel Clinical Alert: Approaches to the FDA "Boxed Warning". A report of the american college of cardiology foundation task force on clinical expert consensus documents and the american heart association endorsed by the society for cardiovascular angiography and interventions and the society of thoracic surgeon. 56(4): p. 321-341.
44. Lau, W.C., T.D. Welch, T. Shields, M. Rubenfire, U.S. Tantry, and P.A. Gurbel, (2011) The effect of St John's Wort on the pharmacodynamic response of clopidogrel in hyporesponsive volunteers and patients: increased platelet inhibition by enhancement of CYP3A4 metabolic activity. J Cardiovasc Pharmacol. 57(1): p. 86-93.
45. Van Booven, D., S. Marsh, H. McLeod, M.W. Carrillo, K. Sangkuhl, T.E. Klein, and R.B. Altman, (2010) Cytochrome P450 2C9-CYP2C9. Pharmacogenetics and genomics. 20(4): p. 277-281.
46. Lima, J.J., C.D. Thomas, J. Barbarino, Z. Desta, S.L. Van Driest, N. El Rouby, J.A. Johnson, L.H. Cavallari, V. Shakhnovich, D.L. Thacker, et al., (2021) Clinical Pharmacogenetics Implementation Consortium (CPIC) Guideline for CYP2C19 and Proton Pump Inhibitor Dosing. Clin Pharmacol Ther. 109(6): p. 1417-1423.
47. LeBlanc, T.W., M.J. McNeil, A.H. Kamal, D.C. Currow, and A.P. Abernethy, (2015) Polypharmacy in patients with advanced cancer and the role of medication discontinuation. The Lancet Oncology. 16(7): p. e333-e341.
48. Murphy, C.C., H.M. Fullington, C.A. Alvarez, A.C. Betts, S.J.C. Lee, D.A. Haggstrom, and E.A. Halm, (2018) Polypharmacy and patterns of prescription medication use among cancer survivors. Cancer. 124(13): p. 2850-2857.
49. Patel, D., R. Bertz, S. Ren, D.W. Boulton, and M. Någård, (2020) A Systematic Review of Gastric Acid-Reducing Agent-Mediated Drug–Drug Interactions with Orally Administered Medications. Clinical Pharmacokinetics. 59(4): p. 447-462.
50. Sharma, M., H.M. Holmes, H.B. Mehta, H. Chen, R.R. Aparasu, Y.T. Shih, S.H. Giordano, and M.L. Johnson, (2019) The concomitant use of tyrosine kinase inhibitors and proton pump inhibitors: Prevalence, predictors, and impact on survival and discontinuation of therapy in older adults with cancer. Cancer. 125(7): p. 1155-1162.
51. Zhang, D., G. Luo, X. Ding, and C. Lu, (2012) Preclinical experimental models of drug metabolism and disposition in drug discovery and development. Acta Pharmaceutica Sinica B. 2(6): p. 549-561.
52. Knights, K.M., D.M. Stresser, J.O. Miners, and C.L. Crespi, (2016) In Vitro Drug Metabolism Using Liver Microsomes. Current Protocols in Pharmacology. 74(1): p. 7.8.1-7.8.24.
53. Sahi, J., S. Grepper, and C. Smith, (2010) Hepatocytes as a tool in drug metabolism, transport and safety evaluations in drug discovery. Curr Drug Discov Technol. 7(3): p. 188-98.
54. Zhao, P., K.L. Kunze, and C.A. Lee, (2005) Evaluation of time-dependent inactivation of cyp3a in cryopreserved human hepatocytes. Drug Metabolism and Disposition. 33(6): p. 853-861.

55. Hariparsad, N., R.S. Sane, S.C. Strom, and P.B. Desai, (2006) In vitro methods in human drug biotransformation research: Implications for cancer chemotherapy. Toxicology in Vitro. 20(2): p. 135-153.
56. *EURL ECVAM Tracking System for Alternative methods towards Regulatory acceptance. Cytochrome P450 (CYP) enzyme induction in vitro method using cryopreserved differentiated human HepaRG™ cells*, E.S.H. Joint Research Centre (JRC), Editor. 2009, European Commission Joint Research Centre's EU Reference Laboratory for Alternatives to Animal Testing.
57. Aninat, C., A. Piton, D. Glaise, T. Le Charpentier, S. Langouët, F. Morel, C. Guguen-Guillouzo, and A. Guillouzo, (2005) Expression of cytochromes p450, conjugating enzymes and nuclear receptors in human hepatoma heparg cells. Drug Metabolism and Disposition. 34(1): p. 75.
58. Guillouzo, A., A. Corlu, C. Aninat, D. Glaise, F. Morel, and C. Guguen-Guillouzo, (2007) The human hepatoma HepaRG cells: A highly differentiated model for studies of liver metabolism and toxicity of xenobiotics. Chemico-Biological Interactions. 168(1): p. 66-73.
59. Andersson, T.B., K.P. Kanebratt, and J.G. Kenna, (2012) The HepaRG cell line: a unique in vitro tool for understanding drug metabolism and toxicology in human. Expert opinion on drug metabolism & toxicology. 8(7): p. 909-920.
60. Anthérieu, S., C. Chesné, R. Li, S. Camus, A. Lahoz, L. Picazo, M. Turpeinen, A. Tolonen, J. Uusitalo, C. Guguen-Guillouzo, et al., (2010) Stable Expression, Activity, and Inducibility of Cytochromes P450 in Differentiated HepaRG Cells. Drug Metabolism and Disposition. 38(3): p. 516.
61. Cerec, V., D. Glaise, D. Garnier, S. Morosan, B. Turlin, B. Drenou, P. Gripon, D. Kremsdorf, C. Guguen-Guillouzo, and A. Corlu, (2007) Transdifferentiation of hepatocyte-like cells from the human hepatoma HepaRG cell line through bipotent progenitor. Hepatology. 45(4): p. 957-967.
62. Michaut, A., D. Le Guillou, C. Moreau, S. Bucher, M.R. McGill, S. Martinais, T. Gicquel, I. Morel, M.-A. Robin, H. Jaeschke, et al., (2016) A cellular model to study drug-induced liver injury in nonalcoholic fatty liver disease: application to acetaminophen. Toxicology and applied pharmacology. 292: p. 40-55.
63. Troadec, M.-B., D. Glaise, G. Lamirault, M. Le Cunff, E. Guérin, N. Le Meur, L. Détivaud, P. Zindy, P. Leroyer, I. Guisle, et al., (2006) Hepatocyte iron loading capacity is associated with differentiation and repression of motility in the HepaRG cell line. Genomics. 87(1): p. 93-103.
64. Jossé, R., C. Aninat, D. Glaise, J. Dumont, V. Fessard, F. Morel, J.-M. Poul, C. Guguen-Guillouzo, and A. Guillouzo, (2008) Long-Term Functional Stability of Human HepaRG Hepatocytes and Use for Chronic Toxicity and Genotoxicity Studies. Drug Metabolism and Disposition. 36(6): p. 1111-1118.
65. Kanebratt, K.P. and T.B. Andersson, (2008) HepaRG Cells as an in Vitro Model for Evaluation of Cytochrome P450 Induction in Humans. Drug Metabolism and Disposition. 36(1): p. 137-145.
66. Kanebratt, K.P. and T.B. Andersson, (2008) Evaluation of HepaRG Cells as an in Vitro Model for Human Drug Metabolism Studies. Drug Metabolism and Disposition. 36(7): p. 1444-1452.
67. Iwatsubo, T., H. Suzuki, and Y. Sugiyama, (1997) Prediction of species differences (rats, dogs, humans) in the *in vivo* metabolic clearance of YM796 by the liver from *in vitro* data. Journal of Pharmacology and Experimental Therapeutics. 283(2): p. 462-469.
68. Boase, S. and J.O. Miners, (2002) In vitro-in vivo correlations for drugs eliminated by glucuronidation: investigations with the model substrate zidovudine. Br J Clin Pharmacol. 54(5): p. 493-503.
69. Knights, K.M., S.M. Spencer, J.K. Fallon, N. Chau, P.C. Smith, and J.O. Miners, (2016) Scaling factors for the in vitro-in vivo extrapolation (IV-IVE) of renal drug and xenobiotic glucuronidation clearance. Br J Clin Pharmacol. 81(6): p. 1153-64.
70. Gómez-Lechón, M.J., T. Donato, X. Ponsoda, and J.V. Castell, (2003) Human hepatic cell cultures: in vitro and in vivo drug metabolism. Altern Lab Anim. 31(3): p. 257-65.

71. Pelkonen, O. and M. Turpeinen, (2007) In vitro-in vivo extrapolation of hepatic clearance: biological tools, scaling factors, model assumptions and correct concentrations. Xenobiotica. 37(10-11): p. 1066-89.
72. Shiran, M.R., N.J. Proctor, E.M. Howgate, K. Rowland-Yeo, G.T. Tucker, and A. Rostami-Hodjegan, (2006) Prediction of metabolic drug clearance in humans: in vitro-in vivo extrapolation vs allometric scaling. Xenobiotica. 36(7): p. 567-80.
73. Chen, W.W., M. Niepel, and P.K. Sorger, (2010) Classic and contemporary approaches to modeling biochemical reactions. Genes & development. 24(17): p. 1861-1875.
74. Duggleby, R.G. and R.B. Clarke, (1991) Experimental designs for estimating the parameters of the Michaelis-Menten equation from progress curves of enzyme-catalyzed reactions. Biochimica et Biophysica Acta (BBA) - Protein Structure and Molecular Enzymology. 1080(3): p. 231-236.
75. Naritomi, Y., S. Terashita, S. Kimura, A. Suzuki, A. Kagayama, and Y. Sugiyama, (2001) Prediction of human hepatic clearance from in vivo animal experiments and in vitro metabolic studies with liver microsomes from animals and humans. Drug Metab Dispos. 29(10): p. 1316-24.
76. Miners, J.O., P.A. Smith, M.J. Sorich, R.A. McKinnon, and P.I. Mackenzie, (2004) Predicting human drug glucuronidation parameters: application of in vitro and in silico modeling approaches. Annu Rev Pharmacol Toxicol. 44: p. 1-25.
77. Ito, K. and J.B. Houston, (2005) Prediction of human drug clearance from in vitro and preclinical data using physiologically based and empirical approaches. Pharm Res. 22(1): p. 103-12.
78. Miners, J.O., K.M. Knights, J.B. Houston, and P.I. Mackenzie, (2006) In vitro-in vivo correlation for drugs and other compounds eliminated by glucuronidation in humans: pitfalls and promises. Biochem Pharmacol. 71(11): p. 1531-9.
79. Čulen, M., P.K. Tuszyński, S. Polak, R. Jachowicz, A. Mendyk, and J. Dohnal, (2015) Development of *In Vitro - In Vivo* Correlation/Relationship Modeling Approaches for Immediate Release Formulations Using Compartmental Dynamic Dissolution Data from "Golem": A Novel Apparatus. BioMed Research International. 2015: p. 328628.
80. Herries, D.G., (1988) Enzyme Kinetics: by A Cornish-Bowden and C W Wharton. pp 77. In Focus series, IRL Press Ltd, Oxford. 1988. £5.95. Biochemical Education. 16(3): p. 179-180.
81. Cornish-Bowden, A., (2015) One hundred years of Michaelis–Menten kinetics. Perspectives in Science. 4: p. 3-9.
82. Michaelis, L. and M.L. Menten, (1913) Die kinetik der invertinwirkung. Biochem. z. 49(333-369): p. 352.
83. Briggs, G.E. and J.B. Haldane, (1925) A Note on the Kinetics of Enzyme Action. The Biochemical journal. 19(2): p. 338-339.
84. Roberts, M.S. and M. Rowland, (1985) Hepatic elimination--dispersion model. J Pharm Sci. 74(5): p. 585-7.
85. Khalil, F. and S. Läer, (2011) Physiologically Based Pharmacokinetic Modeling: Methodology, Applications, and Limitations with a Focus on Its Role in Pediatric Drug Development. Journal of Biomedicine and Biotechnology. 2011: p. 907461.
86. Yu, L.X. and G.L. Amidon, (1999) A compartmental absorption and transit model for estimating oral drug absorption. Int J Pharm. 186(2): p. 119-25.
87. Yu, L.X., (1999) An Integrated Model for Determining Causes of Poor Oral Drug Absorption. Pharmaceutical Research. 16(12): p. 1883-1887.
88. Adiwidjaja, J., A.V. Boddy, and A.J. McLachlan, (2020) Implementation of a Physiologically Based Pharmacokinetic Modeling Approach to Guide Optimal Dosing Regimens for Imatinib and Potential Drug Interactions in Paediatrics. Frontiers in Pharmacology. 10(1672).
89. Li, S., Y. Yu, Z. Jin, Y. Dai, H. Lin, Z. Jiao, G. Ma, W. Cai, B. Han, and X. Xiang, (2019) Prediction of pharmacokinetic drug-drug interactions causing atorvastatin-induced rhabdomyolysis using physiologically based pharmacokinetic modelling. Biomedicine & Pharmacotherapy. 119: p. 109416.

90. Zhang, T., (2015) Physiologically based pharmacokinetic modeling of disposition and drug–drug interactions for atorvastatin and its metabolites. European Journal of Pharmaceutical Sciences. 77: p. 216-229.
91. Zhou, L., X. Tong, P. Sharma, H. Xu, N. Al-Huniti, and D. Zhou, (2019) Physiologically based pharmacokinetic modelling to predict exposure differences in healthy volunteers and subjects with renal impairment: Ceftazidime case study. Basic Clin Pharmacol Toxicol. 125(2): p. 100-107.
92. Rathore, S.S., J.P. Curtis, Y. Wang, M.R. Bristow, and H.M. Krumholz, (2003) Association of serum digoxin concentration and outcomes in patients with heart failure. Jama. 289(7): p. 871-8.
93. Scotcher, D., C. Jones, A. Rostami-Hodjegan, and A. Galetin, (2016) Novel minimal physiologically-based model for the prediction of passive tubular reabsorption and renal excretion clearance. European Journal of Pharmaceutical Sciences. 94: p. 59-71.
94. Scotcher, D., C.R. Jones, A. Galetin, and A. Rostami-Hodjegan, (2017) Delineating the Role of Various Factors in Renal Disposition of Digoxin through Application of Physiologically Based Kidney Model to Renal Impairment Populations. The Journal of pharmacology and experimental therapeutics. 360(3): p. 484-495.
95. Obach, R.S., (2011) Predicting clearance in humans from in vitro data. Curr Top Med Chem. 11(4): p. 334-9.
96. Mallick, P., M. Moreau, G. Song, A.Y. Efremenko, S.N. Pendse, M.R. Creek, T.G. Osimitz, R.N. Hines, P. Hinderliter, H.J. Clewell, et al., (2020) Development and Application of a Life-Stage Physiologically Based Pharmacokinetic (PBPK) Model to the Assessment of Internal Dose of Pyrethroids in Humans. Toxicological Sciences. 173(1): p. 86-99.
97. Riley, R.J., D.F. McGinnity, and R.P. Austin, (2005) A unified model for predicting human hepatic, metabolic clearance from in vitro intrinsic clearance data in hepatocytes and microsomes. Drug Metabolism and Disposition. 33(9): p. 1304-1311.
98. Yeo, K.R., J.R. Kenny, and A. Rostami-Hodjegan, (2013) Application of in vitro-in vivo extrapolation (IVIVE) and physiologically based pharmacokinetic (PBPK) modelling to investigate the impact of the CYP2C8 polymorphism on rosiglitazone exposure. Eur J Clin Pharmacol. 69(6): p. 1311-20.
99. Wilhelm, S.M., C. Carter, L. Tang, D. Wilkie, A. McNabola, H. Rong, C. Chen, X. Zhang, P. Vincent, M. McHugh, et al., (2004) BAY 43-9006 exhibits broad spectrum oral antitumor activity and targets the RAF/MEK/ERK pathway and receptor tyrosine kinases involved in tumor progression and angiogenesis. Cancer Res. 64(19): p. 7099-109.
100. de Lope, C.R., S. Tremosini, A. Forner, M. Reig, and J. Bruix, (2012) Management of HCC. Journal of Hepatology. 56: p. S75-S87.
101. Wilhelm, S.M., L. Adnane, P. Newell, A. Villanueva, J.M. Llovet, and M. Lynch, (2008) Preclinical overview of sorafenib, a multikinase inhibitor that targets both Raf and VEGF and PDGF receptor tyrosine kinase signaling. Molecular Cancer Therapeutics. 7(10): p. 3129-3140.
102. Wilhelm, S., C. Carter, M. Lynch, T. Lowinger, J. Dumas, R.A. Smith, B. Schwartz, R. Simantov, and S. Kelley, (2006) Discovery and development of sorafenib: a multikinase inhibitor for treating cancer. Nature Reviews Drug Discovery. 5(10): p. 835-844.
103. *European Medicines Agency. Nexavar: European Public Assessment Reports (EPAR)-Scientific Discussion.* 2007 March 3, 2007; Available from: http://www.ema.europa.eu/docs/en_GB/document_library/EPAR-Scientific_Discussion/human/000690/WC500027707.pdf.
104. Tlemsani, C., O. Huillard, J. Arrondeau, P. Boudou-Rouquette, A. Cessot, B. Blanchet, A. Thomas-Schoemann, R. Coriat, J.-P. Durand, J. Giroux, et al., (2015) Effect of glucuronidation on transport and tissue accumulation of tyrosine kinase inhibitors: consequences for the clinical management of sorafenib and regorafenib. Expert Opinion on Drug Metabolism & Toxicology. 11(5): p. 785-794.
105. Koschny, R., D. Gotthardt, C. Koehler, D. Jaeger, W. Stremmel, and T.M. Ganten, (2013) Diarrhea is a positive outcome predictor for sorafenib treatment of advanced hepatocellular carcinoma. Oncology. 84(1): p. 6-13.

106. Bracarda, S., E.M. Ruggeri, M. Monti, M. Merlano, A. D'Angelo, F. Ferraù, E. Cortesi, and A. Santoro, (2012) Early detection, prevention and management of cutaneous adverse events due to sorafenib: Recommendations from the Sorafenib Working Group. Critical Reviews in Oncology/Hematology. 82(3): p. 378-386.
107. Llovet, J.M., S. Ricci, V. Mazzaferro, P. Hilgard, E. Gane, J.-F. Blanc, A.C. de Oliveira, A. Santoro, J.-L. Raoul, A. Forner, et al., (2008) Sorafenib in Advanced Hepatocellular Carcinoma. New England Journal of Medicine. 359(4): p. 378-390.
108. Harding, C.V., J.E. Heuser, and P.D. Stahl, (2013) Exosomes: looking back three decades and into the future. J Cell Biol. 200(4): p. 367-71.
109. Zaborowski, M.P., L. Balaj, X.O. Breakefield, and C.P. Lai, (2015) Extracellular Vesicles: Composition, Biological Relevance, and Methods of Study. Bioscience. 65(8): p. 783-797.
110. Raposo, G. and W. Stoorvogel, (2013) Extracellular vesicles: Exosomes, microvesicles, and friends. The Journal of Cell Biology. 200(4): p. 373-383.
111. Masyuk, A.I., T.V. Masyuk, and N.F. LaRusso, (2013) Exosomes in the pathogenesis, diagnostics and therapeutics of liver diseases. Journal of hepatology. 59(3): p. 10.1016/j.jhep.2013.03.028.
112. Camussi, G., M.C. Deregibus, S. Bruno, V. Cantaluppi, and L. Biancone, (2010) Exosomes/microvesicles as a mechanism of cell-to-cell communication. Kidney International. 78(9): p. 838-848.
113. Thery, C., M. Boussac, P. Veron, P. Ricciardi-Castagnoli, G. Raposo, J. Garin, and S. Amigorena, (2001) Proteomic analysis of dendritic cell-derived exosomes: a secreted subcellular compartment distinct from apoptotic vesicles. J Immunol. 166.
114. Greening, D.W., H.P.T. Nguyen, K. Elgass, R.J. Simpson, and L.A. Salamonsen, (2016) Human Endometrial Exosomes Contain Hormone-Specific Cargo Modulating Trophoblast Adhesive Capacity: Insights into Endometrial-Embryo Interactions1. Biology of Reproduction. 94(2): p. 38, 1-15-38, 1-15.
115. Guduric-Fuchs, J., A. O'Connor, B. Camp, C.L. O'Neill, R.J. Medina, and D.A. Simpson, (2012) Selective extracellular vesicle-mediated export of an overlapping set of microRNAs from multiple cell types. BMC Genomics. 13(1): p. 357.
116. Dozio, V. and J.-C. Sanchez, (2017) Characterisation of extracellular vesicle-subsets derived from brain endothelial cells and analysis of their protein cargo modulation after TNF exposure. Journal of Extracellular Vesicles. 6(1): p. 1302705.
117. Conde-Vancells, J., E. Rodriguez-Suarez, N. Embade, D. Gil, R. Matthiesen, M. Valle, F. Elortza, S.C. Lu, J.M. Mato, and J.M. Falcon-Perez, (2008) Characterization and Comprehensive Proteome Profiling of Exosomes Secreted by Hepatocytes. Journal of proteome research. 7(12): p. 5157-5166.
118. Colombo, M., C. Moita, G. van Niel, J. Kowal, J. Vigneron, P. Benaroch, N. Manel, L.F. Moita, C. Thery, and G. Raposo, (2013) Analysis of ESCRT functions in exosome biogenesis, composition and secretion highlights the heterogeneity of extracellular vesicles. J Cell Sci. 126(Pt 24): p. 5553-65.
119. Baietti, M.F., Z. Zhang, E. Mortier, A. Melchior, G. Degeest, A. Geeraerts, Y. Ivarsson, F. Depoortere, C. Coomans, E. Vermeiren, et al., (2012) Syndecan-syntenin-ALIX regulates the biogenesis of exosomes. Nat Cell Biol. 14(7): p. 677-85.
120. Trajkovic, K., C. Hsu, S. Chiantia, L. Rajendran, D. Wenzel, and F. Wieland, (2008) Ceramide triggers budding of exosome vesicles into multivesicular endosomes. Science. 319.
121. Hessvik, N.P. and A. Llorente, (2018) Current knowledge on exosome biogenesis and release. Cell Mol Life Sci. 75(2): p. 193-208.
122. Phuyal, S., N.P. Hessvik, T. Skotland, K. Sandvig, and A. Llorente, (2014) Regulation of exosome release by glycosphingolipids and flotillins. Febs j. 281(9): p. 2214-27.
123. Kajimoto, T., T. Okada, S. Miya, L. Zhang, and S. Nakamura, (2013) Ongoing activation of sphingosine 1-phosphate receptors mediates maturation of exosomal multivesicular endosomes. Nat Commun. 4: p. 2712.
124. Baltes, C., F. Princz-Kranz, M. Rudin, and T. Mueggler, (2011) Detecting amyloid-beta plaques in Alzheimer's disease. Methods Mol Biol. 711: p. 511-33.

125. Esparza, T.J., M. Gangolli, N.J. Cairns, and D.L. Brody, (2018) Soluble amyloid-beta buffering by plaques in Alzheimer disease dementia versus high-pathology controls. PLOS ONE. 13(7): p. e0200251.
126. Wildburger, N.C., F. Gyngard, C. Guillermier, B.W. Patterson, D. Elbert, K.G. Mawuenyega, T. Schneider, K. Green, R. Roth, R.E. Schmidt, et al., (2018) Amyloid-β Plaques in Clinical Alzheimer's Disease Brain Incorporate Stable Isotope Tracer In Vivo and Exhibit Nanoscale Heterogeneity. Frontiers in Neurology. 9(169).
127. Camara, H. and E.A. De-Souza, (2018) β-Amyloid Accumulation Slows Earlier than Expected in Preclinical Alzheimer's Disease Patients. The Journal of Neuroscience. 38(43): p. 9123-9125.
128. Takahashi, R.H., T.A. Milner, F. Li, E.E. Nam, M.A. Edgar, H. Yamaguchi, M.F. Beal, H. Xu, P. Greengard, and G.K. Gouras, (2002) Intraneuronal Alzheimer Aβ42 Accumulates in Multivesicular Bodies and Is Associated with Synaptic Pathology. The American Journal of Pathology. 161(5): p. 1869-1879.
129. Sardar Sinha, M., A. Ansell-Schultz, L. Civitelli, C. Hildesjö, M. Larsson, L. Lannfelt, M. Ingelsson, and M. Hallbeck, (2018) Alzheimer's disease pathology propagation by exosomes containing toxic amyloid-beta oligomers. Acta neuropathologica. 136(1): p. 41-56.
130. Yang, Y., Q. Han, Z. Hou, C. Zhang, Z. Tian, and J. Zhang, (2017) Exosomes mediate hepatitis B virus (HBV) transmission and NK-cell dysfunction. Cellular and Molecular Immunology. 14(5): p. 465-475.
131. Garcia, N.A., J. Moncayo-Arlandi, P. Sepulveda, and A. Diez-Juan, (2016) Cardiomyocyte exosomes regulate glycolytic flux in endothelium by direct transfer of GLUT transporters and glycolytic enzymes. Cardiovascular Research. 109(3): p. 397-408.
132. Valadi, H., K. Ekstrom, A. Bossios, M. Sjostrand, J.J. Lee, and J.O. Lotvall, (2007) Exosome-mediated transfer of mRNAs and microRNAs is a novel mechanism of genetic exchange between cells. Nat Cell Biol. 9.
133. Enderle, D., A. Spiel, C.M. Coticchia, E. Berghoff, R. Mueller, M. Schlumpberger, M. Sprenger-Haussels, J.M. Shaffer, E. Lader, J. Skog, et al., (2015) Characterization of RNA from Exosomes and Other Extracellular Vesicles Isolated by a Novel Spin Column-Based Method. PLOS ONE. 10(8): p. e0136133.
134. Yang, J., J. Hagen, K.V. Guntur, K. Allette, S. Schuyler, J. Ranjan, F. Petralia, S. Gesta, R. Sebra, M. Mahajan, et al., (2017) A next generation sequencing based approach to identify extracellular vesicle mediated mRNA transfers between cells. BMC genomics. 18(1): p. 987-987.
135. Murakami, T., C.M. Yamamoto, T. Akino, H. Tanaka, N. Fukuzawa, H. Suzuki, T. Osawa, T. Tsuji, T. Seki, and H. Harada, (2018) Bladder cancer detection by urinary extracellular vesicle mRNA analysis. Oncotarget. 9(67): p. 32810-32821.
136. Cheng, P., F. Feng, H. Yang, S. Jin, C. Lai, Y. Wang, and J. Bi, (2020) Detection and significance of exosomal mRNA expression profiles in the cerebrospinal fluid of patients with meningeal carcinomatosis. J Mol Neurosci.
137. Reif, S., Y. Elbaum Shiff, and R. Golan-Gerstl, (2019) Milk-derived exosomes (MDEs) have a different biological effect on normal fetal colon epithelial cells compared to colon tumor cells in a miRNA-dependent manner. J Transl Med. 17(1): p. 325.
138. Barceló, M., M. Castells, L. Bassas, F. Vigués, and S. Larriba, (2019) Semen miRNAs Contained in Exosomes as Non-Invasive Biomarkers for Prostate Cancer Diagnosis. Scientific Reports. 9(1): p. 13772.
139. Chiba, M., M. Kimura, and S. Asari, (2012) Exosomes secreted from human colorectal cancer cell lines contain mRNAs, microRNAs and natural antisense RNAs, that can transfer into the human hepatoma HepG2 and lung cancer A549 cell lines. Oncology Reports. 28(5): p. 1551-1558.
140. Helwa, I., J. Cai, M.D. Drewry, A. Zimmerman, M.B. Dinkins, M.L. Khaled, M. Seremwe, W.M. Dismuke, E. Bieberich, W.D. Stamer, et al., (2017) A Comparative Study of Serum Exosome Isolation Using Differential Ultracentrifugation and Three Commercial Reagents. PLOS ONE. 12(1): p. e0170628.

141. Menck, K., A. Bleckmann, M. Schulz, L. Ries, and C. Binder, (2017) Isolation and Characterization of Microvesicles from Peripheral Blood. Journal of Visualized Experiments : JoVE, (119): p. 55057.
142. Nordin, J.Z., Y. Lee, P. Vader, I. Mäger, H.J. Johansson, W. Heusermann, O.P.B. Wiklander, M. Hällbrink, Y. Seow, J.J. Bultema, et al., (2015) Ultrafiltration with size-exclusion liquid chromatography for high yield isolation of extracellular vesicles preserving intact biophysical and functional properties. Nanomedicine: Nanotechnology, Biology and Medicine. 11(4): p. 879-883.
143. Kalra, H., C.G. Adda, M. Liem, C.-S. Ang, A. Mechler, R.J. Simpson, M.D. Hulett, and S. Mathivanan, (2013) Comparative proteomics evaluation of plasma exosome isolation techniques and assessment of the stability of exosomes in normal human blood plasma. Proteomics. 13(22): p. 3354-3364.
144. Gidlöf, O., M. Evander, M. Rezeli, G. Marko-Varga, T. Laurell, and D. Erlinge, (2019) Proteomic profiling of extracellular vesicles reveals additional diagnostic biomarkers for myocardial infarction compared to plasma alone. Scientific Reports. 9(1): p. 8991.
145. *World Health Organization: Cancer fact sheets*. (2018); Available from: http://gco.iarc.fr/today/data/factsheets/cancers/11-Liver-fact-sheet.pdf.
146. Vogel, A., A. Cervantes, I. Chau, B. Daniele, J.M. Llovet, T. Meyer, J.-C. Nault, U. Neumann, J. Ricke, B. Sangro, et al., (2018) Hepatocellular carcinoma: ESMO Clinical Practice Guidelines for diagnosis, treatment and follow-up†. Annals of Oncology. 29(Supplement_4): p. 238-255.
147. Cheng, A.L., Y.K. Kang, Z. Chen, C.J. Tsao, S. Qin, J.S. Kim, R. Luo, J. Feng, S. Ye, T.S. Yang, et al., (2009) Efficacy and safety of sorafenib in patients in the Asia-Pacific region with advanced hepatocellular carcinoma: a phase III randomised, double-blind, placebo-controlled trial. Lancet Oncol. 10(1): p. 25-34.
148. Abou-Alfa, G.K., L. Schwartz, S. Ricci, D. Amadori, A. Santoro, A. Figer, J. De Greve, J.Y. Douillard, C. Lathia, B. Schwartz, et al., (2006) Phase II study of sorafenib in patients with advanced hepatocellular carcinoma. J Clin Oncol. 24(26): p. 4293-300.
149. Trotti, A., A.D. Colevas, A. Setser, V. Rusch, D. Jaques, V. Budach, C. Langer, B. Murphy, R. Cumberlin, C.N. Coleman, et al., (2003) CTCAE v3.0: development of a comprehensive grading system for the adverse effects of cancer treatment. Semin Radiat Oncol. 13(3): p. 176-81.
150. Marrero, J.A., M. Kudo, A.P. Venook, S.-L. Ye, J.-P. Bronowicki, X.-P. Chen, L. Dagher, J. Furuse, J.-F.H. Geschwind, L.L. de Guevara, et al., (2016) Observational registry of sorafenib use in clinical practice across Child-Pugh subgroups: The GIDEON study. Journal of Hepatology. 65(6): p. 1140-1147.
151. Vincenzi, B., D. Santini, A. Russo, R. Addeo, F. Giuliani, L. Montella, S. Rizzo, O. Venditti, A.M. Frezza, M. Caraglia, et al., (2010) Early skin toxicity as a predictive factor for tumor control in hepatocellular carcinoma patients treated with sorafenib. Oncologist. 15(1): p. 85-92.
152. Otsuka, T., Y. Eguchi, S. Kawazoe, K. Yanagita, K. Ario, K. Kitahara, H. Kawasoe, H. Kato, and T. Mizuta, (2012) Skin toxicities and survival in advanced hepatocellular carcinoma patients treated with sorafenib. Hepatol Res. 42(9): p. 879-86.
153. Shomura, M., T. Kagawa, K. Shiraishi, S. Hirose, Y. Arase, J. Koizumi, and T. Mine, (2014) Skin toxicity predicts efficacy to sorafenib in patients with advanced hepatocellular carcinoma. World J Hepatol. 6(9): p. 670-6.
154. Cheng, A.L., Y.K. Kang, D.Y. Lin, J.W. Park, M. Kudo, S. Qin, H.C. Chung, X. Song, J. Xu, G. Poggi, et al., (2013) Sunitinib versus sorafenib in advanced hepatocellular cancer: results of a randomized phase III trial. J Clin Oncol. 31(32): p. 4067-75.
155. Therasse, P., S.G. Arbuck, E.A. Eisenhauer, J. Wanders, R.S. Kaplan, L. Rubinstein, J. Verweij, M. Van Glabbeke, A.T. van Oosterom, M.C. Christian, et al., (2000) New guidelines to evaluate the response to treatment in solid tumors. European Organization for Research and Treatment of Cancer, National Cancer Institute of the United States, National Cancer Institute of Canada. J Natl Cancer Inst. 92(3): p. 205-16.

156. Kawashima, A., H. Takayama, Y. Arai, G. Tanigawa, M. Nin, J. Kajikawa, T. Imazu, T. Kinoshita, Y. Yasunaga, H. Inoue, et al., (2011) One-month relative dose intensity of not less than 50% predicts favourable progression-free survival in sorafenib therapy for advanced renal cell carcinoma in Japanese patients. European Journal of Cancer. 47(10): p. 1521-1526.
157. Wildiers, H. and M. Reiser, (2011) Relative dose intensity of chemotherapy and its impact on outcomes in patients with early breast cancer or aggressive lymphoma. Critical Reviews in Oncology/Hematology. 77(3): p. 221-240.
158. Reiss, K.A., S. Yu, R. Mamtani, R. Mehta, K. D'Addeo, E.P. Wileyto, T.H. Taddei, and D.E. Kaplan, (2017) Starting Dose of Sorafenib for the Treatment of Hepatocellular Carcinoma: A Retrospective, Multi-Institutional Study. J Clin Oncol. 35(31): p. 3575-3581.
159. Gore, M.E., R.J. Jones, A. Ravaud, M. Kuczyk, T. Demkow, A. Bearz, J. Shapiro, U.P. Strauss, and C. Porta, (2017) Sorafenib dose escalation in treatment-naive patients with metastatic renal cell carcinoma: a non-randomised, open-label, Phase 2b study. BJU Int. 119(6): p. 846-853.
160. Hopkins, A.M., M. Van Dyk, A. Rowland, and M.J. Sorich, (2019) Effect of early adverse events on response and survival outcomes of advanced melanoma patients treated with vemurafenib or vemurafenib plus cobimetinib: A pooled analysis of clinical trial data. Pigment Cell Melanoma Res. 32(4): p. 576-583.
161. Tang, E., A. Rowland, R.A. McKinnon, M.J. Sorich, and A.M. Hopkins, (2019) Effect of early adverse events resulting in ado-trastuzumab emtansine dose adjustments on survival outcomes of HER2+ advanced breast cancer patients. Breast Cancer Res Treat. 178(2): p. 473-477.
162. Halmos, B., E.-H. Tan, R.A. Soo, J. Cadranel, M.K. Lee, P. Foucher, T.-C. Hsia, M. Hochmair, F. Griesinger, T. Hida, et al., (2019) Impact of afatinib dose modification on safety and effectiveness in patients with EGFR mutation-positive advanced NSCLC: Results from a global real-world study (RealGiDo). Lung Cancer. 127: p. 103-111.
163. Coriat, R., C. Nicco, C. Chereau, O. Mir, J. Alexandre, S. Ropert, B. Weill, S. Chaussade, F. Goldwasser, and F. Batteux, (2012) Sorafenib-induced hepatocellular carcinoma cell death depends on reactive oxygen species production in vitro and in vivo. Mol Cancer Ther. 11(10): p. 2284-93.
164. Ogawa, C., M. Morita, A. Omura, T. Noda, A. Kubo, T. Matsunaka, H. Tamaki, M. Shibatoge, A. Tsutsui, T. Senoh, et al., (2017) Hand-Foot Syndrome and Post-Progression Treatment Are the Good Predictors of Better Survival in Advanced Hepatocellular Carcinoma Treated with Sorafenib: A Multicenter Study. Oncology. 93(suppl 1)(Suppl. 1): p. 113-119.
165. Hotte, S.J., G.A. Bjarnason, D.Y.C. Heng, M.A.S. Jewett, A. Kapoor, C. Kollmannsberger, J. Maroun, L.A. Mayhew, S. North, M.N. Reaume, et al., (2011) Progression-free survival as a clinical trial endpoint in advanced renal cell carcinoma. Current oncology (Toronto, Ont.). 18 Suppl 2(Suppl 2): p. S11-S19.
166. Pazdur, R., (2008) Endpoints for assessing drug activity in clinical trials. Oncologist. 13 Suppl 2: p. 19-21.
167. Likhitsup, A., N. Razumilava, and N.D. Parikh, (2019) Treatment for Advanced Hepatocellular Carcinoma: Current Standard and the Future. Clinical Liver Disease. 13(1): p. 13-19.
168. *Nexavar: European Public Assessment Reports (EPAR)-Scientific Discussion.* 2007.
169. Liu, C., Z. Chen, Y. Chen, J. Lu, Y. Li, S. Wang, G. Wu, and F. Qian, (2016) Improving Oral Bioavailability of Sorafenib by Optimizing the “Spring” and “Parachute” Based on Molecular Interaction Mechanisms. Molecular Pharmaceutics. 13(2): p. 599-608.
170. Lind, J.S., A.M. Dingemans, H.J. Groen, F.B. Thunnissen, O. Bekers, D.A. Heideman, R.J. Honeywell, E. Giovannetti, G.J. Peters, P.E. Postmus, et al., (2010) A multicenter phase II study of erlotinib and sorafenib in chemotherapy-naive patients with advanced non-small cell lung cancer. Clin Cancer Res. 16(11): p. 3078-87.
171. Fang, Y.H., Y.H. Yang, M.J. Hsieh, M.S. Hung, and Y.C. Lin, (2019) Concurrent proton-pump inhibitors increase risk of death for lung cancer patients receiving 1st-line gefitinib treatment - a nationwide population-based study. Cancer Manag Res. 11: p. 8539-8546.
172. *European Medicines Agency. Sunitinib (SUTENT). Summary of Product Characteristics*. 2015.
173. Lalani, A.A., R.R. McKay, X. Lin, R. Simantov, M.D. Kaymakcalan, and T.K. Choueiri, (2017) Proton Pump Inhibitors and Survival Outcomes in Patients With Metastatic Renal Cell Carcinoma. Clin Genitourin Cancer. 15(6): p. 724-732.

174. Adiwidjaja, J., A.V. Boddy, and A.J. McLachlan, (2020) Implementation of a Physiologically Based Pharmacokinetic Modeling Approach to Guide Optimal Dosing Regimens for Imatinib and Potential Drug Interactions in Paediatrics. Frontiers in pharmacology. 10: p. 1672-1672.
175. Ono, C., P.H. Hsyu, R. Abbas, C.M. Loi, and S. Yamazaki, (2017) Application of Physiologically Based Pharmacokinetic Modeling to the Understanding of Bosutinib Pharmacokinetics: Prediction of Drug-Drug and Drug-Disease Interactions. Drug Metab Dispos. 45(4): p. 390-398.
176. Djebli, N., D. Fabre, X. Boulenc, G. Fabre, E. Sultan, and F. Hurbin, (2015) Physiologically-based Pharmacokinetic Modeling for Sequential Metabolism: Effect of CYP2C19 Genetic Polymorphism on Clopidogrel and Clopidogrel Active Metabolite Pharmacokinetics. Drug Metabolism and Disposition: p. dmd.114.062596.
177. Heimbach, T., W. Lin, F. Hourcade-Potelleret, X. Tian, F.P. Combes, N. Horvath, and H. He, (2019) Physiologically Based Pharmacokinetic Modeling to Supplement Nilotinib Pharmacokinetics and Confirm Dose Selection in Pediatric Patients. Journal of Pharmaceutical Sciences. 108(6): p. 2191-2198.
178. Vogel, A., A. Cervantes, I. Chau, B. Daniele, J.M. Llovet, T. Meyer, J.C. Nault, U. Neumann, J. Ricke, B. Sangro, et al., (2018) Hepatocellular carcinoma: ESMO Clinical Practice Guidelines for diagnosis, treatment and follow-up. Ann Oncol. 29(Suppl 4): p. iv238-iv255.
179. Wang, H.-T. and M. Xia, (2019) A meta-analysis of efficacy and safety of sorafenib versus other targeted agents for metastatic renal cell carcinoma. Medicine. 98(1): p. e13779-e13779.
180. Strumberg, D., J.W. Clark, A. Awada, M.J. Moore, H. Richly, A. Hendlisz, H.W. Hirte, J.P. Eder, H.-J. Lenz, and B. Schwartz, (2007) Safety, Pharmacokinetics, and Preliminary Antitumor Activity of Sorafenib: A Review of Four Phase I Trials in Patients with Advanced Refractory Solid Tumors. The Oncologist. 12(4): p. 426-437.
181. Awada, A., A. Hendlisz, T. Gil, S. Bartholomeus, M. Mano, D. de Valeriola, D. Strumberg, E. Brendel, C.G. Haase, B. Schwartz, et al., (2005) Phase I safety and pharmacokinetics of BAY 43-9006 administered for 21 days on/7 days off in patients with advanced, refractory solid tumours. British Journal of Cancer. 92(10): p. 1855-1861.
182. Moore, M., H.W. Hirte, L. Siu, A. Oza, S.J. Hotte, O. Petrenciuc, F. Cihon, C. Lathia, and B. Schwartz, (2005) Phase I study to determine the safety and pharmacokinetics of the novel Raf kinase and VEGFR inhibitor BAY 43-9006, administered for 28 days on/7 days off in patients with advanced, refractory solid tumors. Ann Oncol. 16(10): p. 1688-94.
183. Jain, L., S. Woo, E.R. Gardner, W.L. Dahut, E.C. Kohn, S. Kummar, D.R. Mould, G. Giaccone, R. Yarchoan, J. Venitz, et al., (2011) Population pharmacokinetic analysis of sorafenib in patients with solid tumours. Br J Clin Pharmacol. 72(2): p. 294-305.
184. Ruanglertboon, W., M.J. Sorich, J.M. Logan, A. Rowland, and A.M. Hopkins, (2020) The effect of proton pump inhibitors on survival outcomes in advanced hepatocellular carcinoma treated with sorafenib. Journal of Cancer Research and Clinical Oncology. 146(10): p. 2693-2697.
185. Au, T.H., E.B. Bailey, S.B. Patel, S.K. Tantravahi, N. Agarwal, and D.D. Stenehjem, (2016) Effect of concomitant proton pump inhibitor (PPI) on effectiveness of tyrosine kinase inhibitor (TKI) in patients with metastatic renal cell carcinoma (mRCC). Journal of Clinical Oncology. 34(2_suppl): p. 608-608.
186. Fukudo, M., T. Ito, T. Mizuno, K. Shinsako, E. Hatano, S. Uemoto, T. Kamba, T. Yamasaki, O. Ogawa, H. Seno, et al., (2014) Exposure-toxicity relationship of sorafenib in Japanese patients with renal cell carcinoma and hepatocellular carcinoma. Clin Pharmacokinet. 53(2): p. 185-96.
187. Ruanglertboon, W., M.J. Sorich, A. Rowland, and A.M. Hopkins, (2020) Effect of early adverse events resulting in sorafenib dose adjustments on survival outcomes of advanced hepatocellular carcinoma patients. Int J Clin Oncol. 25(9): p. 1672-1677.
188. de Wit, D., H.J. Guchelaar, J. den Hartigh, H. Gelderblom, and N.P. van Erp, (2015) Individualized dosing of tyrosine kinase inhibitors: are we there yet? Drug Discov Today. 20(1): p. 18-36.

189. Mueller-Schoell, A., S.L. Groenland, O. Scherf-Clavel, M. van Dyk, W. Huisinga, R. Michelet, U. Jaehde, N. Steeghs, A.D.R. Huitema, and C. Kloft, (2020) Therapeutic drug monitoring of oral targeted antineoplastic drugs. European Journal of Clinical Pharmacology.
190. Semrad, T.J., D.R. Gandara, and P.N. Lara, Jr., (2011) Enhancing the clinical activity of sorafenib through dose escalation: rationale and current experience. Therapeutic advances in medical oncology. 3(2): p. 95-100.
191. Escudier, B., C. Szczylik, T.E. Hutson, T. Demkow, M. Staehler, F. Rolland, S. Negrier, N. Laferriere, U.J. Scheuring, D. Cella, et al., (2009) Randomized phase II trial of first-line treatment with sorafenib versus interferon Alfa-2a in patients with metastatic renal cell carcinoma. J Clin Oncol. 27(8): p. 1280-9.
192. Verheijen, R.B., H. Yu, J.H.M. Schellens, J.H. Beijnen, N. Steeghs, and A.D.R. Huitema, (2017) Practical Recommendations for Therapeutic Drug Monitoring of Kinase Inhibitors in Oncology. Clin Pharmacol Ther. 102(5): p. 765-776.
193. Rowland, A., M. van Dyk, A.A. Mangoni, J.O. Miners, R.A. McKinnon, M.D. Wiese, A. Rowland, G. Kichenadasse, H. Gurney, and M.J. Sorich, (2017) Kinase inhibitor pharmacokinetics: comprehensive summary and roadmap for addressing inter-individual variability in exposure. Expert Opin Drug Metab Toxicol. 13(1): p. 31-49.
194. Kang, J.S. and M.H. Lee, (2009) Overview of therapeutic drug monitoring. The Korean journal of internal medicine. 24(1): p. 1-10.
195. Thomson, A., (1997) TDM - A Multidisciplinary Approach. Therapeutic Drug Monitoring. 19(4): p. 490.
196. Sánchez-Hernández, J.G., N. Rebollo, A. Martin-Suarez, M.V. Calvo, and F. Muñoz, A 3-year prospective study of a multidisciplinary early proactive therapeutic drug monitoring programme of infliximab treatments in inflammatory bowel disease. British Journal of Clinical Pharmacology. n/a(n/a).
197. Sorich, M.J., F. Mutlib, M. van Dyk, A.M. Hopkins, T.M. Polasek, J.C. Marshall, A.D. Rodrigues, and A. Rowland, (2019) Use of Physiologically Based Pharmacokinetic Modeling to Identify Physiological and Molecular Characteristics Driving Variability in Axitinib Exposure: A Fresh Approach to Precision Dosing in Oncology. J Clin Pharmacol. 59(6): p. 872-879.
198. Rowland, A., M. van Dyk, A.M. Hopkins, R. Mounzer, T.M. Polasek, A. Rostami-Hodjegan, and M.J. Sorich, (2018) Physiologically Based Pharmacokinetic Modeling to Identify Physiological and Molecular Characteristics Driving Variability in Drug Exposure. Clin Pharmacol Ther. 104(6): p. 1219-1228.
199. Polasek, T.M. and A. Rostami-Hodjegan, (2020) Virtual Twins: Understanding the Data Required for Model-Informed Precision Dosing. Clinical Pharmacology & Therapeutics. 107(4): p. 742-745.
200. Kluwe, F., R. Michelet, A. Mueller-Schoell, C. Maier, L. Klopp-Schulze, M. van Dyk, G. Mikus, W. Huisinga, and C. Kloft, (2020) Perspectives on Model-Informed Precision Dosing in the Digital Health Era: Challenges, Opportunities, and Recommendations. Clin Pharmacol Ther.
201. Polasek, T.M., S. Polak, M.P. Doogue, A. Rostami-Hodjegan, and J.O. Miners, (2009) Assessment of inter-individual variability in predicted phenytoin clearance. Eur J Clin Pharmacol. 65(12): p. 1203-10.
202. Chetty, M., T. Cain, J. Wedagedera, A. Rostami-Hodjegan, and M. Jamei, (2018) Application of Physiologically Based Pharmacokinetic (PBPK) Modeling Within a Bayesian Framework to Identify Poor Metabolizers of Efavirenz (PM), Using a Test Dose of Efavirenz. Frontiers in Pharmacology. 9(247).
203. Tsamandouras, N., A. Rostami-Hodjegan, and L. Aarons, (2015) Combining the 'bottom up' and 'top down' approaches in pharmacokinetic modelling: fitting PBPK models to observed clinical data. Br J Clin Pharmacol. 79(1): p. 48-55.
204. Tylutki, Z., S. Polak, and B. Wiśniowska, (2016) Top-down, Bottom-up and Middle-out Strategies for Drug Cardiac Safety Assessment via Modeling and Simulations. Current Pharmacology Reports. 2(4): p. 171-177.

205. Polasek, T.M., G.T. Tucker, M.J. Sorich, M.D. Wiese, T. Mohan, A. Rostami-Hodjegan, P. Korprasertthaworn, V. Perera, and A. Rowland, (2018) Prediction of olanzapine exposure in individual patients using physiologically based pharmacokinetic modelling and simulation. British Journal of Clinical Pharmacology. 84(3): p. 462-476.
206. van Dyk, M. and A. Rowland, (2017) PBPK modeling as an approach to evaluate the effect of covariates and drug-drug interactions on variability in EGFR kinase inhibitor exposure. Transl Cancer Res. 6: p. S1600-1615.
207. Rowland Yeo, K., M. Jamei, J. Yang, G.T. Tucker, and A. Rostami-Hodjegan, (2010) Physiologically based mechanistic modelling to predict complex drug-drug interactions involving simultaneous competitive and time-dependent enzyme inhibition by parent compound and its metabolite in both liver and gut - the effect of diltiazem on the time-course of exposure to triazolam. Eur J Pharm Sci. 39(5): p. 298-309.
208. Liu, B., H.K. Crewe, M. Ozdemir, K. Rowland Yeo, G. Tucker, and A. Rostami-Hodjegan, (2017) The absorption kinetics of ketoconazole plays a major role in explaining the reported variability in the level of interaction with midazolam: Interplay between formulation and inhibition of gut wall and liver metabolism. Biopharmaceutics & Drug Disposition. 38(3): p. 260-270.
209. Rowland, A., M. van Dyk, A.A. Mangoni, J.O. Miners, R.A. McKinnon, M.D. Wiese, A. Rowland, G. Kichenadasse, H. Gurney, and M.J. Sorich, (2017) Kinase inhibitor pharmacokinetics: comprehensive summary and roadmap for addressing inter-individual variability in exposure. Expert Opinion on Drug Metabolism & Toxicology. 13(1): p. 31-49.
210. Schwenger, E., V.P. Reddy, G. Moorthy, P. Sharma, H. Tomkinson, E. Masson, and K. Vishwanathan, (2018) Harnessing Meta-analysis to Refine an Oncology Patient Population for Physiology-Based Pharmacokinetic Modeling of Drugs. Clinical Pharmacology & Therapeutics. 103(2): p. 271-280.
211. Minami, H., K. Kawada, H. Ebi, K. Kitagawa, Y.-i. Kim, K. Araki, H. Mukai, M. Tahara, H. Nakajima, and K. Nakajima, (2008) Phase I and pharmacokinetic study of sorafenib, an oral multikinase inhibitor, in Japanese patients with advanced refractory solid tumors. Cancer Science. 99(7): p. 1492-1498.
212. Shebley, M., P. Sandhu, A. Emami Riedmaier, M. Jamei, R. Narayanan, A. Patel, S.A. Peters, V.P. Reddy, M. Zheng, L. de Zwart, et al., (2018) Physiologically Based Pharmacokinetic Model Qualification and Reporting Procedures for Regulatory Submissions: A Consortium Perspective. Clin Pharmacol Ther. 104(1): p. 88-110.
213. Basu, S., Y.T. Lien, V. Vozmediano, J.-F. Schlender, T. Eissing, S. Schmidt, and C. Niederalt, (2020) Physiologically Based Pharmacokinetic Modeling of Monoclonal Antibodies in Pediatric Populations Using PK-Sim. Frontiers in Pharmacology. 11(868).
214. Hennig, S., F. Holthouse, and C.E. Staatz, (2015) Comparing dosage adjustment methods for once-daily tobramycin in paediatric and adolescent patients with cystic fibrosis. Clin Pharmacokinet. 54(4): p. 409-21.
215. Song, L., C.-Y. He, N.-G. Yin, F. Liu, Y.-T. Jia, and Y. Liu, (2017) A population pharmacokinetic model for individualised dosage regimens of vancomycin in Chinese neonates and young infants. Oncotarget. 8(62): p. 105211-105221.
216. Rowland, A., W. Ruanglertboon, M. van Dyk, D. Wijayakumara, L. Wood, R. Meech, P. Mackenzie, A. Rodrigues, J. Marshall, and M. Sorich, (2019) Plasma Extracellular Nanovesicle (Exosome) derived biomarkers for ADME pathways: A novel approach to characterise variability in drug exposure. Br J Clin Pharmacol. 85(1): p. 216-226.
217. Kumar, S., N. Sinha, K.A. Gerth, M.A. Rahman, M.M. Yallapu, and N.M. Midde, (2017) Specific packaging and circulation of cytochromes P450, especially 2E1 isozyme, in human plasma exosomes and their implications in cellular communications. Biochem Biophys Res Commun. 491(3): p. 675-680.
218. Achour, B., Z.M. Al-Majdoub, A. Grybos-Gajniak, K. Lea, P. Kilford, M. Zhang, D. Knight, J. Barber, J. Schageman, and A. Rostami-Hodjegan, (2021) Liquid Biopsy Enables Quantification of the Abundance and Interindividual Variability of Hepatic Enzymes and Transporters. Clin Pharmacol Ther. 109(1): p. 222-232.

219. Ruanglertboon, W., M.J. Sorich, A.M. Hopkins, and A. Rowland, (2021) Mechanistic Modelling Identifies and Addresses the Risks of Empiric Concentration-Guided Sorafenib Dosing. Pharmaceuticals. 14(5): p. 389.
220. Diczfalusy, U., H. Nylén, P. Elander, and L. Bertilsson, (2011) 4β-Hydroxycholesterol, an endogenous marker of CYP3A4/5 activity in humans. Br J Clin Pharmacol. 71(2): p. 183-9.
221. Diczfalusy, U., J. Miura, H.K. Roh, R.A. Mirghani, J. Sayi, H. Larsson, K.G. Bodin, A. Allqvist, M. Jande, J.W. Kim, et al., (2008) 4Beta-hydroxycholesterol is a new endogenous CYP3A marker: relationship to CYP3A5 genotype, quinine 3-hydroxylation and sex in Koreans, Swedes and Tanzanians. Pharmacogenet Genomics. 18(3): p. 201-8.
222. Bai, Y. and H. Zhao, (2018) Liquid biopsy in tumors: opportunities and challenges. Annals of translational medicine. 6(Suppl 1): p. S89-S89.
223. Guibert, N., A. Pradines, G. Favre, and J. Mazieres, (2020) Current and future applications of liquid biopsy in nonsmall cell lung cancer from early to advanced stages. European Respiratory Review. 29(155): p. 190052.
224. Yeo, J.C. and C.T. Lim, (2018) Potential of circulating biomarkers in liquid biopsy diagnostics. Biotechniques. 65(4): p. 187-189.
225. Parikh, A.R., I. Leshchiner, L. Elagina, L. Goyal, C. Levovitz, G. Siravegna, D. Livitz, K. Rhrissorrakrai, E.E. Martin, E.E. Van Seventer, et al., (2019) Liquid versus tissue biopsy for detecting acquired resistance and tumor heterogeneity in gastrointestinal cancers. Nature Medicine. 25(9): p. 1415-1421.
226. Jiang, N., J. Pan, S. Fang, C. Zhou, Y. Han, J. Chen, X. Meng, X. Jin, and Z. Gong, (2019) Liquid biopsy: Circulating exosomal long noncoding RNAs in cancer. Clin Chim Acta. 495: p. 331-337.
227. Mader, S. and K. Pantel, (2017) Liquid Biopsy: Current Status and Future Perspectives. Oncol Res Treat. 40(7-8): p. 404-408.
228. Zhou, B., K. Xu, X. Zheng, T. Chen, J. Wang, Y. Song, Y. Shao, and S. Zheng, (2020) Application of exosomes as liquid biopsy in clinical diagnosis. Signal Transduction and Targeted Therapy. 5(1): p. 144.
229. Zhang, W., W. Xia, Z. Lv, C. Ni, Y. Xin, and L. Yang, (2017) Liquid Biopsy for Cancer: Circulating Tumor Cells, Circulating Free DNA or Exosomes? Cellular Physiology and Biochemistry. 41(2): p. 755-768.
230. Perakis, S. and M.R. Speicher, (2017) Emerging concepts in liquid biopsies. BMC Medicine. 15(1): p. 75.
231. Bronkhorst, A.J., V. Ungerer, and S. Holdenrieder, (2019) The emerging role of cell-free DNA as a molecular marker for cancer management. Biomolecular detection and quantification. 17: p. 100087-100087.
232. Fernandez-Garcia, D., A. Hills, K. Page, R.K. Hastings, B. Toghill, K.S. Goddard, C. Ion, O. Ogle, A.R. Boydell, K. Gleason, et al., (2019) Plasma cell-free DNA (cfDNA) as a predictive and prognostic marker in patients with metastatic breast cancer. Breast Cancer Research. 21(1): p. 149.
233. Volik, S., M. Alcaide, R.D. Morin, and C. Collins, (2016) Cell-free DNA (cfDNA): Clinical Significance and Utility in Cancer Shaped By Emerging Technologies. Mol Cancer Res. 14(10): p. 898-908.
234. Murray, D.H., R.T. Baker, S. Gaur, G.P. Young, and S.K. Pedersen, (2017) Validation of a Circulating Tumor-Derived DNA Blood Test for Detection of Methylated BCAT1 and IKZF1 DNA. J Appl Lab Med. 2(2): p. 165-175.
235. Théry, C., L. Zitvogel, and S. Amigorena, (2002) Exosomes: composition, biogenesis and function. Nature Reviews Immunology. 2(8): p. 569-579.
236. Clayton, A., A. Turkes, S. Dewitt, R. Steadman, M.D. Mason, and M.B. Hallett, (2004) Adhesion and signaling by B cell-derived exosomes: the role of integrins. Faseb j. 18(9): p. 977-9.
237. Palma, J., S.C. Yaddanapudi, L. Pigati, M.A. Havens, S. Jeong, G.A. Weiner, K.M.E. Weimer, B. Stern, M.L. Hastings, and D.M. Duelli, (2012) MicroRNAs are exported from malignant cells in customized particles. Nucleic Acids Research. 40(18): p. 9125-9138.

238. Koga, Y., M. Yasunaga, Y. Moriya, T. Akasu, S. Fujita, S. Yamamoto, and Y. Matsumura, (2011) Exosome can prevent RNase from degrading microRNA in feces. J Gastrointest Oncol. 2(4): p. 215-22.
239. Robbins, P.D. and A.E. Morelli, (2014) Regulation of immune responses by extracellular vesicles. Nat Rev Immunol. 14(3): p. 195-208.
240. Wang, W. and M.T. Lotze, (2014) Good things come in small packages: exosomes, immunity and cancer. Cancer Gene Therapy. 21(4): p. 139-141.
241. Eldh, M., K. Ekström, H. Valadi, M. Sjöstrand, B. Olsson, M. Jernås, and J. Lötvall, (2010) Exosomes communicate protective messages during oxidative stress; possible role of exosomal shuttle RNA. PLoS One. 5(12): p. e15353.
242. Lässer, C., (2012) Exosomal RNA as biomarkers and the therapeutic potential of exosome vectors. Expert Opin Biol Ther. 12 Suppl 1: p. S189-97.
243. Umezu, T., K. Ohyashiki, M. Kuroda, and J.H. Ohyashiki, (2013) Leukemia cell to endothelial cell communication via exosomal miRNAs. Oncogene. 32(22): p. 2747-55.
244. Yin, C., C. Luo, W. Hu, X. Ding, C. Yuan, and F. Wang, (2016) Quantitative and Qualitative Analysis of Circulating Cell-Free DNA Can Be Used as an Adjuvant Tool for Prostate Cancer Screening: A Meta-Analysis. Disease Markers. 2016: p. 3825819.
245. Jackson, L.P., B.A. Tjoa, H. Mellert, and G.A. Pestano, (2020) Development of a TCR beta repertoire assay for profiling liquid biopsies from NSCLC donors. Hepatoma Research. 3(3): p. 563-571.
246. Zanger, U.M., M. Turpeinen, K. Klein, and M. Schwab, (2008) Functional pharmacogenetics/genomics of human cytochromes P450 involved in drug biotransformation. Analytical and Bioanalytical Chemistry. 392(6): p. 1093-1108.
247. Guengerich, F.P., (2008) Cytochrome P450 and Chemical Toxicology. Chemical Research in Toxicology. 21(1): p. 70-83.
248. Lin, J.H. and A.Y. Lu, (2001) Interindividual variability in inhibition and induction of cytochrome P450 enzymes. Annu Rev Pharmacol Toxicol. 41: p. 535-67.
249. Xie, F., X. Ding, and Q.-Y. Zhang, (2016) An update on the role of intestinal cytochrome P450 enzymes in drug disposition. Acta pharmaceutica Sinica. B. 6(5): p. 374-383.
250. Lindell, M., M. Lang, and H. Lennernäs, (2003) Expression of genes encoding for drug metabolising cytochrome P450 enzymes and P-glycoprotein in the rat small intestine; comparison to the liver. European Journal of Drug Metabolism and Pharmacokinetics. 28(1): p. 41-48.
251. Thelen, K. and J.B. Dressman, (2009) Cytochrome P450-mediated metabolism in the human gut wall. Journal of Pharmacy and Pharmacology. 61(5): p. 541-558.
252. Useckaite, Z., A. Mukhopadhya, B. Moran, and L. O'Driscoll, (2020) Extracellular vesicles report on the MET status of their cells of origin regardless of the method used for their isolation. Scientific Reports. 10(1): p. 19020.
253. Lotvall, J. and H. Valadi, (2007) Cell to cell signalling via exosomes through esRNA. Cell adhesion & migration. 1(3): p. 156-158.
254. Shelke, G.V., Y. Yin, S.C. Jang, C. Lässer, S. Wennmalm, H.J. Hoffmann, L. Li, Y.S. Gho, J.A. Nilsson, and J. Lötvall, (2019) Endosomal signalling via exosome surface TGFβ-1. Journal of Extracellular Vesicles. 8(1): p. 1650458.
255. Luan, X., K. Sansanaphongpricha, I. Myers, H. Chen, H. Yuan, and D. Sun, (2017) Engineering exosomes as refined biological nanoplatforms for drug delivery. Acta Pharmacologica Sinica. 38(6): p. 754-763.
256. Bunggulawa, E.J., W. Wang, T. Yin, N. Wang, C. Durkan, Y. Wang, and G. Wang, (2018) Recent advancements in the use of exosomes as drug delivery systems. Journal of Nanobiotechnology. 16(1): p. 81.
257. Lespagnol, A., D. Duflaut, C. Beekman, L. Blanc, G. Fiucci, J.C. Marine, M. Vidal, R. Amson, and A. Telerman, (2008) Exosome secretion, including the DNA damage-induced p53-dependent secretory pathway, is severely compromised in TSAP6/Steap3-null mice. Cell Death Differ. 15(11): p. 1723-33.
258. Osaki, M. and F. Okada, (2019) Exosomes and Their Role in Cancer Progression. Yonago acta medica. 62(2): p. 182-190.

259. Cocucci, E. and J. Meldolesi, (2015) Ectosomes and exosomes: shedding the confusion between extracellular vesicles. Trends Cell Biol. 25(6): p. 364-72.
260. van der Pol, E., F.A. Coumans, A.E. Grootemaat, C. Gardiner, I.L. Sargent, P. Harrison, A. Sturk, T.G. van Leeuwen, and R. Nieuwland, (2014) Particle size distribution of exosomes and microvesicles determined by transmission electron microscopy, flow cytometry, nanoparticle tracking analysis, and resistive pulse sensing. J Thromb Haemost. 12(7): p. 1182-92.
261. Raiborg, C. and H. Stenmark, (2009) The ESCRT machinery in endosomal sorting of ubiquitylated membrane proteins. Nature. 458(7237): p. 445-452.
262. van Niel, G., I. Porto-Carreiro, S. Simoes, and G. Raposo, (2006) Exosomes: a common pathway for a specialized function. J Biochem. 140(1): p. 13-21.
263. Crutchfield, C.A., S.N. Thomas, L.J. Sokoll, and D.W. Chan, (2016) Advances in mass spectrometry-based clinical biomarker discovery. Clinical proteomics. 13: p. 1-1.
264. Zhou, W., E.F. Petricoin, 3rd, and C. Longo, (2017) Mass Spectrometry-Based Biomarker Discovery. Methods Mol Biol. 1606: p. 297-311.
265. Clark-Langone, K.M., J.Y. Wu, C. Sangli, A. Chen, J.L. Snable, A. Nguyen, J.R. Hackett, J. Baker, G. Yothers, C. Kim, et al., (2007) Biomarker discovery for colon cancer using a 761 gene RT-PCR assay. BMC Genomics. 8(1): p. 279.
266. Lohmann, S., A. Herold, T. Bergauer, A. Belousov, G. Betzl, M. Demario, M. Dietrich, L. Luistro, M. Poignée-Heger, K. Schostack, et al., (2013) Gene expression analysis in biomarker research and early drug development using function tested reverse transcription quantitative real-time PCR assays. Methods. 59(1): p. 10-19.
267. Provenzano, M. and S. Mocellin, (2007) Complementary techniques: validation of gene expression data by quantitative real time PCR. Adv Exp Med Biol. 593: p. 66-73.
268. Arya, M., I.S. Shergill, M. Williamson, L. Gommersall, N. Arya, and H.R. Patel, (2005) Basic principles of real-time quantitative PCR. Expert Rev Mol Diagn. 5(2): p. 209-19.
269. Tse, C. and J. Capeau, (2003) [Real time PCR methodology for quantification of nucleic acids]. Ann Biol Clin (Paris). 61(3): p. 279-93.
270. Han, X., A. Aslanian, and J.R. Yates, 3rd, (2008) Mass spectrometry for proteomics. Current opinion in chemical biology. 12(5): p. 483-490.
271. Guerrera, I.C. and O. Kleiner, (2005) Application of mass spectrometry in proteomics. Biosci Rep. 25(1-2): p. 71-93.
272. Domon, B. and R. Aebersold, (2006) Mass spectrometry and protein analysis. Science. 312(5771): p. 212-7.
273. Moon, P.G., J.E. Lee, S. You, T.K. Kim, J.H. Cho, I.S. Kim, T.H. Kwon, C.D. Kim, S.H. Park, D. Hwang, et al., (2011) Proteomic analysis of urinary exosomes from patients of early IgA nephropathy and thin basement membrane nephropathy. Proteomics. 11(12): p. 2459-75.
274. Tracy, T.S., A.S. Chaudhry, B. Prasad, K.E. Thummel, E.G. Schuetz, X.-B. Zhong, Y.-C. Tien, H. Jeong, X. Pan, L.M. Shireman, et al., (2016) Interindividual Variability in Cytochrome P450-Mediated Drug Metabolism. Drug metabolism and disposition: the biological fate of chemicals. 44(3): p. 343-351.
275. Vagner, T., A. Chin, J. Mariscal, S. Bannykh, D.M. Engman, and D. Di Vizio, (2019) Protein Composition Reflects Extracellular Vesicle Heterogeneity. Proteomics. 19(8): p. e1800167.
276. Ang, F.L.I., A. Rowland, N.D. Modi, R.A. McKinnon, M.J. Sorich, and A.M. Hopkins, (2020) Early Adverse Events predict Survival Outcomes in HER2-positive Advanced Breast Cancer Patients treated with Lapatinib plus Capecitabine. Journal of Cancer. 11(11): p. 3327-3333.
277. Branco, F., R.S.M. Alencar, F. Volt, G. Sartori, A. Dode, L. Kikuchi, C.M. Tani, A.L. Chagas, T. Pfiffer, P. Hoff, et al., (2017) The Impact of Early Dermatologic Events in the Survival of Patients with Hepatocellular Carcinoma Treated with Sorafenib. Annals of Hepatology. 16(2): p. 263-268.
278. Nightingale, G., E. Skonecki, and M.K. Boparai, (2017) The Impact of Polypharmacy on Patient Outcomes in Older Adults With Cancer. The Cancer Journal. 23(4): p. 211-218.
279. Shrestha, S., S. Shrestha, and S. Khanal, (2019) Polypharmacy in elderly cancer patients: Challenges and the way clinical pharmacists can contribute in resource-limited settings. Aging medicine (Milton (N.S.W)). 2(1): p. 42-49.

280. Jørgensen, T.L., J. Hallas, S. Friis, and J. Herrstedt, (2012) Comorbidity in elderly cancer patients in relation to overall and cancer-specific mortality. Br J Cancer. 106(7): p. 1353-60.
281. Nobili, A., L. Pasina, M. Tettamanti, U. Lucca, E. Riva, I. Marzona, L. Monesi, R. Cucchiani, A. Bortolotti, I. Fortino, et al., (2009) Potentially severe drug interactions in elderly outpatients: results of an observational study of an administrative prescription database. J Clin Pharm Ther. 34(4): p. 377-86.
282. Dagli, R.J. and A. Sharma, (2014) Polypharmacy: a global risk factor for elderly people. Journal of international oral health : JIOH. 6(6): p. i-ii.
283. Mortazavi, S.S., M. Shati, A. Keshtkar, S.K. Malakouti, M. Bazargan, and S. Assari, (2016) Defining polypharmacy in the elderly: a systematic review protocol. BMJ Open. 6(3): p. e010989.
284. Chu, M.P., J.R. Hecht, D. Slamon, Z.A. Wainberg, Y.J. Bang, P.M. Hoff, A. Sobrero, S. Qin, K. Afenjar, V. Houe, et al., (2017) Association of Proton Pump Inhibitors and Capecitabine Efficacy in Advanced Gastroesophageal Cancer: Secondary Analysis of the TRIO-013/LOGiC Randomized Clinical Trial. JAMA Oncol. 3(6): p. 767-773.
285. Wong, G.G., V. Ha, M.P. Chu, D. Dersch-Mills, S. Ghosh, C.R. Chambers, and M.B. Sawyer, (2019) Effects of Proton Pump Inhibitors on FOLFOX and CapeOx Regimens in Colorectal Cancer. Clin Colorectal Cancer. 18(1): p. 72-79.
286. Mir, O., N. Touati, M. Lia, S. Litière, A. Le Cesne, S. Sleijfer, J.Y. Blay, M. Leahy, R. Young, R.H.J. Mathijssen, et al., (2019) Impact of Concomitant Administration of Gastric Acid-Suppressive Agents and Pazopanib on Outcomes in Soft-Tissue Sarcoma Patients Treated within the EORTC 62043/62072 Trials. Clin Cancer Res. 25(5): p. 1479-1485.
287. Uchida, M., S. Suzuki, H. Sugawara, Y. Suga, H. Kokubun, Y. Uesawa, T. Nakagawa, and H. Takase, (2019) A nationwide survey of hospital pharmacist interventions to improve polypharmacy for patients with cancer in palliative care in Japan. Journal of Pharmaceutical Health Care and Sciences. 5(1): p. 14.
288. Hajjar, E.R., J.T. Hanlon, R.J. Sloane, C.I. Lindblad, C.F. Pieper, C.M. Ruby, L.C. Branch, and K.E. Schmader, (2005) Unnecessary Drug Use in Frail Older People at Hospital Discharge. Journal of the American Geriatrics Society. 53(9): p. 1518-1523.
289. Dash, S., S.K. Shakyawar, M. Sharma, and S. Kaushik, (2019) Big data in healthcare: management, analysis and future prospects. Journal of Big Data. 6(1): p. 54.
290. Agarwal, M., M. Adhil, and A.K. Talukder. *Multi-omics Multi-scale Big Data Analytics for Cancer Genomics*. in *Big Data Analytics*. 2015. Cham: Springer International Publishing.
291. Belle, A., R. Thiagarajan, S.M.R. Soroushmehr, F. Navidi, D.A. Beard, and K. Najarian, (2015) Big Data Analytics in Healthcare. BioMed Research International. 2015: p. 370194.
292. Khatib, R., R. Giacaman, U. Khammash, and S. Yusuf, (2017) Challenges to conducting epidemiology research in chronic conflict areas: examples from PURE- Palestine. Conflict and Health. 10(1): p. 33.
293. Ehrenstein, V., H. Nielsen, A.B. Pedersen, S.P. Johnsen, and L. Pedersen, (2017) Clinical epidemiology in the era of big data: new opportunities, familiar challenges. Clin Epidemiol. 9: p. 245-250.
294. Iwashyna, T.J. and V. Liu, (2014) What's so different about big data?. A primer for clinicians trained to think epidemiologically. Annals of the American Thoracic Society. 11(7): p. 1130-1135.
295. Trifirò, G., J. Sultana, and A. Bate, (2018) From Big Data to Smart Data for Pharmacovigilance: The Role of Healthcare Databases and Other Emerging Sources. Drug Saf. 41(2): p. 143-149.
296. Shebley, M., P. Sandhu, A. Emami Riedmaier, M. Jamei, R. Narayanan, A. Patel, S.A. Peters, V.P. Reddy, M. Zheng, L. de Zwart, et al., (2018) Physiologically Based Pharmacokinetic Model Qualification and Reporting Procedures for Regulatory Submissions: A Consortium Perspective. Clinical Pharmacology & Therapeutics. 104(1): p. 88-110.
297. Grimstein, M., Y. Yang, X. Zhang, J. Grillo, S.-M. Huang, I. Zineh, and Y. Wang, (2019) Physiologically Based Pharmacokinetic Modeling in Regulatory Science: An Update From the U.S. Food and Drug Administration’s Office of Clinical Pharmacology. Journal of Pharmaceutical Sciences. 108(1): p. 21-25.

298. Rowland, A., M. van Dyk, A.M. Hopkins, R. Mounzer, T.M. Polasek, A. Rostami-Hodjegan, and M.J. Sorich, (2018) Physiologically Based Pharmacokinetic Modeling to Identify Physiological and Molecular Characteristics Driving Variability in Drug Exposure. Clinical Pharmacology & Therapeutics. 104(6): p. 1219-1228.
299. Darwich, A.S., K. Ogungbenro, A.A. Vinks, J.R. Powell, J.L. Reny, N. Marsousi, Y. Daali, D. Fairman, J. Cook, L.J. Lesko, et al., (2017) Why has model-informed precision dosing not yet become common clinical reality? lessons from the past and a roadmap for the future. Clin Pharmacol Ther. 101(5): p. 646-656.
300. Euteneuer, J.C., S. Kamatkar, T. Fukuda, A.A. Vinks, and H.T. Akinbi, (2019) Suggestions for Model-Informed Precision Dosing to Optimize Neonatal Drug Therapy. J Clin Pharmacol. 59(2): p. 168-176.
301. Darwich, A.S., T.M. Polasek, J.K. Aronson, K. Ogungbenro, D.F.B. Wright, B. Achour, J.-L. Reny, Y. Daali, B. Eiermann, J. Cook, et al., (2020) Model-Informed Precision Dosing: Background, Requirements, Validation, Implementation, and Forward Trajectory of Individualizing Drug Therapy. Annual Review of Pharmacology and Toxicology.
302. Oxnard, G.R., K.S. Thress, R.S. Alden, R. Lawrance, C.P. Paweletz, M. Cantarini, J.C. Yang, J.C. Barrett, and P.A. Jänne, (2016) Association Between Plasma Genotyping and Outcomes of Treatment With Osimertinib (AZD9291) in Advanced Non-Small-Cell Lung Cancer. J Clin Oncol. 34(28): p. 3375-82.
303. Siravegna, G., S. Marsoni, S. Siena, and A. Bardelli, (2017) Integrating liquid biopsies into the management of cancer. Nat Rev Clin Oncol. 14(9): p. 531-548.
304. Wu, X., J. Li, A. Gassa, D. Buchner, H. Alakus, Q. Dong, N. Ren, M. Liu, M. Odenthal, D. Stippel, et al., (2020) Circulating tumor DNA as an emerging liquid biopsy biomarker for early diagnosis and therapeutic monitoring in hepatocellular carcinoma. International journal of biological sciences. 16(9): p. 1551-1562.
305. Allenson, K., J. Castillo, F.A. San Lucas, G. Scelo, D.U. Kim, V. Bernard, G. Davis, T. Kumar, M. Katz, M.J. Overman, et al., (2017) High prevalence of mutant KRAS in circulating exosome-derived DNA from early-stage pancreatic cancer patients. Ann Oncol. 28(4): p. 741-747.
306. Jonsson, M.K.B., T.A.B.v. Veen, J. Synnergren, and B. Becker, (2016) Towards creating the perfect *in vitro* cell model. Stem Cells International. 2016: p. 3459730.
307. Hudu, S.A., A.S. Alshrari, A. Syahida, and Z. Sekawi, (2016) Cell Culture, Technology: Enhancing the Culture of Diagnosing Human Diseases. Journal of clinical and diagnostic research : JCDR. 10(3): p. DE01-DE5.
308. Zhang, W., X. Zhou, Q. Yao, Y. Liu, H. Zhang, and Z. Dong, (2017) HIF-1-mediated production of exosomes during hypoxia is protective in renal tubular cells. American Journal of Physiology-Renal Physiology. 313(4): p. F906-F913.
309. Ban, J.J., M. Lee, W. Im, and M. Kim, (2015) Low pH increases the yield of exosome isolation. Biochem Biophys Res Commun. 461(1): p. 76-9.
310. Ludwig, N., S.S. Yerneni, E.V. Menshikova, D.G. Gillespie, E.K. Jackson, and T.L. Whiteside, (2020) Simultaneous Inhibition of Glycolysis and Oxidative Phosphorylation Triggers a Multi-Fold Increase in Secretion of Exosomes: Possible Role of 2′,3′-cAMP. Scientific Reports. 10(1): p. 6948.
311. Aebersold, R., A. Bensimon, B.C. Collins, C. Ludwig, and E. Sabido, (2016) Applications and Developments in Targeted Proteomics: From SRM to DIA/SWATH. Proteomics. 16(15-16): p. 2065-7.
312. Tu, C., J. Li, Q. Sheng, M. Zhang, and J. Qu, (2014) Systematic assessment of survey scan and MS2-based abundance strategies for label-free quantitative proteomics using high-resolution MS data. Journal of proteome research. 13(4): p. 2069-2079.
313. Marx, V., (2013) Targeted proteomics. Nat Methods. 10(1): p. 19-22.
314. Borràs, E. and E. Sabidó, (2017) What is targeted proteomics? A concise revision of targeted acquisition and targeted data analysis in mass spectrometry. PROTEOMICS. 17(17-18): p. 1700180.
315. Lange, V., P. Picotti, B. Domon, and R. Aebersold, (2008) Selected reaction monitoring for quantitative proteomics: a tutorial. Mol Syst Biol. 4: p. 222.

316. Venkitakrishnan, R.P., E. Zaborowski, D. McElheny, S.J. Benkovic, H.J. Dyson, and P.E. Wright, (2004) Conformational changes in the active site loops of dihydrofolate reductase during the catalytic cycle. Biochemistry. 43(51): p. 16046-55.
317. Hammes, G.G., (2002) Multiple Conformational Changes in Enzyme Catalysis. Biochemistry. 41(26): p. 8221-8228.
318. Hammes, G.G., (1964) MECHANISM OF ENZYME CATALYSIS. Nature. 204: p. 342-3.
319. Gagné, D., R.L. French, C. Narayanan, M. Simonović, P.K. Agarwal, and N. Doucet, (2015) Perturbation of the Conformational Dynamics of an Active-Site Loop Alters Enzyme Activity. Structure (London, England : 1993). 23(12): p. 2256-2266.
320. Watt, E.D., H. Shimada, E.L. Kovrigin, and J.P. Loria, (2007) The mechanism of rate-limiting motions in enzyme function. Proceedings of the National Academy of Sciences. 104(29): p. 11981-11986.
321. Benkaidali, L., F. André, G. Moroy, B. Tangour, F. Maurel, and M. Petitjean, (2017) The Cytochrome P450 3A4 has three Major Conformations: New Clues to Drug Recognition by this Promiscuous Enzyme. Molecular Informatics. 36(10): p. 1700044.
322. Keerthikumar, S., L. Gangoda, M. Liem, P. Fonseka, I. Atukorala, C. Ozcitti, A. Mechler, C.G. Adda, C.-S. Ang, and S. Mathivanan, (2015) Proteogenomic analysis reveals exosomes are more oncogenic than ectosomes. Oncotarget. 6(17): p. 15375-15396.
323. Demory Beckler, M., J.N. Higginbotham, J.L. Franklin, A.J. Ham, P.J. Halvey, I.E. Imasuen, C. Whitwell, M. Li, D.C. Liebler, and R.J. Coffey, (2013) Proteomic analysis of exosomes from mutant KRAS colon cancer cells identifies intercellular transfer of mutant KRAS. Mol Cell Proteomics. 12(2): p. 343-55.
324. Bernasconi, C., O. Pelkonen, T.B. Andersson, J. Strickland, I. Wilk-Zasadna, D. Asturiol, T. Cole, R. Liska, A. Worth, U. Müller-Vieira, et al., (2019) Validation of in vitro methods for human cytochrome P450 enzyme induction: Outcome of a multi-laboratory study. Toxicology in vitro : an international journal published in association with BIBRA. 60: p. 212-228.

APPENDIX 1: MATERIALS

Appendix Table A. Chemicals and reagents

Items	Manufacturers/Suppliers
0.5% Trypsin-EDTA (10x) (cat# 15400-054)	Gibco by Life Technologies, Canada
1 M HEPES (cat# 15630080)	Thermo Fisher Scientific, Australia
1,4-dithiothreitol (DTT-RO)	Roche, Switzerland
10 mM Tris-HCl; 1 mM EDTA buffer (BioUltra, for molecular biology, pH 7.4)	Sigma-Aldrich, USA
100x L-Glutamine (cat# 25030081)	Thermo Fisher Scientific, Australia
1-hydroxy Midazolam (cat# H948420)	Toronto Research Chemicals, Canada
30% Acrylamide/Bis solution (29:1) (cat# 1610156)	Biorad, USA
Acetonitrile hypergrade for LC-MS (LiChrosolv® 2.5 Litre, cat# 1000292500)	Sigma-Aldrich, USA
Ammonium Bicarbonate (Reagent plus®, ≥ 99%, cat# A6141)	Sigma-Aldrich, USA
Amplification grade DNase I (cat# 18068015)	Thermo Fisher Scientific, Australia
Biorad Protein assay reagent (cat #5000006)	Biorad, USA
Bovine serum albumin (BSA), heat shock fraction, pH 7, ≥ 98% (cat# A9647)	Sigma-Aldrich, USA
Denatured absolute alcohol F3 (Ethyl Alcohol) (cat# 1502186968)	Thermo Fisher Scientific, Australia
Dimethyl Sulfoxide (cat# D8418-100ML)	Sigma-Aldrich, USA
di-Potassium hydrogen orthophosphate (K_2HPO_4) (cat# 2221-500G)	Univar, USA
di-Sodium hydrogen phosphate anhydrous (Na_2HPO_4) (cat# 4741)	May & Baker Pty Ltd, Australia
Dulbecco phosphate buffer saline (DPBS) (cat# D5652)	Sigma-Aldrich, USA
Exosome-depleted Foetal Bovine Serum (cat# A25904DG)	Gibco by Life Technologies, USA
Foetal Bovine Serum (cat# 61538)	Scientifix Life, Australia
Folin & Ciocalteu's Phenol reagent (cat# 3264)	BDH Laboratory Supplies, England

Formic acid 98-100% (Suprapur® 250 mL, cat# 1.11670.0250)	Merck Millipore, Australia
GlutaMAX™-I (100x) (cat# 35050061)	Gibco by Life Technologies, Canada
GoTaq® qPCR Master Mix (cat# A6001)	Promega, USA
Hydrocortisone sodium succinate (Solu-Cortef®) (cat# AUST R 12264)	Pfizer Inc., USA
Insulin solution from bovine pancreas (cat# I0516-5ML)	Sigma-Aldrich, USA
Iodoacetamide (BioUltra, cat# I1149)	Sigma-Aldrich, USA
Methanol hypergrade for LC-MS (LiChrosolv® 2.5 Litre, cat# 1.06018.2500)	Merck Millipore, Australia
Micro BCA protein assay kit (cat# 23235)	Thermo Fisher Scientific, Australia
Midazolam (cat# M343000)	Toronto Research Chemicals, Canada
N, N, N', N'- Tetramethly-1-2-diamiomethane (TEMED) (cat# T9281)	Sigma-Aldrich, USA
Nitrocellulose membrane, Roll, 0.2 µm, 30 cm x 3.5 m (cat# 1620112)	Biorad, USA
Nuclease-free water (cat# P1193)	Promega, USA
NxGen® M-MuLV Reverse Transcriptase (cat# 30222-1)	Lucigen, Wisconsin, USA
NxGen® RNase Inhibitor (cat# 30281-1)	Lucigen, Wisconsin, USA
Penicillin-Streptomycin (Solution stabilized, with 10,000 units penicillin and 10 mg streptomycin/mL, sterile-filtered, cat# P4333-100 mL)	Sigma-Aldrich, USA
Piece MicroBCA™ Assay kit (cat# 23235)	Thermo Fisher Scientific, Australia
Rifadin (rifampin 150 mg)	Sanofi Aventis, USA
Sequencing Grade Modified Trypsin (cat# V511A)	Promega, USA
Serum-free Induction medium supplement for HepaRG (cat# HPRG650)	Thermo Fisher Scientific, Australia
SuperScript™ VILO™ cDNA Synthesis Kit (cat# 11754250)	Thermo Fisher Scientific, Australia
SuperSignal West Pico chemiluminescent (ECL) HRP substrate (cat# 34579)	Thermo Fisher Scientific, Australia

Thaw, seed and general-purpose additive for HepaRG (cat# HPRG670)	Thermo Fisher Scientific, Australia
Tris (hydroxymethyl) aminomethane (TRIS) (cat# 2525C271)	VWR Life Science AMRESCO®, Australia
TRizol reagent (cat# 15596026)	Thermo Fisher Scientific, Australia
Trypan Blue stain (0.4%) (cat# 15250061)	Thermo Fisher Scientific, Australia
Trypsin Resuspension Buffer (cat# V542A)	Promega, USA
Tween-20 (cat# BIO0777-500ML)	Astral Scientific, Australia
William's E media with no phenol red (1x) (cat# A1217601)	Thermo Fisher Scientific, Australia
Williams' Medium E with no glutamine(1x) (cat# 12551032)	Thermo Fisher Scientific, Australia
β-Nicotinamide adenine dinucleotide 2′-phosphate reduced tetrasodium salt hydrate (cat# N1630-250MG)	Sigma-Aldrich, USA

Appendix Table B. Commercial kits.

Items	Manufacturers/Suppliers
Amicon® Ultra-4 Centrifugal Filter Units (cat# UFC803024)	Merck Millipore, Billerica, MA, USA
exoRNeasy Serum Plasma Kits (cat# 77044)	Qiagen, Germany
qEV 2/70 nm (Product Code: SP4)	Izon Science
qEV original/70 nm (Product Code: SP1)	Izon Science
QIAGEN exoEasy Serum/Plasma Maxi Kit (20) (cat# 160015170)	Qiagen, Germany
QIAGEN exoEasy Serum/Plasma Midi Kit (50) (cat# 157053808)	Qiagen, Germany
QIAzol Lysis Reagent (cat# 79306)	Qiagen, Germany
TFF-Easy -tangential flow filtration concentrator, 20 nm cut-off filter (cat# HBM-TFF/1)	Lonza, Australia

Appendix Table C. General laboratory consumables

Items	Manufacturers/Suppliers
10 mL Serological Pipette (cat# 86.1254.001)	Sarstedt, Germany

100-1250 µL Pipette tips (cat# 651C6-651G)	Edwards, USA
2 mL Serological Pipette (cat# 160210)	LP Italiana SPA, Italy
200 µL Pipette tips (cat# 70.760.002)	Sarstedt, Germany
25 mL Serological Pipette (cat# 86.1685.001)	Sarstedt, Germany
5 mL Serological Pipette (cat# 86.1253.001)	Sarstedt, Germany
50 mL Tube 114 x 28 mm, PP (cat# 62.547.254)	Sarstedt, Germany
BD Syringe 10 mL (cat# 302146)	Becton Dickinson, Singapore
Disposable cuvettes for spectrophotometers (semi-micro) (cat# 634-0678)	VWR International, USA
Micro tube 1.5 mL (cat# 72.690.001)	Sarstedt, Australia
Minisart® Syringe Filter 0.2 µm (cat# 16534)	Sartorius AG, Germany
Minisart® Syringe Filter 0.45 µm (cat# 16592)	Sartorius AG, Germany
Protein LoBind tubes 2 mL (cat#0030108132)	Eppendorf, Australia
Protein LoBind tubes 5 mL (cat#0030108302)	Eppendorf, Australia
RotorGene 3000 Four-Channel Multiplexing System	Corbette Research, Australia
Thinwall Polypropylene Tube (cat#344367)	Beckman Coulter, Australia
Nunc™ MicroWell™ 96-Well, Nunclon Delta-Treated, Flat-Bottom Microplate (cat# 167008)	Thermo Fisher Scientific, Australia
Ted-Pella B 300M carbon-coated grids	Ted-Pella, Redding, CA, USA
21-gauge Vacuette Safety BloodCollection sealed vacuum device	Greiner Bio-One, Frickenhausen, Germany
Z Serum Sep Clot Activatortubes	Greiner Bio-One, Frickenhausen, Germany

Appendix Table D. Instruments

Items	Manufacturers/Suppliers
1200 Series High Performance Liquid Chromatography	Agilent Technologies, USA
7-Litre Shaking Water Bath	RATEK Instruments, Australia
AdvanceBio Peptide Mapping, 2.7 µm, 2.1 x 100 mm (Part no. 655750-902)	Agilent Technologies, USA
Agilent Triple Quadrupole LC/MS 6495B	Agilent Technologies, USA
Beckman Coulter optima XPN80 (Part no. A95765)	Beckman Coulter, Australia
Cary 300 Conc UV-Visible Spectrophotometer	Varian, USA
FEI TECNAI^{TM} Spirit G2 TEM	FEI company, USA

JA-20 Fixed-Angle Aluminium Rotor, 8 x 50 mL, 20,000 rpm, 48,400 x g (Part no. 334831)	Beckman Coulter, Australia
Mini Trans-Blot® Cell (cat# 1703930)	Biorad, USA
NanoDrop™ 2000/2000c Spectrophotometers	Thermo Fisher Scientific, Australia
NanoSight NS300	Malvern Panalytical, UK
Olympus CKX53 Microscope	Olympus, Australia
PIPETMAN® Classic P1000 Pipette	Gilson, Australia
PIPETMAN® Classic P2 Pipette	Gilson, Australia
PIPETMAN® Classic P20 Pipette	Gilson, Australia
PIPETMAN® Classic P200 Pipette	Gilson, Australia
SpectraMax iD5 Multi-Mode Microplate reader	Molecular Devices, USA
SW 32.1 Ti Swinging-Bucket Rotor Package (Part no. 369694) include 369650 SW 32.1 Ti Rotor Assembly, 331186 Bucket Holder Rack, 335456 Overspeed Disks)	Beckman Coulter, Australia
TSX Series ultra-low freezers (-80 °C)	Thermo Fisher Scientific, Australia
ZORBAX RRHD Eclipse Plus C18, 95Å, 2.1 x 50 mm, 1.8 µm, 1200 bar pressure limit (Part no. 959757-902)	Agilent Technologies, USA

Working reagents

The following buffer formulae were used to make up appropriate buffers throughout the duration of this work:

CYP450 enzyme activity assay

- Alamethicin (10 mg/mL, A.G. Scientific): Alamethicin was dissolved in methanol to a concentration of 10 mg/mL and stored at -20 ºC for up to 1 year.
- Trypsin Gold (Promega) powder was resuspended in 100 µL of supplied trypsin resuspension buffer (Promega) and stored at -20 ºC for up to 1 year.

Mobile phase for Liquid chromatography

- Mobile phase: 0.1% Formic acid in Acetonitrile:0.1% Formic acid in water (50:50 ratio)
- Potassium-Phosphate buffer (1 M): 40 mL of 1 M KH_2PO_4 (136.09 g/mol) solution with

- of 160 mL of 1 M K_2HPO_4 (MW = 174.18 g/mol) solution. pH was adjusted to 7.4 by adding 1 M KH_2PO_4.

Mammalian tissue culture

- 1 M Dulbecco's Phosphate Buffered Saline (D-PBS): Weight 9.6 g of dry powder D-PBS (Sigma-Aldrich) per 1 litre of autoclaved distilled water.
- 1 M Phosphate Buffered Saline: 137 mM NaCl, 2.7 mM KCl, 10 mM Na_2HPO_4 and 2 mM KH_2PO_4, pH 7.4.

Proteomics: in-gel digestion

All reagents were made fresh before use:

- 50 mM ammonium bicarbonate (ABC, pH 7.8): 253 µL of Milli-Q water was added per 1 mg of ABC
- 50 mM calcium chloride: 136.04 µL of 50 mM ABC was added per 1 mg of calcium chloride
- 50 mM dithiothreitol (DTT): 129.5 µL of 50 mM ABC was added per 1 mg of DTT
- 100 mM iodoacetamide (IAA): 54 µL of 50 mM ABC was added per 1 mg of IAA

Proteomics: in-solution digestion

All reagents were made fresh before use:

- 50 mM ABC (pH 7.8): 253 µL of Milli-Q water was added per 1 mg of ABC
- 200 mM DTT: dissolve 3.1 mg per 100 µL Milli-Q water.
- IAA 400 mM: dissolve 7.4 mg per 100 µL Milli-Q water.
- Formic acid 10% v/v in Milli-Q water.

Immunoblotting

- SDS-PAGE running buffer: 25 mM Tris pH 8.3, 192 mM glycine, 0.1% SDS.
- SDS-PAGE transfer buffer: 25 mM Tris pH 8.3, 192 mM glycine, 20% methanol.
- Tris-buffered saline (TBS): 50 mM Tris pH 7.4, 150 mM NaCl.
- SDS loading buffer: 0.2 M Tris-HCl, 4.3 M Glycerol, 277 mM SDS, 6 mM Bromophenol blue, 0.4 M DTT.

APPENDIX 2: GENERAL METHODS FOR DETERMINATION OF PROTEIN CONCENTRATION

Lowry assay

Protein concentration of cells lysates was determined using Lowry assay. Cells lysates were diluted 1:10 in distilled water. 25 µL of diluted sample was mixed with 475 µL of distilled water and subsequently with 2 mL of Lowry reagent. The Folin-Ciocalteau reagent (250 µL) was added to initiate the colour forming reaction. A calibration curve was generated using Bovine Serum Albumin (BSA). The calibration curve was prepared over the concentration range 5 – 100 mg/L. Protein content in all samples and BSA standards was measured using the absorbance at 660 nm. The UV-spectrophotometry was zeroed using a distilled water instead of protein. All samples and standard were analysed in duplicate. Calibration curve was plotted between protein content and absorbance. Protein concentration of samples was determined using the following equation:

$$[protein\ content] = dilution\ factor\ x\ \frac{absorbance}{calibration\ curve\ slope}\ x\ \frac{1}{sample\ volume}$$

microBCA protein assay

A set of BSA protein standards was prepared as per manufacturer's protocol. Briefly, serial dilution of BSA stock concentration (2 mg/mL) was performed to obtain protein standard range from 0 – 200 µg/mL. The Micro BCA working solution was prepared by mixing 25 parts of Micro BCA reagent A and 24 parts Micro BCA reagent B with 1 part of Micro BCA reagent C (Ratio 25:24:1). 150 µL of BSA standard or samples was pipetted in duplicate into 96-well plate, followed by the addition of 150 µL Micro BCA working solution. The 96-well plate was incubated at 37°C for 2 hours. Following incubation, the plate was left to stand at room temperature for 5 minutes and absorbance was measured using a SpectraMax iD5 Multi-Mode Microplate Readers (Molecular Devices, USA) set to 562 nm wavelength.

APPENDIX 3: CULTURING AND VALIDATION OF HEPARG

Methods

Cell culture

Undifferentiated HepaRG cells (passage 13) were obtained from Biopredic international (Rennes, France) under MTA agreement. Upon arrival, cells were stored in liquid nitrogen tank immediately. Cell bank was set up according to the standard instruction protocol (Rennes, France). Cells were seeded at 2 million cells in T75 cell culture flask and were cultured in growth media; William's E media supplemented with 2 mM Glutamax, 10% foetal bovine serum (FBS), 100 IU/mL penicillin, 100 µg/mL streptomycin, 5 µg/mL bovine insulin, and 50 µM hydrocortisone hemisuccinate. Cells were maintained in growth media for 14 days to allow cell proliferation. At day 15, cells cell growth media was replaced with media containing 1% DMSO for 3 days, before subsequently changing to cell differentiation media containing 2% DMSO and grown for another 14 days. Media was renewed every 2-3 days throughout the entire culturing process.

To passage cells, media was removed from the flaks and cells were washed with sufficient amount of sterile D-PBS to completely remove any remaining media. Cells were detached from the flasks by adding 2 mL (for T75 flasks) 0.05% trypsin/0.53 mM EDTA in PBS solution and incubating at 37°C for 2 – 3 minutes. Trypsin was neautralised by adding complete growth media. To determine cell count, 20 µL of cell suspension was mixed with an equal volume of 0.2% trypan blue, 10 µL of mixture was loaded onto a Neubauer Haemocytometer Cell Counting Chamber (Adelab Scientific, Australia), covered with coverglass and cells were counted using Olympus CK2 microscope.

Induction study

For induction study, HepaRG were cultured in induction media; William's E media supplemented with 2 mM Glutamax, 100 IU/ml penicillin, 100 µg/mL streptomycin, 4 µg/ml bovine insulin, and 50 µM hydrocortisone hemisuccinate. Induction media composition was similar to cell growth media, with a modification of depleting FBS and lowering the concentration of insulin. Induction media was used to lower the CYP3A4 and the other enzyme activity to basal level, as DMSO in differentiation maintained the activity of enzymes to the highest extent. Rifampicin was dissolved in DMSO at 1,000-fold to the desired final concentration in order to minimise DMSO concentration to less than 0.1% at the incubation step. Cells were cultured in induction media with the presence or the absence of 10 µM rifampicin for 48 hours, with media and drug renewal every 24 hours. At 48 hours, cells were harvested by removing media, washing briefly with Dulbecco's phosphate-buffered saline (D-PBS) and collecting cells using a cell scrapper before transferring them to the collection tubes.

To generate stocks of cells for subsequent use, HepaRG cells were counted and 1.5 million cells per Nunc cryotube vial were frozen. Briefly, freezing media containing growth media supplemented with 20% DMSO was used for freezing cells for the biobank storage. Cells were harvested and centrifuged at 500 g for 3 minutes at 4°C to obtain a cell pellet. Cell pellets were re-suspended in 250 µL of growth media and placed on ice immediately. Slowly, 250 µL of freezing media was added to the Cryovials, each containing 500 µL of final mixture (1.5 million of cells) and they were stored at -80°C for 24 hours before transferring to liquid nitrogen for long term storage. Upon removal from liquid nitrogen, cell stocks were thawed by dropping gently 1 mL growth media directly to the frozen cells and transferring the cell suspension to the T25 cell culture flask containing HepaRG cell growth media. The following day, media was replaced with fresh growth media to completely remove any traces of DMSO.

EV isolations

The process of EVs isolation was provided in **Chapter 5** under methods section.

Determination of CYP3A4 enzyme activity.

The metabolite formation of 1OH-midazolam was used to determine CYP3A4 enzyme activity in HepaRG cells. Cell lysates (80 µg) were incubated with 5 µM midazolam in presence of 0.1 M phosphate buffer and 1 mM NADPH for 60 minutes in a shaking water bath at 37°C. Reactions were terminated with ice-cold acetonitrile containing 0.1% formic acid. Samples were centrifuged at 16,000 *g* for 15 minutes at 4ºC. 300 µL of clear supernatant were transferred to LC-MS vials filled with 400 µL pull-point glass inserts. Vials were then capped and transferred to the LC-MS for analysis.

Extraction of total RNA from mammalian cells.

RNA extraction was performed as per TRIzol manufacturer's protocol. Briefly, HepaRG cells were washed in D-PBS and harvested in 1 mL of TRIzol (Life Technologies, Victoria, Australia) per 10-25 cm^2 of surface area of cells grown. Samples were transferred to a new 1.5 mL microcentrifuge tubes and 200 µL of chloroform was added per 1 mL of TRIzol and mixed vigorously. Samples were centrifuged at 12,000 g for 15 minutes at 4°C. Top aqueous layer containing the RNA was transferred to a fresh 1.5 mL microcentrifuge tube. RNA was precipitated by adding 500 µL of isopropanol per 1 mL TRIzol starting volume. Samples were incubated at room temperature for 10 minutes, and then centrifuged at 12,000 g, 4°C for 10 minutes. Samples were washed with 1 mL of 75% ethanol per 1 mL of TRIzol. Supernatant was discarded, and samples were air-dried for 30 minutes. Samples were resuspended (a white pellet might be visible) in 20-30 µL of RNase-free water and heated to 60°C for 10 minutes. Store the samples in -80°C until required for downstream analysis.

cDNA synthesis using Lucigen kit (Lucigen Corporation)

RNA concentration was measured using NanoDrop™ 2000/2000c Spectrophotometers (Thermo Fisher Scientific, Australia). A 2 µg aliquot of total RNA was transferred to a new 1.5 mL microfuge tube and 1 U of DNA I (1 U/1 µL) amplification grade DNase I in 20 mM Tris-HCl (pH 8.4), 2 mM MgCl2 and 50 mM KCl and inculated at room temperature for 15 minutes. Inactivation of DNase I was done by adding EDTA to a final concentration of 2.5 mM, and samples were incubated at 65°C for 10 minutes. One microgram (8 µL) of DNase-treated RNA was added to a 20 µL reaction volume containing 1 µL 10 mM dNTPs, 1 µL 53 ng/µL random hexamers (NEB) and 6 µL RNase-free water. Samples were incubated at 65°C for 5 minutes then cooled on ice for 2 minutes. 2 µL of M-MulV Reverse Transcriptase buffer (10x), 1 µL RNase inhibitor and 1 µL Reverse Transcriptase were added and the reaction volume was brought up to 20 µL. Reverse transcriptase reaction was performed at 42°C for 1 hour, followed by an increase temperature to 90°C, and followed by a 10 minutes hold. cDNA was diluted 1:10 with sterile RNase-free water before using in PCR.

Determination of CYP3A4 mRNA expression.

Cells were seeded and cultured in 6-well plates following the standard process of growth, differentiation and induction as mentioned prior. After 48 hours, cells were washed with 1xPBS before harvesting using Trizol lysis reagent (1 mL per well). NanoDrop™ 2000/2000c spectrophotometer was used to determine the concentration and purity of all RNA samples. RNA was reverse transcribed to cDNA using the SuperScript™ VILO™ cDNA Synthesis Kit according to manufacturer's protocol (Invitrogen, Cat no: 11754050). The 20 µL reaction mixture contained 5 µL cDNA product, 1 µL TaqMan Gene expression Assay (20x), 10 µL TaqMan® Gene Expression Master mix (2x). PCR reactions were run at 50°C for 2 minutes and then 95 °C for 10 minutes, followed by 40 cycles of 95°C for 15 seconds and 60°C for 1 minute. Expression level of mRNA was analysed using the Rotor-Gene 6 software (Corbett Life Science). 18S and GAPDH were used as normalizing controls (TaqMan® Gene Expression Assay IDs Hs99999901_s1 and Hs02786624_g1 respectively).

Appendix Table E. Real-time PCR: TaqMan® *CYP3A4* gene expression assay.

List	Details
Assay ID	Hs00604506_m1
Lot number	P160610-006A03
Vial type	Matrix Tube
Vial ID	213832522
Assay Mix concentration	20x
Forward Primer Name	Hs00604506_m1_F
Forward Primer Concentration	18

Reverse Primer Name	Hs00604506_m1_R
Reverse Primer	18
Reporter 1 Name	Hs00604506_m1_M
Reporter 1 Dye	FAM
Reporter 1 Concentration	5
Reporter 1 Quencher	NFQ

Results

Cell morphology

HepaRG demonstrated a morphology of elongated cells during the first 5 days after seeding (**Appendix Figure A**). Cells actively propagated until they reached confluency at around day 10 – 11. Upon reaching the confluency, cells underwent morphology change together with forming colonies of granular epithelial cells. Adding of DMSO at day 14 facilitated HepaRG cell differentiation. At day 35, HepaRG cells were at a differentiated stage with approximately 40-50% of the cells were hepatocyte-like cell (**Appendix Figure B**).

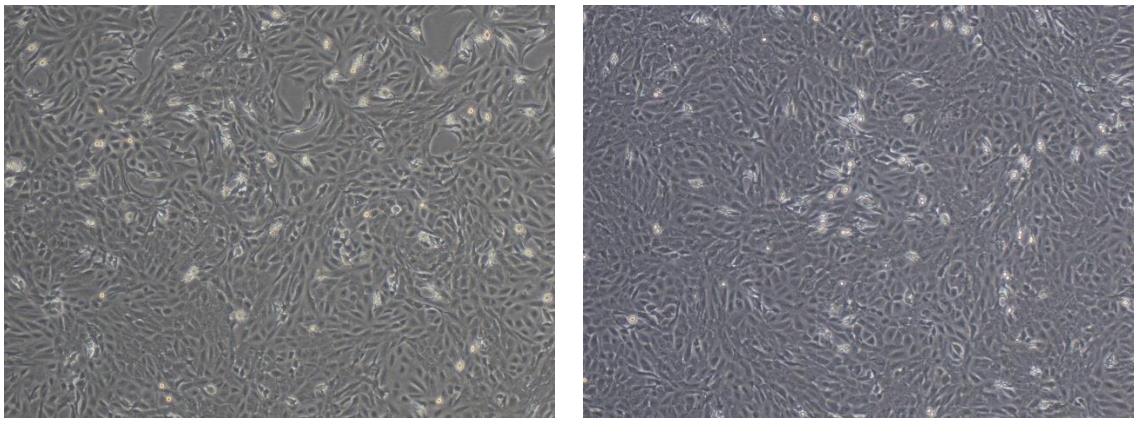

Appendix Figure A – Phase contrast photomicrograph of HepaRG cultured at day 10 in growth media. Cells were seeded at 2x10^6 cells per T75 flask. The morphology observed a diversity of shapes with nearly 100% confluency.

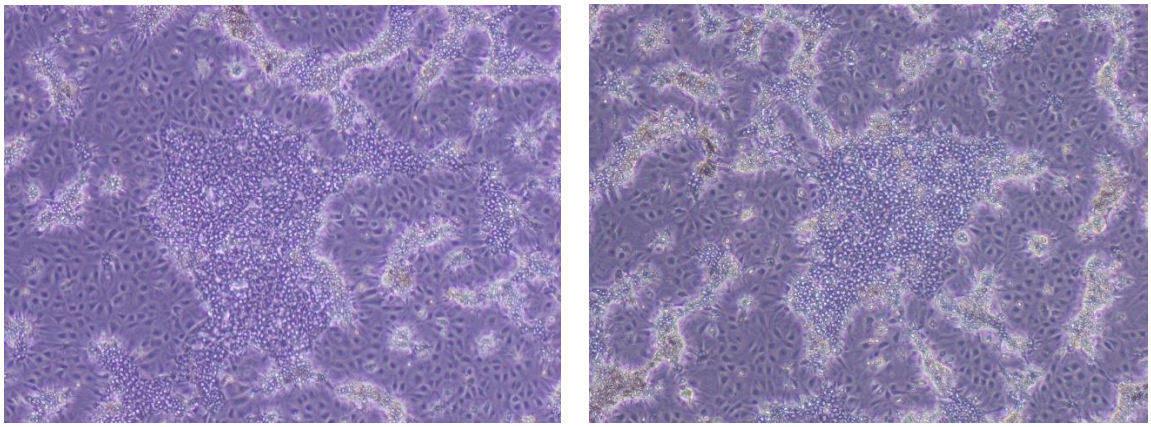

Appendix Figure B – Phase contrast photomicrograph of HepaRG cultured for 35 days. Cells were cultured in growth media in absence of DMSO for 14 days before transition to be cultured in the media containing 2 % DMSO. The morphology observed predominantly of hepatocyte-like cells with substantial present of bile canaliculus-like structure.

CYP3A4 enzyme activity following rifampicin induction.

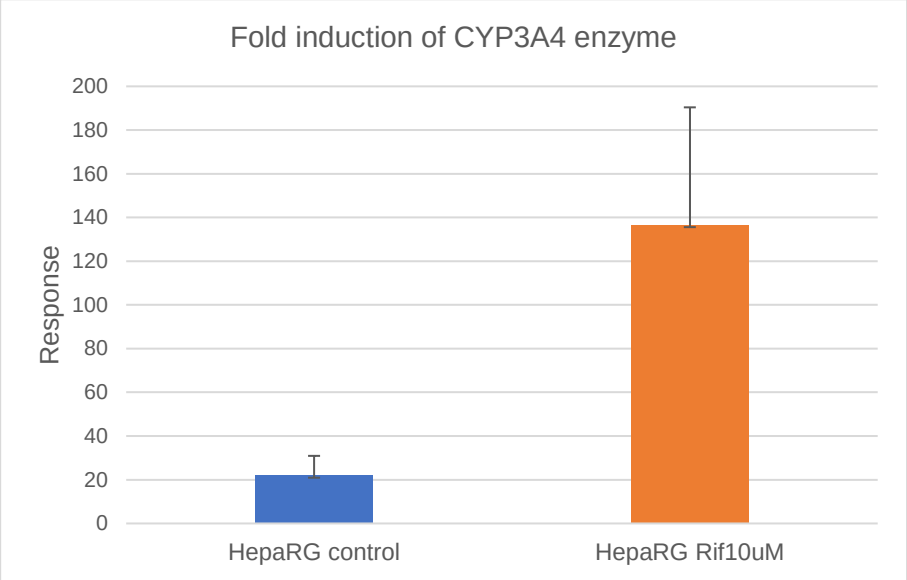

Appendix Figure C – Overall fold induction of rifampicin on HepaRG. Data were generated from four biological replicates. HepaRG treated with 10 µM rifampicin observed approximately 6.3-fold change of CYP3A4 enzyme activity compared to the control group.

Induction of P450 enzyme observed a dramatically pronounced after 48 hours exposure to enzyme inducer as reported in previous literatures [65]. In this validation study, rifampicin at 10 µM was served as CYP3A4 inducing agent [324]. Midazolam 5 µM was the specific CYP3A4 substrate used in the metabolite formation method to observe 1OH midazolam which is the metabolite generated from midazolam via CYP3A4.

Four biological replicates were conducted to evaluate the inducibility of CYP3A4 in HepaRG cells. CYP3A4-catalysed 1OH-midazolam activity was induced by rifampicin with the average 6.3-fold induction (**Appendix Figure C**).

Expression of CYP3A4 mRNA following rifampicin induction.

HepaRG treated with rifampicin (10 µM) for 48 hours observed average *CYP3A4* mRNA induction of 10-fold compared to untreated HepaRG. Data was normalised to *GAPDH* mRNA levels (**Appendix Figure D**).

Size distribution of EVs isolated from HepaRG conditioned media.

EVs isolated from conditioned media collected 24 hours after induction media was introduced showed a uniformity of the particle size in which range between 88 – 105 nm. The size distribution of EVs isolated from the conditioned media before the induction study showed a similar profile to the EVs isolated 48 hour after introducing induction media to HepaRG **(Appendix Figure E).**

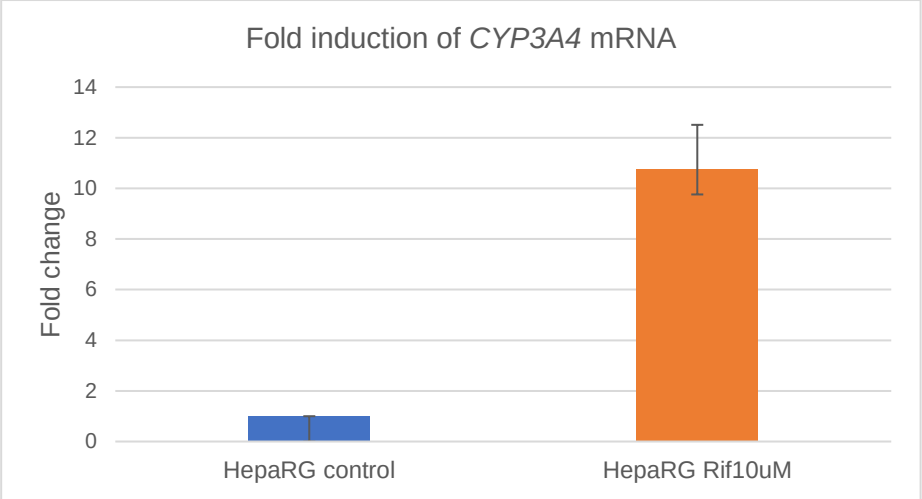

Appendix Figure D – Overall fold induction of rifampicin on *CYP3A4* mRNA expression. Data were generated from three biological replicates. HepaRG treated with 10 µM rifampicin observed approximately 10-fold change of *CYP3A4* mRNA expression compared to the control group.

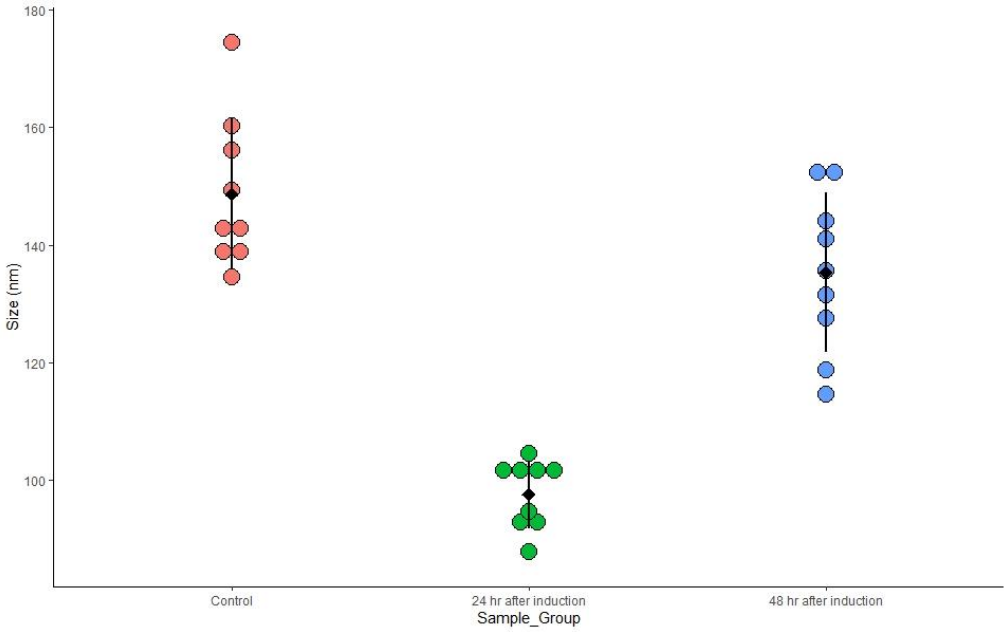

Appendix Figure E – Size distribution of EVs isolated from HepaRG in different state of culturing. Data were generated from three biological replicates.

APPENDIX 4: PEPTIDE SEQUENCES

Appendix Table F. Peptide sequences for CYP3A4.

List	Details
Protein name	Cytochrome P450 3A4
Gene	*CYP3A4*
Domain	Transmembrane
Peptides sequences	10 20 30 40 50 60 MALIPDLAME TWLLLAVSLV LLYLYGTHSH GLFKKLGIPG PTPLPFLGNI LSYHKGFCMF 70 80 90 100 110 120 DMECHKKYGK VWGFYDGQQP VLAITDPDMI KTVLVKECYS VFTNRRPFGP VGFMKSAISI 130 140 150 160 170 180 AEDEEWKRLR SLLSPTFTSG KLKEMVPIIA QYGDVLVRNL RREAETGKPV TLKDVFGAYS 190 200 210 220 230 240 MDVITSTSFG VNIDSLNNPQ DPFVENTKKL LRFDFLDPFF LSITVFPFLI PILEVLNICV 250 260 270 280 290 300 FPR**EVTNFLR** KSVKRMKESR LEDTQKHRVD FLQLMIDSQN SKETESHKAL SDLELVAQSI 310 320 330 340 350 360 IFIFAGYETT SSVLSFIMYE LATHPDVQQK LQEEIDAVLP NKAPPTYDTV LQMEYLDMVV

	370 380 390 400 410 420 NETLRLFPIA MRLERVCKKD VEINGMFIPK GVVVMIPSYA LHRDPKYWTE PEKFLPERFS 430 440 450 460 470 480 KKNKDNIDPY IYTPFGSGPR NCIGMRFALM NMKLALIRVL QNFSFKPCKE TQIPLKLSLG 490 500 GLLQPEKPVV LKVESRDGTV SGA
UniProt ID	P08684
Amount	25 nmol

APPENDIX 5: METHOD DEVELOPMENT OF SORAFENIB METABOLISM USING HLM AS PROTEIN SOURCE

Methods

Sorafenib metabolism by CYP3A4 with HLM

HLM samples (80 µg) were incubated with 0.1 M phosphate buffer, 1 mM NADPH, water and sorafenib (2.5 – 160 µM) in a total volume 200 µL. Incubations were performed over 60 minutes at 37°C in shaking water bath. Reactions were terminated with 400 µL ice-cold acetonitrile containing 0.1% formic acid and proceed to LC-MS analysis.

Determination the metabolite of sorafenib by LC-MS

The LC condition was Agilent; mobile phase A: 0.1 % (v/v) formic acid in water; mobile phase B: 0.1 % (v/v) formic acid in Acetonitrile; gradient, 0 minutes to 4 minutes at 10 to 60 % B, 4 minutes to 6 minutes at 60 to 90% B; flow rate, 0.3 mL/minute; column temperature, 26.57°C; and injection volume, 5 µL. The MS/MS detector used was a quadrupole tandem mass spectrometer (Agilent, USA). Samples were analysed using electrospray ionization in the positive model. Data were collected and analysed by MassHunter Sorafenib N-oxide was monitored at *m/z* 481.09 > 286 (collision energy 30) and 481.09 > 211 (collision energy 40 eV).

Results

Appendix Table G. Kinetic profile of sorafenib using HLM as protein source.

Sorafenib concentration [S]	**Accounted for the non-specific binding**	**Velocity [V]**	**[V]/[S]**
2.5	0.5	404050.7	808101.5
5	1	1044693	1044693
7.5	1.5	2274328	1516219
10	2	3148950	1574475
15	3	4463584	1487861
20	4	6111969	1527992
80	16	14104466	881529.1
105	21	14319596	681885.5
110	22	14696111	668005
120	24	14609008	608708.7
130	26	13651062	525040.8
160	32	13188422	412138.2

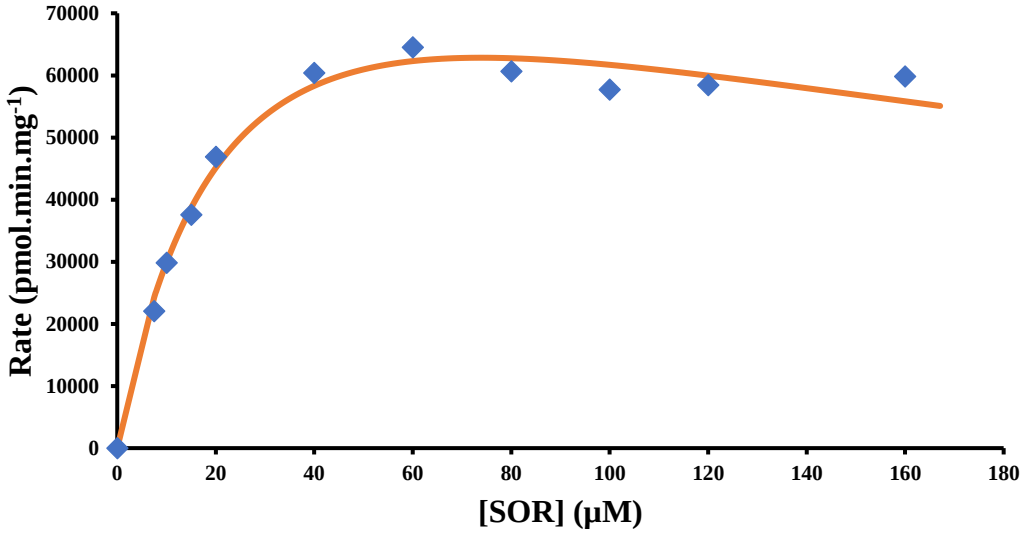

Appendix Figure F – Velocity versus substrate concentration plot for sorafenib metabolism by HLM.

LC-MS/MS Conditions

Five-µL of sample supernatant was injected onto a ZORBAX Eclipse Plus C18 2.1 x 50 mm 1.8-µm HPLC column (Agilent Technologies). Mobile phase consisted of Milli-Q water with 0.1% (v/v) formic acid (A) and acetonitrile with 0.1% (v/v) formic acid (B) at a flow rate of 0.3 mL/minute (see **Appendix Table H** and **I** for gradient). Total run time was 5.5 minutes per sample.

Appendix Table H. LC mobile phase gradient for 1OH-midazolam.

Time (minute)	A (%)	B (%)
0.00	90	10
1.00	90	10
3.00	40	60
3.10	90	10

Appendix Table I. LC mobile phase gradient for sorafenib N-oxide

Time (minute)	A (%)	B (%)
0.00	90	10
4.00	40	60
6.00	10	90
6.10	90	10

MS was operated in Electrospray Ionisation+ (ESI+) and Multiple Reaction Monitoring (MRM) was used to monitor transitions from the 1OH- midazolam precursor ion (m/z 342.01) to several product ions outlined in **Appendix Table J**. Sorafenib N-oxide precursor ion and its product ion as shown in **Appendix Table K**. Other relevant MS settings are outlined in **Appendix Table L**.

Appendix Table J. 1OH- midazolam product ions and relevant acquisition settings.

Product ion (m/z)	Dwell (ms)	Collision energy (eV)	Cell accelerator voltage
342.1 (quantifier)	200	24	4
289 (qualifier)	50	32	4
203 (qualifier)	100	44	4
176 (qualifier)	50	44	4
168 (qualifier)	100	44	4

Appendix Table K. Sorafenib N-oxide product ions and relevant acquisition settings.

Product ion (m/z)	Dwell (ms)	Collision energy (eV)	Cell accelerator voltage
286 (quantifier)	200	30	4
211 (qualifier)	200	40	4

Appendix Table L. Additional relevant MS settings.

Parameter	Value
Delta EMV (+)	200
Capillary	3000 V
Nozzle Voltage	0 V
Nebuliser	20 psi

APPENDIX 6: PUBLICATIONS ARISING DIRECTLY FROM THIS THESIS

International Journal of Clinical Oncology
https://doi.org/10.1007/s10147-020-01698-7

ORIGINAL ARTICLE

Effect of early adverse events resulting in sorafenib dose adjustments on survival outcomes of advanced hepatocellular carcinoma patients

Warit Ruanglertboon[1] · Michael J. Sorich[1] · Andrew Rowland[1] · Ashley M. Hopkins[1]

Received: 20 January 2020 / Accepted: 1 May 2020

Abstract

Background Sorafenib is a current first-line treatment option for advanced hepatocellular carcinoma (HCC). This study aimed to evaluate the impact of early adverse events (AEs) requiring sorafenib dose adjustment on survival outcomes of patients with advanced HCC.

Methods The study was a secondary analysis of the phase III clinical trial NCT00699374. A landmark Cox proportional hazard analysis was used to evaluate the association between early AEs requiring sorafenib dose adjustment with survival outcomes. The primary outcome was overall survival (OS) with progression-free survival (PFS) as secondary.

Results AEs requiring sorafenib dose adjustment within the first 28 days of therapy were significantly associated with OS (HR [95% CI]; dose interruption = 0.9 [0.7–1.2]; dose reduction = 0.6 [0.5–0.9]; discontinuation = 1.7 [0.9–3.4]; $P = 0.005$). No statistically significant association with PFS was identified ($P = 0.148$).

Conclusion Sorafenib dose interruptions and reduction due to AEs did not compromise the survival outcomes of patient with advanced HCC. Patients who required a sorafenib dose reduction were observed to have more favourable OS compared to those who did not experience an AE which required a dose adjustment.

Keywords Sorafenib · Adverse events · Dose adjustment · Prediction · Survival · Response

Introduction

Hepatocellular carcinoma (HCC) is the third most common cause of cancer-related death [1]. Sorafenib, a tyrosine kinase inhibitor (TKI), is the recommended first-line treatment option for advanced/metastatic HCC with demonstrated improvements in overall survival (OS) and progression-free survival (PFS) compared to previous options [2, 3]. Nevertheless, there is still heterogeneity in survival outcomes and adverse outcomes between patients who receive sorafenib therapy [2–4].

Sorafenib is initiated at a dose of 400 mg twice daily for the treatment of advanced HCC [5]. Within clinical trials approximately 40% of patients treated with sorafenib require a dose interruption and 30% require a dose reduction due to adverse events (AEs). Studies indicate that AEs most commonly occur within the first month of sorafenib therapy, with frequent AEs including hand-foot syndrome and diarrhoea [2, 6–8]. Studies have demonstrated that diarrhoea and hand-foot syndrome early after sorafenib initiation were associated with improved survival outcomes [9, 10]. However, studies have not investigated the associations between dose adjustments due to sorafenib-induced AEs and survival outcomes. The primary aim of the study was to evaluate the impact of early AEs requiring sorafenib dose interruptions or dose reductions on survival outcomes in patients with advanced HCC. An exploratory analysis of the association between pre-treatment patient characteristic and early sorafenib dose adjustments induced by AEs was conducted.

Electronic supplementary material The online version of this article (https://doi.org/10.1007/s10147-020-01698-7) contains supplementary material, which is available to authorized users.

✉ Warit Ruanglertboon
warit.ruanglertboon@flinders.edu.au

[1] Department of Clinical Pharmacology, College of Medicine and Public Health, Flinders University, Adelaide, Australia

Published online: 16 May 2020

Methods

Study design and patients

The study was a secondary analysis of the sorafenib arm of phase III clinical trial NCT00699374 which included participants with locally advanced or metastatic HCC [11]. Participants were initiated on sorafenib at 400 mg twice daily on 4-week cycles. Dose reductions and treatment interruptions were permitted in response to AEs according to the registered product insert [11]. When necessary, doses were reduced to 400 mg once daily, and then 400 mg dose every other day.

Individual participant data (IPD) were accesses in this study from https://www.projectdatasphere.org. Secondary analysis of anonymized IPD was deemed negligible risk research by the Southern Adelaide Local Health Network, Office for Research and Ethics and was exempt from review.

Predictors and outcome data

The primary outcome was OS, with PFS assessed as a secondary. PFS was evaluated according to the Response Evaluation Criteria in Solid Tumours (RECIST) version 1.0 [12].

AEs were defined by grade according to the Common Terminology Criteria for Adverse Events version 3.0 (CTCAE) [5]. AEs requiring sorafenib dose adjustments were categorised as 'dose reduction', 'dose interruption' and 'discontinuation'. AE within the first 28 days of sorafenib therapy leading to dose adjustment were the primary focus of this analysis.

Supplementary analyses were undertaken for hand-foot syndrome AEs occurring in the first 28 days of sorafenib therapy and relative dose intensity (actual divided by planned cumulative dose [13, 14]) of sorafenib over the first 28 days of therapy. Sorafenib relative dose intensity was calculated and classified into two groups ($< 50\%$ vs $\geq 50\%$) as previously described [13].

Available pre-treatment characteristic data included sex, age, race, weight, Eastern Cooperative Oncology Group performance status (ECOG PS), estimated glomerular filtration rate, Barcelona Clinic Liver Cancer (BCLC) staging, history of hepatitis B or C infection, number of metastatic site, the presence of liver metastases, oesophageal varices, liver cirrhosis, non-alcoholic steatohepatitis and portal vein thrombosis.

Statistical analysis

A landmark Cox proportional hazard analysis was used to evaluate the association between early AEs requiring sorafenib dose adjustments and OS/PFS. Associations were reported as hazard ratios (HR; event outcomes) with 95% confidence intervals (95% CI) and P values. The landmark was set at 28 days (end of 1st cycle) after sorafenib initiation, with individuals who progressed or died within the first 28 days of therapy excluded from analysis. The landmark was derived according to a balance of being as early as possible (as early markers of response are more useful, and there is a loss of individuals/power as the landmark time increases due to the event occurring before the landmark) and ensuring enough AEs had occur before the landmark time (as only AEs before the landmark count in the analysis technique). Kaplan–Meier analysis was used to estimate and plot survival outcomes according to sorafenib dose adjustment categories.

As an exploratory analysis, univariable Cox proportional hazard analysis was used to evaluate the association between pre-treatment characteristics and early AEs requiring sorafenib dose adjustments within the first 28 days of therapy.

Results

Patient characteristics

Data from 542 patients with advanced HCC who received sorafenib therapy were available. Table 1 provides a summary of the patient characteristics. Prior to day 28th, 16 participants were excluded from the analysis due to disease progression, including 10 participants who died. Median follow-up in the population was 22 [95% CI 21–24] months.

Dose adjustment and predictors

Figure 1 presents the incidence of AEs requiring dose adjustments of sorafenib within each of the first ten cycles of therapy. Within the first 28 days, 128 (51.6%) had a dose interruption, 97 (39.1%) had a dose reduction and 23 (9.3%) discontinued the treatment.

Univariable Cox proportional analysis data identified older age, Asian race, lower weight, history of hepatitis C infection, and absence of liver metastases as associated with an increased risk of experiencing an AEs within the first 28 days of sorafenib therapy which requires a dose adjustment ($P < 0.05$; Supplementary Table 2).

Effect of early AE-related dose adjustment on survival outcomes:

At day 28, there was a significant relationship between early AEs requiring sorafenib dose adjustment within the first 28 days with OS (HR [95%CI]; dose interruption = 0.9

Table 1 Summary of patient characteristics

Parameters	Total No. 542
Sex	
Female	85 (16%)
Male	457 (84%)
Age (years)	
[18, 50]	128 (24%)
[50, 60]	148 (27%)
[60, 70]	149 (27%)
[70, 84]	115 (21%)
Missing	2 (0%)
Race	
Asian	417 (77%)
Non-Asian	125 (23%)
Weight at baseline	64 (57–74)
Baseline ECOG score	
0	289 (53%)
1	250 (46%)
Missing	3 (1%)
BCLC stage	
B	89 (16%)
C	452 (83%)
Missing	1 (0%)
Involved disease site—liver	495 (91%)
Number of involved disease sites (including liver)	
1	223 (41%)
2	214 (39%)
3	89 (16%)
4	16 (3%)
Oesophageal varices	
Yes	156 (29%)
No	376 (69%)
Missing	10 (2%)
Hepatitis B	
Yes	287 (53%)
No	245 (45%)
Missing	10 (2%)
Hepatitis C	
Yes	118 (22%)
No	414 (76%)
Missing	10 (2%)
Liver cirrhosis	
Yes	247 (46%)
No	285 (53%)
Missing	10 (2%)
Estimated glomerular filtration rate (ml/min/1.73 m^2)	
[90, 257]	301 (56%)
[60, 90]	190 (35%)
[45, 60]	30 (6%)
[6, 45]	19 (4%)
Missing	2 (0%)

Table 1 (continued)

Data are median (IQR) or number of patients (%)

[0.7–1.2]; dose reduction = 0.6 [0.5–0.9]; discontinuation = 1.7 [0.9–3.4]; $P = 0.005$) (Table 2). There was no significant relationship between early AEs requiring sorafenib dose adjustment with PFS (HR [95% CI]; dose interruption = 1.2 [1–1.5]; dose reduction = 0.9 [0.7–1.1]; discontinuation = 1.1 [0.2–7.7]; $P = 0.148$) (Table 2). Figure 2 presents Kaplan–Meier estimates of OS and PFS by AE induced dose adjustment category within the first 28 days of sorafenib therapy. Supplementary Fig. 1 presents a forest plot of OS by patient subgroups for AEs requiring dose reductions versus no action in the first 28 days of sorafenib treatment—indicative that the association between dose reduction due to AEs within the first 28 days of sorafenib and favourable OS was consistent across patient subgroups.

Supplementary analyses

Higher sorafenib dose intensity (≥ 50% vs < 50%) over the first 28 days was associated with less favourable OS (HR [95% CI]; 1.4 [1.0–1.9], $P = 0.035$), however, there was no significant association with PFS (HR [95% CI]; 1.0 [0.8–1.4], $P = 0.775$) (Supplementary Table 3). Hand-foot syndrome in the first 28 days of sorafenib therapy was associated with favourable OS (HR [95% CI]; 0.9 [0.8–0.9], $P = 0.005$) but not PFS (HR [95% CI]; 1.0 [0.9–1.1], $P = 0.785$).

Discussion

To the best of the authors' knowledge, this is the first study to report on the effects of dose adjustment of sorafenib due to AEs on survival outcomes of advanced HCC patients. Our analysis showed that dose adjustments were not associated with worse survival outcomes. In addition, patients who experienced dose reduction due to AEs within the first 28 days of therapy had more favourable OS compared to patients who required no dose adjustments.

The precision dosing of cancer medicines requires evidence to inform the effect of dose changes on cancer patient outcomes. This information is currently lacking for sorafenib use in advanced HCC. Several studies have explored alternate dosing strategies for sorafenib [15, 16]. A retrospective study assessed initiating sorafenib at < 800 mg daily, identifying non-inferior outcomes compared to 800 mg daily [15]. Meanwhile, dose escalation above 800 mg daily has been observed to improve survival in a subset of patients [16]. The current recommended dosing strategy of sorafenib in HCC is 800 mg daily, with dose reduction in response

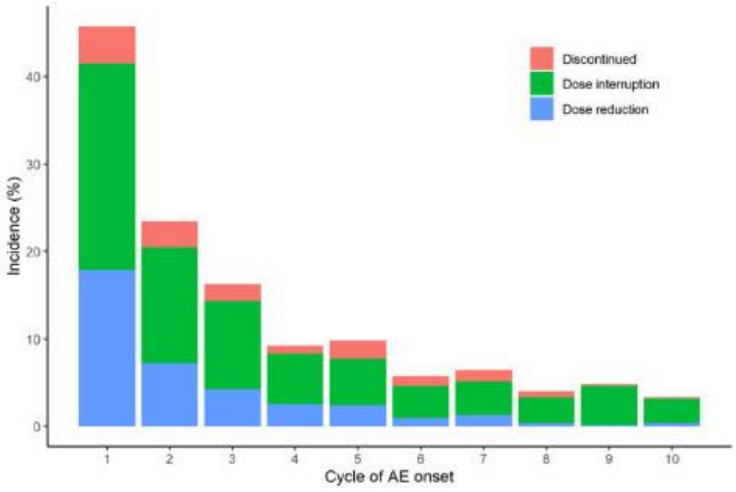

Fig. 1 Proportion of the study cohort with an adverse event leading to adjustment of sorafenib dosing over the first 10 cycles of sorafenib treatment

Table 2 Summary of the association between dose adjustment following AEs within first 28 days of sorafenib treatment with OS and PFS

Action	*N*	OS			PFS		
		Median [95% CI] time to event (months)	HR [95% CI]	*P*	Median [95% CI] time to event (months)	HR [95% CI]	*P*
No action	292	10 [8–11]	1	0.005	4 [3–4]	1	0.148
Dose interruption	125	9 [8–15]	0.91 [0.7–1.2]		3 [3–4]	1.2 [1–1.5]	
Dose reduction	95	15 [12–22]	0.6 [0.5–0.9]		4 [3–6]	0.9 [0.7–1.1]	
Discontinuation	14	3 [2–NA]	1.7 [0.9–3.4]		NA	1.1 [0.2–7.7]	

N - sample size, *CI* - confidence interval, *HR* - hazard ratio, *OS* - overall survival, *PFS* - progression-free survival, *NA* - no data

to AEs. In this study, HCC patients initiated sorafenib at 800 mg daily and dose interruptions and reductions in response to toxicity were not observed to worsen survival outcomes, in fact, patients who required a dose reduction had favourable OS. Such evidence provides strong support for the current dosing guidelines of sorafenib in HCC. Thus, our study highlights a need for caution when investigating lower than recommended initial doses—there is the potential that high initial doses/plasma concentrations ultimately drive long term benefits. In addition, this study supports future investigations of dose escalation strategies in patients who have not experienced AEs, as a mechanism to improve survival in patient who have not required a dose adjustment.

A finding that sorafenib dose adjustments due to AEs are not associated with worse survival outcomes is not surprising. Similar results have been shown for other targeted cancer medicines including vemurafenib, afatinib and ado-trastuzumab emtansine [17–19]. In part, this is due to AEs potentially reflecting a subgroup of patients with high plasma concentrations or patients more pharmacodynamically sensitive to the medicine—particularly where AE reflects an 'on-target' toxicity. Supporting the findings of this study, prior research has demonstrated a concentration-effect relationship for sorafenib and that the early occurrence of hand-foot syndrome and diarrhoea with sorafenib may be associated with improved survival outcomes [20–22]. A similar association between the occurrence of hand-foot syndrome in the first 28 days of sorafenib therapy with favourable OS was observed in this study on supplementary analysis.

In this study, it was identified that older age, Asian race, lower weight, history of hepatitis C infection, and absence of liver metastases were associated with increased dose adjustments of sorafenib due to AEs. Such evidence provides support for subgroups of patients who require increased monitoring to minimise the negative quality

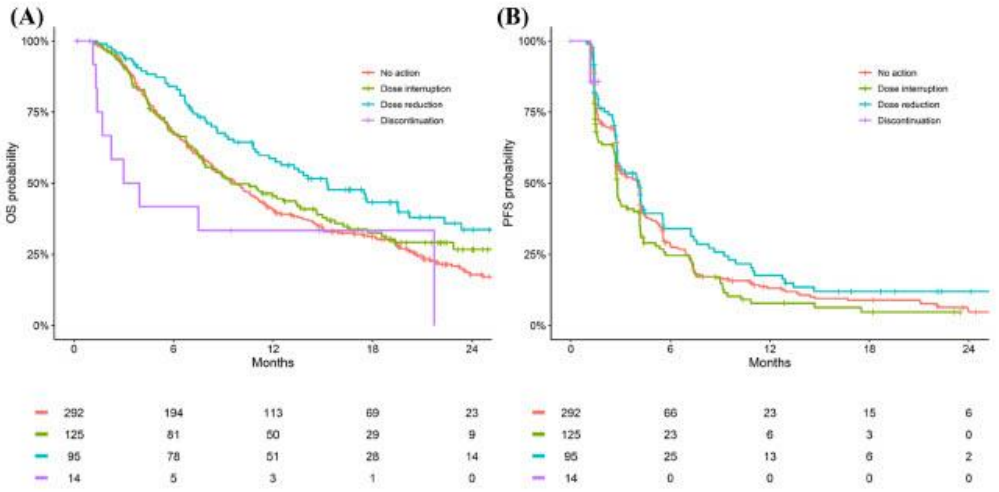

Fig. 2 Kaplan–Meier estimates of OS (**a**) and PFS (**b**) by AE induced dose adjustment category within the first 28 days of sorafenib therapy

of life impacts of AEs which ultimately require dose adjustments.

This study used large high-quality data, consistent with contemporary practice. A landmark approach was utilised to avoid potential time biases. Furthermore, the landmark time of 28 days is an early time to provide functional information for clinical decisions, while capturing a significant of portion of required dose adjustments. Another significant strength of the study was that the association between dose reductions and favourable OS was consistent with supplementary analysis of sorafenib dose intensity and findings across patient subgroups (Supplementary Fig. 1). Variability in associations of sorafenib dose adjustment with OS/PFS were identified, this may be due to PFS being an imperfect surrogate affected by variability in timing of assessments, investigators and measurement biases [23, 24]. Further OS associations may be confounded by subsequent therapies or crossover [23, 24]. Nonetheless, dose adjustment of sorafenib due to AEs did not worsen PFS or OS. Thus, both endpoints are in concordance with supporting current dosing guidelines.

In conclusion, dose adjustment of sorafenib due to AEs did not compromise the survival outcomes of advanced HCC patients, with dose reduction associated with improved OS. Furthermore, older age, Asian race, lower weight, history of hepatitis C infection, and absence of liver metastases were associated with an increased risk of experiencing AEs requiring a sorafenib dose adjustment. Such evidence provides support for the current dosing guidelines of sorafenib in advanced HCC, and an indication of subgroups who require increased monitoring to minimise the potential quality of life impacts of AEs.

Acknowledgements This publication uses information obtained from https://www.projectdatasphere.org, which is maintained by Project Data Sphere, LLC. Neither Project Data Sphere, LLC nor the owners of any information from the web site have contributed to, approved or are in any way responsible for the contents of this publication.

Author contributions All authors contributed to study design, interpretation, and preparation the manuscript.

Funding Ashley Hopkins is an early career researcher funded by a Fellowship from the National Breast Cancer Foundation, Australia. Warit Ruanglertboon was supported by the Royal Thai Government Scholarship, Thailand. Andrew Rowland (mid-career) and Michael Sorich (principal) are funded by a Beat Cancer Fellowships from Cancer Council of South Australia, Australia. Research undertaken with the financial support of Cancer Council South Australia's Beat Cancer Project on behalf of its donors and the State Government through the Department of Health (Grant ID: 1159924 and 1127220).

Compliance with ethical standards

Conflict of interest M. J. S. and A. R. report investigator-initiated project grants from Pfizer, outside the scope of the submitted work. A. M. H. and W. R. have no conflicts of interest to disclose.

References

1. World Health Organization: Cancer fact sheets. (2018). https://gco.iarc.fr/today/data/factsheets/cancers/11-Liver-fact-sheet.pdf.

2. Vogel A, Cervantes A, Chau I et al (2018) Hepatocellular carcinoma: ESMO Clinical Practice Guidelines for diagnosis, treatment and follow-up†. Ann Oncol 29(Supplement_4):238–255
3. Cheng AL, Kang YK, Chen Z et al (2009) Efficacy and safety of sorafenib in patients in the Asia-Pacific region with advanced hepatocellular carcinoma: a phase III randomised, double-blind, placebo-controlled trial. Lancet Oncol 10(1):25–34
4. Abou-Alfa GK, Schwartz L, Ricci S et al (2006) Phase II study of sorafenib in patients with advanced hepatocellular carcinoma. J Clin Oncol 24(26):4293–4300
5. Trotti A, Colevas AD, Setser A et al (2003) CTCAE v3.0: development of a comprehensive grading system for the adverse effects of cancer treatment. Semin Radiat Oncol 13(3):176–181
6. Marrero JA, Kudo M, Venook AP et al (2016) Observational registry of sorafenib use in clinical practice across Child-Pugh subgroups: the GIDEON study. J Hepatol 65(6):1140–1147
7. Vincenzi B, Santini D, Russo A et al (2010) Early skin toxicity as a predictive factor for tumor control in hepatocellular carcinoma patients treated with sorafenib. Oncologist 15(1):85–92
8. Llovet JM, Ricci S, Mazzaferro V et al (2008) Sorafenib in advanced hepatocellular carcinoma. N Engl J Med 359(4):378–390
9. Otsuka T, Eguchi Y, Kawazoe S et al (2012) Skin toxicities and survival in advanced hepatocellular carcinoma patients treated with sorafenib. Hepatol Res 42(9):879–886
10. Shomura M, Kagawa T, Shiraishi K et al (2014) Skin toxicity predicts efficacy to sorafenib in patients with advanced hepatocellular carcinoma. World J Hepatol 6(9):670–676
11. Cheng AL, Kang YK, Lin DY et al (2013) Sunitinib versus sorafenib in advanced hepatocellular cancer: results of a randomized phase III trial. J Clin Oncol 31(32):4067–4075
12. Therasse P, Arbuck SG, Eisenhauer EA et al (2000) New guidelines to evaluate the response to treatment in solid tumors. European Organization for Research and Treatment of Cancer, National Cancer Institute of the United States, National Cancer Institute of Canada. J Natl Cancer Inst 92(3):205–216
13. Kawashima A, Takayama H, Arai Y et al (2011) One-month relative dose intensity of not less than 50% predicts favourable progression-free survival in sorafenib therapy for advanced renal cell carcinoma in Japanese patients. Eur J Cancer 47(10):1521–1526
14. Wildiers H, Reiser M (2011) Relative dose intensity of chemotherapy and its impact on outcomes in patients with early breast cancer or aggressive lymphoma. Crit Rev Oncol Hematol 77(3):221–240
15. Reiss KA, Yu S, Mamtani R et al (2017) Starting dose of sorafenib for the treatment of hepatocellular carcinoma: a retrospective, multi-institutional study. J Clin Oncol 35(31):3575–3581
16. Gore ME, Jones RJ, Ravaud A et al (2017) Sorafenib dose escalation in treatment-naive patients with metastatic renal cell carcinoma: a non-randomised, open-label, Phase 2b study. BJU Int 119(6):846–853
17. Hopkins AM, Van Dyk M, Rowland A et al (2019) Effect of early adverse events on response and survival outcomes of advanced melanoma patients treated with vemurafenib or vemurafenib plus cobimetinib: a pooled analysis of clinical trial data. Pigment Cell Melanoma Res 32(4):576–583
18. Tang E, Rowland A, McKinnon RA et al (2019) Effect of early adverse events resulting in ado-trastuzumab emtansine dose adjustments on survival outcomes of HER2+ advanced breast cancer patients. Breast Cancer Res Treat 178(2):473–477
19. Halmos B, Tan E-H, Soo RA et al (2019) Impact of afatinib dose modification on safety and effectiveness in patients with EGFR mutation-positive advanced NSCLC: results from a global real-world study (RealGiDo). Lung Cancer 127:103–111
20. Coriat R, Nicco C, Chereau C et al (2012) Sorafenib-induced hepatocellular carcinoma cell death depends on reactive oxygen species production in vitro and in vivo. Mol Cancer Ther 11(10):2284–2293
21. Ogawa C, Morita M, Omura A et al (2017) Hand-foot syndrome and post-progression treatment are the good predictors of better survival in advanced hepatocellular carcinoma treated with sorafenib: a multicenter study. Oncology 93(suppl 1):113–119
22. Koschny R, Gotthardt D, Koehler C et al (2013) Diarrhea is a positive outcome predictor for sorafenib treatment of advanced hepatocellular carcinoma. Oncology 84(1):6–13
23. Hotte SJ, Bjarnason GA, Heng DYC et al (2011) Progression-free survival as a clinical trial endpoint in advanced renal cell carcinoma. Curr Oncol (Toronto, Ont.) 18(Suppl 2):S11–S19
24. Pazdur R (2008) Endpoints for assessing drug activity in clinical trials. Oncologist 13(Suppl 2):19–21

Journal of Cancer Research and Clinical Oncology
https://doi.org/10.1007/s00432-020-03261-3

ORIGINAL ARTICLE – CLINICAL ONCOLOGY

The effect of proton pump inhibitors on survival outcomes in advanced hepatocellular carcinoma treated with sorafenib

Warit Ruanglertboon[1] · Michael J. Sorich[1] · Jessica M. Logan[2] · Andrew Rowland[1] · Ashley M. Hopkins[1]

Received: 8 May 2020 / Accepted: 14 May 2020

Abstract

Purpose Sorafenib is an oral tyrosine kinase inhibitor (TKI) and first-line treatment option for advanced hepatocellular carcinoma (HCC). Preliminary evidence indicates proton pump inhibitors (PPI) may affect the absorption of TKIs through decreased gut dissolution. This study aims to evaluate the impact of PPI use on the survival outcomes of advanced HCC patients treated with sorafenib.

Methods The study was a secondary analysis of individual-participant data from the phase III clinical trial NCT00699374. Cox proportional hazard analysis was used to evaluate the association between baseline PPI use and survival outcomes. Overall survival (OS) was the primary outcome with progression-free survival (PFS) secondary.

Results In a cohort of 542 advanced HCC patients initiating sorafenib treatment, 122 were concomitantly using a PPI at baseline. No significant associations between baseline PPI use and OS were identified on univariable (HR [95% CI]; 1.01 [0.80–1.28], $P=0.93$) and adjusted (1.10 [0.82–1.41], $P=0.62$) analysis. Furthermore, no significant associations between baseline PPI use and PFS were identified on univariable (0.96 [0.76–1.21], $P=0.73$) and adjusted (1.11 [0.86–1.44], $P=0.41$) analysis.

Conclusion In a large high-quality dataset, PPI use was not observed to compromise the survival outcomes of advanced HCC patients initiated on sorafenib.

Keywords Sorafenib · Proton pump inhibitors · Prediction · Survival outcomes

Introduction

Sorafenib is an oral tyrosine kinase inhibitor (TKIs) and the current mainstay first-line treatment for advanced hepatocellular carcinoma (HCC) (Likhitsup et al. 2019). Sorafenib acts as a potent inhibitor of vascular endothelial growth factor (VEGFR) subtype 1, 2 and 3, platelet-derived growth factor-beta (PDGFRβ) and fibroblast growth factor receptor 1 (FGFR1) (Wilhelm et al. 2006, 2008).

Recently, clinical studies reported a high degree of inter-individual variability in the pharmacokinetic profile of sorafenib (Nexavar: European Public Assessment Reports (EPAR)-Scientific Discussion. 2007). It is suggested that sorafenib has a limited absorption capacity in the gastrointestinal (GI) tract due to its low solubility profile. In addition, sorafenib's oral bioavailability may be limited by factors that increase intragastric pH, which resultantly decrease the solubility and potentially lower the fraction of sorafenib absorbed from the gastrointestinal tract (f_a) (Sharma et al. 2019).

In clinical practice, cancer patients often take both cancer and non-cancer medicines. Medicines for chronic diseases such as metabolic syndromes and acid-lowering agents being among the most reportedly used non-cancer medicines in cancer patients (LeBlanc et al. 2015; Murphy et al. 2018). A current hypothesis is that concurrent proton pump inhibitor (PPI) administration may reduce the bioavailability of oral TKIs, particularly those with dissolution profiles sensitive to pH changes (Lind et al. 2010; Liu et al. 2016; Nexavar:

Electronic supplementary material The online version of this article (https://doi.org/10.1007/s00432-020-03261-3) contains supplementary material, which is available to authorized users.

✉ Warit Ruanglertboon
warit.ruanglertboon@flinders.edu.au

[1] Department of Clinical Pharmacology, College of Medicine and Public Health, Flinders University, Adelaide, Australia

[2] Mechanisms in Cell Biology and Disease Research Group, Clinical and Health Sciences, Cancer Research Institute, University of South Australia, Adelaide, Australia

Published online: 24 May 2020

European Public Assessment Reports (EPAR)-Scientific Discussion 2007). Recent research indicated that PPIs may impact the survival of cancer patients treated with gefitinib (Fang et al. 2019) and erlotinib (Ohgami et al. 2018). Furthermore, Sharma et al. (Sharma et al. 2019) indicated that PPIs may impact TKIs as a class, albeit the data were dominated by lung cancer patients treated with erlotinib. However, the efficacy and dissolution profile of all TKIs are not the same and to date there has been no large high-quality analysis to investigate the impact of PPI use on the survival outcomes of advanced HCC patients treated with sorafenib.

Thus, using individual-participant data from the phase III clinical trial NCT00699374, this study aimed to evaluate the impact of PPI use on the survival outcomes of advanced HCC patients initiating sorafenib treatment.

Methods

Patient population

The study was a secondary analysis of the phase III clinical trial NCT00699374 (sorafenib arm only) (Cheng et al. 2013). Participants were assigned to receive sorafenib at 400 mg twice daily on 4-week cycles for the treatment of locally advanced or metastatic HCC.

Individual-participant data (IPD) were accessed in this study via www.projectdatasphere.org. Secondary analysis of anonymized IPD was deemed negligible risk research by the Southern Adelaide Local Health Network, Office for Research and Ethics and was exempt from review.

Predictors and outcomes

The primary assessed outcome was overall survival (OS), with progression-free survival (PFS) assessed as the secondary outcome. PFS was evaluated according to Response Evaluation Criteria in Solid Tumours (RECIST) version 1.0 (Therasse et al. 2000). PPI use at the time of sorafenib initiation (baseline) was assessed as the primary covariate. Baseline PPI use was the focus, as PPIs are commonly used for extended time periods.

Available pre-treatment characteristic data included age, sex, weight, race, Eastern Cooperative Oncology Group performance status (ECOG PS), number of metastatic sites, alpha-fetoprotein (AFP), neutrophil-to-lymphocyte ratio, Barcelona clinic liver cancer stage (BCLC), sum of longest diameter of target lesions, history of hepatitis B or C infection, history of alcohol abuse, liver cirrhosis, oesophageal varices, portal vein thrombosis, non-alcoholic steatohepatitis, serum haemoglobin and gamma glutamyl transferase concentrations.

Statistical analysis

Cox proportional hazard analysis was used to evaluate the association between baseline PPI use and OS/PFS. Associations were reported as hazard ratios (HR) with 95% confidence intervals (95% CI) and probability (P) values. Univariable and analyses adjusted for known prognostic factors were conducted. Complete case analyses were conducted. Kaplan–Meier analysis was used to estimate and plot survival outcomes. Statistical analyses were performed using R version 3.5.

Results

Patient population

There were 542 patients with advanced HCC who received sorafenib in the clinical trial, 122 patients were concomitantly using a PPI at baseline. A summary of patient characteristics is presented in Supplementary Table 1. Median follow-up in the population was 22 [95% CI 21–24] months.

Of the 122 using a PPI at baseline, 34 were using esomeprazole, 19 lansoprazole, 22 omeprazole, 28 pantoprazole and 19 rabeprazole. The indications for PPI use were ulcers ($n=37$), gastritis ($n=36$), gastroesophageal reflux disease ($n=20$) and others ($n=29$). Of the 122 using a PPI at baseline, 81 used PPI therapy for the entire period of receiving sorafenib treatment. Of the 41 patients who had PPI free periods while on sorafenib, the median [inter-quartile range] number of days on PPI therapy within the first month was 30 [19–30]—an indication that even in these patients PPI use was frequent.

The effect of concomitant use of sorafenib and PPI on survival outcomes

On univariable analysis, there were no associations between baseline PPI use and OS (HR [95% CI] 1.01 [0.80–1.28], $P=0.93$) nor PFS (0.96 [0.76–1.21], $P=0.73$) in advanced HCC initiated on sorafenib (Table 1, Fig. 1). Further on adjusted analysis, no significant association with OS (1.10 [0.82–1.41], $P=0.62$) nor PFS (1.11 [0.86–1.44], $P=0.41$) was identified (Table 1).

Discussion

Orally administered cancer medicines can be affected pharmacokinetically or pharmacodynamically by other co-administered drugs. For example, rifampicin which

Table 1 Summary of association between baseline PPI use status and survival outcomes

PPI	Univariable			*n*	Adjusted[a]	*P*
	n	HR (95% CI)	*P*		HR (95% CI)	
OS						
No	420	1.00	0.93	377	1.00	0.62
Yes	122	1.01 (0.80–1.28)		105	1.10 (0.82–1.41)	
PFS						
No	420	1.00	0.73	377	1.00	0.41
Yes	122	0.96 (0.76–1.21)		105	1.11 (0.86–1.44)	

CI confidence interval, *HR* hazard ratio, *n* number of subjects

[a]Analysis adjusted for age, sex, weight, race, baseline ECOG, number of metastatic site, baseline AFP, neutrophil to lymphocyte ratio, baseline BCLC, sum of longest diameter of target lesion at baseline, history of hepatitis B or C infection, history of alcohol abuse, liver cirrhosis, oesophageal varices, portal vein thrombosis, non-alcoholic steatohepatitis, baseline haemoglobin, baseline gamma glutamyl transferase

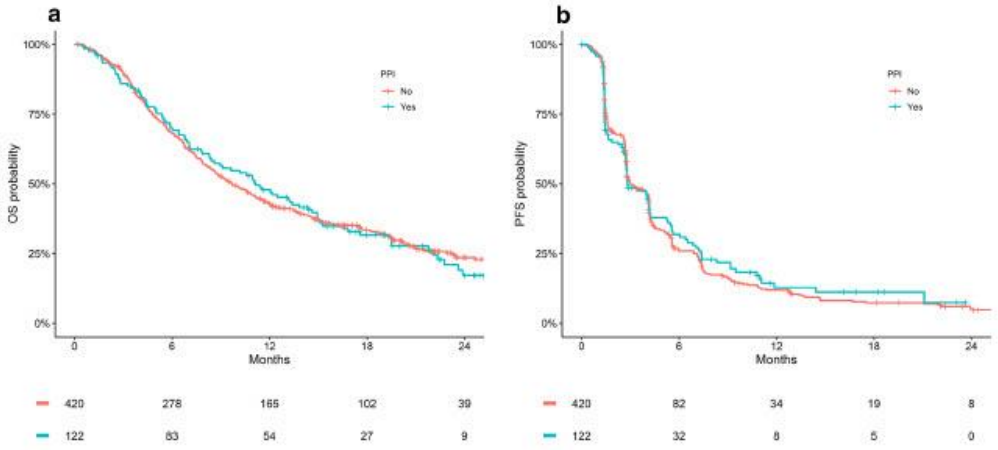

Fig. 1 Kaplan–Meier estimates of OS (a) and PFS (b) by PPI status

is a potent CYP3A4 inducer, reduces the area under the curve (AUC) and C_{max} of sunitinib exposure by 23 and 46%, respectively (European Medicines Agency. Sunitinib (SUTENT). Summary of Product Characteristics 2015; Ohgami et al. 2018). Similarly, it is mechanistically rationalised that PPIs irreversibly bind to the H^+/K^+-ATPase pumps altering intragastric pH from being highly acidic (pH 1–4) to less acidic (pH > 6), thus potentially reducing gastrointestinal dissolution and absorption of oral TKIs (Ohgami et al. 2018). It is further hypothesised that this effect may be unfavourable to the survival outcomes achieved with TKIs, which require an acidic environment for intestinal absorption. However, the potential impact of PPIs on outcomes of advanced HCC patients treated with sorafenib has been minimally explored. Here, we highlighted that concomitant PPI use with sorafenib in advanced HCC patients was not associated with altered survival outcomes.

To date, there has been preliminary research on the effect of PPIs on the therapeutic outcomes associated with TKIs. For example, Sharma et al. (2019) conducted a pooled analysis of Surveillance, Epidemiology, and End Results (SEER)-Medicare database indicating that concomitant PPI use with a TKI was associated with an increased risk of death. However, the dissolution and pharmacodynamic profiles of all TKIs are not the same. Thus, while Sharma et al. (2019) indicated PPI use was associated with negative outcomes for TKIs and specifically erlotinib (the majority of the population), no effects on imatinib or sunitinib were identified and the associations for sorafenib were not presented. Thus, to the best of our knowledge, the present study is the largest analysis of the association between concomitant PPI use and

survival outcomes of advanced HCC patients treated with sorafenib–of which no association with altered survival outcomes was identified. These results are similar to the Lalani et al. (2017) study which found no association between PPI use and survival outcomes in a pooled cohort of renal cell carcinoma (RCC) patients, treated with sorafenib, sunitinib or axitinib.

While a post hoc analysis, the data used in this study were large high-quality data collected within clinical trial and the dosing strategy assessed is consistent with contemporary practice. Another strength of this study is the result of no association between concomitant PPI use and sorafenib outcomes was demonstrated for both OS and PFS (on univariable and adjusted analysis). It is acknowledged that Child–Pugh class A, ECOG PS of 0 or 1 and adequate organ function were inclusion criteria, and the presence of clinically relevant ascites was an exclusion criteria of NCT00699374 (Cheng et al. 2013). A notable limitation was an inability to assess the type, dose or compliance to the documented PPI use. Nonetheless, at least 80% of those using a PPI at baseline did so for a condition requiring long-term treatment. Future research will aim to confirm if the results are consistent between specific PPIs and if the non-association extends to other acid-lowering agents such as H2 receptor antagonists. A limitation of this study is the restricted range of settings evaluated. Future research should include the evaluation of sorafenib used for advanced RCC and its use in other lines of therapy.

Conclusions

The concomitant use of a PPI with sorafenib in advanced HCC patients was not associated with altered survival outcomes. Our analysis further shows the importance of assessing the impact of PPIs on TKIs on a per medicine basis as the dissolution and pharmacokinetic profile of all TKIs are not the same.

Author contributions WR contributed to conception, design, analysis, interpretation, and manuscript drafting. MJS contributed to conception, design, data acquisition and analysis, interpretation, supervision and manuscript drafting. JML contributed to design, interpretation, and manuscript drafting. AR contributed to conception, design, interpretation, supervision and manuscript drafting. AMH contributed to conception, design, data acquisition and analysis, interpretation, supervision and manuscript drafting. All authors have read and approved the submission of this manuscript.

Funding Ashley Hopkins is an early career researcher funded by a Fellowship from the National Breast Cancer Foundation, Australia (PF-17-007). Warit Ruanglertboon was supported by the Royal Thai Government Scholarship, Thailand. Andrew Rowland (mid-career) and Michael Sorich (principal) are funded by a Beat Cancer Fellowships from Cancer Council of South Australia, Australia. Research undertaken with the financial support of Cancer Council South Australia's Beat Cancer Project on behalf of its donors and the State Government through the Department of Health (Grant ID: 1159924 and 1127220). The funder had no role in the design and conduct of the study; collection, management, analysis, and interpretation of the data; preparation, review, or approval of the manuscript; and decision to submit the manuscript for publication.

Availability of data and materials Individual participant data (IPD) were accessed in this study via www.projectdatasphere.org.

Compliance with ethical standards

Conflict of interest Dr. Sorich and Dr. Rowland report grants from Pfizer, outside the submitted work. No potential conflicts of interest were reported by the other authors.

Ethics approval The study was a secondary analysis of individual participant data (IPD). IPD was accessed in this study via www.projectdatasphere.org, according to Pfizer's policy and process for data sharing. Secondary analysis of anonymized IPD was deemed negligible risk research by the Southern Adelaide Local Health Network, Office for Research and Ethics and was exempted from review. The NCT00699374 trial conducted by Pfizer was performed in accordance with Good Clinical Practice guidelines and the provisions of the Declaration of Helsinki. Protocol approval was obtained from an independent ethics committee at each study site. All patients provided written informed consent (Cheng et al. 2013).

Consent for publication All patients provided written informed consent.

Code availability Data and statistical analyses were performed using R version 3.5.

References

Cheng A-L, Kang Y-K, Lin D-Y et al (2013) Sunitinib versus sorafenib in advanced hepatocellular cancer: results of a randomized phase III trial. J Clin Oncol 31:4067–4075. https://doi.org/10.1200/jco.2012.45.8372

European Medicines Agency (2015) Sunitinib (SUTENT). Summary of product characteristics

Fang YH, Yang YH, Hsieh MJ et al (2019) Concurrent proton-pump inhibitors increase risk of death for lung cancer patients receiving 1st-line gefitinib treatment—a nationwide population-based study. Cancer Manag Res 11:8539–8546. https://doi.org/10.2147/cmar.S222278

Lalani AA, McKay RR, Lin X et al (2017) Proton pump inhibitors and survival outcomes in patients with metastatic renal cell carcinoma. Clin Genitourin Cancer 15:724–732. https://doi.org/10.1016/j.clgc.2017.05.019

LeBlanc TW, McNeil MJ, Kamal AH et al (2015) Polypharmacy in patients with advanced cancer and the role of medication discontinuation. Lancet Oncol 16:e333–e341. https://doi.org/10.1016/S1470-2045(15)00080-7

Likhitsup A, Razumilava N, Parikh ND (2019) Treatment for advanced hepatocellular carcinoma: current standard and the future. Clin Liver Dis 13:13–19. https://doi.org/10.1002/cld.782

Lind JS, Dingemans AM, Groen HJ et al (2010) A multicenter phase II study of erlotinib and sorafenib in chemotherapy-naive patients

with advanced non-small cell lung cancer. Clin Cancer Res 16:3078–3087. https://doi.org/10.1158/1078-0432.Ccr-09-3033

Liu C, Chen Z, Chen Y et al (2016) Improving oral bioavailability of sorafenib by optimizing the "spring" and "parachute" based on molecular interaction mechanisms. Mol Pharm 13:599–608. https://doi.org/10.1021/acs.molpharmaceut.5b00837

Murphy CC, Fullington HM, Alvarez CA et al (2018) Polypharmacy and patterns of prescription medication use among cancer survivors. Cancer 124:2850–2857. https://doi.org/10.1002/cncr.31389

Nexavar: European Public Assessment Reports (EPAR)-Scientific Discussion. (2007) https://www.ema.europa.eu/docs/en_GB/document_library/EPAR-Scientific_Discussion/human/000690/WC500027707.pdf. Accessed 3 Mar 2007

Ohgami M, Kaburagi T, Kurosawa A et al (2018) Effects of proton pump inhibitor coadministration on the plasma concentration of erlotinib in patients with non-small cell lung cancer. Ther Drug Monit 40:699–704. https://doi.org/10.1097/ftd.0000000000000552

Sharma M, Holmes HM, Mehta HB et al (2019) The concomitant use of tyrosine kinase inhibitors and proton pump inhibitors: prevalence, predictors, and impact on survival and discontinuation of therapy in older adults with cancer. Cancer 125:1155–1162. https://doi.org/10.1002/cncr.31917

Therasse P, Arbuck SG, Eisenhauer EA et al (2000) New guidelines to evaluate the response to treatment in solid tumors. J Natl Cancer Inst 92:205–216. https://doi.org/10.1093/jnci/92.3.205

Wilhelm S, Carter C, Lynch M et al (2006) Discovery and development of sorafenib: a multikinase inhibitor for treating cancer. Nat Rev Drug Discov 5:835–844. https://doi.org/10.1038/nrd2130

Wilhelm SM, Adnane L, Newell P et al (2008) Preclinical overview of sorafenib, a multikinase inhibitor that targets both Raf and VEGF and PDGF receptor tyrosine kinase signalling. Mol Cancer Ther 7:3129–3140. https://doi.org/10.1158/1535-7163.Mct-08-0013

pharmaceuticals

MDPI

Article

Mechanistic Modelling Identifies and Addresses the Risks of Empiric Concentration-Guided Sorafenib Dosing

Warit Ruanglertboon *, Michael J. Sorich, Ashley M. Hopkins and Andrew Rowland

College of Medicine and Public Health, Flinders University, Bedford Park, SA 5042, Australia; michael.sorich@flinders.edu.au (M.J.S.); ashley.hopkins@flinders.edu.au (A.M.H.); andrew.rowland@flinders.edu.au (A.R.)

* Correspondence: warit.ruanglertboon@flinders.edu.au

Abstract: The primary objective of this study is to evaluate the capacity of concentration-guided sorafenib dosing protocols to increase the proportion of patients that achieve a sorafenib maximal concentration (C_{max}) within the range 4.78 to 5.78 µg/mL. A full physiologically based pharmacokinetic model was built and validated using Simcyp® (version 19.1). The model was used to simulate sorafenib exposure in 1000 Sim-Cancer subjects over 14 days. The capacity of concentration-guided sorafenib dose adjustment, with/without model-informed dose selection (MIDS), to achieve a sorafenib C_{max} within the range 4.78 to 5.78 µg/mL was evaluated in 500 Sim-Cancer subjects. A multivariable linear regression model incorporating hepatic cytochrome P450 (CYP) 3A4 abundance, albumin concentration, body mass index, body surface area, sex and weight provided robust prediction of steady-state sorafenib C_{max} ($R^2 = 0.883$; $p < 0.001$). These covariates identified subjects at risk of failing to achieve a sorafenib $C_{max} \geq 4.78$ µg/mL with 95.0% specificity and 95.2% sensitivity. Concentration-guided sorafenib dosing with MIDS achieved a sorafenib C_{max} within the range 4.78 to 5.78 µg/mL for 38 of 52 patients who failed to achieve a $C_{max} \geq 4.78$ µg/mL with standard dosing. In a simulation setting, concentration-guided dosing with MIDS was the quickest and most effective approach to achieve a sorafenib C_{max} within a designated range.

Keywords: concentration-guided dosing; model informed dosing; physiologically based pharmacokinetics; sorafenib

Citation: Ruanglertboon, W.; Sorich, M.J.; Hopkins, A.M.; Rowland, A. Mechanistic Modelling Identifies and Addresses the Risks of Empiric Concentration-Guided Sorafenib Dosing. *Pharmaceuticals* **2021**, *14*, 389. https://doi.org/10.3390/ph14050389

Academic Editors: Mary J. Meegan and Niamh M O'Boyle

Received: 11 March 2021
Accepted: 19 April 2021
Published: 21 April 2021

1. Introduction

Sorafenib is an orally administered small molecule kinase inhibitor (KI) used in the treatment of advanced hepatocellular (HCC) and renal cell (RCC) carcinomas. Sorafenib is a potent inhibitor of multiple kinase receptors including the vascular endothelial growth factor receptor (VEGFR), endothelial growth factor (subtype 1, 2 and 3), platelet-derived growth factor-beta (PDGFRβ) and fibroblast growth factor receptor 1 (FGFR1). Variability in sorafenib exposure between individuals and within an individual over time has been identified as a potential source of heterogeneity in treatment efficacy and tolerability [1,2]. The area under the plasma concentration curve (AUC) and maximal concentration (C_{max}) for sorafenib following has been reported to vary more than 50% with standard 400 mg dosing [3–5]. Variability in gastrointestinal absorption due to limited and pH dependent solubility has been proposed as a major source of variability in exposure [6], however concomitant proton pump inhibitor (PPI) use, which is reported to reduce KI absorption [7], has been demonstrated to have no impact on survival outcomes in HCC [8] and RCC [9,10] patients treated with sorafenib.

A sorafenib $C_{max} \geq 4.78$ µg/mL has been associated with superior overall survival in RCC and HCC patients, albeit with a higher incidence of hypertension, while a sorafenib $C_{max} \geq 5.78$ µg/mL has been associated with an increased incidence of grade II toxicity, the most common of which is hand foot skin reactions [11,12]. While the evidence for these thresholds is derived from a single observational study in 52 individuals, these values

have been cited as target concentrations in multiple reviews addressing individualised sorafenib dosing [13,14]. The dose escalation protocol that has been proposed for sorafenib to increase from 400 mg to 600 mg twice daily [15]. This approach is based on a sub-analysis of a phase II trial demonstrating a clinical benefit in patients who increased from 400 mg to 600 mg sorafenib twice daily following disease progression at the 400 mg dose [16]. Notably the association of this dose escalation with sorafenib plasma concentration has not been evaluated.

The potential benefits of individualised KI dosing have gained interest in recent years [17–19] and a number of strategies are available to both inform initial dose selection and facilitate dose adaption [20]. Therapeutic drug monitoring (TDM) is an established method to facilitate concentration-guided dose adaption but requires significant clinical and analytical resources to quantify the drug of interest and establish a robust evidence base. To date, few cancer medicines have met the level of evidence required to implement TDM in a clinical setting [21–23].

Model-informed initial dose selection (MIDS), often underpinned by a population pharmacokinetic (pop-PK) or physiologically based pharmacokinetic (PBPK) model, has emerged as a strategy to assist initial dose selection either to complement or replace TDM [24–27]. PBPK modelling and simulation is an established tool in drug discovery and development, where it is used to predict factors affecting PK and support the design of clinical trials [28,29]. PBPK is a 'bottom-up' approach whereby the concentration–time profile of a drug is simulated based on physiochemical and in vitro data [30,31]. Novel clinical applications for PBPK have been proposed involving the prediction of clinical drug–drug interactions, identification of physiological covariates impacting drug exposure and informing initial dose selection [25,31–33].

The primary objective of this study is to evaluate the capacity of concentration-guided sorafenib dose adjustment, with and without MIDS, to increase the proportion of patients that achieve a sorafenib C_{max} within a concentration range of 4.78 to 5.78 µg/mL. A full body PBPK model for sorafenib was first developed and validated, then used to identify physiological and molecular covariates associated with between subject variability in sorafenib exposure.

2. Results

2.1. Verification of the Sorafenib PBPK Compound Model

The accuracy of the sorafenib compound model was assessed in nineteen age and sex matched cohorts from single or multiple ascending dose (100 to 800 mg) trials. Mean simulated and observed AUC and C_{max} values and the corresponding simulated/observed ratios are presented in Table S1 along with a summary of the verification trial characteristics (i.e., age range, sex, sample size and dose). The mean (±standard deviation; SD) simulated/observed AUC and C_{max} ratios for the single-dose cohorts (n = 37) were 1.92 (±1.11) and 1.50 (±1.7), respectively. The mean (±SD) simulated/observed AUC and C_{max} ratios for the multiple-dose (typically 14 days) cohorts (n = 14) were 1.50 (±0.72) and 1.17 (±0.63), respectively. Variability in model performance, indicated by large SD for parameter ratios, was driven by heterogeneity in observed parameters between trials. A representative sorafenib concentration–time profile depicting overlayed with the mean concentration–time profile and 90% confidence interval (CI) for the observed data is shown in Figure 1. The accuracy of the sorafenib compound model was considered acceptable on the basis that mean simulated parameters were within two-fold of the respective mean observed parameter and contained within the 90% CI for the observed parameter. Simulated Day 14 and Day 28 sorafenib C_{max} values were divided by 1.17 to account for simulation to observed MFE in multiple dose studies when evaluating the simulated parameters against the observed target C_{max} range. Results of sensitivity analyses performed to evaluate the impact of input parameters with measurement uncertainty (C_{lint} for CYP3A4 and UGT1A9 pathways, fraction unbound, B/P ratio and LogP) on sorafenib kinetic parameters are shown in Figure S1.

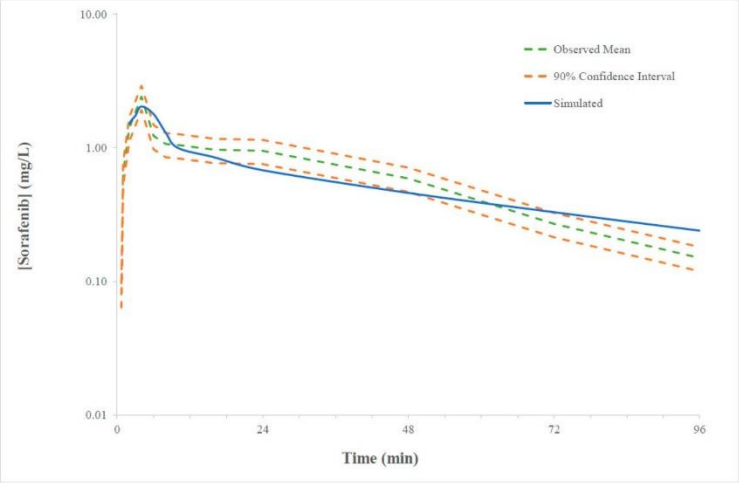

Figure 1. Representative overlay of simulated and observed (range) plasma concentration time curve of sorafenib (0–96 h) following 400 mg twice a day dosing. Solid blue line represented the mean model predicted exposure, dashed green line represented the mean observed exposure and dashed orange represented minimal and maximal 90% confidence intervals for the observed data.

2.2. Sorafenib Exposure in Cancer Patient

The summary of the mean, SD and range of steady-state sorafenib AUC and C_{max} parameters defining exposure in 1000 virtual cancer patients is presented in Table S2. Consistent with the reported clinical trial data [4,5,34], the simulation revealed variability of greater than an order of magnitude in sorafenib exposure; the steady state AUC ranged from 22.7 to 270 mg/L·h (mean 99.2 mg/L·h), while C_{max} ranged from 2.3 to 23.2 µg/mL (mean 8.9 µg/mL).

2.3. Physiological and Molecular Characteristics Driving Variability in Sorafenib Exposure

Univariate logistic regression analysis evaluated correlations between physiological and molecular characteristics and sorafenib steady state C_{max} threshold at > 4.78 mg/L (Table S3) in a cohort of 1000 Sim-Cancer subjects. Statistical analysis of multivariable linear regression with stepwise inclusion of parameters revealed the primary covariates driving variability in sorafenib AUC were hepatic CYP3A4 abundance, albumin concentration, body mass index (BMI), body surface area (BSA), sex and weight (Figure 2).

A summary of the performance characteristics for the multivariable linear regression model is shown in Table 1. The covariate most strongly associated with variability in sorafenib AUC was hepatic CYP3A4 abundance, inclusion of albumin concentration and BMI resulted in substantial improvement in multivariable model fit. Stepwise inclusion of additional the covariates BSA, sex and weight resulted in minor improvements in model performance (R^2 change $\leq$ 0.010). No other covariate met the stepwise inclusion criteria (probability of F to enter $\leq$ 0.05). These parameters formed the basis of the MIDS. The AUC of the ROC for the MIDS predicted steady state AUC was 0.991 (Figure 3). Sixty-three subjects (6.3%) from the Sim-Cancer cohort failed to achieve a Day 14 C_{max} > 4.78 µg/mL. MIDS predicted individuals that failed to achieve a therapeutic sorafenib C_{max} with 95.2% sensitivity (60/63 sub-therapeutic individuals) and 95.0% specificity (809/937 therapeutic individuals) (Table 2, Figure 3). Shown in Figure S2, differences in albumin concentration between participants were associated with changes in f_u.

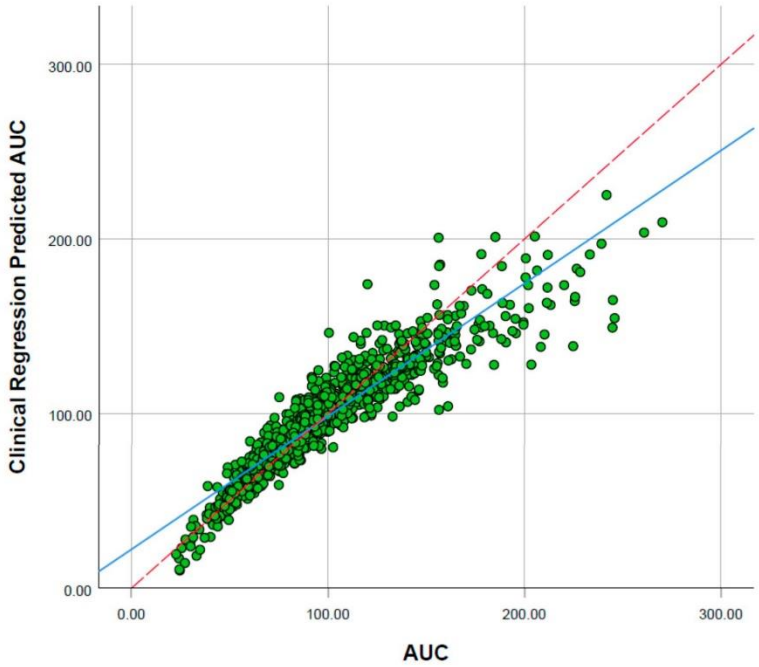

Figure 2. Correlation of model predicted steady-state sorafenib concentration predicted sorafenib AUC.

Table 1. Multivariable linear regression model performance characteristics.

Model	R^2	Std. Error of the Estimate	R^2 Change	AUC ROC	AUC ROC Change
a	0.631	0.24141	0.631	0.953	0.953
b	0.781	0.18614	0.150	0.981	0.028
c	0.868	0.14458	0.087	0.990	0.009
d	0.873	0.14156	0.006	0.991	0.001
e	0.883	0.13619	0.010	0.991	-
f	0.883	0.13595	0.001	0.991	-

Model predictors (a) hepatic CYP3A4 abundance; (b) hepatic CYP3A4 abundance, albumin concentration; (c) hepatic CYP3A4 abundance, albumin concentration, BMI; (d) hepatic CYP3A4 abundance, albumin concentration, BMI, body surface area; (e) hepatic CYP3A4 abundance, albumin concentration, BMI, body surface area, sex; (f) hepatic CYP3A4 abundance, albumin concentration, BMI, body surface area, sex, weight; (g) hepatic CYP3A4 abundance, albumin concentration, BMI, body surface area, sex and weight.

Table 2. Classification matrixes describing the capability of linear regression models to identify individuals with a sub-therapeutic sorafenib steady state $C_{max.}$

		Predicted Therapeutic C_{max}		Percentage Correct
		Sub-Therapeutic	Therapeutic	
Observed Therapeutic C_{max}	Sub-therapeutic	60 (true negative)	3 (false negative)	95.2
	Therapeutic	47 (false positive)	890 (true positive)	95.0

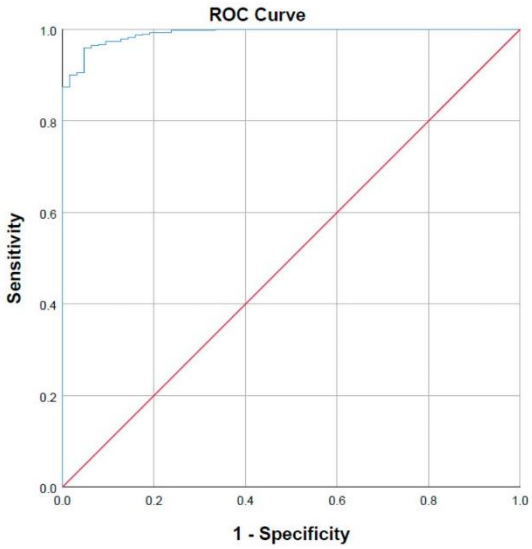

Figure 3. Receiver operating characteristic (ROC) curve demonstrating the prediction performance of a predicted steady state sorafenib AUC.

2.4. Impact of Dose Individualisation

The proportion of participants with a simulated sorafenib C_{max} below, within and above the target 4.78 to 5.78 µg/mL range at Day 14 and Day 28 based on following flat 400 mg dosing, concentration-guided dosing and concentration-guided dosing with MIDS is reported in Table 3. Concentration-guided sorafenib dosing without MIDS identified that 12.4% of subject (62/500) failed to achieve a Day 14 $C_{max} \geq 4.78$ µg/mL with 400 mg twice daily dosing. Increasing the sorafenib dose to 600 mg twice daily in individuals who failed to achieve a Day 14 sorafenib $C_{max} > 4.78$ µg/mL, while retaining the 400 mg twice daily dose for those who did achieve a Day 14 sorafenib $C_{max} \geq 4.78$ µg/mL resulted in 99% of subjects (495/500) achieving a Day 28 $C_{max} \geq 4.78$ µg/mL. Concentration-guided sorafenib dosing without MIDS resulted in an additional 43 subjects achieving a Day 28 $C_{max} > 5.78$ µg/mL compared to flat 400 mg dosing.

Table 3. Number of participant below, within and above target concentration range with different sorafenib dosing protocols.

Dosing Protocol	Day 14			Day 28		
	<4.78 µg/mL	4.78 to 5.78 µg/mL	>5.78 µg/mL	<4.78 µg/mL	4.78 to 5.78 µg/mL	>5.78 µg/mL
Flat dosing	62	116	322	62	116	322
Concentration-guided dosing	62	116	322	5	130	365
Concentration-guided dosing with MIDS	34	135	331	5	164	336

On the basis of MIDS, 52 subjects were allocated to receive an initial sorafenib dose of 500 mg and 448 subjects were allocated to receive an initial sorafenib dose of 400 mg. Concentration-guided sorafenib dosing with MIDS resulted in 6.8% (34/500) subjects failing to achieve a Day 14 $C_{max} \geq 4.78$ µg/mL. Increasing the sorafenib dose to 600 mg twice daily in individuals who failed to achieve a Day 14 sorafenib $C_{max} \geq 4.78$ µg/mL, while retaining the MIDS informed twice daily dose for those who did achieve a Day 14

sorafenib $C_{max} \geq 4.78$ µg/mL resulted in 99% (495/500) of subjects achieving a Day 28 $C_{max} \geq 4.78$ µg/mL. Concentration-guided dosing with MIDS resulted in an additional 9 subjects achieving a Day 28 $C_{max} > 5.78$ µg/mL compared to flat 400 mg dosing. Post-hoc analysis demonstrated that three of these subjects would have a $C_{max} < 4.78$ µg/mL with 400 mg dosing, while the remaining six subjects could have retained a Day 28 $C_{max} \geq 4.78$ µg/mL while avoiding a Day 28 $C_{max} > 5.78$ µg/mL with a dose reduction from 500 mg to 400 mg following assessment of C_{max} on Day 14, however dose reduction was not incorporated into the simulation protocol.

3. Discussion

The present study demonstrated that concentration-guided dosing with MIDS facilitates therapeutic sorafenib exposure in 99% of subjects within 28 days while minimising the number of additional subjects at risk of supra-therapeutic dosing compared to concentration-guided dosing alone. Multivariable linear regression modelling demonstrated that variability in simulated sorafenib AUC and C_{max} is associated with hepatic CYP3A4 abundance, albumin concentration, BMI, sex, age and weight. Logistic regression modelling of these covariates predicted individuals likely to fail to achieve sorafenib $C_{max} \geq 4.78$ mg/L with high sensitivity and specificity (95.2% and 95%, respectively). Incorporation of these parameters into an MIDS algorithm that allocated subjects to a 400 mg or 500 mg initial sorafenib dose resulted in a 50% reduction in the number of subjects that failed to achieve a Day 14 $C_{max} \geq 4.78$ mg/L. When used in conjunction with concentration-guided dosing at Day 14, this protocol resulted in 99% of subjects attaining a Day 28 $C_{max} \geq 4.78$ mg/L.

The current study also highlights the potential danger of empiric concentration-guided dosing in terms of placing patients at an increased risk of toxicity. In the absence of MIDS, 69% of subjects (43/62) that underwent a dose escalation from 400 to 600 mg on Day 14 experienced a C_{max} on Day 28 that is associated with increased risk of grade II toxicity. Compared to concentration-guided dosing alone, the concentration-guided dosing with MIDS protocol reduced the number of additional subjects at increased risk of grade II toxicity on Day 28 ($C_{max} \geq 5.78$ mg/L) from 43 to 9.

PBPK modelling and simulation is an established tool to support drug discovery and development, and is a core element of the regulatory approval process in many jurisdictions [35]. Recent studies have further demonstrated the potential role of PBPK in predicting covariates affecting variability in drug exposure resulting from either patient characteristics or the drugs' physicochemical properties [24,25], giving rise to the intriguing potential for this platform to support model informed precision dosing [26,32]. Since the introduction of imatinib in 2001 there has been a growing evidence base supporting a role for concentration-guided KI dosing, despite this implementation of KI dose individualisation has remained challenging. Many early studies focussed on a potential role for TDM-guided KI dosing, however, sufficient evidence has yet to be generated to support widespread implementation for any KI. This has led to the exploration of novel approaches to facilitate precision KI dosing, which have included model informed precision dosing based on integrated simulation/prediction platforms such as PK-Sim®, GastroPlus™, Phoenix™, and Simcyp® [26,36–38].

The target concentration range and dose escalation protocol used in the current study were based on the best current evidence [11,16]. The main limitation to this study remains the lack of independent verification of the 4.78 to 5.78 µg/mL target C_{max} range. Further, when considering the clinical implementation, it is also important to note that the rate at which sorafenib is absorbed from the GIT varies >five-fold [6]. Variability in the rate of intestinal absorption results in marked variability in the time taken to reach C_{max} for sorafenib (1 to 6 h). As such, in the absence of full PK (AUC) sampling, which is not practical in a clinical setting, concentration-guided sorafenib dosing based on a C_{max} target is unlikely to be robust.

Liver CYP3A4 abundance was identified as the dominant characteristic driving variability in sorafenib AUC and C_{max}. By accounting for this characteristic alone, it was possible to identifying subjects with a sub-therapeutic sorafenib C_{max} with a specificity of 74.6% and a sensitivity of 96.3%. When hepatic CYP3A4 abundance was considered along with readily attained data regarding albumin concentration, BMI, BSA, sex and weight in combination with albumin concentration, these two parameters accounted for >88% of multivariable model performance in terms of R^2, specificity and sensitivity (Table 1). These data suggest that consideration of liver CYP3A4 abundance may provide sufficient power to prospectively identify patients who are likely to require a higher sorafenib dose in order to achieve a therapeutic plasma concentration. Importantly, recent work in this [39] and other [40,41] laboratories has demonstrated that quantification of extracellular vesicle (EV)-derived CYP3A protein, mRNA and ex vivo activity robustly describes variability in CYP3A activity in humans.

This study identified the major physiological and molecular characteristics associated with between subject variability in sorafenib exposure to be hepatic CYP3A4 abundance, albumin concentration, BMI, BSA, sex and weight. Initial dose selection informed by a model accounting for these covariates resulted a quicker and more effective concentration-guided sorafenib dosing.

4. Materials and Methods

4.1. Development and Verification of the Sorafenib PBPK Model Structural Model

Sorafenib absorption was simulated using the advanced dissolution, absorption, and metabolism (ADAM) sub-model which incorporates membrane permeability, intestinal metabolism and transporter-mediated uptake and efflux. The ADAM sub-model was used in conjunction with a full-body PBPK model, containing compartments and drug distribution characteristics for all organs. All simulations were performed using Simcyp® (version 19.1, Certara, UK). The differential equations underpinning the model have been described previously [42].

4.2. Development of the Sorafenib Compound Model

The physicochemical, blood binding, absorption, distribution, elimination parameters utilised to construct the sorafenib compound model are summarised in Table 4. Physicochemical properties were based on published literature and documents [43,44]. Metabolism and elimination parameters were incorporated based on reported intersystem extrapolation factor (ISEF) adjusted in vitro CYP and UDP-glucuronosyltransferase (UGT) data (Figure 4).

Table 4. Model inputs used to build the sorafenib compound model.

Parameter	Value	Source
Physicochemical properties		
Molecular weight	464.82 g/mol	
Log $P_{o:w}$	4.54	[43]
Hydrogen bond donor	3	
Species	Base	[43]
Protein binding		
B/P	0.55	[43]
f_{up}	0.0048	[43]
Absorption (ADAM model)		
f_a	0.99	Predicted
k_a (L/h)	1.75	Predicted
Permeability		
P_{eff}, man (10^{-4} cm/s)	4.01	Predicted
Caco-2 (10^{-6} cm/s)	24.1	
Formulation		
Solid formulation	Immediate release	[43]
In vivo pharmacokinetic properties (full PBPK model)		
Prediction model	1	
K_p scalar	0.7	Predicted
CYP metabolism: ISEF adjusted recombinant enzyme kinetics (CL_{int}; µL/min/pmol)		
CYP3A4	2.6	[18]
UGT metabolism: ISEF adjusted recombinant enzyme kinetics (CL_{int}; µL/min/mg)		
UGT1A9	20.1	[18]

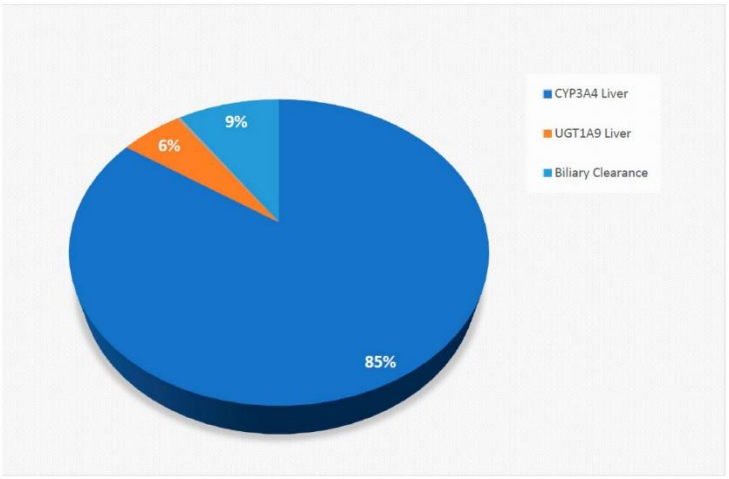

Figure 4. The pie chart demonstrated the relative contribution of CYP and UGT to simulated sorafenib elimination based on the predicted model.

4.3. Population Model

As no clinical trials evaluating sorafenib exposure have been performed in healthy volunteers, verification of the sorafenib compound model was performed using Sim-Cancer population cohort. Simulations performed to assess the physiological and molecular characteristics driving between-subject variability in sorafenib exposure at steady state also

utilised the Sim-Cancer population cohort. The physiological and pathological characteristics of the Sim-cancer population have been determined based on a meta-analysis of cancer patients enrolled in clinical trials [45].

4.4. Simulated Trial Designs

During the model development stage, simulations included 10 trials with 10 subjects per trial (100 subjects total). During the verification stage, simulations were performed in 10 trials matched for sample size, dose, age range and sex distribution in the protocol described for the observed trial. Unless specified otherwise, parameters defining sorafenib exposure were assessed over 24 h following a single dose at 9:00 a.m. on day 1.

4.5. Validation of the Sorafenib Compound Model

The sorafenib compound model was validated by comparing simulated AUC and C_{max} values to reported observed values from matched clinical trials undertaken in cancer patients. A mean simulated parameter estimated within two-fold of the mean observed parameter and contained within the 90% confidence interval for the observed parameter was applied as the criteria to accept the model accuracy. The model goodness-of-fit was further verified by visual inspection of the overlay of mean simulated and observed sorafenib concentration-time profiles from individual clinical trials. Simulated C_{max} values were normalised to account for the mean fold error (MFE) between simulated and observed values determined from multiple dose validation studies when evaluating simulations against the observed target concentration range (4.78 to 5.78 μg/mL).

4.6. Physiological and Molecular Characteristics Driving Variability in Sorafenib Exposure

The validated sorafenib compound model was used to evaluate associations between physiological and molecular covariates and steady-state sorafenib AUC and C_{max} [24]. A trial comprising 1000 subjects from the Sim-Cancer population was simulated over 15 days with 400 mg of sorafenib administered orally in a fasted-state every 12 h for 14 days starting at 9:00 a.m. on Day 1. The steady state sorafenib AUC was determined over 12 h following the final dose of sorafenib at 9:00 p.m. on Day 14. The steady state sorafenib C_{max} was determined as the maximum concentration following the final dose at 9:00 p.m. on Day 14.

Associations between physiological and molecular characteristics and sorafenib log transformed AUC and C_{max} were evaluated by univariate and multivariate linear regression. Continuous variables were checked for normality and non-linearity of association, sex was coded as a binary variable. A multivariable linear regression model to predict the log transformed sorafenib C_{max} was developed by stepwise forward inclusion of individually significant characteristics identified in the univariable regression analysis based on a probability of F to enter ≤ 0.05. The multivariable model (MIDS) predicted C_{max} was determined by back transformation of the model predicted log transformed C_{max}. The capacity of MIDS to identify subjects with a sub-therapeutic simulated sorafenib C_{max} determined by scaling the reported threshold for simulation accuracy was evaluated using classification matrix analysis and is summarised as model sensitivity and specificity. The predictive performance of MIDS was assessed by receiver operating characteristic curve (ROC) analysis. Statistical analysis was conducted using R version 4.0.2 and IBM SPSS Statistics for Windows version 23 (Release 2015, IBM, Armonk, NY, USA).

4.7. Impact of Dose Individualisation

A simulation was conducted to evaluate the capacity of concentration-guided sorafenib dose adjustment to achieve a steady state sorafenib C_{max} within the range 4.78 to 5.78 μg/mL. Sorafenib exposure was simulated in a cohort of 500 subjects from the Sim-Cancer population (20 to 50 years old, 50% female) over 14 days with 400 mg sorafenib administered orally in a fasted-state every 12 h starting at 9:00 a.m. on Day 1. Sorafenib C_{max} was determined following the final dose at 9:00 p.m. on Day 14. Sorafenib exposure

in subjects who failed to achieve a Day 14 normalised simulated $C_{max} \geq 4.78$ µg/mL was simulated over an additional 14 days with sorafenib administered at a dose of 600 mg every 12 h starting at 9:00 a.m. on Day 15. The post dose adjustment sorafenib C_{max} was determined following the final dose at 9:00 p.m. on Day 28.

A simulation was conducted in the same cohort to evaluate the benefit of MIDS at baseline in conjunction with concentration-guided sorafenib dose adjustment. Demographic characteristics for the Sim-Cancer cohort were used to predict the normalised simulated Day 14 sorafenib C_{max} based on the multivariable model described previously. Based on MIDS subjects with a predicted sorafenib $C_{max} \geq 4.78$ µg/mL received 400 mg sorafenib twice daily, while subjects with predicted sorafenib $C_{max} < 4.78$ µg/mL received 500 mg sorafenib twice daily. Sorafenib exposure was simulated over 28 days as described for concentration-guided sorafenib dose adjustment without MIDS, with C_{max} evaluated at Day 14 and Day 28 and a dose increase to 600 mg between Day 15 and Day 28 for individuals who failed to achieve a Day 14 $C_{max} \geq 4.78$ µg/mL.

Supplementary Materials: The following are available online at https://www.mdpi.com/article/10.3390/ph14050389/s1. Table S1: Verification of the impact of drug interactions on sorafenib exposure. Table S2: Summary of physiological and molecular characteristic considered in regression analyses. Table S3: Logistic regression analysis of therapeutic C_{max} threshold of >5.5926 mg/L.

Author Contributions: Conceptualisation, W.R., M.J.S., A.M.H. and A.R.; methodology, W.R., M.J.S., A.M.H. and A.R.; software, A.R.; validation, A.R. and W.R.; formal analysis, W.R. and A.R.; investigation, W.R. and A.R.; resource, A.R.; data curation, W.R. and A.R.; writing—original draft preparation, W.R..; writing—review and editing, W.R., A.R., A.M.H. and M.J.S.; visualisation, W.R. and A.R.; supervision, M.J.S., A.M.H. and A.R.; project administration, M.J.S., A.M.H. and A.R.; funding acquisition, A.R. All authors have read and agreed to the published version of the manuscript.

Funding: WR is supported by a Royal Thai Government Scholarship. A.R. and M.J.S. are supported by Cancer Council Beat Cancer Fellowships. A.M.H. is supported by a National Breast Cancer Foundation Fellowship.

Institutional Review Board Statement: Not applicable.

Informed Consent Statement: Not applicable.

Data Availability Statement: The data that support the findings of this study are available from the corresponding author upon reasonable request.

Conflicts of Interest: A.R. and M.J.S. report investigator-initiated project grants from Pfizer, outside the scope of the submitted work. W.R. and A.M.H. have no conflicts of interest to disclose.

References

1. Vogel, A.; Cervantes, A.; Chau, I.; Daniele, B.; Llovet, J.M.; Meyer, T.; Nault, J.C.; Neumann, U.; Ricke, J.; Sangro, B.; et al. Hepatocellular carcinoma: ESMO Clinical Practice Guidelines for diagnosis, treatment and follow-up. *Ann Oncol.* **2018**, *29* (Suppl. 4), 238–255. [CrossRef]
2. Wang, H.-T.; Xia, M. A meta-analysis of efficacy and safety of sorafenib versus other targeted agents for metastatic renal cell carcinoma. *Medicine* **2019**, *98*, e13779. [CrossRef]
3. Strumberg, D.; Clark, J.W.; Awada, A.; Moore, M.J.; Richly, H.; Hendlisz, A.; Hirte, H.W.; Eder, J.P.; Lenz, H.-J.; Schwartz, B. Safety, Pharmacokinetics, and Preliminary Antitumor Activity of Sorafenib: A Review of Four Phase I Trials in Patients with Advanced Refractory Solid Tumors. *Oncologist* **2007**, *12*, 426–437. [CrossRef] [PubMed]
4. Awada, A.; Hendlisz, A.; Gil, T.; Bartholomeus, S.; Mano, M.; de Valeriola, D.; Strumberg, D.; Brendel, E.; Haase, C.G.; Schwartz, B.; et al. Phase I safety and pharmacokinetics of BAY 43-9006 administered for 21 days on/7 days off in patients with advanced, refractory solid tumours. *Br. J. Cancer* **2005**, *92*, 1855–1861. [CrossRef]
5. Moore, M.; Hirte, H.W.; Siu, L.; Oza, A.; Hotte, S.J.; Petrenciuc, O.; Cihon, F.; Lathia, C.; Schwartz, B. Phase I study to determine the safety and pharmacokinetics of the novel Raf kinase and VEGFR inhibitor BAY 43-9006, administered for 28 days on/7 days off in patients with advanced, refractory solid tumors. *Ann. Oncol.* **2005**, *16*, 1688–1694. [CrossRef]
6. Jain, L.; Woo, S.; Gardner, E.R.; Dahut, W.L.; Kohn, E.C.; Kummar, S.; Mould, D.R.; Giaccone, G.; Yarchoan, R.; Venitz, J.; et al. Population pharmacokinetic analysis of sorafenib in patients with solid tumours. *Br. J. Clin. Pharmacol.* **2011**, *72*, 294–305. [CrossRef]

7. Sharma, M.; Holmes, H.M.; Mehta, H.B.; Chen, H.; Aparasu, R.R.; Shih, Y.-C.T.; Giordano, S.H.; Johnson, M.L. The concomitant use of tyrosine kinase inhibitors and proton pump inhibitors: Prevalence, predictors, and impact on survival and discontinuation of therapy in older adults with cancer. *Cancer* **2019**, *125*, 1155–1162. [CrossRef] [PubMed]
8. Ruanglertboon, W.; Sorich, M.J.; Logan, J.M.; Rowland, A.; Hopkins, A.M. The effect of proton pump inhibitors on survival outcomes in advanced hepatocellular carcinoma treated with sorafenib. *J. Cancer Res. Clin. Oncol.* **2020**, *146*, 2693–2697. [CrossRef] [PubMed]
9. Lalani, A.A.; McKay, R.R.; Lin, X.; Simantov, R.; Kaymakcalan, M.D.; Choueiri, T.K. Proton Pump Inhibitors and Survival Outcomes in Patients With Metastatic Renal Cell Carcinoma. *Clin. Genitourin. Cancer* **2017**, *15*, 724–732. [CrossRef] [PubMed]
10. Au, T.H.; Bailey, E.B.; Patel, S.B.; Tantravahi, S.K.; Agarwal, N.; Stenehjem, D.D. Effect of concomitant proton pump inhibitor (PPI) on effectiveness of tyrosine kinase inhibitor (TKI) in patients with metastatic renal cell carcinoma (mRCC). *J. Clin. Oncol.* **2016**, *34* (Suppl. 2), 608. [CrossRef]
11. Fukudo, M.; Ito, T.; Mizuno, T.; Shinsako, K.; Hatano, E.; Uemoto, S.; Kamba, T.; Yamasaki, T.; Ogawa, O.; Seno, H.; et al. Exposure-toxicity relationship of sorafenib in Japanese patients with renal cell carcinoma and hepatocellular carcinoma. *Clin. Pharmacokinet.* **2014**, *53*, 185–196. [CrossRef] [PubMed]
12. Ruanglertboon, W.; Sorich, M.J.; Rowland, A.; Hopkins, A.M. Effect of early adverse events resulting in sorafenib dose adjustments on survival outcomes of advanced hepatocellular carcinoma patients. *Int. J. Clin. Oncol.* **2020**, *25*, 1672–1677. [CrossRef] [PubMed]
13. de Wit, D.; Guchelaar, H.J.; den Hartigh, J.; Gelderblom, H.; van Erp, N.P. Individualized dosing of tyrosine kinase inhibitors: Are we there yet? *Drug Discov. Today* **2015**, *20*, 18–36. [CrossRef] [PubMed]
14. Mueller-Schoell, A.; Groenland, S.L.; Scherf-Clavel, O.; van Dyk, M.; Huisinga, W.; Michelet, R.; Jaehde, U.; Steeghs, N.; Huitema, A.D.R.; Kloft, C. Therapeutic drug monitoring of oral targeted antineoplastic drugs. *Eur. J. Clin. Pharmacol.* **2020**, *29*, iv238–iv255. [CrossRef]
15. Semrad, T.J.; Gandara, D.R.; Lara, P.N., Jr. Enhancing the clinical activity of sorafenib through dose escalation: Rationale and current experience. *Ther. Adv. Med. Oncol.* **2011**, *3*, 95–100. [CrossRef]
16. Escudier, B.; Szczylik, C.; Hutson, T.E.; Demkow, T.; Staehler, M.; Rolland, F.; Negrier, S.; Laferriere, N.; Scheuring, U.J.; Cella, D.; et al. Randomized phase II trial of first-line treatment with sorafenib versus interferon Alfa-2a in patients with metastatic renal cell carcinoma. *J. Clin. Oncol.* **2009**, *27*, 1280–1289. [CrossRef] [PubMed]
17. Verheijen, R.B.; Yu, H.; Schellens, J.H.M.; Beijnen, J.H.; Steeghs, N.; Huitema, A.D.R. Practical Recommendations for Therapeutic Drug Monitoring of Kinase Inhibitors in Oncology. *Clin. Pharmacol. Ther.* **2017**, *102*, 765–776. [CrossRef]
18. Rowland, A.; van Dyk, M.; Mangoni, A.A.; Miners, J.O.; McKinnon, R.A.; Wiese, M.D.; Rowland, A.; Kichenadasse, G.; Gurney, H.; Sorich, M.J. Kinase inhibitor pharmacokinetics: Comprehensive summary and roadmap for addressing inter-individual variability in exposure. *Expert Opin. Drug Metab. Toxicol.* **2017**, *13*, 31–49. [CrossRef] [PubMed]
19. Darwich, A.; Ogungbenro, K.; Hatley, O.; Rostami-Hodjegan, A. Role of pharmacokinetic modeling and simulation in precision dosing of anticancer drugs. *Transl. Cancer Res.* **2017**. [CrossRef]
20. Hopkins, A.M.; Menz, B.D.; Wiese, M.D.; Kichenadasse, G.; Gurney, H.; McKinnon, R.A.; Rowland, A.; Sorich, M.J. Nuances to precision dosing strategies of targeted cancer medicines. *Pharmacol. Res. Perspect.* **2020**, *8*, e00625. [CrossRef]
21. Kang, J.S.; Lee, M.H. Overview of therapeutic drug monitoring. *Korean J. Intern. Med.* **2009**, *24*, 1–10. [CrossRef] [PubMed]
22. Thomson, A. TDM—A Multidisciplinary Approach. *Ther. Drug Monit.* **1997**, *19*, 490. [CrossRef]
23. Sánchez-Hernández, J.G.; Rebollo, N.; Martin-Suarez, A.; Calvo, M.V.; Muñoz, F. A 3-year prospective study of a multidisciplinary early proactive therapeutic drug monitoring programme of infliximab treatments in inflammatory bowel disease. *Br. J. Clin. Pharmacol.* **2020**, *86*, 1165–1175. [CrossRef] [PubMed]
24. Sorich, M.J.; Mutlib, F.; van Dyk, M.; Hopkins, A.M.; Polasek, T.M.; Marshall, J.C.; Rodrigues, A.D.; Rowland, A. Use of Physiologically Based Pharmacokinetic Modeling to Identify Physiological and Molecular Characteristics Driving Variability in Axitinib Exposure: A Fresh Approach to Precision Dosing in Oncology. *J. Clin. Pharmacol.* **2019**, *59*, 872–879. [CrossRef] [PubMed]
25. Rowland, A.; van Dyk, M.; Hopkins, A.M.; Mounzer, R.; Polasek, T.M.; Rostami-Hodjegan, A.; Sorich, M.J. Physiologically Based Pharmacokinetic Modeling to Identify Physiological and Molecular Characteristics Driving Variability in Drug Exposure. *Clin. Pharmacol. Ther.* **2018**, *104*, 1219–1228. [CrossRef] [PubMed]
26. Polasek, T.M.; Rostami-Hodjegan, A. Virtual Twins: Understanding the Data Required for Model-Informed Precision Dosing. *Clin. Pharmacol. Ther.* **2020**, *107*, 742–745. [CrossRef]
27. Kluwe, F.; Michelet, R.; Mueller-Schoell, A.; Maier, C.; Klopp-Schulze, L.; van Dyk, M.; Mikus, G.; Huisinga, W.; Kloft, C. Perspectives on Model-Informed Precision Dosing in the Digital Health Era: Challenges, Opportunities, and Recommendations. *Clin. Pharmacol. Ther.* **2020**, *109*, 29–36. [CrossRef]
28. Polasek, T.M.; Polak, S.; Doogue, M.P.; Rostami-Hodjegan, A.; Miners, J.O. Assessment of inter-individual variability in predicted phenytoin clearance. *Eur. J. Clin. Pharmacol.* **2009**, *65*, 1203–1210. [CrossRef]
29. Chetty, M.; Cain, T.; Wedagedera, J.; Rostami-Hodjegan, A.; Jamei, M. Application of Physiologically Based Pharmacokinetic (PBPK) Modeling Within a Bayesian Framework to Identify Poor Metabolizers of Efavirenz (PM), Using a Test Dose of Efavirenz. *Front. Pharmacol.* **2018**, *9*, 247. [CrossRef]
30. Tsamandouras, N.; Rostami-Hodjegan, A.; Aarons, L. Combining the 'bottom up' and 'top down' approaches in pharmacokinetic modelling: Fitting PBPK models to observed clinical data. *Br. J. Clin. Pharmacol.* **2015**, *79*, 48–55. [CrossRef]

31. Tylutki, Z.; Polak, S.; Wiśniowska, B. Top-down, Bottom-up and Middle-out Strategies for Drug Cardiac Safety Assessment via Modeling and Simulations. *Curr. Pharmacol. Rep.* **2016**, *2*, 171–177. [CrossRef]
32. Polasek, T.M.; Tucker, G.T.; Sorich, M.J.; Wiese, M.D.; Mohan, T.; Rostami-Hodjegan, A.; Korprasertthaworn, P.; Perera, V.; Rowland, A. Prediction of olanzapine exposure in individual patients using physiologically based pharmacokinetic modelling and simulation. *Br. J. Clin. Pharmacol.* **2018**, *84*, 462–476. [CrossRef]
33. Van Dyk, M.; Rowland, A. PBPK modeling as an approach to evaluate the effect of covariates and drug-drug interactions on variability in EGFR kinase inhibitor exposure. *Transl. Cancer Res.* **2017**, *6*, S1600–S1615. [CrossRef]
34. Minami, H.; Kawada, K.; Ebi, H.; Kitagawa, K.; Kim, Y.-I.; Araki, K.; Mukai, H.; Tahara, M.; Nakajima, H.; Nakajima, K. Phase I and pharmacokinetic study of sorafenib, an oral multikinase inhibitor, in Japanese patients with advanced refractory solid tumors. *Cancer Sci.* **2008**, *99*, 1492–1498. [CrossRef] [PubMed]
35. Shebley, M.; Sandhu, P.; Riedmaier, A.E.; Jamei, M.; Narayanan, R.; Patel, A.; Peters, S.A.; Reddy, V.P.; Zheng, M.; de Zwart, L.; et al. Physiologically Based Pharmacokinetic Model Qualification and Reporting Procedures for Regulatory Submissions: A Consortium Perspective. *Clin. Pharmacol. Ther.* **2018**, *104*, 88–110. [CrossRef]
36. Basu, S.; Lien, Y.T.; Vozmediano, V.; Schlender, J.-F.; Eissing, T.; Schmidt, S.; Niederalt, C. Physiologically Based Pharmacokinetic Modeling of Monoclonal Antibodies in Pediatric Populations Using PK-Sim. *Front. Pharmacol.* **2020**, *11*, 868. [CrossRef] [PubMed]
37. Hennig, S.; Holthouse, F.; Staatz, C.E. Comparing dosage adjustment methods for once-daily tobramycin in paediatric and adolescent patients with cystic fibrosis. *Clin. Pharmacokinet.* **2015**, *54*, 409–421. [CrossRef] [PubMed]
38. Song, L.; He, C.-Y.; Yin, N.-G.; Liu, F.; Jia, Y.-T.; Liu, Y. A population pharmacokinetic model for individualised dosage regimens of vancomycin in Chinese neonates and young infants. *Oncotarget* **2017**, *8*, 105211–105221. [CrossRef]
39. Rowland, A.; Ruanglertboon, W.; van Dyk, M.; Wijayakumara, D.; Wood, L.; Meech, R.; Mackenzie, P.; Rodrigues, A.; Marshall, J.; Sorich, M. Plasma Extracellular Nanovesicle (Exosome) derived biomarkers for ADME pathways: A novel approach to characterise variability in drug exposure. *Br. J. Clin. Pharmacol.* **2019**, *85*, 216–226. [CrossRef]
40. Kumar, S.; Sinha, N.; Gerth, K.A.; Rahman, M.A.; Yallapu, M.M.; Midde, N.M. Specific packaging and circulation of cytochromes P450, especially 2E1 isozyme, in human plasma exosomes and their implications in cellular communications. *Biochem. Biophys. Res. Commun.* **2017**, *491*, 675–680. [CrossRef]
41. Achour, B.; Al-Majdoub, Z.M.; Grybos-Gajniak, A.; Lea, K.; Kilford, P.; Zhang, M.; Knight, D.; Barber, J.; Schageman, J.; Rostami-Hodjegan, A. Liquid Biopsy Enables Quantification of the Abundance and Interindividual Variability of Hepatic Enzymes and Transporters. *Clin. Pharmacol. Ther.* **2021**, *109*, 222. [CrossRef] [PubMed]
42. Rowland Yeo, K.; Jamei, M.; Yang, J.; Tucker, G.T.; Rostami-Hodjegan, A. Physiologically based mechanistic modelling to predict complex drug-drug interactions involving simultaneous competitive and time-dependent enzyme inhibition by parent compound and its metabolite in both liver and gut-the effect of diltiazem on the time-course of exposure to triazolam. *Eur. J. Pharm. Sci.* **2010**, *39*, 298–309. [PubMed]
43. European Medicines Agency. Nexavar: European Public Assessment Reports (EPAR)-Scientific Discussion. 3 March 2007. Available online: http://www.ema.europa.eu/docs/en_GB/document_library/EPAR-Scientific_Discussion/human/000690/WC500027707.pdf (accessed on 20 February 2021).
44. Liu, B.; Crewe, H.K.; Ozdemir, M.; Yeo, K.R.; Tucker, G.; Rostami-Hodjegan, A. The absorption kinetics of ketoconazole plays a major role in explaining the reported variability in the level of interaction with midazolam: Interplay between formulation and inhibition of gut wall and liver metabolism. *Biopharm. Drug Dispos.* **2017**, *38*, 260–270. [CrossRef] [PubMed]
45. Schwenger, E.; Reddy, V.P.; Moorthy, G.; Sharma, P.; Tomkinson, H.; Masson, E.; Vishwanathan, K. Harnessing Meta-analysis to Refine an Oncology Patient Population for Physiology-Based Pharmacokinetic Modeling of Drugs. *Clin. Pharmacol. Ther.* **2018**, *103*, 271–280. [CrossRef]